UNIVERSITÉ DE MONTRÉAL

GENE SILENCING USING CHITOSAN BASED SIRNA DELIVERY SYSTEMS IN CELLS AND ANIMALS

MOHAMAD ALAMEH

INSTITUT DE GÉNIE BIOMÉDICAL

ÉCOLE POLYTECHNIQUE DE MONTRÉAL

THÈSE PRÉSENTÉE EN VUE DE L'OBTENTION

DU DIPLÔME DE PHILOSOPHIAE DOCTOR

(GÉNIE BIOMÉDICAL)

JUIN 2017

© Mohamad Alameh, 2017.

UNIVERSITÉ DE MONTRÉAL

ÉCOLE POLYTECHNIQUE DE MONTRÉAL

Cette thèse intitulée :

GENE SILENCING USING CHITOSAN BASED SIRNA DELIVERY SYSTEMS IN CELLS AND ANIMALS

présentée par : ALAMEH Mohamad

en vue de l'obtention du diplôme de : Philosophiae Doctor

a été dûment acceptée par le jury d'examen constitué de :

Mme HOEMANN Caroline, Ph. D., présidente

M. BUSCHMANN Michael, Ph. D., membre et directeur de recherche

M. LAVERTU Marc, Ph. D., membre et codirecteur de recherche

M. DAMHA Masad José, Ph. D., membre

M. GREEN Jordan J, Ph. D., membre externe

DEDICATION

To my mother,

My sister

&

My family and to all those who had or still have a grudge against me

ACKNOWLEDGEMENTS

I would like to express my special gratitude towards my supervisor, Dr. Michael Buschmann who has been a tremendous mentor for me. His knowledge and motivation has allowed me to grow as a research scientist. I appreciate his contributions of time and ideas to make my Ph. D. experience productive and stimulating. He has always given me the freedom to pursue projects independently which has instilled confidence in my abilities. By providing me the opportunity to lead the group, he has expressed immense belief in my capabilities, for which I am extremely grateful.

I would also like to thank my co-supervisor, Dr. Marc Lavertu. His guidance and constant feedback have been extremely instrumental in achieving my Ph.D. I acknowledge the stimulating conversations which have provided critical insights into my projects and much needed breakthroughs throughout my research. In addition, I would like to recognize the role of Dr. Caroline Hoemann in letting me develop my teaching capabilities. I am thankful to her, and to Michael Buschmann for providing me the opportunities to teach several courses and mentor students which have led to the development of my communication and presentation skills.

I am indebted to the contribution of Chi-Yuan Chang in my research. He has been extremely supportive and instrumental in executing several of critical and challenging experiments of my research. Yuan was also a good listener, a confident in time of need, and a staunch supporter that stood for me. My deep appreciation goes out to Anik, Genevieve, Ashkan, Ousamah, Etienne and Nicolas for their time and assistance which have been immensely instrumental in the progress of my project.

Fun times with friends provide the much needed respite from the research life. I have deep appreciation for my friends Ghazal, Ashkan (or *MY Akhi*), Ibtissam, Emily-Jane, Fadi & Racha & Anthony Aris (Like father like son ☺, let's hope for the BB ya abo el fouf), Sana B, Imad Nasrallah, Abdallah Alameh (or *THE khal*), Mariam G, Daniel Del Balso, Pierrino Torbey, Bourak Gockcinar & Teoman, Mike Syrmakesian and Mohamad Karnib. I am extremely thankful to them for always being there in times of need and helping me face the challenges during Ph.D. I extend a special thanks to Garima Dwivedi, a true friend and very competent colleague, Colleen, Ashkan and Nic for their invaluable advices and feedback on my research. More often than not, they had faith in my intellect and encouraged me to work harder.

I would also like to express heartfelt gratitude towards Prime Minister Saad Rafik Hariri, Minister Marwan Hamadeh and Christiane Buck for their support, help and advices which has aided me in numerous ways during several phases of my PhD project and beyond.

Undertaking this PhD has been a truly life-changing experience for me and it would not have been possible to do without the support and guidance that I received from my family. Despite her own hardships in life, my mother has always supported my dreams, was and will always be the role model for me. I owe my success to her sacrifices and constant encouragement. She has always lent a patient ear to my venting in frustrating and testing times. I feel extremely fortunate to have a supportive and loving sister Lily-Isabelle, who has always been a sweet and lovely pain since childhood ☺. I am also thankful to my grandmothers for their unconditional love and warmth throughout life which has constantly driven me towards achieving my goals. Finally, I would like to thank my dad, my grandfather, and my father figure Dr Talaat J, who have inspired me with their patience and life philosophies.

Thank you all

RÉSUMÉ

Le développement de vecteurs de livraison non viraux à des fins thérapeutiques a pris de l'ampleur dans les dernières années. Le chitosane est un polymère cationique naturel ayant la capacité de former des nanoparticules lorsqu'il est mélangé à des molécules polyanioniques comme les petits ARN interférents (pARNi). Les efforts pour identifier les paramètres moléculaires favorisant une bioactivité optimale n'ont pas été concluants en raison de différences expérimentales, d'un manque d'uniformité des protocoles de transfection, de la faible caractérisation du polymère et des différences au niveau des sources de chitosane utilisé. Cette thèse a été entreprise afin de répondre aux objectifs suivants: **1)** Tester et valider l'efficacité de transfection de formulations, précédemment identifiées comme optimales pour la livraison d'ADN plasmidique, **2)** Examiner l'influence des paramètres intrinsèques (dégrée de deacetylation (DDA), la masse moléculaire (Mn) et le ratio N:P) et extrinsèques (sérum, pH, force ionique et conditions de mélange) sur les caractéristiques physicochimiques des particules, leur internalisation dans les cellules, l'efficacité de silençage, la toxicité métabolique, la génotoxicité et l'hémocomptabilité, en utilisant une chimiothèque de chitosanes hautement caractérisés, et **3)** Sélectionner des formulations ayant des caractéristiques optimales relatives à la taille, le potentiel zêta, l'intégrité des nanoparticules et la capacité de ces dernières à induire un silençage spécifique du gène en question tout en étant sécuritaire, et **4)** Caractériser la biodistribution des nanoparticules, leurs toxicités et leurs potentiel de silençage génique suite à des injections intraveineuses chez la souris.

Une étude initiale a démontré que le chitosane interfère avec l'extraction d'acide nucléique de cellules transfectées *in vitro*. Une méthode enzymatique simple et peu coûteuse a permis de récupérer l'ARN totale pour des applications moléculaires tel que la PCR en temps réel. De plus, cette étude a permis de réduire le biais (~ 10-15 %) associé aux nanoparticules adsorbées à la surface des cellules lors de mesures du niveau d'internalisation par cytométrie en flux.

En outre, la digestion enzymatique du chitosane pourrait être effectuée en présence de guanidium, un agent chaotropique présent dans le tampon de lyse, démontrant ainsi l'efficacité et la simplicité de cette méthode. Avec la résolution de cet obstacle technique, nous avons sélectionné des formulations ayant démontré, auparavant, une efficacité de transfection élevée pour la livraison d'ADN plasmidique. Ces formulations ont été caractérisés pour leur taille, leur forme, leur potentiel

surfacique (potentiel zêta), leur capacité de protéger les pARNi contre les nucléases et leur efficacité à transfecter, de façon non toxique, différentes lignées cellulaires.
Les nanoparticules ainsi formées étaient sphériques et leur taille variait entre 40 et 100 nm. De plus, les résultats ont démontré que la protection contre les nucléases dépendait de la masse moléculaire et du ratio N:P. Par ailleurs, une haute efficacité (~80%) de silençage génique, en présence de sérum (10%), a pu être atteinte dans plusieurs lignées cellulaires. Pour la première fois, des nanoparticules avaient pu être obtenues à un faible ratio N:P marquant ainsi une différence frappante avec la littérature. Nos résultats ont pu démontrer la cause de ce bais favorisant la sélection de nanoparticules à haut ratio N :P testée dans la littérature.

Dans la perspective de comprendre l'influence du degré de désacétylation (DDA) et de la masse moléculaire (Mn) du chitosane ainsi que du ratio N :P sur l'efficacité de transfection *in vitro*, la toxicité, la génotoxicité, l'hémocompatibilité et la biodistribution *in vivo*, une chimiothèque de chitosans hautement caractérisés a été produite à de différents DDA (98%, 92%, 80% et 72%) et Mn (5, 10, 40, 80 et 120 kDa) et mélangée avec des pARNi à des ratios N :P de 5 :1 et 30 :1. Les nanoparticules, ainsi formées, ont été caractérisées pour leurs tailles et potentiel surfacique en présence de 10 et 150 mM de sel. L'efficacité d'encapsulation (EE) et de transfection a été mesurée à pH 6.5 et 8 (EE) et à pH 6.5 et 7.4 respectivement. Les formulations les plus performantes ont été sélectionnées pour une caractérisation plus poussée de l'influence de la Mn et du ratio N:P sur l'internalisation des nanoparticules, l'activité métabolique cellulaire, la génotoxicité et l'efficacité de transfection *in vitro* en présence de sérum. L'hémocompatibilité et la biodistribution *in vivo* ont également été examinées pour différents Mn, ratios N :P et doses. Nos résultats ont démontré que l'internalisation des nanoparticules et l'efficacité de silençage étaient positivement corrélées à l'augmentation du potentiel surfacique, obtenu en augmentant le DDA et la Mn. Une longueur minimale de ~60-70 monomères (Mn ~10 kDa) était requise pour garantir une stabilité et un silençage en présence ou absence de sérum. L'efficacité de silençage a atteint des niveaux équivalents (~ 80-90%) à ceux du contrôle positif (DharmaFECT®) sans toxicité métabolique ou génotoxicité démontrant ainsi la supériorité de notre système comparativement aux lipides cationiques qui ont diminué l'activité métabolique des cellules. La présence de concentration croissante de sérum a négativement influencé la transfection *in vitro*. Nos résultats indiquent que l'influence négative du sérum est inversement proportionnelle à une augmentation du DDA, de la

Mn et du ratio N :P. L'hémocompatibilité s'est révélée être dépendante de la dose, du DDA et de la masse moléculaire suggérant ainsi l'utilisation d'acide hyaluronique (HA), un polymère anionique et biocompatible, pour diminuer l'interaction avec les composantes du sang et améliorer la stabilité colloïdale.

Les études de toxicité *in vivo* ont démontré que les nanoparticules de chitosane formulées à N:P 5 pourraient être tolérées jusqu'à une dose de 2.5mg/kg siRNA, tandis que celles revêtues de HA améliorent la tolérabilité par un facteur d'au moins 4.

Contrairement aux nanoparticules lipidiques, les nanoparticules avec ou sans revêtement n'ont ni entraîné l'expression de cytokines pro-inflammatoires (ex. IL-1β, IL-6, TNF-α, IFN-γ et KC) ni l'augmentation de biomarqueurs sérologiques tels que l'ALT, AST, ALP, l'urée sanguine, et la créatinine. Une diminution des thrombocytes a été uniquement observée avec les formulations lipidiques soulignant ainsi des différences majeures avec le chitosane.

L'analyse histopathologique des tissus et le suivit des masses corporelles ont confirmés le profil d'innocuité observé avec le chitosane. L'étude de biodistribution chez la souris démontre une accumulation spécifique de nanoparticules dans les tubules épithéliaux proximaux du rein où 40-50% de silençage a été observé, suggérant ainsi des applications potentielles du système au niveau des maladies rénales.

ABSTRACT

Research to develop safe and efficient non-viral gene delivery vectors for clinical applications has gained momentum in recent years. Chitosan is a natural cationic polymer with a characteristic property of self-assembly with small interfering RNA (siRNA) to form nanoparticles with high *in vitro* and *in vivo* transfection efficiencies. Previous efforts to identify molecular parameters favoring optimal bioactivity failed to produce conclusive results because of experimental discrepancies, lack of uniformity in transfection protocols, differences in chitosan sources, and poor characterization. In the light of these lacunae, The project presented in this thesis was carried out with the following objectives **1)** Test and validate the transfection efficiency of formulations, previously identified as optimal for plasmid DNA, **2)** Investigate the effect of intrinsic (DDA, Mn and N:P ratio) and extrinsic parameters (serum, pH, ionic strength and mixing conditions) on nanoparticle physicochemical characteristics, *in vitro* cell uptake, knockdown efficiency, metabolic toxicity, genotoxicity and hemocompatibility using a library of precisely characterized chitosans, and **3)** Identify formulations with optimal characteristics with respect to size, surface charge, integrity, knockdown, toxicity followed by the characterization of their *in vivo* biodistribution; toxicity and gene knockdown potential following intravenous administration.

An initial study demonstrated that chitosan interferes with column based extractions of total RNA from low cell numbers. The digestion of chitosan using a relatively simple and inexpensive enzymatic method permitted total recovery of high-quality RNA. In addition, surface bound chitosan was shown to bias flow cytometry data, evaluating nanoparticle uptake through fluorescently labeled siRNA. Treatment of cells using the chitosanase method reduced false positive events by around 10-15%. Surprisingly, enzymatic digestion could be performed in guanidium, a chaotropic agent, containing lysis buffer demonstrating the convenience of the method and allowing for the extracted RNA to be used in quantitative PCR experiment. With the technical hurdle solved, specific formulations based on designs parameters for plasmid DNA were characterized for their size, shape, surface charge, nuclease protection and ability to transfect different cell lines and produce non-toxic target specific knockdown. In contrast to plasmid DNA, nanoparticles formed with siRNA were all spherical, and their size ranged from 40-100 nm. For the first time, nanoparticles could be obtained at low N:P ratio in striking difference with the literature. Nuclease protection was found to be molecular weight dependent, and gene silencing in

the presence of 10 % serum reached around 80%. This study demonstrated that nanoparticles formulated at low N:P ratio were able to form stable nanoparticles and induce target knockdown.

In an attempt to understand the influence of chitosan molecular weight and degree of deacetylation on *in vitro* transfection efficiency, toxicity, genotoxicity, hemocompatibility and *in vivo* biodistribution, a library of precisely characterized chitosans was produced at different DDAs (98%, 92%, 80% and 72%) and Mn (5, 10, 40, 80 and 120 kDa). They were then mixed with siRNA at N:P ratios of 5:1 and 30:1, and nanoparticles were characterized for their size and surface charge in the presence of 10 and 150 mM salt. Encapsulation (EE) and transfection efficiencies were characterized at pH 6.5 and 8 for EE and pH 6.5 and 7.4 for *in vitro* transfection. Formulations were selected for further characterization of the influence of Mn and N:P ratio on nanoparticle uptake, metabolic activity, genotoxicity, and *in vitro* transfection in the presence of increasing concentrations of serum. Hemocompatibility and *in vivo* biodistribution were also investigated for several Mn, N:P ratio, and dose. Nanoparticle uptake and gene silencing correlated positively with increased surface charge, which in turn was obtained at high DDA and high Mn. A minimum polymer length of ~60-70 monomers, or Mn of ~10kDa, was required for stability and *in vitro* knockdown in the presence or absence of serum. *In vitro* knockdown reached levels equivalent to the DharmaFECT® (~ 80-90%) with no metabolic toxicity or genotoxicity, the former in contrast to the lipid-based control which severely impaired metabolic activity. Serum had negative dose-dependent effects on biological performance, which correlated inversely with increased DDA, Mn and N:P. The poor *in vitro* performance above 50% serum concentration is believed to be multifactorial in cause and could not be elucidated. Despite the negative effect of serum on *in vitro* transfection efficiency, several reports have demonstrated *in vivo* efficacy. Hemocompatibility was found to be dose-dependent and increased with both Mn and DDA prompting the use of hyaluronic acid (HA), a biocompatible and negatively charged polymer, to coat nanoparticles for limited blood interaction and improved colloidal stability. Single ascending dose toxicity studies showed that uncoated chitosan-formulated at N:P 5 could be tolerated up to 2.5mg/kg siRNA dose, with nanoparticle coating improving tolerability by at least 4-folds. In contrast to commercially available, and liver-restricted lipid nanoparticles (LNPs), both uncoated and HA-coated did not induce pro-inflammatory cytokines such as. IL-1β, IL-6, TNF-α, IFN-γ, and KC, nor had obvious effects on the liver (ALT, AST, ALP) and kidney (BUN, Creatinine) biomarkers. Thrombocytopenia was only observed with the LNPs formulated with a native siRNA sequence

confirming previous reports and highlighting differences with chitosan. Repeated administration and histopathological analysis confirmed the safety profile of chitosan *versus* LNPs. *In vivo* biodistribution in mice showed accumulation of nanoparticles in the proximal epithelial tubules of the kidney, where 40-50% functional knockdown was observed and confirmed using multiple techniques, suggesting potential applications in kidney diseases.

TABLE OF CONTENTS

DEDICATION III

ACKNOWLEDGEMENTS IV

RÉSUMÉ VI

ABSTRACT IX

TABLE OF CONTENTS XII

LIST OF TABLES XXI

LIST OF SUPPLEMENTARY TABLES XXIII

LIST OF FIGURES XXIV

LIST OF SUPPLEMENTARY FIGURES XXXIX

LIST OF BOXES XLIII

LIST OF SYMBOLS AND ABBREVIATIONS XLIV

CHAPTER 1 INTRODUCTION 1

1.1 Introduction 1

1.2 Problematic 3

1.3 Research Hypotheses and Objectives 4

1.3.1 General objective 4

1.3.2 Study 1 4

1.3.2.1 Hypothesis 1 4

1.3.2.2 Objective 1 4

1.3.3 Study 2 5

1.3.3.1 Hypothesis 2 5

1.3.3.2 Objective 2 5

1.3.4 Study 3 6

1.3.4.1 Hypothesis 3 6

1.3.4.2 Objective 3 7

1.4 Brief structure of the thesis 7

CHAPTER 2 LITERATURE REVIEW 8

2.1 RNAi mechanism of action 8

2.2 Pharmacokinetic and pharmacodynamic considerations for effective RNAi 10

2.2.1 Physiological barriers to siRNA delivery 10

2.2.2 Structural factors affecting siRNA-induced RNAi 12

2.2.3 Potential toxicities 12

2.2.3.1 MicroRNA like off-target effects 12

2.2.3.2 Immune stimulation properties 14

2.2.3.3 Sequence-independent off-target effects. 15

2.2.4 Improvement of siRNA PK/PD properties through chemical modifications 15

2.3 Strategies for siRNA delivery 20

2.3.1 Nanoparticles based systems 20

2.3.1.1 Lipid nanoparticles (LNPs) 20

2.3.2 Polymer-based systems or polymer based nanoparticles 26

2.3.2.1 Polyethyleneimine (PEI) 26

2.3.2.1 Poly (β-amino ester) (PBAE) systems 27

2.3.2.2 Cyclodextrin-based systems 28

2.3.3 Conjugation-based systems 30

2.3.3.1 Lipid-siRNA conjugates 30

2.3.3.2 Dynamic Polyconjugates (DPC) 33

2.3.3.3 GalNAc conjugates 35

2.3.4 Chitosan for gene delivery 38

2.3.4.1 Chitosan for the delivery of plasmid DNA 40

2.3.4.2 Chitosan for the delivery of small interfering RNAs 42

2.4 Mechanisms of cell entry and endosomal escape of siRNA delivery systems 44

2.4.1 Mechanism of escape of lipid nanoparticles 47

2.4.2 Mechanism of escape of cationic polymers and cytoplasmic release 48

2.4.3 Mechanism of escape of molecular conjugates 48

CHAPTER 3 ORGANIZATION OF ARTICLES 49

CHAPTER 4 ARTICLE 1: CHITOSANASE-BASED METHOD FOR RNA ISOLATION FROM CELLS TRANSFECTED WITH CHITOSAN/SIRNA NANOCOMPLEXES FOR REAL-TIME RT-PCR IN GENE SILENCING 52

4.1 Introduction 53

4.2 Materials and Methods 55

4.2.1 Preparation of chitosan/siRNA polyplexes 55

4.2.2 Cell culture 55

4.2.3 Transfection with chitosan/siRNA nanoparticle complexes 56

4.2.4 Transfection with Dharmafect1™ 56

4.2.5 Chitosanase treatment of transfected cells and polyplexes degradation 56

4.2.6 FACS analysis 57

4.2.7 Confocal imaging 57

4.2.8 RNA extraction and assessment methods (yield, purity and integrity) 58

4.2.9 TaqMan® Gene Expression Assays – Endogenous controls 58

4.2.10 Universal Probe Library (UPL) Assays 58

4.2.11 Detection and analysis 59

4.2.12 Statistical Analysis 59

4.3 Results 60

4.3.1 Cellular Uptake 60

4.3.1 Effect of low molecular weight chitosan on RNA recovery 62

4.3.2 Effect of lysis buffer on Chitosanase activity 63

4.3.3 Gene silencing 65

4.4 Discussion 66

4.5 Conclusion 68

CHAPTER 5 ARTICLE 2: LOW MOLECULAR WEIGHT CHITOSAN NANOPARTICULATE SYSTEM AT LOW N:P RATIO FOR NONTOXIC POLYNUCLEOTIDE DELIVERY. 73

5.1 Introduction 75

5.2 Materials and methods 78

5.2.1 Synthesis siRNAs and dsODNs as a structural model of siRNA 78

5.2.2 Preparation and characterization of depolymerized chitosan 78

5.2.3 Preparation of chitosan nanoparticles 79

5.2.4 Nanoparticle size and ζ-potential analysis 80

5.2.5 High-vacuum scanning electron microscopy (ESEM) 80

5.2.6 Nanoparticle stability assessment by polyacrylamide gel electrophoresis 80

5.2.7 Nuclease protection assay 81

5.2.8 *In vitro* cell transfection 81

5.2.8.1 Cell culture 81

5.2.8.2 Cell transfection 82

5.2.8.3 Transfection with DharmaFECT 82

5.2.9 *In vitro* cell viability assay 82

5.2.10 Uptake analysis by flow cytometry and confocal microscopy 83

5.2.10.1 Fluorescence-activated cell sorting (FACS) analysis.....83

5.2.10.2 Confocal microscopy.....84

5.2.11 Quantitative PCR (qPCR) analysis of RecQL1 and ApoB mRNA knockdown....84

5.2.11.1 RNA extraction and assessment methods (yield, purity, and integrity).....84

5.2.11.2 Reverse transcription.....85

5.2.11.3 Gene expression assays 85

5.2.11.4 Detection and analysis.....85

5.2.12 Statistical analysis 86

5.3 Results 86

5.3.1 Size and ζ-potential of chitosan nanoparticles 86

5.3.2 Chitosan/dsODN nanoparticle stability.....87

5.3.3 Nanoparticle protection assay 89

5.3.4 *In vitro* cell uptake analysis by flow cytometry and confocal microscopy.....90

5.3.5 Specific gene silencing and cell cytotoxicity evaluation of chitosan nanoparticles in different cell lines.....94

5.4 Discussion 96

CHAPTER 6 ARTICLE 3: SIRNA DELIVERY WITH CHITOSAN: INFLUENCE OF CHITOSAN MOLECULAR WEIGHT, DEGREE OF DEACETYLATION AND AMINE TO PHOSPHATE RATIO ON IN VITRO SILENCING EFFICIENCY, HEMOCOMPATIBILITY, BIODISTRIBUTION AND IN VIVO EFFICACY 109

6.1 Introduction 111

6.2 Materials and methods 113

6.2.1 siRNA sequences and chitosan characterization.....113

6.2.2 Preparation of nanoparticles by manual mixing.....116

6.2.3 Determination of nanoparticle size and surface charge 116

6.2.4 Encapsulation efficiency and siRNA release 116

6.2.4.1 siRNA release at different pH 117

6.2.4.2 siRNA release in the presence of heparin 117

6.2.4.3 siRNA release in the presence of serum albumin 117

6.2.5 Cell culture 118

6.2.6 *In vitro* transfection 118

6.2.7 Assessment of EGFP knockdown and nanoparticle uptake using flow cytometry .. 118

6.2.8 MIQE compliant quantitative real-time PCR (qPCR) 119

6.2.9 Assessment of nanoparticle toxicity using the alamarBlue® assay 120

6.2.10 Assessment of nanoparticle genotoxicity using the comet or single cell gel electrophoresis assay. 121

6.2.11 Assessment of nanoparticle hemocompatibility at doses relevant for *in vivo* administration 121

6.2.12 *In vivo* biodistribution and efficacy studies 122

6.2.12.1 Determination of chitosan-siRNA biodistribution using *ex-vivo* whole organ imaging 123

6.2.12.2 Determination of *in vivo* functional gene knockdown 123

6.2.13 Assessment of *in vitro* knockdown and nanoparticle biodistribution using confocal microscopy 125

6.2.14 Statistical analysis 125

6.3 Results 127

6.3.1 Chitosan dictate nanoparticle uptake, target knockdown, ζ-potential and encapsulation efficiency at physiological pH while increasing Mn and N:P ratio have positive effects ... 127

6.3.2 In *vitro* knockdown efficiency is Mn independent above a certain threshold with chitosan found to disturb global gene expression. 136

6.3.3 *In vitro* lipid nanoparticle (LNP) like potency (EC_{50}) can be achieved, in the presence of serum, using chitosans with increasing Mn and N:P ratio 144

6.3.4 Reduction in knockdown efficiency due to serum can be mitigated by increasing Mn and N:P ratio 146

6.3.5 Metabolic and genotoxic testing demonstrate the safety of chitosan-siRNA nanoparticles at low/high Mn and N:P ratios 148

6.3.6 Chitosan induce Mn- and dose-dependent hemolysis and aggregation of red blood cells 151

6.3.7 Chitosan promotes extrahepatic siRNA delivery to proximal epithelial tubular cells of the kidney and induces target specific functional knockdown. 155

6.4 Discussion 160

6.5 Conclusion 166

CHAPTER 7 ARTICLE 4: CHITOSAN SIRNA NANOPARTICLES PRODUCE SIGNIFICANT NON-TOXIC FUNCTIONAL GENE SILENCING IN KIDNEY CORTICES 175

7.1 Introduction 177

7.2 Material and Methods 179

7.2.1 Materials 179

7.2.2 siRNA sequences and chitosan characterization 180

7.2.3 Preparation of chitosan-based nanoparticles 182

7.2.3.1 Preparation of chitosan, hyaluronic acid, and siRNA working solutions 182

7.2.3.2 Preparation, lyophilization and reconstitution of uncoated and HA-coated anti-ApoB nanoparticles (NPs) for the assessment of *in vivo* toxicity 182

7.2.3.3 Preparation of uncoated and HA-coated anti-GAPDH nanoparticles for assessment of *in vivo* target knockdown 183

7.2.4 Preparation of Invivofectamine®-siRNA-lipid nanoparticles (LNPs) 183

7.2.5 Determination of size and surface charge 184

7.2.6 Hemocompatibility 184

7.2.7 *In vivo* studies 185

7.2.7.1 Determination of chitosan-siRNA biodistribution using *ex-vivo* organ imaging 185

7.2.7.2 Determination of chitosan-siRNA nanoparticle in *vivo* toxicity 186

7.2.7.3 Hematological and serological parameters 186

7.2.7.4 Determination of cytokine levels 186

7.2.8 Determination of chitosan-siRNA nanoparticle in *vivo* efficacy 187

7.2.8.1 Assessment of GAPDH enzymatic activity using the KDalert® assay 187

7.2.8.2 Western blotting 188

7.2.8.3 Clinical signs and body weight 189

7.2.8.4 Histology and immunohistochemistry 189

7.2.8.5 Confocal laser scanning microscopy 189

7.2.9 Statistical analysis 190

7.3 Results 191

7.3.1 Uncoated chitosan NPs induced hemolysis and hemagglutination at high doses which were abrogated by hyaluronic acid (HA) coating 191

7.3.2 Uncoated and HA coated chitosan NPs promoted extrahepatic delivery of siRNA to kidney proximal tubular epithelial cells (PTEC) 194

7.3.3 Characterization of the injected nanoparticles 196

7.3.4 Unlike Lipid nanoparticles, uncoated and HA coated chitosan NPs did not induce immune stimulation and hematologic toxicity upon intravenous administration 198

7.3.5 Liver and kidney biomarkers remain unchanged with uncoated and HA coated chitosan NPs while high doses of lipid NPs led to increased transaminase levels 203

7.3.6 Despite normal clinical signs post-administration of NPs, a decrease in body weight was observed with cationic lipid nanoparticles, specifically following multiple injections 205

7.3.7 Uncoated and HA coated chitosan NPs did not induce histopathological changes in main organs following I.V injection at low and high doses 210

7.3.8 Uncoated chitosan NPs demonstrated functional gene-specific knockdown in kidney cortex independent of polymer length (Mn) 214

7.4 Discussion 217

7.5 Conclusion 224

CHAPTER 8 GENERAL DISCUSSION 234

CHAPTER 9 CONCLUSION AND RECOMMENDATIONS 244

BIBLIOGRAPHY 248

LIST OF TABLES

Table 2-1 Biological barriers for siRNA delivery, the impact of each barrier on performance and strategies to overcome the barriers. 11

Table 2-2 GalNAc based clinical candidates in development 36

Table 4-1: Effect of chitosanase treatment on RNA extraction, Relative Integrity Number (RIN) and real-time PCR (qPCR) analysis in three different DPP-IV expressing cell lines. Inhibition percentages of DPP-IV gene expression in siRNA/polyplexes transfected cells were determined in comparison with non-transfected cells: Effect of chitosanase treatment on RNA extraction, Relative Integrity Number (RIN) and real-time PCR (qPCR) analysis in three different DPP-IV expressing cell lines. Inhibition percentages of DPP-IV gene expression in siRNA/polyplexes transfected cells were determined in comparison with non-transfected cells 65

Table 5-1: Physicochemical characteristics of bulk chitosans 79

Table 5-2: Size and zeta potential values obtained by dynamic light scattering for chitosan/dsODN-RecQL1 and chitosan/dsODN-ApoB nanoparticles 87

Table 5-3: Safety and performance criteria for the development of effective nonviral gene delivery systems 98

Table 6-1 Characterization of chitosans tested in this study. Different chitosans are denoted according to their chemical composition using the nomenclature [DDA-Mn] and are represented in the first column of the table. The degree of deacetylation (DDA) was determined by ^{1}H NMR. The number and weight average molecular weight (Mn and Mw) were determined by gel permeation chromatography (GPC). The polydispersity index (PdI) was calculated as M_w/M_n. The degree of polymerization (Dp) or chain length was computed using the following equation $Dp = (Mn\ chitosan)/(Mw\ monomer\ at\ specific\ DDA)$ 115

Table 6-2 Effect of Mn and N:P ratio on in vitro dose-dependent knockdown. EC_{50} values were derived from a 4-parameter sigmoid curve fitted to data derived from 2 independent experiments with 2 technical replicates per experiment; Figure S. 6-5 in supplemental data for more information, p-value <0.05 145

Table 6-3 Effect of Mn and dose (concentration) on red blood cell agglutination. Agglutination was measured qualitatively and scored. (-) No aggregation, (+) Low agglutination, few aggregates (++) Medium agglutination, several large aggregates, (+++) Strong agglutination, clumps, (++++) Very strong agglutination, large clumps.....154

Table 7-1 Characterization of chitosans tested in this study. Different chitosans are denoted according to their chemical composition using the nomenclature [DDA-Mn] and are represented in the first column of the table. The degree of deacetylation (DDA) was determined by ^{1}H NMR. The number and weight average molecular weight (Mn and Mw) were determined by gel permeation chromatography (GPC). The polydispersity index (PdI) was calculated as M_w/M_n. The degree of polymerization (Dp) or chain length was computed using the following equation $\boldsymbol{Dp = Mn\ chitosan Average\ monomer\ molar\ mass\ at\ specific\ DDA}$.....181

Table 7-2 Clinical signs collected following a single ascending dose of LNPs, uncoated and HA coated chitosan-siRNA nanoparticles. General aspect score (GAS), or the general physical aspect of the animal (i.e. hunchback position, piloerection, vocalization …), the natural behaviour score (NBS), or the behavioral aspect of the animal relative to its habitat and littermates (i.e. litter aspect, activity, nesting …) and the provoked behaviour score (PKBS), or the animal response to stimuli (i.e. pen tap on the cage …) were collected by three independent scorers and reported in this table along with the frequency. 208

LIST OF SUPPLEMENTARY TABLES

Table S 6-2 Efficiency of the primer-probe pairs used in this study. Reference gene specific primer-probe pairs were tested for their amplification efficiency on complementary DNA (cDNA) prepared from total RNA extracted from non-treated $EGFP^+$ H1299 cells. In order to validate that chitosan treatment does not affect reaction efficiency, primer-probe pairs specific to β2M and RPL13A were also tested on cDNA prepared from total RNA extracted from cells treated (transfected) with 92-10-30. Formulations were designated [DDA(%)-Mn (kDa)-N:P ratio]. High N:P was chosen to ensure maximum potential contamination of total RNA with chitosan. Data show that almost all primer-probe pairs passed, except for ACTB, and that chitosan does not affect amplification efficiency 142

Table S 6-3 Descriptive statistics of the data collected for genotoxicity parameters 151

LIST OF FIGURES

Figure 2-1: Mechanism of RNA interference induced the siRNA (left side) and the miRNA (right side) pathways. Adapted from [8]. Copyright 2017, with Nature Publishing Group permission. 9

Figure 2-2: The different categories of off-target effects observed with small interfering RNAs. The cartoon depicts the on-target, or the intended effect (left), the off-target, or miRNA-like off-target silencing, occurring after siRNA recognition of imperfectly matched 3'UTRs sequences in the transcriptome (middle) and the immune stimulation off-target effect of siRNA and/or delivery material used i.e. lipid nanoparticle (right). Note: other off-target effects such as RISC saturation are not depicted in this cartoon. Image adapted from [5]. Copyright 2017, with Nature publishing group permission.....13

Figure 2-3: Different chemical modification used in siRNA design. RNA, ribonucleic acid; PS, phosphothioate, PS2, phosphodithioate; EA, 2 0 -aminoethyl; DNA, deoxyribonucleic acid; 20 -F, 20 -fluoro; 20 -OMe 20 -O-methyl; 2 0 -MOE, 20 -O-methoxyethyl; F-ANA, 20 -deoxy-20 -fluoro-β-d-arabinonucleic acid; HM, 40 -C-hydroxymethyl-DNA; LNA, locked nucleic acid; carboxylic LNA 2 0 ,40 -carbocyclic-LNA-locked nucleic acid; OXE, oxetane-LNA; UNA, unlocked nucleic acid; 40 -S, 40 -thioribonucleis acid; F-SRNA, 2 0 -deoxy-20 -fluoro-40 -thioribonucleic acid; ME-SRNA, 2 0 -O-Me-40 -thioribonucleic acid; 40 -S-F-ANA, 20 -fluoro-40 -thioarabinonucleic acid; ANA, altritol nucleic acid; HNA, hexitol nucleic acid; B, base. Adapted from [106]. Copyright 2017, with permission from Frontiers. 17

Figure 2-4: Different architectures of siRNA used in the literature. The canonical 21-nt siRNA is the most popular siRNA design and continue to be used in most of the studies. Dicer-substrate siRNAs such as 27-nt siRNA, shRNA, pre-miRNA mimics, or fork siRNA have been associated with enhanced potency. Asymmetrical siRNAs (aiRNA), asymmetric shorter-duplex siRNA (asiRNA), bulge-siRNAs and sisiRNA were shown to improve silencing specificity and when associated with lipophilic conjugates become self-delivering. Blunt-end siRNA are reported to be more nuclease resistant but can be recognized by PRK and RIG-1. Single-stranded siRNAs (ss-siRNAs) and 16 nt are functional but may require higher siRNA concentrations. Dumbbell-shaped circular siRNAs may have longer silencing duration.

Passenger strands are shown in black and guide strands in red. Adapted from [106]. Copyright 2017, with permission from Frontiers. 19

Figure 2-5 Molecular structure and local arrangement of nucleic acid in lipid nanoparticles. A) Schematic of the local arrangement of the nucleic acid between the lipid bilayers of multilamellar (MLV) lipid nanoparticles. B) Cryo-TEM images of fusion of DOTAP/Cholesterol (1:1) liposomes induced by the addition of oligonucleotides. Black arrows indicate membrane junctions and white arrows indicate a paired membrane. Scale bar: 50 nm. C) Schematic model of MLV liposome or lipoplex formation. Adapted from [136]. Copyright, 2017, Elsevier with permission. 22

Figure 2-6: Structure of the major siRNA delivery systems. A) First generation lipid nanoparticle (LNP) used in pre-clinical and clinical settings [12, 121]. This type of LNPs is composed of a mixture of helper lipids i.e. DSPC (yellow), cholesterol (orange), the ionizable lipid DLinDMA and PEG-C-DMA. b) Cyclodextrin-based polymer nanoparticle (CDP). CDPs are synthesized through polymerization of diaminated cyclodextrin (dark green) yielding an oligomer with diamine groups (blue). The polymer is end-capped with imidazole to improve endosomal escape. Adamantan (AD), a hydrophobic molecule is used to conjugate both PEG and targeting ligands. AD incorporate into the cyclic core of the cyclodextrin. c) First generation dynamic polyconjugate composed of PBAVE, GalNAc, PEG and the siRNA. d) Trivalent GalNAs siRNA conjugate. The metabolically stabilized siRNA is conjugated at the 3´ terminus of the passenger strand to three GalNAc molecules through a triantennary spacer molecule. GalNAc mediates hepatocyte entry through receptor-based recognition and subsequent endocytosis. Adapted from [59]. Copyright 2017, Nature Publishing Group with permission. 23

Figure 2-7: Chemical structure of chitosan (A and D units represent N-acetyl-D-glucosamine and D-glucosamine, respectively). Adapted from [28] Copyright 2017, with Elsevier's permission. 39

Figure 2-8: Spontaneous assembly of a chitosan-nucleic acid polyelectrolyte complex, or nanoparticle through electrostatic interactions. The nucleic acid depicted in this figure is a circular supercoiled plasmid DNA with a negatively charged phosphate backbone (blue) and the polymer is positively charged (red). The ball of wool or scrambled egg like structure has

pKa above the pKa of free polymer (pKa ~6.5). Adapted from [209]. Copyright 2017, with American Chemical Society permission. 40

Figure 2-9: Different type of endocytosis. Image adapted from [227]. Copyright 2017, Dove Press with permission. 46

Figure 2-10 Schematic illustration of the uptake pathway and mechanism of endosomal release of cationic lipid nanoparticles. The schematic considers a receptor-independent mechanism of uptake. The same principle is believed to occur for ionizable lipid nanoparticles following PEG hydrolysis and ionization in the acidic environment of the endosome lumen. Adapted [136], Copyright 2017, Elsevier with permission. 47

Figure 4-1. FACS analysis of chitosan/DPP-IVODN polyplexes uptake in HepG2 cell line. Uptake of 5'-6FAM labeled DPP-IVODN in chitosanase treated and untreated cells 24 hours post transfection. a) Transfection efficiency was calculated as the percentage of 5'FAM-D 61

Figure 4-2. Confocal imaging of polyplexes uptake. Confocal microscopy images of HepG2 live cells 24 h post transfection with chitosan/DPP-IV_{ODN} polyplexes (N/P=5). Chitosan 92-10 (DDA, MW) was labeled with Rhodamine (red), the DPP-IV_{ODN} with 6FAM at the 5'extremity (green) and the cell membranes were stained prior to imaging with cell mask (blue). Membrane staining was performed to differentiate between internalized and membrane bound polyplexes.....61

Figure 4-3: Effect of *Streptomyces griseus* chitosanase on yield and integrity of total RNA extraction. Total RNA extraction was performed on HepG2 cells transfected with 10 pmol and 50 pmol of nanoparticles siRNA/chitosan at 3 different N/P ratios indicated by the formulation code 92-10-5, 92-10-10 or 92-10-20 (DDA, MW, N/P). Chitosanase was resuspended in DMEM pH 6.5 and directly applied to cells at a final concentration of 6.12mU/µg of chitosan. Total RNA was extracted from chitosan transfected cell treated with or without chitosanase. The different extractions were compared to control Dharmafect™ 1 transfected cells and non-transfected (NT) cells. (nt) = nucleotide, L= standard ladder, the green band is a lower marker, which allows sample alignment and permits comparison for RIN calculation. RIN= RNA integrity number, is an algorithm based numbering system that calculate RNA integrity with 10 being the most intact and 1 being fully degraded. 62

Figure 4-4: Polyacrylamide gel electrophoresis of chitosan/DPP-IV_{ODN} polyplexes bearing different DDAs and N/P ratios, treated with or without Streptomyces griseus chitosanase. a) chitosan migration b) ODN migration. Lane 1 to 4 corresponds to chitosan/DPP-IV_{ODN} directly incubated with chitosanase during 60 minutes at 37ºC. Chitosan digestion allows the ODN release. Lane 5 to 8 corresponds to chitosan/DPP-IV_{ODN} incubated at the similar conditions without chitosanase. Faster chitosan migration was observed when comparing lanes 5 and 6 due to different MW of theses formulations. Increased band intensity (lane 4-8) results from greater amounts of chitosan at higher N/P ratios 63

Figure 4-5: Total RNA extraction from HepG2 transfected cells with 10 pmol siRNA. Following transfection, cells were treated with chitosanase for: a) 30 min, b) 60 and c) 60 min in lysis buffer. 64

Figure 5-1: Environmental scanning electron microscopy images of spherical chitosan/dsODN nanoparticles. (A) 92-10-5 chitosan/dsODN-RecQL1 nanoparticles; (B) 80-40-5 chitosan/dsODN-RecQL1 nanoparticles; (C) 80-10-10 chitosan/dsODN-RecQL1 nanoparticles; (D) 92-10-5 chitosan/dsODN-ApoB nanoparticles; (E) 80-80-5 chitosan/dsODN-ApoB nanoparticles, and (F) 80-10-10 chitosan/dsODN-ApoB nanoparticles.....86

Figure 5-2: Chitosan nanoparticle temporal stability. Stability was assessed at 0.5, 4, and 24 hours after complex formation using polyacrylamide gel electrophoresis at a pH of 6.5 (MES 1X) and pH8 (TAE 1X). Chitosan 92-10 at different N:P ratios (0.5, 2, and 10) was complexed with (A) dsODN-RecQL1 at pH of 6.5; (B) dsODN-RecQL1 at a pH of 8; (C) ds-ODN-ApoB at a pH of 6.5, and (D) ds-ODN-ApoB at a pH of 8. Unstable nanoparticles release dsODNs which become visible following EtBr staining on polyacrylamide gel following eethidium bromide staining of the polyacrylamid gel.....88

Figure 5-3: Nuclease protection assays of chitosan/dsODN nanocomplexes. (A) Chitosan (92-10-5, 80-40-5 or 80-10-10) complexed with dsODN-RecQL1. (B) dsODN-RecQL1 remaining after the DNAse I digestion was assessed using the signal intensity of the treated samples with the control (ie, 0 U DNAse I = 100% intensity). This comparison was made between the samples of the same chitosan formulation. (C) Chitosan (92-10-5, 80-80-5 or 80-10-10)

complexed with dsODN-ApoB. (D) dsODN-ApoB remaining after the DNAse I digestion was similarly assessed as in (B). 90

Figure 5-4. Polyacrylamide gel electrophoresis of chitosan/DPP-IV$_{ODN}$ polyplexes bearing different DDAs and N/P ratios, treated with or without Streptomyces griseus chitosanase. a) chitosan migration b) ODN migration. Lane 1 to 4 corresponds to chitosan/DPP-IV$_{ODN}$ directly incubated with chitosanase during 60 minutes at 37ºC. Chitosan digestion allows the ODN release. Lane 5 to 8 corresponds to chitosan/DPP-IV$_{ODN}$ incubated at the similar conditions without chitosanase. Faster chitosan migration was observed when comparing lanes 5 and 6 due to different MW of theses formulations. Increased band intensity (lane 4-8) results from greater amounts of chitosan at higher N/P ratios 91

Figure 5-5: Cellular uptake of dsODN-ApoB nanoparticles 24 hours post transfection in HEK293, Raw269.7, and HepG2 cell lines. Chitosan formulations 92-10-5, 80-80-5, and 80-10-10 were complexed to (6FAM) 5′ labeled dsODN-ApoB and transfected at 60 pmol/well 24 hours prior to fluorescence-activated cell sorting analysis. (A) Uptake efficiency of ApoB dsODN in percentage (%). (B) Uptake efficiency of ApoB dsODN in HepG2 cells at different passage number. DharmaFECT was used as the positive uptake control.....92

Figure 5-6: Confocal imaging of chitosan/dsODN nanocomplex uptake 24 hours post transfection. Chitosan 92-10 (DDA, M_n) was labeled with rhodamine (red) and dsODNs were 5′ labeled with (6FAM) (green). Chitosan 92-10 was complexed to dsODNs at an N:P ratio of 5. Cell membranes were stained prior to imaging with CellMask™ (blue) to differentiate between internalized and membrane-bound nanoparticles. Images shown represent each separate channel, with dsODNs in green, chitosan in red, membrane in blue, differential interference contrast image in grey, and the merged images shown on the bottom left quadrant. (A) LS174T cells transfected with chitosan/ dsODN-RecQL1 nanoparticles. (B) HepG2 cells transfected with chitosan/dsODN-ApoB nanoparticles. (C) HEK293 cells transfected with chitosan/dsODN-ApoB nanoparticles. (D) Raw 294.7 cells transfected with chitosan/dsODN-ApoB nanoparticles. 93

Figure 5-7: Real-time polymerase chain reaction analysis of the inhibition of RecQL1 and ApoB gene expression in specific cell lines. LS174T cells were transfected with chitosan (92-10-5, 80-40-5, and 80-10-10)/siRNA-RecQL1 nanoparticles, whereas HepG2 cells were transfected

with chitosan (92-10-5)/siRNA-ApoB nanoparticles. The inhibition percentage was obtained by comparing the transfected and nontransfected cells, using the ΔΔCT method. 95

Figure 5-8: Cell viability assessment using the alamarBlue® assay 24 hours post transfection with different chitosan/siRNA formulations. To alleviate the apoptotic effect of RecQL1 gene silencing for a proper assessment of chitosan-siRNA toxicity, mock siRNA was used for transfection in the LS174T cell line. The HepG2 cell line was transfected with ApoB siRNA. DharmaFECT was used for comparison purposes whereas dimethyl sulfoxide was used as a positive control of toxicity. 96

Figure 6-1 Nanoparticle size and ζ-potential as a function of DDA, Mn, and amine to phosphate ratio (N:P) measured in the presence of 10 and 150 mM NaCl. A) Nanoparticle size (Z-ave diameter) vs DDA, Mn and N:P ratio in the presence of low ionic strength (10 mM NaCl, pH 5.5, measurement at 2.5 min post incubation in medium). B) Nanoparticle surface charge (ζ-potential) vs DDA, Mn and N:P ratio in the presence of low ionic strength (10 mM NaCl, pH 5.5). C) Nanoparticle size vs DDA, Mn and N:P ratio in the presence of high ionic strength (150 mM NaCl, pH 5.5). D) Nanoparticle surface charge (ζ-potential) vs DDA, Mn and N:P ratio in the presence of high ionic strength (150 mM NaCl, pH 5.5). Data represent the average ± standard deviation of 3 independent experiments with 2 technical replicates per experiment (N=3, n=6). Measurements in 150 mM NaCl were taken immediately after adding 150 mM NaCl. Measurements in 10 mM NaCl were stable over time (see Supp Info Figure S. 6-1) 128

Figure 6-2 Effect of DDA, Mn and N:P ratio on the encapsulation efficiency at two different pH. Nanoparticles were formed in water and incubated either in 25 mM MES (pH 6.5) or 1X TAE (pH 8.0) for 24 hours then assayed for siRNA release using the Quant-iT™ RiboGreen® assay. The percentage of siRNA release provided the percent encapsulation efficiency (% EE) computed relative to naked siRNA (N:P 0). Red color corresponds to 100% encapsulation efficiency (no release) while magenta corresponds to 0% encapsulation efficiency (all released). Average values from 2 independent experiments with 3-4 technical replicates per experiment. At pH 6.5, complete encapsulation (0% release) of the payload is observed at all DDA, Mn and N:P ratio used to form nanoparticles. However, at pH 8.0, chitosan glucosamine units become deprotonated and their interaction with siRNA phosphate groups decreases

promoting payload release. At pH 8, an increase in DDA, Mn and N:P ratio is required to maintain nanoparticle integrity.....130

Figure 6-3 Effect of DDA, Mn, N:P ratio and pH on the biological performance of chitosan-siRNA nanoparticles. Nanoparticles were formed in water following 1:1 (v/v) mixing of chitosan to siRNA (0.1 mg/mL). $EGFP^+$ H1299 cells were transfected at a final siRNA concentration of 100 nM. Data represent average ± standard deviation of at least 3 independent experiments with at least 2-3 technical replicates in each experiment (N=3, n=6-9).....132

Figure 6-4 Cell uptake, knockdown, correlations to size and charge, cell toxicity. A) The effects of DDA, Mn and N:P ratio on uptake were measured in the $EGFP^+$ H1299 cell line 48 hours post transfection at 100 nM siRNA B) Lack of correlation between EGFP knockdown and nanoparticle size measured at low and high ionic strength. C) Strong correlation between EGFP knockdown and nanoparticle surface charge (ζ-potential) measured at low and high ionic strength. D) Effect of different formulations prepared at N:P 5 on metabolic toxicity. All experiments in these figures were performed at pH 7.2-7.4 in the absence of serum. Media over cells was aspirated and replenished with complete media 44 hours before analysis. All data shown represent average of at least 3 independent experiments with 2-3 technical replicates per experiment (N=3, n=6-9). Correlation graphs represent average values of size or ζ-potential correlated with average values of EGFP knockdown. 135

Figure 6-5 Effect of Mn at 92% DDA (92-Mn) and N:P ratio on uptake and knockdown. The $EGFP^+$ H1299 cell line was transfected in the presence of 10% serum at a final siRNA concentration of 100 nM. A) Uptake of DY^{647} labeled siRNA expressed as median fluorescence intensity (MFI). B) EGFP knockdown post transfection with anti EGFP nanoparticles. C) Lack of EGFP knockdown post transfection with non-targeting siNT nanoparticles; siNT represents a scrambled siRNA and is an indicator of specificity to the target siRNA sequence. D) Lack of EGFP knockdown following transfection with chitosan only. Data represent the average ± standard deviation of 3 independent experiments with 2 technical replicates per experiment (N=3, n=6).....137

Figure 6-6 Effect of FBS, chitosan Mn and N:P ratio at 92% deacetylation on EGFP knockdown in H1299 cells. A) EGFP knockdown measured as the average fluorescence intensity (FI) relative to untreated cells 48 h post transfection with siEGFP. $EGFP^+$ H1299 cells were

transfected in the absence or presence of 10% serum for a period of 5 hours, media aspirated and replenished with complete RPMI-1640 media (pH 7.2-7.4, 290 mOsm) and incubated for 44 hours before analysis. B) EGFP mRNA knockdown measured using qPCR, normalized using the geometric average of EIF, PUM-1, and GAPDH and calibrated to untreated cells. $EGFP^+$ H1299 cells were treated as described in A. C) Representative confocal laser scanning microscopy (CLSM) images. EGFP is indicated in green. In all experiments, siRNA was delivered at a final concentration of 100 nM and data in A and B expressed as the average value of 3 independent experiments with 2-3 technical replicates per experiment (N=3, n=6-9), *p-value < 0.01. 139

Figure 6-7 Effect of chitosan and DharmaFect® 2 treatment on reference gene stability. A panel of 10 reference genes was tested for expression stability under diverse experimental conditions. $EGFP^+$ H1299 cells were transfected with the following formulations i.e. 92-10-5, 92-10-30, 92-120-5, 92-120-30, 98-10-5, 98-10-30 and DharmaFect® 2 at a final siRNA concentration of 100 nM. Untreated cells were included in the analysis. A) panel shows the classification of the least to most stable (left to right) reference gene based on the average expression stability values, or geNorm M-Score, computed on the remaining control genes during stepwise exclusion of the least stable control gene, for samples from all treatments. B) panel shows the effect of the exclusion of DharmaFect® 2 from the statistical analysis. C) Panel shows the effect of the exclusion of both DharmaFect® 2 and untreated cells from the analysis. The M-Scores were computed using the geNorm statistical package on the average Cq of two independent experiments.....141

Figure 6-8 Effect of increasing concentration of serum on the biological performance of nanoparticles. A) Effect of increasing serum concentration on EGFP knockdown. B) Percent loss of EGFP knockdown in the presence of 94% serum compared to transfection without serum. C) Effect of physiological concentration of heparin sulfate (2.5 µg/mL) on payload release. Low (10 kDa) and high (120 kDa) 92% deacetylated chitosan was formulated with siRNA at different N:P ratio and incubated for 1 hour in the absence and presence of heparin sulfate (pH 7.4). Increased fluorescence indicates increased payload release D) Effect of physiological concentration of BSA (25 mg/mL) on payload release. Low (10 kDa) and high (120 kDa) 92% DDA chitosan was formulated with siRNA at different N:P ratio and incubated for 1 hour in the absence and presence of BSA (pH 7.4).....147

Figure 6-9 Effect of chitosan Mn and N:P ratio at 92% DDA on in vitro toxicity and genotoxicity. A) Metabolic activity relative to untreated EGFP^{+} H1299 cells measured by the alamarBlue® assay. Activity was measured 48 h posttransfection. Mock chitosan (M) was used at N:P 30 to assess the effect of siRNA encapsulation on metabolic activity. DharmaFect® 2 (DF), a commercial lipid-based system, was used as a comparator. Dimethyl sulfoxide (DS) was used as positive control of toxicity. B) Effect of increasing Mn and N:P ratio on genotoxicity as measured using the comet assay parameter "% DNA in tail (PDT)". The PDT represents the percentage of DNA migrated in the tail of the comet or the proportion of damage to total DNA. C) Effect of increasing Mn and N:P ratio on genotoxicity as measured using the parameter "Olive tail moment (OTM)". OTM represents a parameter that is insensitive to the measurement of tail length. D) Correlation between median PDT and N:P ratio for 10 vs 120 kDa chitosan. For the alamarBlue® assay, data represent average metabolic activity ± standard deviation of 3 independent experiments with 2-3 technical replicates per experiment (N=3, n=6-9). For the comet assay, box plots were constructed from data of 2 independent experiments with more than 100 comet/experiment/treatment. 149

Figure 6-10 Effect of Mn and dose on hemocompatibility via red blood cell (RBC) lysis. Low (10 kDa) versus high (120 kDa) molecular weight chitosans were formulated with HPLC-grade siRNA at an N:P ratio of 5. Increasing doses of siRNA were mixed with human pooled blood and % hemolysis determined as per ASTM-E2524 [43]. The concentration of chitosan (mg/mL) in the test vial (equivalent to the concentration in total circulating blood volume or tCBV), the equivalent chitosan dose in mg/kg of body weight and the corresponding siRNA dose in mg/kg for N:P of 5 are shown. The inset shows data from positive and negative controls. Poly-L-Lysine (PLL), Triton-X-100 (TX-100), Polyethylene glycol (PEG), buffer (excipients at 1% trehalose, 5.8 mM histidine, pH 6.5), Hyaluronic acid 866 kDa (HA) and siRNA. Data represent the average ± standard deviation of 2 independent experiments with 3-6 technical replicate per experiment (N=2, n= 6-12). 153

Figure 6-11Effect of Mn on the bio-distribution of chitosan-siRNA nanoparticles. Nanoparticles were injected in Balb/c nude mice at a dose of 0.5 mg/kg of DY^{647} labeled siRNA (equivalent dose of 1.4 mg/kg of chitosan) and organs imaged ex-vivo 4 hours post administration. ...156

Figure 6-12 Histological and CLSM images of nanoparticles accumulated in PTEC. Nanoparticles were injected in Balb/c nude mice at a dose of 0.5 mg/kg of DY^{647} labeled siRNA (equivalent dose of 1.4 mg/kg of chitosan), organs perfused and collected 4 hours post administration, fixed and cryosectioned (5 µm). For CLSM, sections were stained with phalloidin red and Hoechst. (PBS) Phosphate Buffered Saline, (siNaked) naked DY^{647} labeled siRNA, (InV LNP) Invivofectamine® 2.0-DY^{647} siRNA-lipid nanoparticles, (PTEC) Proximal epithelial tubular cells, (NPs) Nanoparticles. DY^{647} siRNA = Green, Nucleus = Blue and Brush borders= Red (actin staining). 157

Figure 6-13 Effect of DDA and Mn on in vivo knockdown in the kidney. A) Size of the injected nanoparticles. Nanoparticles were rehydrated in excipients to reach a target dose of 2.5 mg/kg, injected and the remaining volume, diluted 1:8 in excipients and assessed for size using dynamic light scattering. B) Polydispersity index (PdI) of injected nanoparticles. The PdI was automatically computed during DLS in A. C) Changes in body weight following multiple injections. Mice body weight was monitored for a period of 8 days and measured before injection and at euthanasia as an indirect assessment of general toxicity. Arrows and cross represent injection and euthanasia respectively. D) Functional target knockdown in the kidney. Nanoparticles were manually prepared, freeze-dried, rehydrated with excipients and injected in Balb/c mice at a dose of 2.5 mg/kg siRNA. Seventy-two hours after the last administration, kidneys were collected, excised, lysed and the GAPDH enzymatic activity assessed using the KDalert® assay and normalized to total protein content. Cleveland dot plot represents 3 animals per treatment group, with average and standard deviation represented in the form of bars. Statistical significance was computed with One-Way ANOVA followed by Tukey test for multiple comparisons: *$p< 0.01$, **$p <0.001$, ***$p < 0.00001$ 158

Figure 7-1 Hemocompatibility profiling of uncoated and HA coated chitosan-siRNA nanoparticles via red blood cell (RBC) lysis. Low (10 kDa) versus high (120 kDa) molecular weight chitosans were formulated with HPLC-grade siRNA at an N:P ratio of 5. HA coated formulations were formulated at an N:P:C of 2:1:1.5. Increasing doses of siRNA were mixed with human pooled blood and % hemolysis determined as per ASTM-E2524 [49]. The concentration of chitosan (mg/mL) in the test vial (equivalent to the concentration in total circulating blood volume or tCBV), the equivalent chitosan dose in mg/kg of body weight and the corresponding siRNA dose in mg/kg for N:P of 5 are shown. Inset shows data from

positive and negative controls. Poly-L-Lysine (PLL), Triton-X-100 (TX-100), Polyethylene glycol (PEG), Excipients (1% trehalose, 5.8 mM histidine, pH 6.5), Hyaluronic acid 866 kDa (HA), siRNA (8 mg/kg) and Invivofectamine® 2.0 (1 versus 8 mg/kg of siRNA). Data represent the average ± standard deviation of 2 independent experiments with 3-6 technical replicates per experiment (N=2, n= 6-12). 192

Figure 7-2 *In vivo* Biodistribution of uncoated and HA coated chitosan-siRNA nanoparticles. A) Effect of Mn and HA coating on the biodistribution of chitosan-siRNA nanoparticles. Uncoated nanoparticles were injected in Balb/c nude mice at a dose of 0.25 mg/kg of DY^{647} labelled siRNA (equivalent dose of 0.7 mg/kg of chitosan), HA coated nanoparticles were injected at a dose of 0.165 mg/kg of DY^{647} labelled siRNA (equivalent dose of 0.2 mg/kg of chitosan) and organs imaged ex-vivo 4 hours post administration. B) Histological and CLSM images of nanoparticles accumulated in PTEC. Nanoparticles were injected as described above, organs perfused and collected 4 hours post-administration, fixed and cryosectioned (5 µm). For CLSM insets, sections were stained with phalloidin red and DAPI. (PBS) Phosphate Buffered Saline, (siNaked) naked DY^{647} labeled siRNA, (Invivofectamine) lipid nanoparticles, (PTEC) Proximal epithelial tubular cells, (NPs) Nanoparticles. Lumen (L), DY^{647} siRNA = Green, Nucleus (N) = Blue and Brush borders= Red (actin staining). 195

Figure 7-3 Size, polydispersity index and surface charge (ζ-potential) of chitosan-based siRNA nanoparticles and lipid-based nanoparticles (LNPs). Invivofectamine® 2.0 (Inv LNP) were formulated with unmodified (siApoB Nat) or 2'O-methyl modified anti-ApoB siRNA (2'Ome siApoB) sequences (panels A, B and C). Invivofectamine® 3.0 and Altogen LNPs were formulated with LNA-modified anti-GAPDH siRNA (panels D, E and F). Low molecular weight chitosan, with a degree of deacetylation of 92% and molecular weight (Mn) of 10 kDa (92-10) was formulated with siApoB Nat or 2'Ome siApoB at an amine to phosphate ratio (N:P ratio) of 5 (panels A, B and C). Low Mn (10 kDa) and high Mn (120 kDa) chitosans were formulated with LNA-modified anti-GAPDH siRNA at an N:P ratio of 5 (panels D, E and F). Hyaluronic acid (HA, 866 kDa) coated chitosan nanoparticles (HA92-10) were prepared at an N:P ratio of 2 and coated with HA at a phosphate to carboxyl ratio (P:C) of 1.5 (panels A, B, C, D, E and F). Size, PdI and ζ-potential of lipid nanoparticles (LNPs) were measured in phosphate buffered saline (PBS, pH 7.4). Size, PdI and ζ-potential of uncoated and HA coated chitosan-siRNA nanoparticles were measured in excipients (1% trehalose

(w/w), 5.8 or 3.5 mM histidine, pH 6.5). A) Size (Z-ave diameter in nm), B) Polydispersity index (pdI), and C) Surface charge (ζ-potential) of nanoparticles injected for the assessment of toxicity. D) Size (Z-ave diameter in nm), E) Polydispersity index (pdI), and F) Surface charge (ζ-potential) of nanoparticles injected for the assessment of in vivo knockdown efficacy. Data represent the average ± standard deviation of 3 independent experiments with 2 technical replicates per experiment (N=3, n=6). 197

Figure 7-4 Cytokine induction 4 hours post injection of a single ascending dose of Invivofectamine® 2.0, uncoated and HA coated chitosan-siRNA nanoparticles in CD-1® (ICR) mice. PBS (Phosphate buffered saline), LPS (Lipopolysaccharide), Inv LNP (Invivofectamine® 2.0-siRNA Lipid Nanoparticles), siApoB Nat (unmodified anti-ApoB siRNA sequence), siApoB 2'Ome (2'O methyl-modified anti-ApoB siRNA sequence), and HA (Hyaluronic acid, 866 kDa). Mice were I.V. injected with test articles, serum collected and analyzed 4 hours post injection using the BioPlex™ 200 system. Each symbol represents an animal and data represent average values ± standard deviation of 5-7 animals. Statistical significance versus PBS-treated animals was computed with One-Way ANOVA followed by Dunnett test for multiple comparisons: *p< 0.01, **p <0.001, ***p < 0.00001. Note: In order to not bias the average, cytokine levels (animals) below the range of detection (< OOR) were excluded and not considered as 0 or LLOQ (pg/mL).....199

Figure 7-5 Hematological profiling of Invivofectamine® 2.0, uncoated and HA coated chitosan-siRNA nanoparticles following single ascending dose administration in CD-1® (ICR) mice. PBS (Phosphate buffered saline), LPS (Lipopolysaccharide), Inv LNP (Invivofectamine® 2.0-siRNA Lipid Nanoparticles), siApoB Nat (unmodified anti-ApoB siRNA sequence), siApoB 2'Ome (2'O methyl-modified anti-ApoB siRNA sequence), and HA (Hyaluronic acid, 866 kDa). Mice were intravenously injected with test articles, blood collected and analyzed 24 hours post injection at IDEXX Laboratories. Each symbol represents an animal and lines represent average values ± standard deviation of 5-7 animals except for InvLNP siApoB Nat (8 mg/kg) where 3 animals were assayed for hematology. The gray shaded area represents the normal values (95% confidence interval, N= 266 divided as 133 ♀ and 133 ♂) of 8-12 week old CD-1® (ICR) mice from Charles Rivers Laboratories (North American colonies) [59]. Statistical significance versus PBS-treated animals was computed with One-Way ANOVA followed by Dunnett test for multiple comparisons: *p< 0.01, **p <0.001, ***p < 0.00001.

Note: Normal range limits in this figure are not firm boundaries and should be used as guidelines since a large range of values was reported in the literature and could be accounted for by variation in age, sex, sampling technique and testing methodology (i.e. instrument, technique …). 202

Figure 7-6 Serological profiling of Invivofectamine® 2.0, uncoated and HA coated chitosan-siRNA nanoparticles following single ascending dose administration in CD-1® (ICR) mice. PBS (Phosphate buffered saline), LPS (Lipopolysaccharide), Inv LNP (Invivofectamine® 2.0-siRNA Lipid Nanoparticles), siApoB Nat (unmodified anti-ApoB siRNA sequence), siApoB 2'Ome (2'O methyl-modified anti-ApoB siRNA sequence), and HA (Hyaluronic acid, 866 kDa), BUN (Blood Urea Nitrogen), ALT (alanine transaminase), AST (aspartate transaminase), ALP (Alkaline phosphatase), γGTT (gamma glutamyl transferase). Mice were intravenously injected with test articles, blood collected and analyzed 24 hours post injection at IDEXX Laboratories. Each symbol represents an animal and data represent average values ± standard deviation of 5-7 animals except for InvLNP siApoB Nat (8 mg/kg) where 3 animals were assayed for hematology. The gray shaded area represents the normal values (95% confidence interval, N= 266 divided as 133 ♀ and 133 ♂) of 8-12 week old CD-1® (ICR) mice from Charles Rivers Laboratories (North American colonies) [59]. Statistical significance versus PBS-treated animals was computed with One-Way ANOVA followed by Dunnett test for multiple comparisons: *p< 0.01, **p <0.001, ***p < 0.00001. Note: Normal range limits in this figure are not firm boundaries and should be used as guidelines since a large range of values was reported in the literature and could be accounted for by variation in age, sex, sampling technique and testing methodology (i.e. instrument, technique …). 204

Figure 7-7 Changes in body weight following intravenous nanoparticle administration. A) Percent change in body weight following a single intravenous injection in CD-1® (ICR) mice. Invivofectamine® 2.0 lipid nanoparticles (Inv LNP) were formulated with unmodified (siApoB Nat) and 2'O-methyl modified ApoB siRNA (siApoB 2'Ome) and injected at 1 and 8 mg/kg. Uncoated chitosan was formulated with siApoB Nat and siApoB 2'Ome at an N:P ratio of 5 and injected at 1 and 2.5 mg/kg. Hyaluronic acid (HA, 866 kDa) coated nanoparticles were prepared at an N:P:C of 2:1:1.5 and injected at 1 and 8 mg/kg. The injected doses were chosen from the hemocompatibility data (Figure 7-1) where the maximum dose results in hemolysis below the ASTM threshold. B) Percent change in body weight following three I.V.

injections in Balb/c mice. Invivofectamine® 3.0 (Inv LNP) and Altogen (Altogen LNP) lipid nanoparticles were formulated with LNA-modified GAPDH siRNA (siGAPDH) and injected at 2.5 mg/kg. Low Mn (10 kDa) and high Mn (120 kDa) chitosan nanoparticles were formulated with siGAPDH at an N:P ratio of 5 and I.V. injected at 1 mg/kg. Hyaluronic acid (HA, 866 kDa) coated nanoparticles were prepared at an N:P:C of 2:1:1.5 and injected at 8 mg/kg. The injected doses were chosen from the hemocompatibility data (Figure 7-1) where the maximum dose results in hemolysis below the ASTM threshold and following personal communication with the manufacturers of Invivofectamine® 3.0 and Altogen. For panel A and B, body weight (g) was collected before each injection and at euthanasia. Red arrows and crosses illustrate injection and euthanasia respectively. Data represent the average ± standard deviation of 5-7 mice/group. Phosphate buffered saline (PBS) and lipopolysaccharide (LPS) were used as controls.....207

Figure 7-8 Histopathological comparison of liver and kidney tissue sections following intravenous administration of high doses of uncoated and HA coated nanoparticles. Uncoated and HA coated nanoparticles were formulated with both unmodified (siApoB Nat) and 2'O-methyl modified ApoB siRNA sequences (2'Ome siApoB) at an N:P:C of 5:1:0 for uncoated and 2:1:1.5 for HA-coated formulations, freeze-dried, rehydrated using excipients and I.V. injected at a dose of 2.5 (uncoated) and 8 (HA coated) mg/kg siRNA. Animals were euthanatized 24 hours post-administration, organ collected, fixed and processed for histopathological analysis. Phosphate buffered saline (PBS) and lipopolysaccharide (LPS) were used as controls. Organs from at least two animals per treatment group were processed and analyzed. Heart, Lungs and Spleen tissues from low (1 mg/kg) and high doses (2.5 and 8 mg/kg) are depicted in Supplemental Figure S. 7-4. Tissues show the absence of morphological changes, alterations, clots, apoptotic/necrotic cells or infiltration of immune cells.....210

Figure 7-9 Efficacy of in vivo target knockdown. A) GAPDH activity (U) normalized per tissue mass (mg). Kidneys were collected, snap frozen in liquid nitrogen, and cortex excised, homogenized, protein extracted and assayed using the GAPDH KDalert™ enzymatic kit. (ns) non-significant and numbers express % knockdown relative to PBS. B) Western blot detection of GAPDH in kidney lysate. GAPDH signal was normalized to the vinculin loading control. The inset shows an actual example of a western blot membrane used for quantification. The

membrane shows three different animals injected with PBS (control) and with 92-10-5 (1 mg/kg siGAPDH). Numbers in the histogram columns represent % knockdown relative to PBS. C) Qualitative assessment of GAPDH knockdown in the kidney by immunohistochemistry. Panels a, b, c, and d show a kidney section collected from a PBS-treated animal, stained with anti-GAPDH antibody (a and b) and isotype control (c and d). Panels e, f, g, and h show a kidney section collected from a chitosan (92-10-5) treated animal, stained with anti-GAPDH antibody (e and f) and isotype control (g and h). Data represent average values ± standard deviation of 5 animals except for 92-120-5 siGAPDH (1 mg/kg) where 4 animals were assayed. Statistical significance versus PBS-treated animals was computed with One-Way ANOVA followed by Dunnett test for multiple comparisons: *p< 0.01, **p <0.001, ***p < 0.00001. 216

LIST OF SUPPLEMENTARY FIGURES

Figure S. 6-1 Nanoparticle colloidal stability versus time. The effect of polymer length on nanoparticle size was investigated in medium containing 10 and 150mM salt (NaCl) over a period of 1h. Nanoparticles were prepared in water by manual mixing of chitosan and siRNA (0.1mg/mL) at 1:1 v/v to reach an N:P ratio of 5, diluted 1:8 in media and size measured over time. Measurements were conducted at 0, 7.5, 15, 30 and 60 minutes post dilution. Data represent the average of 2 independent experiments. Each DLS measurement consisted of 15 repeats.....129

Figure S. 6-2 Effect of EGFP$^+$ H1299 cell number on the reduction of alamarBlue®. Increasing cell numbers were seeded in 96 well plate, one day prior to the addition of alamarBlue®. Absorbance at 570 and 600nm was read 4 hours post-incubation and % reduction calculated using the following equation: $\%\,reduction = eOX\lambda 2A\lambda 1 - eOX\lambda 1A\lambda 2eRED\lambda 1A'\lambda 2 - eRED\lambda 2A'\lambda 1$ where the ε_{ox} is the molar extinction coefficient (ε) of alamarBlue® oxidized form, ε_{RED} is the molar extinction coefficient of the reduced form, A absorbance of test well, A' absorbance of negative well (media+ alamarBlue® only), λ_1 is 570nm and λ_2 is 600nm. The optimal number of cells to be seeded 24 hours post transfection and tested for toxicity 48 hours post transfection with nanoparticles was determined to be 5,000 cells/well.....134

Figure S. 6-3 siRNA encapsulation efficiency of low and high Mn chitosan. Nanoparticles were formed in water by manual mixing of siRNA (0.1mg/mL) with chitosan at different N:P ratio, incubated in low ionic strength pH controlled buffers (MES pH 6.5, TE pH 7.4 and TAE pH 8.0) for 24 hours and siRNA release quantified using the Quant-iT™ RiboGreen® Assay. The percent siRNA release was quantified relative to naked siRNA or N:P 0. At pH 6.5, complete siRNA encapsulation was observed regardless of the Mn and N:P ratio used. At pH 7.4 and 8.0, siRNA release shows a Mn and N:P dependence with higher Mn and N:P ratio required for efficient encapsulation. However, at physiological pH and at N:P ratio of 5, the 5 and 10kDa chitosans were able to encapsulate siRNA 60 and 80% respectively.....138

Figure S. 6-4 Pairwise comparison on normalization factors to determine the minimum number of reference genes needed for accurate normalization using the Vandsompele model. A) All treatments, B) Excluding DharmaFect® 2, C) Excluding DharmaFect® 2 and untreated cells.

A minimum of 3 reference genes needs to be used for accurate normalization when comparing all treatments. 144

Figure S. 6-5 Effects of charge density, chain length and N:P ratio on dose-dependent EGFP knockdown. Nanoparticles were formulated with either siEGFP (anti-EGFP) or siNT (non-targeting) and $EGFP^+$ H1299 cells transfected in the presence of 10% FBS at increasing siRNA concentrations. DharmaFect® 2 was used a positive control to benchmark efficacy. EGFP knockdown was analyzed 48 hours post transfection using flow cytometry. Data represent average values ± standard deviation of 2 independent experiments with 2 technical replicates per experiment. 146

Figure S. 6-6 Representative images of comets 48 hours post transfection with nanoparticles. The montage was prepared with ImageJ. Hydrogen peroxide (H_2O_2) at 100 and 200 µM was used as positive control for genotoxicity. DharmaFect® 2 siRNA nanoparticles were used as a comparator. Formulations at low and high Mn (92-10 and 92-120) were prepared at different N:P ratio (5, 30, 60 and 120) and transfected at final siRNA concentration of 100 nM (~0.00132 mg/mL). Equivalent concentration of chitosan at specific N:P ratio was 0.004, 0.018, 0.037 and 0.074 mg/mL for the N:P 5, 30, 60 and 120 respectively. Naked chitosan, or mock (M), was used as a control to account for the effect of the siRNA sequence. Typical comets are observed post treatment with the positive control. A dose-dependent increase in comet tail length can be seen when comparing 100 vs 200 µM H_2O_2. 150

Figure S. 6-7 Effect of siRNA and salt concentration on nanoparticle size. In a previous experiment (Figure 6-1, A), the effect of DDA and N:P ratio on nanoparticle size was found to be negligible relative to Mn, when particles were mixed with siRNA (0.1mg/mL) and suspended in 10mM NaCl (pH 5.5). As a consequence, one chitosan and one N:P ratio i.e. DDA 92%; N:P 5 were selected to further study the effect of siRNA (mg/mL) and NaCl (mM) concentration on nanoparticle size. The latter was measured in 10mM NaCl using 10 versus 120kDa following manual mixing with specific siRNA concentration (mg/mL). For size measurements using dynamic light scattering, particles were formed as described in the materials and methods of this manuscript and diluted (1:8) either in 10 or 150mM NaCl and size measured after 2.5 min post-incubation. A) 92-10-5 B) 92-120-5. Data represent the

average ± standard deviation of two independent experiment with a technical triplicate in each experiment (N=2, n=6). 159

Figure S. 7-1Hemocompatibility profiling of uncoated and HA coated chitosan-siRNA nanoparticles via erythrocyte aggregation. Low (10 kDa) versus high (120 kDa) molecular weight chitosans were formulated with HPLC-grade siRNA at an N:P ratio of 5. HA coated formulations were formulated at an N:P:C of 2:1:1.5. Increasing doses of siRNA were mixed with human pooled blood, incubated and imaged for qualitative assessment of hemagglutination. In the absence of hemagglutination, erythrocytes (RBC) deposit in the bottom of the U-shaped well and form a ring (see Non-treated, PEG, siRNA in **B**). In contrast, when hemagglutination occurs, aggregates become visible, stay suspended in solution and depending on the extent of agglutination may prevent the formation of the ring. **A)** Treatment samples at different doses of siRNA. **B)** Controls. 193

Figure S. 7-2 Cytokine levels pre-injection of Invivofectamine® 2.0, uncoated and HA coated chitosan-siRNA nanoparticles into CD1 mice. PBS (Phosphate buffered saline), LPS (Lipopolysaccharide), Inv LNP (Invivofectamine® 2.0-siRNA Lipid Nanoparticles), siApoB Nat (unmodified anti-ApoB siRNA sequence), siApoB 2'Ome (2'O methyl-modified anti-ApoB siRNA sequence), and HA (Hyaluronic acid, 866kDa). Mice were intravenously injected with test articles, serum collected and analyzed 4 hours post injection using the BioPlex 200 system. Each symbol represents an animal. Note: In order to not artificially manipulate the average, cytokine levels (animals) that were below the range of detection (< OOR) were excluded and not considered as 0 or LLOQ (pg/mL). 200

Figure S. 7-3 Histopathological comparison of liver and kidney tissue sections following intravenous administration of low doses of uncoated and HA coated nanoparticles. Uncoated and HA coated nanoparticles were formulated with unmodified (siApoB Nat) at an N:P:C ratio of 5:1:0 for uncoated and 2:1:1.5 for HA-coated formulations, freeze-dried, rehydrated using excipients and intravenously injected at a dose of 1 mg/kg siRNA. Animals were euthanatized 24 hours post-administration, organ collected, fixed and processed for histopathological analysis. Tissues show the absence of morphological changes, alterations, clots, apoptotic/necrotic cells or infiltration of immune cells. 211

Figure S. 7-4 Histopathological comparison of spleen, heart and lung tissue sections following intravenous administration of high doses of uncoated and HA coated nanoparticles. Uncoated and HA coated nanoparticles were formulated with either unmodified (siApoB Nat) or 2'O-methyl modified ApoB siRNA (2'Ome ApoB) at an N:P:C ratio of 5:1:0 for uncoated and 2:1:1.5 for HA-coated formulations, freeze-dried, rehydrated using excipients and intravenously injected at a dose of 2.5 (uncoated) and 8 (HA coated) mg/kg siRNA. Animals were euthanatized 24 hours post-administration, organ collected, fixed and processed for histopathological analysis. Phosphate buffered saline (PBS) and lipopolysaccharide (LPS) were used as controls. Organs from at least two animals per treatment group were processed and analyzed. Tissues show absence of morphological changes, alterations, clots, apoptotic/necrotic cells or infiltration of immune cells. 213

LIST OF BOXES

Box. 2-1 The hepatic ASGP receptor.....38

Box. 2-2 Endocytosis definition, pathways, and dynamics.....46

LIST OF SYMBOLS AND ABBREVIATIONS

µ	Micro
^{1}H-NMR	Nuclear magnetic resonance
2'Ome	2'O methyl modified base
ACTB	Actin B
ALP	Alkaline phosphatase
ALT	Alanine transaminase
ANOVA	Analysis of Variance
ApoB	Apolipoprotein B
AS	Anti-sense strand
AST	Aspartate Transaminase
ASTM	American Section of the International Association for Testing Materials
Balb/C	Bagg albino mice is a general purpose inbred mice
bPEI	Branched Polyethylenimine
BSA	Bovine serum albumin
BUN	Blood Urea Nitrogen
CD-1 (ICR)	Cluster of differentiation 1 (CD-1) mice, is a general purpose Swiss albino outbred mice
CLSM	Confocal Laser Scanning Microscopy

Cr	Creatinine
CS	Chitosan
Da	Dalton, molar mass unit
DDA	Degree of deacetylation
DLS	Dynamic light Scattering
DMEM-HG	Dulbecco's Minimal Essential Media with high glucose content (4.5g/L)
DOE	Design of experiments; statistical method to design conclusive experiment with minimal trials and/or samples
DPC	Dynamic Polyconjugate
dTBH	Diluted total blood hemoglobin
DY647	Fluorescent dye from Dharmacon
EGFP	Enhanced Green Fluorescent Protein
EPR	Enhanced retention and permeation effect
ESEM	Environmental Scanning Electron Microscopy
EU	Endotoxin Unit
FAM	Fluorescein isothiocyanate
FBS	Fetal bovine serum
FDA	Food and Drug administration
GalNAc	N-acetylagalactosamine

GAPDH	Glyceraldehyde 3-phosphate
GPC	Gel permeation chromatography
H1299	Human adenocarcinoma lung cell line
HA	Hyaluronic acid
Hb	Hemoglobin
HPLC	High Performance Liquid Chromatography
HRP	Horseradish peroxidase
ICH	International Conference on Harmonization
IgG	Immunoglobulin G
IL-1β	Interleukin- 1 beta
IL-6	Interleukin- 6
IFN-γ	Interferon Gamma
Inv	Invivofectamine; A commercially available cationic lipid formulation
KC	Chemokine homologue to IL-8
KD	Knockdown
kDa	Kilo Dalton, 1000 dalton
LNA	Locked nucleic acid

LNP	Lipid nanoparticles; In this thesis LNP is used as an umbrella term referring to cationic, ionisable, neutral or any lipid based system able to encapsulate and deliver nucleic acid into cells
lPEI	Linear Polyethylenimine
LPS	Lipopolysaccharide; lipid molecules composing the outer membrane of gram negative bacterial. LPS are potent inducers of cytokines and activate TLR-4
MIQE	Minimum Information for Publication of Quantitative Real-Time PCR Experiments
miRNA	microRNA
Mn	Average number molecular weight
mRNA	Messenger RNA
mV	Milli-volt
Mw	Molecular weight
N:P ratio	Nitrogen to phosphate molar ratio
N:P:C ratio	Nitrogen to phosphate to carboxyl molar ratio
NBF	Neutral Buffered Saline
nm	Nanometer
NT	Non-treated
NHP	Non-Human Primate
ODN	Oligonucleotides

PBS	Phosphate buffered Saline
pDNA	Plasmid DNA
PEG	Polyethylene glycol
PEI	Polyethylenimine
PFH	Plasma free hemoglobin, proportion of hemoglobin free in the plasma without RBC lysis
PS	Phosphotioate
qPCR	Quantitative real time PCR
R^2	Pearson correlation coefficient
RISC	RNA inducing Silencing Complex
RNA	Ribonucleic acid
RNAi	RNA interference
RPMI-1640	Roswell Park Memorial Institute medium number 1640
SDS	Sodium Dodecyl Sulfate
PAGE	Polyacrylamid Gel electrophoresis
siRNA	Small interfering RNA
TBH	Total blood hemoglobin
TLR	Toll-Like Receptors
TNF-α	Tumor necrosis factor alpha
ζ-potential	Zeta potential ; Nanoparticule surface charge

Chapter 1 INTRODUCTION

1.1 Introduction

The traditional drug-based toolbox employs small molecules, and biologics, as target agonists or antagonists to promote the intended therapeutic effects. This approach has been historically effective in controlling, and sometimes alleviating, symptoms without completely remediating the fundamental causes of the disease. Advancement in the understanding of molecular mechanisms underlying pathologies, protein-protein interactions and the mechanism of action of small molecules enabled the discovery of new targets, and improvement of treatment modalities without curing the disease. Gene therapy is an experimental technique that uses genes to treat or prevent diseases. In contrast to the traditional drug-based toolbox, i.e. small molecules and biologics, gene therapy offers the potential and promise to correct the underlying cause of the disease. Traditionally, the concept relied on the idea of replacing a defective gene with the correct sequence for proper expression. However, the discovery of RNA interference (RNAi), a process by which short single or double stranded oligonucleotides induce gene knockdown, has revolutionized the concept.

In the RNAi process, short double-stranded RNAs (siRNA) are recognized by a protein complex and guide, through base complementarity, the cleavage of target genes [1]. This powerful and specific technique was later found to be difficult to implement as a therapeutic modality due to nuclease sensitivity and rapid elimination through the kidneys [2-4]. In addition, off-target effects have been associated with the introduction of siRNAs in the body. These off-target effects were divided into two categories *viz.* sequence-dependent and sequence-independent effects [5]. Sequence-dependent mechanisms are related to either the partial complementarity of the siRNA sequence to other transcripts in the cell cytoplasm or through recognition of the siRNA sequence by endogenous pattern recognition receptors (PRR) and subsequent immune stimulation [5, 6]. Sequence-independent effects occur when exogenous siRNA sequences compete with endogenous regulators of gene expression for the RNAi machinery resulting in dysregulated gene expression patterns (i.e. inhibition and/or expression of genes and pathways). Altogether, these barriers limit the translation of siRNA into a clinical reality. Early human trials failed to produce the intended effect and were associated with toxicities [4, 7, 8].

Strategies to improve nuclease resistance and reduce off-target effects were developed and include chemical modifications and the use of delivery systems. The latter provide means to protect the payload by physically encapsulating and isolating it from nucleases. In addition, delivery systems augment cell entry and facilitate payload release into the cell cytoplasm [9, 10]. Endosomal release can be achieved by different means and depends on the material used for delivery. The most advanced systems in clinical trials are composed of lipid- and polymer-based nanoparticles or molecular conjugates [11-13]. Lipid nanoparticles (LNPs) demonstrate high efficiency *in vivo* but are associated with severe toxicity [14-17] and limit payload delivery to the liver prompting the development of safer delivery systems with hepatic and extrahepatic capabilities [4, 18].

Chitosan is a natural cationic polymer characterized by its tunable properties, biodegradability, ease of production, low cost and is generally recognized as safe [19]. In acidic conditions, chitosan spontaneously forms nanoparticles in the presence of nucleic acid, and molecular properties (i.e. degree of deacetylation and molecular weight) can be adjusted to favor nanoparticle stability and efficient transfection [19-21]. Most reports evaluating physicochemical parameters for efficient *in vitro* siRNA delivery were performed using partly deacetylated (DDA ~ 80-85%) chitosan-formulated at very high amine to phosphate ratio (N:P ratio >25) [20, 22-27]. Such formulations could pose significant practical problems for *in vivo* delivery such as premature dissociation, limited dosing, blood incompatibility and non-specific effects due to large quantities of free excess chitosan. Although potent *in vitro* gene knockdown (KD) has been achieved, experimental discrepancies, differences in chitosan sources, and lack of characterization rendered results inconclusive in identifying optimal parameters for siRNA delivery [28]. Reports correlating *in vitro* transfection efficiency (TE) as a function of chitosan degree of deacetylation (DDA), molecular weight (Mn) and N:P ratio have been contradictory [20, 21, 23, 25, 29]. In addition, due to its cationic nature, chitosan can interact with blood components, activate platelets, induce erythrocyte lysis [30] and, depending on its DDA, cause cytokine expression through macrophage/monocyte stimulation following *in vitro* stimulation or local administration [31, 32]. These aspects of toxicity, at least in the nanoparticle field, have been neglected [20-25, 27, 29, 33-40] with *in vivo* reports often using extremely high N:P ratios, based on *in vitro* findings, without reporting any signs of toxicity and/or parameters such as clinical signs, hematological and/or serological biomarkers [22, 24, 41-44]. In addition, and in contrast to LNPs, *in vivo* induction of cytokines was never characterized. Therefore, a systemic study with accurately characterized chitosans that investigates

the effect of intrinsic (DDA, Mn and N:P ratio) and extrinsic parameters (serum, pH, ionic strength and mixing conditions) on cell uptake, *in vitro* transfection efficiency, toxicity, genotoxicity, hemocompatibility and *in vivo* biodistribution, acute toxicity and demonstrates knockdown following I.V. administration of nanoparticles is needed to ensure successful translation of this promising polymer into an effective delivery system with potential applications in the clinic.

The research presented in this thesis attempts to address the aforementioned issues and elucidate the effect of chitosan molecular parameters on nanoparticle physicochemical characteristics and bioactivity. In addition, the research aims to characterize the toxicity and biodistribution profiles of chitosan nanoparticles following intravenous administration and compare it to commercially available lipid nanoparticles.

1.2 Problematic

Several papers have been published demonstrating the efficacy of chitosan and chitosan-based nanoparticles to induce *in vitro* and *in vivo* target specific knockdown. Attempts to identify molecular properties favoring efficient knockdown failed to generate conclusive results as to the role of chitosan degree of deacetylation (charge), molecular weight (chain length), and amine to phosphate ratio (mixing ratio) on nanoparticle physicochemical characteristics and bioactivity. In addition, the role of extrinsic factors such as pH, serum proteins, and ionic strength was not elucidated for chitosan-based nanoparticles encapsulating siRNA and was simply assumed based on previous experiences with plasmid. Earlier studies have reported application of nanoparticles formed at high molecular weight and mixing ratio (N:P ratio > 25), therefore limiting dosing and potentially causing dramatic *in vivo* side effects. Buschmann *et al* as well as several other groups clearly stated, while reviewing past data, that lack of uniformity in transfection protocols, and differences in chitosan sources, cell lines, methods and poor characterization render general conclusions difficult.

Moreover, none of the published work characterized the acute or chronic *in vivo* toxicity following single or repeated administration. Therefore, data on immune stimulation, hematological and serological (systemic) toxicities is much needed to understand the limitations of the system and mechanisms thereof. Therefore, three objectives were elaborated to decorticate the aforementioned problematic, and are stated in section 1.3 of this chapter.

1.3 Research Hypotheses and Objectives

1.3.1 General objective

The research presented here was carried out with an objective to explore and identify molecular properties, or parameters (factors), favoring efficient and non-toxic delivery of small interfering RNA, both *in vitro* and *in vivo*. Furthermore, acute toxicity, biodistribution and potency of selected formulations were investigated in animal studies designed as per regulatory guidelines and compared to lipid nanoparticles.

1.3.2 Study 1

The purpose of this study was to test selected formulations proven to be optimal for *in vitro* plasmid DNA delivery and demonstrate the efficiency of said formulations to transfect multiple cells lines and induce potent gene knockdown at low N:P ratio.

1.3.2.1 Hypothesis 1

We hypothesized that, contrary to previous literature [20, 22, 23, 25, 26], low molecular weight chitosans complexed at low N:P ratios represent suitable formulations for siRNA delivery and gene knockdown; *similar to observations with plasmid DNA*. Specific hypotheses tested through this study included the following:

- low molecular weight chitosans formulated at low N:P ratio are able to transfect multiple cell lines and induce potent gene knockdown;
- formulations at low N:P ratios assure sufficient protection and efficient delivery of the siRNA cargo;
- the requirement for high N:P ratio observed in the previous literature is due to erroneous assessment of nanoparticle stability at high pH and subsequent selection of stable nanoparticles for *in vitro* assessment.

1.3.2.2 Objective 1

Select formulations based on design parameters in Lavertu *et al*, prepare nanoparticles at a low N:P ratio and characterize their physicochemical properties (i.e. size, surface charge, stability at different pH), and ability to transfect multiple cell lines.

1.3.3 Study 2

The purposes of this study were to **1)** understand the correlation between nanoparticle physicochemical properties and knockdown efficiency, **2)** identify molecular parameters favoring efficient delivery and potent target gene knockdown and **3)** characterize the effects of these parameters on cell viability and genotoxicity.

1.3.3.1 Hypothesis 2

We hypothesized that molecular parameters favoring efficient siRNA delivery are different than those found for plasmid DNA. Specific hypotheses tested through this study included the following:

- nanoparticle surface charge is the most important parameter dictating transfection efficiency;
- in contrast to plasmid DNA delivery, transfection and knockdown efficiencies are not influenced by media pH, and nanoparticles integrity is conserved at high pH with an increase in the degree of deacetylation, molecular weight and N:P ratio;
- in contrast to plasmid DNA delivery, nanoparticles prepared at high degrees of deacetylation and molecular weights are able to transfect cells and induce potent gene knockdown;
- serum has a negative impact on low molecular weight formulations through nanoparticle destabilization;
- increasing both molecular weight and N:P ratio does not influence toxicity and genotoxicity;
- nanoparticle hemocompatibility shows a dose, degree of deacetylation and molecular weight dependence;
- nanoparticle hemocompatibility can be abrogated with hyaluronic acid coating permitting improved *in vivo* dosing.

1.3.3.2 Objective 2

Produce and screen a library of fully characterized chitosans to investigate the influence of physicochemical parameters (i.e. degree of deacetylation, molecular weight and N:P ratio) on

nanoparticle size, surface charge (ζ-potential), integrity (± serum and at different pH), metabolic toxicity, genotoxicity, hemocompatibility, cell uptake and target knockdown efficiency.

1.3.4 Study 3

The aims of this study were to **1)** investigate *in vivo* biodistribution, **2)** investigate immunological (i.e. cytokine production), hematological, serological and histopathological toxicity of single ascending dose, and **3)** investigate the efficacy of chitosan-siRNA nanoparticles following intravenous administration in mice.

1.3.4.1 Hypothesis 3

We hypothesized that administration of sub-hemolytic doses of chitosan is non-toxic compared to lipid nanoparticles and induces potent gene knockdown at the site of accumulation. Specific hypotheses tested through this study included the following:

- both uncoated and hyaluronic acid coated nanoparticles do not induce cytokine expression following intravenous administration;
- both uncoated and hyaluronic acid coated nanoparticles do not induce hematological and serological toxicities such as thrombocytopenia, and increased kidney and liver biomarkers;
- both uncoated and hyaluronic acid coated nanoparticles do not induce histopathological changes in main tissues and losses in body weights;
- similar to polyethyleneimine (PEI), uncoated chitosan nanoparticles are eliminated by the reticuloendothelial system and accumulate in lungs, liver, spleen and kidney where they induce potent gene knockdown;
- hyaluronic acid coated nanoparticles have a different biodistribution pattern compared to uncoated formulations;
- hyaluronic acid nanoparticles demonstrate higher knockdown efficiency in accumulated sites due to improved hemocompatibility and increased doses.

1.3.4.2 Objective 3

Inject nanoparticles to mice and investigate biodistribution using whole animal *in vivo* imaging to define the site of accumulation, and confirm findings using *ex-vivo* imaging followed by confocal microscopy. Formulate nanoparticles with a native (inflammatory) and chemically modified (non-inflammatory) siRNA sequences, and inject (at increasing doses) into mice via the tail vein. Assess pro-inflammatory cytokine induction 4 hours post-administration using a multiplex system, collect blood and main organs 24 hours post-administration of nanoparticles and assess hematological, serological and histopathological toxicity. Formulate nanoparticles with a chemically modified siRNA targeting the glyceraldehyde-3 phosphate gene (GAPDH) as a model to demonstrate functional gene knockdown in target tissues.

1.4 Brief structure of the thesis

The thesis is composed of nine chapters, starting with a general introduction of the subject, and a brief description of the problematic, objectives and thesis structure. **Chapter 2** presents a concise literature review of the following subject matters **1)** RNAi mechanism of action, **2)** the pharmacokinetic and pharmacodynamics considerations for the proper translation of small interfering RNA (siRNA) based RNAi, **3)** the main delivery systems including chitosan and **4)** a brief description of the mechanism of cell entry and endosomal escape in order to familiarize the reader with the subject of this thesis. **Chapter 3** introduces the core of the thesis, and describes subsequent chapters. **Chapters 4**, **5**, **6** and **7**, present the main findings as published and submitted manuscripts. These manuscripts are incorporated in the thesis with modifications only in the formatting and represent an exact copy of the published or submitted material. The thesis concludes with the last two chapters composed of a short discussion in **Chapter 8**, and conclusions/future perspectives in **Chapter 9**. The bibliography of **Chapters 4**, **5**, **6** and **7**, can be found at the end of each chapter, while the bibliography of chapters **1**, **2**, and **8** can be found at the end of the thesis.

Chapter 2 LITERATURE REVIEW

Small interfering RNA (siRNA) and antisense oligonucleotides (ASO) are potent molecules with therapeutic potential [2, 4, 12, 13, 45, 46]. The pharmacokinetic (PK) and pharmacodynamics (PD) properties of these molecules depend on several factors such as structure, modifications, formulation, and route of administration [2, 4]. This chapter presents a brief summary of the RNAi process, pharmacodynamics, and kinetic properties, chemical modification, different delivery systems, including chitosan and the mechanism of endosomal entry and escape. In this chapter, the reader is referred to reviews of more limited scope and of greater depth on particular topics.

2.1 RNAi mechanism of action

RNA interference (RNAi) was discovered in 1998 and quickly recognized as a promising approach to block disease-promoting genes via gene-specific silencing. RNAi revolutionized the concept of gene regulation and shed light on the function of non-coding sequences in the genome. RNAi was found to be responsible for the regulation of vital processes such as cell growth, tissue differentiation, and cell proliferation. Dysregulation in the endogenous RNAi process was linked to cardiovascular and neurological diseases as well as a plethora of cancers [1]

In the RNAi process, gene-specific silencing is guided by three types of small noncoding double stranded oligonucleotides namely microRNAs (miRNA), PIWI-interacting RNAs (piRNA) and small interfering RNAs (siRNA). PIWI-interacting RNAs are restricted to germline cells and will not be further explored in this chapter. microRNAs are naturally transcribed from intragenic regions of the genome or within introns as long double-stranded primary microRNA (pri-miRNAs); such transcripts are at least 1000 nt long and contain single or clustered double-stranded hairpins (Figure 2-1). The pre-miRNA is processed in the nucleus into an approximately 70 nucleotides (~ 70nt) stem-loop structure called the precursor microRNA (pre-miRNA) [47, 48] by the microprocessor complex (MPC). The MCP is composed of Drosha [47, 48], a type 2 ribonuclease III with an important role in ribosomal RNA possessing [49], and the dsRNA-binding protein Pasha [50]. The pre-miRNA is exported to the cytoplasm [51] via an Exportin-5 mediated process [52] where it is further shortened by a type III RNase enzyme called Dicer into an approximately 22-nucleotide mature double-stranded miRNA (Figure 2-1). One of the duplex strands, the guide strand, also known as the antisense strand (AS), is recognized and incorporated

into a nucleic acid-protein complex called RISC (RNA-Induced Silencing Complex), where AGO2, a member of the conserved Argonaute family of proteins, is the catalytic core in plants and animals [53]. The miRNA guide strand directs RISC to the 3' untranslated (3'UTR) region of the target messenger RNA (mRNA) (Figure 2-1).

In contrast to miRNA, small interfering RNAs are exogenous 21 nucleotide duplexes (Figure 2-4) and bypass the processing steps of miRNA and directly enter the RNAi pathways through direct RISC loading. As for miRNA, the siRNA guide, or AS strand is incorporated into RISC which then guides the silencing complex to the target mRNA (Figure 2-1). Both miRNA and siRNA duplexes demonstrate strand asymmetry summarized by preferential loading of one of the strands into RISC. It was proposed that the duplex strand displaying weaker thermodynamic energy (binding energy) at its 5' end is always incorporated into the RISC and mediates gene silencing [54, 55] through direct sequence specific mRNA cleavage (PTGS) or translational repression (TR). The choice between PTGS and TR is dictated by the extent of sequence complementarity between the seed region and target mRNA; *with full sequence complementarity promoting PTGS while partial complementarity, as in the case of most miRNAs, favors translational repression and accumulation of mRNA in P bodies* (Figure 2-1).

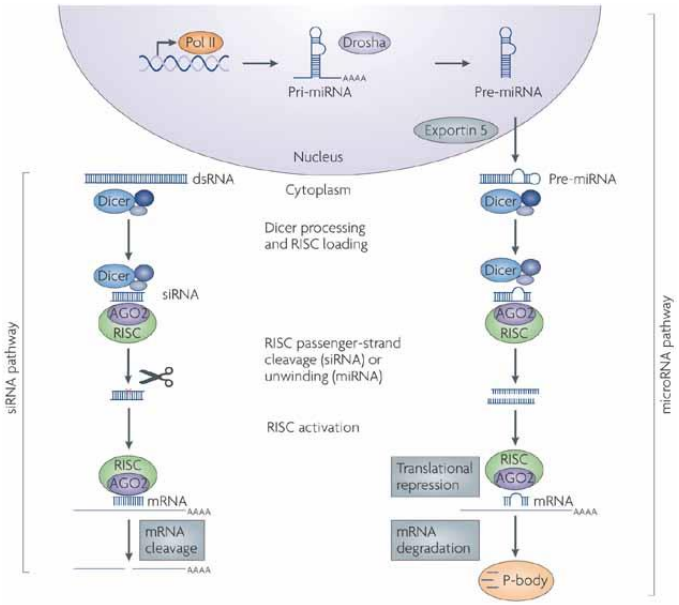

Figure 2-1: Mechanism of RNA interference induced the siRNA (left side) and the miRNA (right side) pathways. Adapted from [8]. Copyright 2017, with Nature Publishing Group permission.

2.2 Pharmacokinetic and pharmacodynamic considerations for effective RNAi

Several factors limit the efficacy of siRNA to induce the intended effects in the cell cytoplasm (pharmacological site of action). These barriers affect both the pharmacokinetics and pharmacodynamics of siRNA and are presented in section 2.2.1, 2.2.2, and 2.2.3 of this chapter.

2.2.1 Physiological barriers to siRNA delivery

In order to mediate their intended effects, the relatively large (~ 14 kDa), hydrophilic and polyanionic siRNA molecules need to **1)** circulate in the bloodstream, **2)** extravasate to the intended target tissue, **3)** diffuse locally, **4)** pass through the cytoplasmic membrane, **5)** escape from the acidic environment of the endosome and finally **6)** load into the RNAi machinery; *the first two steps are eliminated in the case of local delivery*. In each and every step of this process, a defense mechanism has been warranted through evolution in order to protect the integrity of cells and their higher structures. In blood, naked and unmodified siRNA face rapid recognition and degradation by serum endo- and exo-nucleases. In addition, siRNAs and their degradation products are readily eliminated through glomerular filtration and hepatobiliary excretion [56]. Rapid renal elimination occurs due to the relatively small size of the siRNA molecules (size below the ~ 8-10 nm pores [57] of the filtration slits in the glomeruli). Numerous studies have shown that naked, and non-chemically modified siRNAs were rapidly eliminated from the bloodstream with half-lives of less than 5 minutes [41, 58]. In contrast to naked siRNA, metabolically stabilized siRNAs have been shown to circulate up to 50 minutes [41, 58]. For instance, phosphorothioate (PS) modification of the backbone favors interactions with serum proteins and limits renal secretion. Although such modification improves nuclease resistance, permitting extravasation to tissue, additional hurdles such as specific targeting and cellular translocation remain. Moreover, electrostatic repulsion forces between the negatively charged siRNA phosphate and the negatively charged membrane limit passive diffusion [2]. Encapsulation, or conjugation, of siRNA (see section 2.3) breaks down several of these barriers permitting potent gene knockdown (reviewed in [2, 4, 11, 59]). However, delivery materials face similar challenges with endosomal escape being the most rate-limiting step [2, 9, 13, 60, 61].

Table 2-1 Biological barriers for siRNA delivery, the impact of each barrier on performance and strategies to overcome the barriers.

Barriers	**Impact**	**Solutions**
Serum proteins and nucleases	➢ Aggregation ➢ Rapid clearance ➢ Nonspecific uptake ➢ Toxicity	➢ Surface modifications e.g. PEGylation ➢ Physical encapsulation of payload ➢ Payload metabolic stabilization (e.g. chemical modifications)
Tissue specificity	➢ Nonspecific uptake	➢ Size
Cell uptake or internalization	➢ Poor intended effect	➢ Nanoparticle decoration or payload conjugation with tissue or cell specific ligands (e.g. antibodies, transferrin, galactose, GalNAc, etc)
Endosomal escape	➢ Poor target knockdown efficiency	➢ Endosomal escape agents i.e. cell penetrating peptides, membrane destabilizing agents (e.g. Mellitin, PBAVE). ➢ Optimization of lipid formulations, composition, and inclusion of fusogenic lipids and cholesterol ➢ Acid labile bonds ➢ Optimization of lipid pKa (e.g. ionizable lipids)
RISC loading		➢ Optimization of payload sequence (e.g. thermodynamics), 5’stabilization
Off-target effects	➢ Toxicity (e.g. immune stimulation, knockdown of unspecific genes, genotoxicity	➢ Payload designs ➢ *In vitro* high throughput screening ➢ Metabolic stabilization and pattern designs

2.2.2 Structural factors affecting siRNA-induced RNAi

Several factors can affect the potency of the RNAi effect. For instance, incorrect strand selection can trigger the silencing of off-target genes complementary to the intended passenger, or sense, strand and decrease the potency of the antisense strand. Increasing the asymmetry of the duplex through A-U enrichment in the 5' end of the AS strand helps to ensure that the desired strand (i.e. antisense) is selected by RISC. In addition, strategies such as the incorporation of unlocked nucleic acids (UNA) into the 5' end of the AS strand enhance asymmetry and strand selection [62]. Asymmetry can also be enhanced by blocking intracellular phosphorylation of the 5'-OH using selective modification (i.e. methylation) of the hydroxyl group at the 5' end of the sense strand during solid phase synthesis [63]. As activated RISC are devoid of helicase activity [1, 64], mRNA secondary structures can block access to the target site and reduce potency. Several algorithms (i.e. OligoWalk) were developed in order to optimize the design of siRNA duplexes, and select potent sequences for further *in vitro* screening. These algorithms not only take into account mRNA structures [65] but also incorporate design rules to consider the internal stability of the duplex [66]. The general rules for effective siRNA can be summarized as follows **1)** Low G/C content (36 to 50%), **2)** A or U base preferred in position 1 of the AS strand, **3)** a bias toward low internal stability at the S strand 3'- terminus (5' AS terminus); **4)** absence of internal repeats, **5)** at least 3 A/U bases at position 15–19, 6) A/U bases at position 10 (substrate for Ago2 cleavage) and 19, and 7) AU-richness in positions 1-7 [66]. Irrespective of how accurate these predictive algorithms are, it is always encouraged to carry out *in vitro* screening for potency and validate on- and off-target effects using proper controls [7].

2.2.3 Potential toxicities

Three types of toxicities or off-target effects have been reported in the literature and are described in sections 2.2.3.1, 2.2.3.2 and 2.2.3.3 below. It is important to mention that these off-target effects or toxicities are dependent not only upon the siRNA sequence but also upon the composition of the delivery vehicle.

2.2.3.1 MicroRNA like off-target effects

In general, miRNA-like off-target effects occur through non-specific partial complementarity between the antisense sequence and the 3'untranslated regions (3'UTR) of the mRNA pool [5]

(Figure 2-2). miRNA like off-target effects were discovered when different siRNA sequences targeting the same gene led to different transcriptomic signatures [67]. In a follow-up study, Jackson *et al* showed that nucleotide mismatch in the AS strand (5' position) decreased off-target knockdown, but introduced new genomic signatures with a new set of genes being silenced [68]. The analysis of the off-target transcript sequences revealed partial complementarities with the seed region of the siRNA; *the seed region is a sequence of 8-nucleotides that plays a key role in target recognition through base complementarity*. miRNA off-target effects are not restricted to 3'UTRs but could also be induced if siRNA share partial complementarity with coding regions (ORFs) [67]. Design algorithms, incorporating basic local alignment search tools (BLAST), have been developed to select for minimal seed region complementarity with 3'UTR [69-71]. However, these strategies are not error proof and/or are limited since partial homology with available 3'UTR is unavoidable [71]. In addition to careful designs, chemical modifications such as methylation (2'OMe) have demonstrated impressive use in mitigating miRNA like-off target effects [68]. Incorporation of other chemical modifications such as UNA (seed region) and locked nucleic acid (LNA) abrogated the number of off-target transcripts by more than 90% [72]. Both these modifications seem to affect the interaction between the AS and Ago2 (RISC) and decrease complementarity with the 3'UTRs without affecting potency [62, 68, 73].

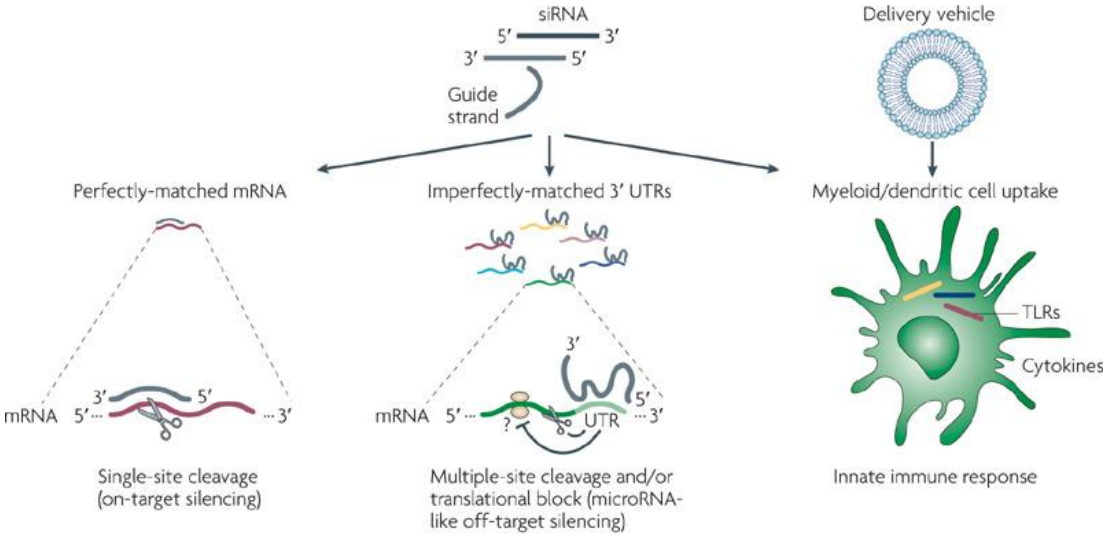

Figure 2-2: The different categories of off-target effects observed with small interfering RNAs. The cartoon depicts the on-target, or the intended effect (left), the off-target, or miRNA-like off-

target silencing, occurring after siRNA recognition of imperfectly matched 3'UTRs sequences in the transcriptome (middle) and the immune stimulation off-target effect of siRNA and/or delivery material used i.e. lipid nanoparticle (right). Note: other off-target effects such as RISC saturation are not depicted in this cartoon. Image adapted from [5]. Copyright 2017, with Nature publishing group permission

2.2.3.2 Immune stimulation properties

siRNA, and the delivery materials (section 2.3), have the potential to activate the innate immune response and stimulate the production of cytokines. Immune activation is generally associated with the activation of pattern recognition receptors (PRR) such as Toll-Like Receptors (TLR) (Figure 2-2). siRNA-dependent immune stimulation has been associated with the endosome bound TLR-3, TLR-7, and TLR-8; TLR-3 is also expressed on plasma membranes. The interaction between a TLR and a siRNA sequence activates downstream signaling pathways leading to the transcription and subsequent expression of proinflammatory genes (i.e. cytokines) such as Tumor Necrosis Factor-alpha (TNF-α) and Interleukin-6 (IL-6). In contrast to TLR-3, the activation of TLR-7 and 8 have been demonstrated to be sequence dependent [74-78]. Beside TLRs, cytoplasmic sensors such as the retinoic acid inducible gene (RIG-1) and protein kinase R (PKR) are able to recognize double-stranded RNA and mediate interferon (IFN) responses [6, 79]. These intracytoplasmic sensors represent a second layer of protection that evolved to counteract direct cytoplasmic loading of dsRNA (viruses) or poor TLR recognition. In an attempt to relate sequence motifs and TLRs, several groups revealed the importance of features such as RNA length, sequence and structure of siRNA on immune activation. However, no consensus on either the nature of the immune-stimulatory motifs or on the design rules has been reported to date. It seems that uridine (U) and guanosine (G) rich sequences including UG dinucleotides and 5'-UGU-3' are potent activators of TLR [5, 80]. Nevertheless, GU-rich sequences do not account for all immune responses to siRNA since sequences lacking U and G nucleotides can still elicit potent TLR activation [76, 78]. These findings demonstrate the difficulty in defining immune-stimulatory motifs and suggest that proper selection of inert sequences is best achieved through experimental screening. However, the most promising strategy to reduce immune stimulation seems to involve chemical modifications (Section 2.2.4). For instance, it has been established that 2' modification of the ribose ring can reduce or even eliminate the innate immune response. Judge *et al* demonstrated that a minimum of two

modifications is required in selected positions to abrogate immune stimulation in PBMCs [81]. Several other types of modifications (i.e. LNA, UNA, 2'-F, etc.) described in section 2.2.4 have also been demonstrated to inhibit immune activity to some extent.

2.2.3.3 Sequence-independent off-target effects.

As siRNA and endogenous microRNA share the same machinery, competition between these two types of molecules can potentially disturb endogenous gene regulation. Several studies demonstrated the saturability of the RNAi pathway and showed toxic effects both in vitro and *in vivo* [82-85]. For instance, mice lethality was demonstrated following the delivery of plasmid DNA encoding short hairpin RNA (shRNA); *shRNA are transcribed in the nucleus, mimic pre-microRNA, processed by Drosha and exported to the cytoplasm via Exportin-5 where they are further processed by Dicer, load RISC and mediate RNAi* [84]. The observed lethality was related to Exportin-5 saturation and impairment of nuclear transport due to the improper cleavage by Drosha [85, 86]. Sequence-independent off-target effects were also demonstrated to occur downstream of Exportin-5, in the cytoplasm, via direct competition for RISC loading [83, 87].

Although chemical modification can abrogate sequence-dependent off-target effects, improve nuclease resistance, reduce immune stimulation (section 2.2.4) and improve potency, they are unable to reduce such sequence independent off-target effects. In fact, chemical modifications, especially with novel chemistries being incorporated could increase this type of negative effects. In light of a recent report demonstrating long-lasting knockdown (6 month) following single administration in human [13], and the subsequent announcement by Alnylam Pharmaceuticals, that immunoprecipitation experiments in mouse hepatocytes showed that siRNA AS strands remain loaded into RISC months after dosing [88], sequence independent off-target effects should, therefore, be seriously investigated for long-term toxicity.

2.2.4 Improvement of siRNA PK/PD properties through chemical modifications

RNAi clinical application has met with some significant obstacles such as low cellular uptake due to the polyanionic nature of siRNA, serum instability, and low pharmacokinetics, off-target effects, toxicity and potent immune stimulation. A variety of chemical modification has been proposed to address these issues. Such modifications can be classified into four major categories: **1)** sugar

modifications, **2)** backbone modifications, **3)** base modifications and **4)** terminal modifications. A number of successful siRNA modifications have focused on the 2' position in the sugar moiety since the 2'-OH is not required for siRNA activity [89]. Such modifications include 2'-O-methylation (2'-O-ME), 2'-O-methoxylethyl (2'-O-MOE), 2'-O-allyl, 2'-O-ethylamine, 2'-O-alkylamine, fluorine modification (2'-F), 2'-deoxy-2'-fluoroarabinonucleic acid (2'F ANA) and Locked Nucleic Acid (LNA) among others (Figure 2-3). In general, all these modifications improve serum stability, binding affinity and reduce immune stimulation while preserving potency. 2'-O-methylation of sugar moieties can be well tolerated throughout the duplex siRNA making it one of the most popular and versatile siRNA modifications. However, contradicting results have been observed with some groups reporting that large numbers of 2'-O-Me modification on either strand decrease siRNA activity [89-92] while others reported that fully modified siRNA are functional [93]. 2'-O-MOE modified siRNA has been used to target the pain related cation-channel P2X3 and resulted in successful gene targeting *in vivo* [94]. This modification was found to be most effective when used on the 3'-overhang in the siRNA sequence most probably due to the fact that bulkier nucleotides are not well tolerated in the siRNA duplexes.

The fluorine modification is probably one of the best-known siRNA modifications that confer improved serum stability [95] and increased binding affinity (Figure 2-3). Reports demonstrated that 2'-F modification is well tolerated when a partial modification is performed on both strands [89, 96, 97] or when the siRNA sequence is fully modified [98]. Change in the stereochemistry of 2'-F RNA leads to 2'-F ANA, a well-tolerated modification that increases serum stability and binding affinity [99, 100] that was initially developed as a DNA analog [101, 102]. Another kind of accepted modifications involves the use of DNA bases. Such modifications are well tolerated as 3'-overhangs and/or in limited numbers within the base-paired region of a siRNA duplex [103]. Substitution with the dsDNA in the 8-nt region at the 5'-end of the guide strand gives active duplexes with reduced off-target effects [104, 105].

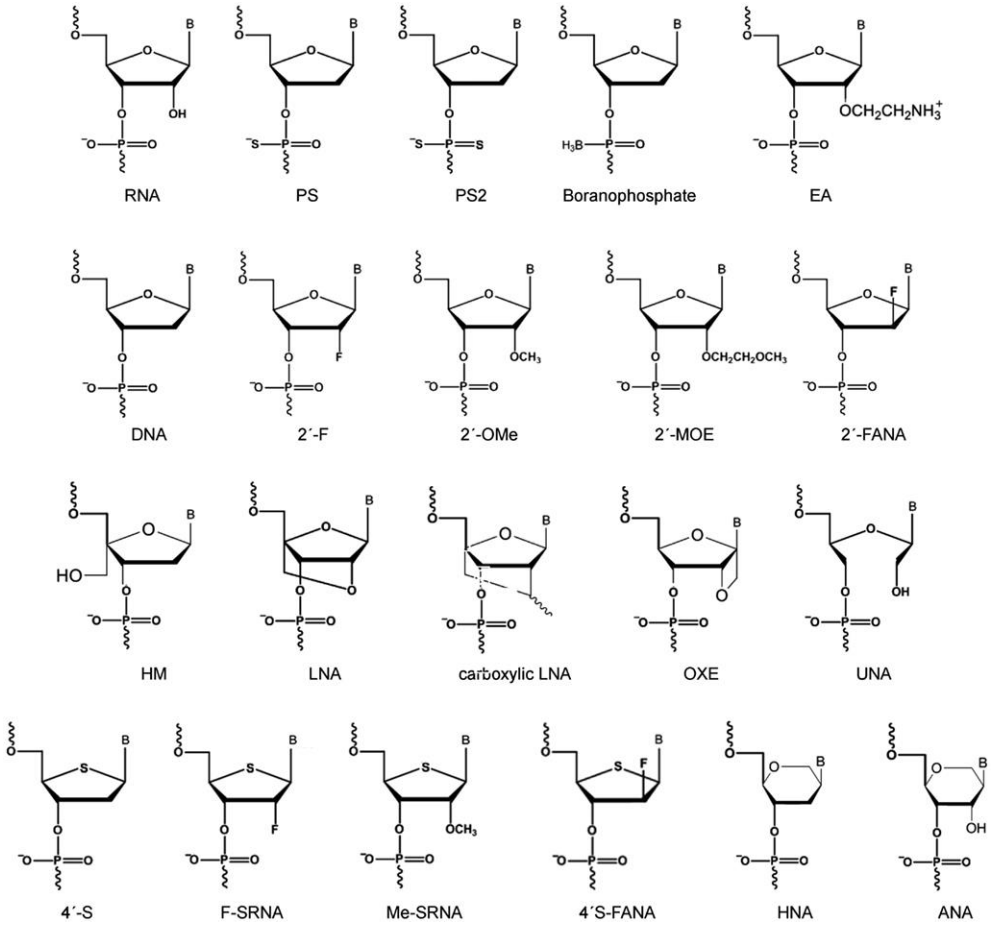

Figure 2-3: Different chemical modification used in siRNA design. RNA, ribonucleic acid; PS, phosphothioate, PS2, phosphodithioate; EA, 2 0 -aminoethyl; DNA, deoxyribonucleic acid; 20 -F, 20 -fluoro; 20 -OMe 20 -O-methyl; 2 0 -MOE, 20 -O-methoxyethyl; F-ANA, 20 -deoxy-20 -fluoro-β-d-arabinonucleic acid; HM, 40 -C-hydroxymethyl-DNA; LNA, locked nucleic acid; carboxylic LNA 2 0 ,40 -carbocyclic-LNA-locked nucleic acid; OXE, oxetane-LNA; UNA, unlocked nucleic acid; 40 -S, 40 -thioribonucleis acid; F-SRNA, 2 0 -deoxy-20 -fluoro-40 -thioribonucleic acid; ME-SRNA, 2 0 -O-Me-40 -thioribonucleic acid; 40 -S-F-ANA, 20 -fluoro-40 -thioarabinonucleic acid; ANA, altritol nucleic acid; HNA, hexitol nucleic acid; B, base. Adapted from [106]. Copyright 2017, with permission from Frontiers.

Backbone modifications include the phosphorothioate (PS), the boranophosphate, the amide linked and the 2’,5’ linked nucleotide. PS offers comparable [97, 107] or lower potencies [89] compared

to native siRNA. Excessive or fully modified duplexes were associated with increased toxicity [107] and decreased potency when modifications occur at the center of the duplex [108]. Boranophosphate modified siRNA demonstrated increased performance – potency and serum stability – compared to native and PS modified siRNAs [109]. The 2',5'-linkage was shown to be a viable option for the sense strand and demonstrated a reduction in potency [110]. Base modification such as 2-thiouracil and the c-linked Ψ-uracil (ΨU) [111-113] was shown to increase potency and specificity when appropriately placed within the duplex. On the contrary, A-U stabilizing bases such as 5-I-Ura instead of uracil and diamino purine instead of adenine demonstrated a reduction in siRNA activity [89]. Pyrimidine methylation is a common modification in conjunction with sugar modification such as DNA, 2'F ANA and LNA. Terminal modifications such as the addition of lipids and steroid moieties or DNA bases at the 3' overhangs were successfully used to improve potency and stability [58, 114]; *refer to section 2.3.3.1 for details regarding lipophilic conjugation*.

The duplex architecture was also demonstrated to be an important aspect influencing siRNA stability, immune activation, off-target effects, and potency [115]. For example, small internally segmented interfering RNA (sisiRNA), a three strand siRNA, demonstrated increased potency and reduced off-target effects [116] (Figure 2-4). Another example of a successful non-canonical architecture is the single stranded antisense RNA. The latter enters the RNAi pathway with similar potency as siRNAs [107, 117]. An alternative strategy to increase potency consists of increasing duplex length [118]. However, it is necessary to keep in mind that siRNA duplexes above 30 nt are potent activators of the interferon response [119].

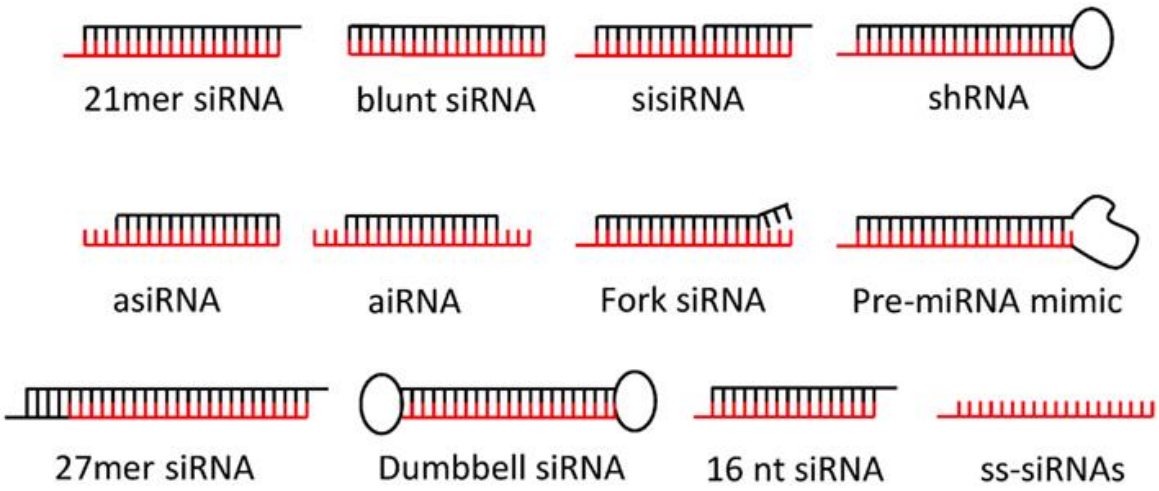

Figure 2-4: Different architectures of siRNA used in the literature. The canonical 21-nt siRNA is the most popular siRNA design and continue to be used in most of the studies. Dicer-substrate siRNAs such as 27-nt siRNA, shRNA, pre-miRNA mimics, or fork siRNA have been associated with enhanced potency. Asymmetrical siRNAs (aiRNA), asymmetric shorter-duplex siRNA (asiRNA), bulge-siRNAs and sisiRNA were shown to improve silencing specificity and when associated with lipophilic conjugates become self-delivering. Blunt-end siRNA are reported to be more nuclease resistant but can be recognized by PRK and RIG-1. Single-stranded siRNAs (ss-siRNAs) and 16 nt are functional but may require higher siRNA concentrations. Dumbbell-shaped circular siRNAs may have longer silencing duration. Passenger strands are shown in black and guide strands in red. Adapted from [106]. Copyright 2017, with permission from Frontiers.

In spite of the fact that these modifications enhance nuclease resistance, increase potency, reduce off-target effects and reduce immune stimulation; they do not resolve cell or tissue specific targeting, the delivery into the pharmacological site of action, biodistribution and endosomal escape. Therefore, safe and efficient siRNA delivery systems are still required to achieve the full potential of RNAi. Several strategies to improve tissue/cell targeting, and delivery siRNA into the cytoplasm are presented in section 2.3 below.

2.3 Strategies for siRNA delivery

Improvement in siRNA design, selection, and chemical modifications confer drug-like properties and demonstrate potency to mediate specific target knockdown with no off-target effects. However, a key challenge with respect to the translation of the broad potential of siRNA-based therapeutics is the delivery problem. As a consequence, strategies including chemical conjugation with targeting moieties or encapsulation in delivery systems were developed and, some, have reached clinical trials. These strategies include the use of lipids, polymers, proteins (including antibodies) and aptamers to address the challenges of *in vivo* delivery.

In this section, a concise review of systems that are considered most promising and/or those that reached clinical trials is presented.

2.3.1 Nanoparticles based systems

Nucleic acid encapsulation into nanoparticles provides multiple attractive properties such as nuclease protection, improved circulation time, targeting, cellular internalization and endosomal release. In the subsequent section, lipid and polymeric based nanoparticles will be presented.

2.3.1.1 Lipid nanoparticles (LNPs)

Lipid nanoparticles (LNPs), or liposomes, represent the most advanced nucleic acid carrier, or platform enabling *in vivo* delivery of siRNA. LNPs have reached clinical trials for the treatment of hypercholesterolemia, transthyretin-mediated amyloidosis, hepatitis B and liver cancers [11, 12, 18]. LNPs are endowed with natural hepatocyte targeting through LDLr-ApoE mediated endocytosis [120] and exhibit potent gene knockdown activity in rodents and non-human primates [120-123]. Electrostatic interaction between the cationic head group and the negatively charged siRNA generates multilamellar structures with positively charged lipid bilayers separated from one another by sheets of negatively charged siRNA (Figure 2-5) [10]. Different types of structures, such as unilamellar or electron dense nanoparticles, can also be fabricated using different processes (Figure 2-6). N-[1-(2,3-dioleyloxy) propyl]-N, N,N-trimethylammonium chloride (DOTMA), a quaternary amine-containing lipid, that was used for nucleic acid delivery [124] in the presence or absence of co-lipids, and form small sized unilamellar liposomes (< 100 nm). The addition of co-

lipids such as dioleoyl phosphatidylethanolamine (DOPE) improved transfection efficiency of cationic lipids.

The use of DOTMA, or other cationic lipids, in the presence or absence of co-lipids, confers a net positive charge to the liposome facilitating interaction with negatively charged membranes and subsequent nanoparticle endocytosis [9, 125]. However, cationic lipids, or liposomes, with constitutive or net positive charge, due to quaternary amine group, have been associated with spontaneous dissociation [126-128], rapid clearance, severe *in vivo* toxicity, and unfavorable biodistribution via interaction with blood components, aggregation, and activation of immune responses (i.e. cytokine and/or complement) [14-16, 128, 129]. Rapid clearance of positively charged liposomes, or lipid nanoparticles, by the reticuloendothelial system (RES) in liver and spleen, has been correlated to protein deposition and surface interactions with higher PB parameter (protein binding ability expressed as g of protein/mol lipids) associated with accelerated clearance profiles [130, 131]. Elimination, via accumulation in the capillary beds in the lungs, has been observed and is believed to be the result of aggregation [131]. Strategies to improve stability and reduce blood interaction – and RES clearance – mainly consist in nanoparticle decoration with hydrophilic polyethylene glycol (PEG), or the use of neutral or negatively charged LNPs. PEGylation has the benefit of reducing toxicity at the cost of compromising potency owing to decreased nanoparticle-cell interactions. Increased potency was achieved with PEG coatings designed to dissociate at constant rates thereby dynamically shifting the equilibrium from a stable to a transfection competent nanoparticle over time [132]. The diffusion rate, or shedding, of the PEG depends on the length of the lipid anchor with shorter chains (C14) dissociating faster [133]. In addition, the lipid anchor and its length were demonstrated to play a crucial role in the immunogenicity of PEGylated LNPs with long acyl anchors promoting antibody-mediated clearance upon multiple administration [134, 135].

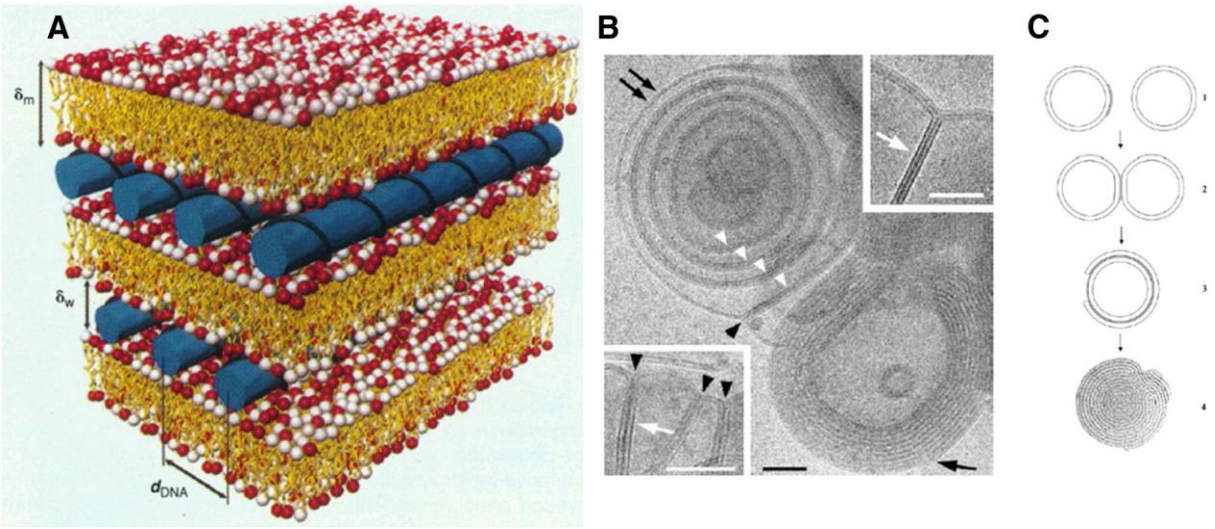

Figure 2-5 Molecular structure and local arrangement of nucleic acid in lipid nanoparticles. A) Schematic of the local arrangement of the nucleic acid between the lipid bilayers of multilamellar (MLV) lipid nanoparticles. B) Cryo-TEM images of fusion of DOTAP/Cholesterol (1:1) liposomes induced by the addition of oligonucleotides. Black arrows indicate membrane junctions and white arrows indicate a paired membrane. Scale bar: 50 nm. C) Schematic model of MLV liposome or lipoplex formation. Adapted from [136]. Copyright, 2017, Elsevier with permission.

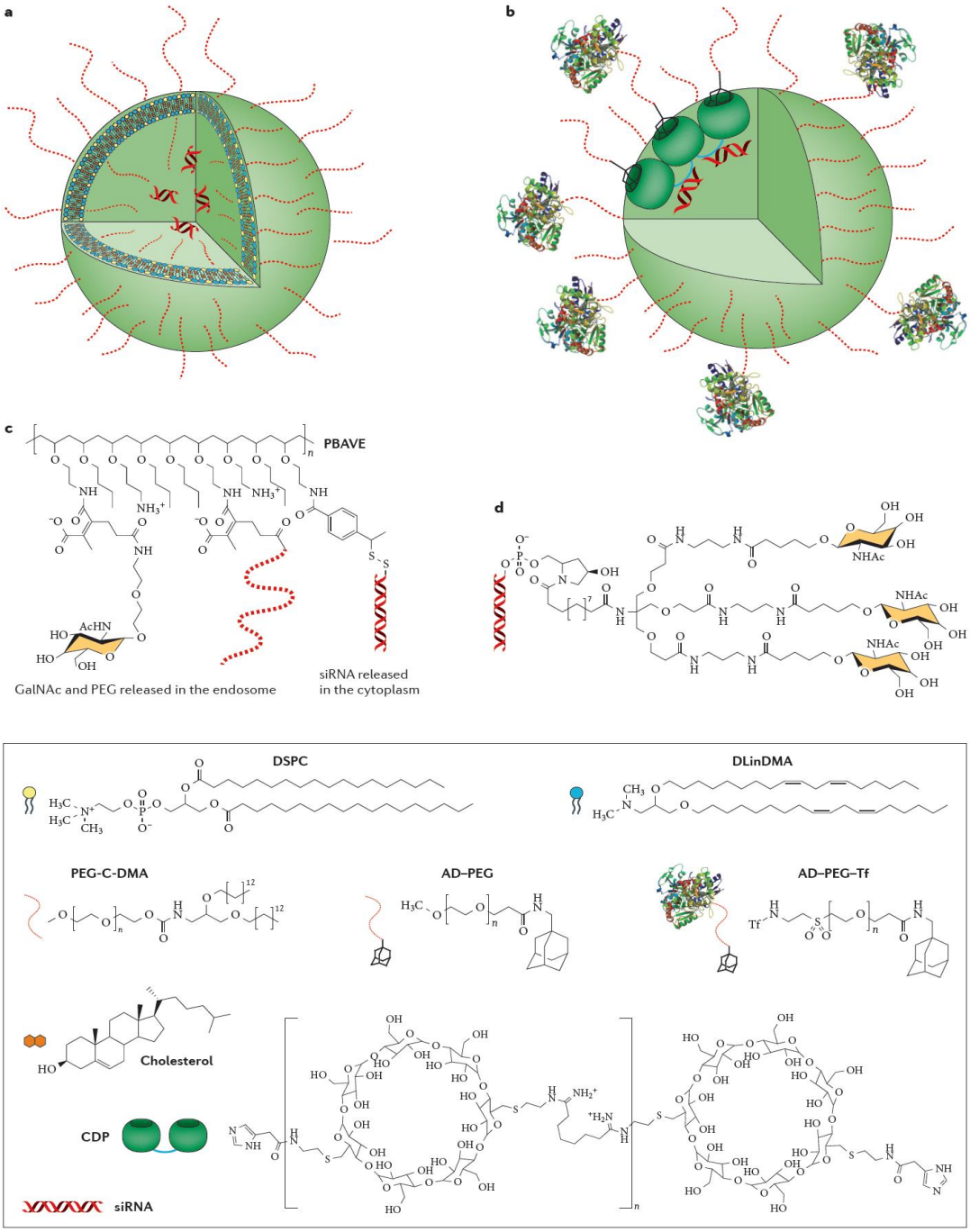

Figure 2-6: Structure of the major siRNA delivery systems. A) First generation lipid nanoparticle (LNP) used in pre-clinical and clinical settings [12, 121]. This type of LNPs is composed of a mixture of helper lipids i.e. DSPC (yellow), cholesterol (orange), the ionizable lipid DLinDMA and PEG-C-DMA. b) Cyclodextrin-based polymer nanoparticle (CDP). CDPs are synthesized through polymerization of diaminated cyclodextrin (dark green) yielding an oligomer with

diamine groups (blue). The polymer is end-capped with imidazole to improve endosomal escape. Adamantan (AD), a hydrophobic molecule is used to conjugate both PEG and targeting ligands. AD incorporate into the cyclic core of the cyclodextrin. c) First generation dynamic polyconjugate composed of PBAVE, GalNAc, PEG and the siRNA. d) Trivalent GalNAs siRNA conjugate. The metabolically stabilized siRNA is conjugated at the 3´ terminus of the passenger strand to three GalNAc molecules through a triantennary spacer molecule. GalNAc mediates hepatocyte entry through receptor-based recognition and subsequent endocytosis. Adapted from [59]. Copyright 2017, Nature Publishing Group with permission.

To avoid *in vivo* toxicity, increase stability, and augment potency of cationic lipids, ionizable head groups with primary, secondary and tertiary amines have been developed. Ionizable lipids are positively charged at low pH (pH < pKa), and neutral in circulation. This property is beneficial since it allows siRNA encapsulation at low pH, reduced protein and blood interaction at physiological pH and promotes endosomal escape following re-ionization in acidic conditions. Significant improvement occurred since the introduction of the first ionizable lipid (1,2- dioleoyl-3-dimethylammonium propane or DODAP) [137] with the number of double bonds in acyl chains controlling encapsulation and gene knockdown. Maximization of *in vitro* knockdown occurred with acyl chains containing 2 and 3 double bonds while payload encapsulation seemed optimal with 2 double bonds containing lipids [138]. As a consequence, the linoleyl lipid (Lin) became the acyl chain of choice and demonstrated potent *in vivo* knockdown in NHPs [121]. The plasma half-life was extended to 38 minutes when siRNA was formulated with linoleyl containing LNPs. However, this formulation showed limited efficacy and caused cytokine induction and complement activation in initial clinical trials [12]. Immune stimulation is a major problem with lipid-based nanoparticles and is responsible for the discontinuation of several programs that were halted by the US Food and Drug Administration after severe flu-like symptoms occurring during or post-infusion [12]. Innate stimulation can be significantly reduced with metabolic stabilization of the payload (i.e. 2'OMe modification) and/or co-administration anti-inflammatory steroids [81, 135, 139]. Immune stimulation would benefit from increased potency since toxicity is a concept related to both dose and exposure. Therefore, significant improvement in potency, and consequently safety has been achieved through **1)** rational design and/or **2)** generation of libraries and screening for novel formulations. The first approach identified two ionizable lipids i.e. DLin-KC2-DMA and

DLin-MC3-DMA with superior potency (100 and 1000-fold respectively) in comparison with the 1st generation DLin-DMA lipid [122, 140]. Maximization of potency, or the decrease in median effective dose (ED50), was strongly correlated with the pKa of ionizable lipids (optimal at 6.44) and their ability to adopt cone structures in acidic environments [140]. In fact, data suggest that the final liposome pKa is more important than the pKa of individual lipid constituents [122]. DLin-MC3-DMA based lipid nanoparticles demonstrated potent TTR knockdown in NHP and moved to clinical trials [12]. Although increased potency at lower doses was obtained, clinical administration of the second generation LNPs (DLin-MC3-DMA) still requires steroid pre-treatment to alleviate infusion reactions [46, 141]. The results of Patisiran phase III study, a DLin-MC3-DMA LNPs targeting the transthyretin protein (TTR) are expected in the third quarter of 2017 and a potential FDA approval in 2018.

In spite of the high potency and advanced clinical development, optimization and screening for new formulations are still ongoing. In an attempt to improve biodegradability, or intracellular β-oxidation, of DLin-MC3-DMA, ester groups were introduced in the alkyl chain [123]. These ester-modified lipids were well tolerated in mice and readily eliminated from tissues while retaining exceptional potency.

A recent approach using chemical libraries of lipid-like molecules termed lipidoids (L), combined with cholesterol and PEG-ceramide, identified L98N12-5 as a novel formulation with high tolerability, and *in vivo* potency in both mice and NHPs [142, 143]. L98N12-5 was administered at doses comparable to the first generation LNPs described by Zimmermann *et al* [121]. In contrast, an epoxide-derived lipidoid library identified a formulation, C12-200, with outstanding knockdown efficacy in mice and NHP. Target gene knockdown exceeded 80% at a dose of 0.1 mg/kg [144]. The clinical translation of these two lipids, as well as the aforementioned ester modified DLin-MC3-DMA, and their performance in human is still pending strategic decisions in a space where GalNAc is rapidly replacing LNPs for liver delivery. As seen in this section, LNPs appears to be restricted to the liver through natural targeting properties to accumulate in liver hepatocytes. The mechanism of liver accumulation and endosomal escape will be presented in section 2.4.1 of this chapter.

2.3.2 Polymer-based systems or polymer based nanoparticles

2.3.2.1 Polyethyleneimine (PEI)

Polyethyleneimine (PEI) is one of the most broadly used cationic polymers for the delivery of nucleic acids [9, 145]. PEI can be synthesized in a linear (lPEI) or branched (bPEI) forms and its molecular weight controlled [9]. Linear PEIs have demonstrated decreased *in vitro* toxicity and improved *in vivo* tolerability profiles compared to their branched counterparts [146-148] motivating their frequent use in the literature. Bonnet *et al*, showed that intravenous administration of lPEI induces potent gene knockdown with no significant increase in pro-inflammatory cytokines or liver transaminases [147]. However, PEIs are generally associated with toxicity [8, 149] and colloidal instability [150] limiting their use in clinical trials. PEI cytotoxicity was characterized as a two-phase process where polycation-cell interaction induces loss of cell membrane integrity and initiation of programmed cell death [151]. Insights into the molecular mechanisms of toxicity revealed the importance of physical interactions between the polycation and the mitochondria leading to the release of proapoptotic proteins and subsequent initiation of apoptosis. *In vivo*, lPEI demonstrates rapid blood clearance (1-5 minutes) and predominately accumulate in the lungs followed by liver, spleen, and kidneys [41]. The two to ten-fold increased accumulation in lungs is hypothesized to be due to salt and protein induced colloidal instability in serum and subsequent physical capture within pulmonary capillary beds.

Improved pharmacokinetic and altered biodistribution profiles can be achieved with PEI surface modification [152, 153]. PEG decorated PEIs (PEG-PEI) showed decreased liver accumulation indicative of improved stability and longer circulation time with no activation of the complement system [154]. Despite the encouraging results, PEG-PEI dissociated upon liver passage underscoring the shortcomings of this system for systemic application [154].

PEI-siRNA systems have been used for local administration with high target knockdown demonstrated in lungs and other organs. Despite numerous reports of cytotoxicity and limited performance following systemic administration [148, 155], PEI-based systems are being tested in clinical trials in Europe, Canada, and Israel. PEI-based nanoparticles (lPEI, 25kDa) were locally injected into pancreatic tumors using ultrasound endoscopy [156]. Buscail *et al* reported a favorable in human safety profile with mild treatment-related toxicities in 4/22 patients (↑ transaminases). A dose-dependent increase in CYL-02 transgene expression was demonstrated with no objective

clinical responses. However, nine patients (9/22) showed stable disease and two of these patients (2/9) experienced long-term survival demonstrating that PEI could potentially be used for local clinical applications [156].

Newer generations of PEI-based systems, based on polycaprolactone-block-PEG copolymers, poly D, L-lactic acid-coglycolic acid (PLGA), or lipid conjugation, are being developed for improved colloidal stability and increased potency [150]. Nevertheless, PEI systems have been associated with off-target and transcriptomic effects [148] that need to be fully investigated, in different cell lines (and potentially *in vivo*) in order to establish proper safety profiles and allow clinical translation.

2.3.2.1 Poly (β-amino ester) (PBAE) systems

Poly (β-amino ester), or PBAE, represents an interesting class of polymers that was first developed in the Langer laboratory at MIT by Lynn *et al* [157]. These polymers offer facile synthesis through classical or combinatorial approaches to construct screening libraries for structure-activity relationship (SAR) and selection of efficient formulations. PBAE are synthesized by the conjugation of amine (side chains) to diacrylates monomers (backbone) using a one-step chemical reaction; *Michael addition reaction* [158, 159]. The diacrylate-terminated polymer can be end capped with a variety of molecules increasing its versatility/modularity. Surface modifications can be performed via conjugation or electrostatic coating with negatively charged peptides/ molecules (i.e. poly E) [160] to reduce deleterious effects associated with cationic surfaces and improved/controlled targeting to tissues.

Due to their positive charge and amine content (primary, secondary and tertiary), PBAE polymers are able to spontaneously condense nucleic acid into nanoparticles and escape the endosome. Initial studies of these polymers showed that optimal formulations had Mn ≥10 kDa and effective diameters below 250 nm with quasi-neutral ζ-potentials (~10 mV) [83, 161]. In comparison with PEI, Poly (β-amino esters) showed at least 4 to 8-fold improvement in transfection efficiency (TE) coupled with decreased cytotoxicity. The latter is attributed to the biodegradable ester bond in PBAEs; *with a half-life between 2-7h depending on the polymer* [159]. Although, PEI and PBAE have a quasi-similar proton buffering capabilities [162], or ability to escape from the endosomes, the enhanced TE observed with PBAE *versus* PEI can be attributed to improved endosomal escape probably via hydrophobic interactions in the endosomal compartment, differences in SAR, nucleic

acid binding/unpacking, and most probably their degradability/low toxicity. As PBAE degrade inside cells and cause less toxicity compared to nondegradable polymers (i.e. PEI), higher polymer/nucleic acid mass ratio can be used to achieve a higher extrinsic buffering capacity per mass of nucleic acid [163]. Principal component analysis (PCA) revealed that hydrophobicity and molecular weights represent major parameters which increase transfection efficiency between related PBAE structures [164]. Studies from the same group (i.e. Green J.J. at John Hopkins), showed that different PBAE polymers are needed for the delivery of siRNA *versus* plasmid DNA, and that chemical composition of the PBAE end group (capping monomer), rather than the core polymer, play a major role in promoting cellular uptake [159, 165, 166]. This is probably due to the role of the end-group in mediating/facilitating an interaction between the surface of the nanoparticles and cells and/or the influence of the end group on the bio-nano interface.

PBAE have been administered *in vivo* using different routes of administration (i.e. intravenous, intraperitoneal, intraocular, etc.) [158-160, 167] and are currently the focus for intratumoral injection in the brain [159]. Intravenous administration of PBAE nanoparticles lead to accumulation in major organs causing toxicity. Electrostatic coating with negatively charged peptides (i.e. Poly-E) alleviate *in vivo* toxicity and directs nanoparticles to either the liver or the bone marrow depending on the coating density [160]. Intracranial CED delivery of PBAE nanoparticles encoding the herpes simplex virus induced thymidine kinase (HSVtk) demonstrated good tumor penetrability reaching the tumor margins and achieved significant survival benefits in rat gliosarcoma models [168]. These polymers continue to be developed in the Green and Langer laboratories for different applications (i.e. mRNA delivery [169]) and show promising results. However, further development needs to be conducted to improve their PK/PD profiles and to understand why PBAE polymers require bio reducible disulfide bonds for siRNA delivery and not another type of nucleic acids.

2.3.2.2 Cyclodextrin-based systems

Cyclodextrin polymers (CDP) are polycationic oligomers synthesized by step-growth polymerization between diamine containing cyclodextrin monomers and dimethyl subermidate to generate oligomers with amidine functional groups. CDPs mediate efficient condensation of nucleic acids, including siRNA, at very low amidine to phosphate ratio (N:P ratio less than 3) due to the strong basicity – or positive charge – of the functional groups. Endosomal release is usually

dependent on imidazole functional groups grafted by end-capping. *In vivo* application of these systems required PEGylation to prevent protein induced aggregation in serum. Non-covalent PEG shielding was performed following conjugation with a hydrophobic molecule, adamantane (AD), that incorporates through hydrophobic interactions into the cyclic, and hydrophobic, core of the cyclodextrin structure (Figure 2-6). PEG shielding, improves colloidal stability, and reduce *in vitro* and *in vivo* transfection efficacy through reduced nanoparticle-cell interaction. Modification of the AD-PEG with targeting ligands such a transferrin (Tf) or mannose (M), rescues the efficacy of the CDP NPs lost with PEG shielding through receptor-mediated interaction and subsequent endocytosis.

The CDP targeted system, developed in the Mark Davis Lab at the California Institute of Technology, was the first targeted nanoparticle system to be tested in clinical trials and to demonstrate the application of RNAi in humans [11, 45]. The system was injected as a two vial component that is mixed at the bedside prior to an intravenous infusion protocol of 30 minutes.

In vivo delivery of siRNA using the CDP system was demonstrated in multiple animal models across species. Potent knockdown and antiproliferative effects were displayed in a syngeneic subcutaneous mouse tumor model and in a xenograft model for Ewing Sarcoma, respectively [170, 171]. Positive data from these initial experiments prompted the initiation of a pre-clinical program where clinical translatability was evaluated in non-human primates. The targeted-CDP system was found to be tolerated following intravenous administration at doses up to 27 mg/kg and demonstrated a large therapeutic index (potency ~0.6-1.2mg/kg, toxicity ~ above 27 mg/kg) with mild activation of pro-inflammatory cytokines [172]. Evidence of RNAi was shown for the first time in a human phase I clinical trial using 5'Rapid Amplification of cDNA Ends (RACE) [45]. Although the system demonstrated fast translatability into clinical trials, mainly due to properties such as low toxicity in preclinical studies, high encapsulation efficiency, the inclusion of targeted moieties and PEG stabilization, phase I clinical trial failed to progress into subsequent phases (i.e. Phase II and III). Arrowhead Research, parent company owning Calando Pharmaceuticals, terminated the Phase Ib trial with the CDP based investigational product CALAA-01; *Phase Ib trials are usually extension studies*. In-depth analysis of the clinical data and correlation with preclinical animal models showed dose-dependent toxicities in several patients, infusion reactions that were correlated with increased pro-inflammatory cytokine release, and acute dose-dependent hematological toxicities (i.e. thrombocytopenia and lymphopenia) [173]. Importantly, all patients

had no objective tumor responses (79%) as per RECIST 1.0 criteria and 7/19 patients had increased tumor size highlighting the absence of therapeutic effect. Pharmacokinetic data correlated between animal and human accompanied with rapid elimination of CALAA-01 occurring through kidney and bladder without liver toxicity. Kidney toxicity was rate limiting in animal studies but not in human despite accumulation and elimination of the CALAA-01 system through the glomeruli [173]. These findings indicate that the system seems to lack stability in blood and needs further investigation. In addition, poor pharmacodynamics and immune stimulation were potentially related to the use of poorly selected siRNA (IC50 in nM *versus* pM range for current designs) and its immune stimulating potential in the absence of chemical modifications. However, the system continues to be evaluated in preclinical models where CDP has been used for the delivery of siRNA to mesangial cells of the kidney [174]. Both Tf and M targeting revealed mesangial accumulation of siRNA and knockdown with potential application in kidney diseases.

In summary, the lessons learned from the CDP system provide guidelines for the design of future polymeric and polycationic systems. These include **1)** dosing in humans which could be achieved at least twice a week with repeated administration, **2)** infusion could be tolerated with premedication, **3)** long term stability (CMC) is an important issue that hinders PD and plays an important role in toxicity, and **4)** NPs can accumulate in tumor following systemic administration and the enhanced permeation retention effect (EPR) which constitute a positive news in respect to the growing skepticism about EPR effect in humans.

2.3.3 Conjugation-based systems

2.3.3.1 Lipid-siRNA conjugates

Lipophilic conjugation was first introduced by Soutschek *et al* in 2004. Cholesterol-conjugated siRNA (Chol-siRNA) displayed improved pharmacokinetic (PK) properties with increased circulation time ($t_{1/2}$ 95 min) compared to its unconjugated form ($t_{1/2}$ 6 min). Improved PK was attributed to increased binding to serum proteins such as albumin [58], which limits renal clearance and promotes endothelial transcytosis. Tissue distribution improved following conjugation with siRNA detected in liver, heart, kidney and adipose tissues 24 hours post administration *versus* none with the unconjugated siRNA. This enhanced PK and biodistribution profile led to potent apoB-1

knockdown in liver and jejunum (~ 57 % mRNA and 68% protein) and a subsequent phenotypic decrease in low density lipoprotein (40%), high density lipoprotein (25%), chylomicron (50%) and plasma cholesterol (37%) levels [58].

Wolfrum *et al* demonstrated that cholesterol (C27), stearoyl (C18), and docosanyl (C22)-siRNA conjugates exhibit potent apoB-1 knockdown following multiple injections (3 injections at 50 mg/kg) confirming previous results and showing that long chain sterols – or bile acids – could be used as lipophilic conjugates [175]. In addition, the authors showed that altered biodistribution profile and improved circulation time (↑ $t_{1/2}$) were not dependent on albumin binding, as hypothesized by Soutschek *et al* [58], but on the incorporation of lipophilic conjugates into serum lipoproteins. In normal physiology, both high (HDL) and low-density lipoprotein (LDL) play a critical role in cholesterol transport and exchange [176, 177]. FPLC analysis revealed that cholesterol, and long chain lipid-siRNA conjugates, selectively associate with HDL, LDL, and albumin with a small fraction remaining unbound following incubation in plasma. It became clear that association with lipoproteins improves nuclease protection and promote tissue-specific distribution responsible of potent knockdown observed in liver and jejunum. The mechanism of cell uptake was determined to be independent of HDL and LDL endocytosis but required association between these lipoproteins and their receptors (scavenger receptor B 1 (SR-B1) and LDL receptor) and the subsequent transfer of conjugates through a mechanism involving, in part, the mammalian homologue of SID-1; *a transmembrane receptor involved in systemic dsRNA uptake* [178]. It is believed that HDL and LDL loaded particles, after association between the lipophilic conjugate and lipoproteins, bind to their receptor and transfer the lipophilic conjugate through SID1T mediated dsRNA recognition and subsequent internalization.

Lipophilic conjugates with lipoprotein pre-treatments (i.e. HDL) demonstrate improved knockdown (~ 8 to 15 fold) *versus* conjugates with albumin, or without, pre-treatment indicating that: **1)** lipophilic conjugates (i.e. cholesterol-siRNA) do not readily associate with lipoproteins following systemic administration, **2)** albumin-bound fraction is not functional and/or cannot be internalized in hepatocytes, and **3)** lipoprotein particles are efficient delivery systems for lipophilic-siRNA conjugates.

α-tocopherol (vitamin E) conjugation of a Dicer substrate siRNA (DsiRNA) (Figure 2-4) inhibited apoB-1 gene expression in the liver following single administration of a 2 mg/kg dose [179]. The

α-tocopherol conjugate demonstrated liver-specific accumulation, dose-dependent knockdown and resulted in phenotypic changes in serum triglyceride and cholesterol without induction of IFN-α/β. The improved potency (~ 25 fold) relative to cholesterol-siRNA conjugates, used as a control, or in [58, 175], might be attributed to differences in payload potency, mechanism of conjugate internalization into hepatocytes and endosomal release. Although the mechanism of cell uptake was not investigated, it was hypothesized that binding of α-tocopherol to serum lipoproteins – other than LDH and HDL – mediated receptor specific endocytosis in hepatocytes. The improved potency *versus* cholesterol-siRNA conjugates requires further investigation, including a systemic study on the effect of conjugate position *vis-à-vis* the siRNA strands, to identify α-tocopherol-siRNA mechanism of uptake, and endosomal release. In order to improve cholesterol based conjugates, the length of the linker between the cholesterol and the siRNA has been investigated. Petrova *et al* found that increased length improved *in vitro* knockdown efficiency [180]. In comparison with first-generation lipid nanoparticles (LNPs) administered in mice and non-human primate [121], lipophilic conjugates demonstrated very low *in vivo* potency (~100 fold). Factors such as 1) poor endosomal escape and 2) metabolic stabilization of the siRNA might have contributed in the low *in vivo* potency. The concomitant delivery of a reversibly masked endosomolytic polymer and a cholesterol-siRNA conjugate ameliorated (500 fold) *in vivo* potency [181] indicating that endosomal escape is a major bottleneck for these lipophilic-conjugate systems. The rate of receptor recycling and the extent of metabolic stabilization of siRNA are considered to be extremely important for the potency of GalNAc conjugates [2, 4, 182].

Despite the low potency, when administered without endosmolytic agents, lipophilic conjugation seems to survive in the RNAi delivery system space with novel hydrophobic conjugates being developed for local delivery [2, 4]. Lipophilic conjugation with asymmetric siRNA induce potent gene silencing *in vitro* and support robust *in vivo* efficacy following local injections [183, 184] and are in phase I/IIa clinical trials (NCT02030275, NCT02079168, NCT02599064, NCT02246465).

Efforts led by the Khvorova group, at the University of Massachusetts, led to the identification of molecules that could be co-delivered with lipophilic-siRNA conjugates to enhance *in vitro* potency [185], and could, in the future, be used in formulations for, at least, local delivery. In addition, strategies to conjugate fatty acids – i.e. docosahexaenoic acid (DHA) – with intrinsic anti-inflammatory properties and improved tissue diffusion [184] indicate that extrahepatic, and mainly local, delivery using these systems could be achievable [4].

2.3.3.2 Dynamic Polyconjugates (DPC)

Dynamic Polyconjugates (DPC) were modeled based on the physical characteristics of viruses and designed to break down intracellular barriers limiting the delivery process. The delivery system was designed to incorporate several components intended to play particular roles under specific physiological conditions. A fundamental characteristic of this prototypical delivery system (Figure 2.5) is the reversible modification of the poly-butyl amino vinyl ether (PBAVE) polymer with polyethylene glycol (PEG) and tissue-specific ligands (L) for increased stability, reduced toxicity and tissue-specific targeting. PBAVE has amphipathic side chains that include alkyl groups interspersed with primary amine (NH_2) functional groups. The polymer was chosen for its membrane lytic potential, that is dependent on both the positively charged amines and the hydrophobic alkyls side chains; *with longer chains (i.e. propyl or butyl) demonstrated to improve membrane disrupting properties of the polymer* [186]. In order to prevent non-specific interactions with serum proteins and hemolytic activity *vis-à-vis* erythrocytes, amine groups were modified, or masked, using carboxy dimethylmaleic anhydride (CDM) containing PEG and targeting ligands to form acid-labile maleamate groups. These CMD linkers are relatively stable at pH 7.2-7.4 but fully reversible in acidic environments such as those present in the endosomes and lysosomes. Unmasking of the amines reactivate the membrane lytic activity and promote endosomal disruption. In order to induce gene knockdown, siRNA is conjugated to the polymer side chains by a disulfide linker allowing for payload release under bio-reducing conditions (i.e. cytoplasm). The prototypical DPC was designed to target liver hepatocytes by attaching the asialoglycoprotein receptor (ASGPR) ligand GalNAc.

This first generation GalNAc targeted DPCs (DPC™ 1.0) demonstrated potent apolipoprotein B-1 (*apob-1*) and peroxisome proliferator-activated receptor alpha (*ppara*) gene knockdown in mice. apob-1 showed dose-dependent knockdown reaching ~80% when administered at 2 mg/kg (50 µg) and translated in phenotypic responses such as reduction (~ 40%) in serum cholesterol [187]. The decreases in apob-1 mRNA and cholesterol remained significant for 10 and 4 days respectively and returned to nadir around 15 days. Liver transaminase levels and pro-inflammatory cytokine expression (TNF-α and IL-6) transiently increased and returned to baseline less than 48 hours post-administration. The importance of the targeting moieties and the reversible linkage (maleate linkage) was demonstrated to be critical for tissue-specific accumulation and knockdown efficiency. Mannose targeting directed DPC uptake to nonparenchymal liver cells expressing the

receptor. Shielding with non-hydrolysable linkers abrogated knockdown highlighting the importance of unmasking, or polymer reversal from inert-to-membrane lytic states, for optimal endosomal release [187].

The uncontrolled nature of the polymerization process used in the production of PBAVE led to heterogeneity in respect to size and composition; therefore, limiting manufacturing reproducibility and entailing the development of sophisticated purification and analytical methods [188]. The clinical translation of this potent technology, at least from a control and manufacturing (CMC) and regulatory standpoint, required an improved synthesis process. Homogeneous polymers amenable to large scale manufacturing were therefore developed using novel chemistries such as atom transfer radical polymerization (ATRP) and reversible addition-fragmentation chain transfer (RAFT) [11, 188]. In addition, the incorporation of hydrolyzable bonds in both the polymer backbone and side chains was used to reduce toxicity upon multiple administration; preventing cytoplasmic accumulation of membrane lytic polymers. However, the aforementioned improvements did not alleviate the manufacturing complexity associated with the conjugation chemistry or product stability [188].

Exploiting the natural liver-targeting properties of lipophilic-siRNA conjugates, possibly through LDL and HDL incorporation and subsequent shuttling to the liver [175], Wong *et al* showed that PBAVE co-administration improves apob-1 knockdown (~ 500 fold) in mice and non-human primates [181]. Consistent with PBAVE blood clearance and liver accumulation kinetics [189], separately injected components – i.e. polymer and lipophilic-siRNA – were able to colocalize in endosomes and trigger potent knockdown within two hours. This co-administration strategy simplifies the manufacturing process – i.e. decreased conjugation steps, increased yield, etc. – and permit exploration and use of alternative membrane disrupting agents. Indeed, the original PBAVE polymer has been replaced with a reversibly masked mellitin-like peptide (MLP) [190]. The exact reasons for the replacement of PBAVE with MLP (EX®1) are not publicly available but could be due to manufacturing and/or toxicity problems. The novel MLP based DPC system demonstrated potent and safe gene knockdown in mice and NHP [190] and tested in phase II clinical trials for the treatment of hepatitis B (HBV) [191] and reductions of liver α-1 antitrypsin [192]. Two clinical drug candidates (ARC-520 and 521) contain two cholesterols–siRNAs targeting conserved regions of HBV transcripts show potent knockdown in human with mild adverse events reported [193]. The tolerability of ARC-520, ARC-521, and ARC-AAT in human clinical trials appears to be

favorable; *with more than 300 patients generally tolerating the infusions (e.g. 6% infusion reaction and 3 serious adverse events (SAE) were reported for ARC-520* [191, 193]. Despite human tolerability, Arrowhead Pharmaceuticals decided to discontinue the EX®1-containing programs, following the death of an NHP injected at the highest dose, and deploy its resources to develop subcutaneously (SubQ) administered GalNAc targeted systems [194].

2.3.3.3 GalNAc conjugates

N-acetylgalactosamine (GalNAc) conjugates are emerging as important components of the oligonucleotide liver-targeted delivery toolbox. GalNAc conjugates are rapidly replacing LNPs in clinical trials with major companies (i.e. Alnylam, Arrowhead, Dicerna, Ionis, and Silence) shifting toward the GalNAc technology and dropping their LNP or proprietary based pipelines products [2, 194]. Increased interest stems from **1)** simplistic design (i.e. direct conjugation) *versus* LNP (i.e. multi-component) or DPCs (i.e. complex chemistry), **2)** high efficiency to deliver oligonucleotides, including siRNAs, to hepatocytes, **3)** induce potent target specific knockdown in said cells and **4)** their facile and straightforward manufacturing process. GalNAc conjugated siRNA can be synthesized using solid-state synthesizers and characterized using mass spectrometry [195, 196].

The trivalent GalNAc system is designed to bind with high avidity to the hepatocyte lectin asialoglycoprotein receptor (ASGPr) (Box. 2-1). In this system, GalNAc is attached to the 3’ end of the siRNA sense – or passenger – strand using a linker (Figure 2-6). The system for siRNA delivery was developed at Alnylam Pharmaceuticals under the leadership of Manoharan [195-197]. The potency of the system increased with increased GalNAc valence [195]; *with trivalent siRNAs demonstrating highest uptake and knockdown in mouse primary hepatocytes*. The specificity of the GalNAc system to target hepatocytes was demonstrated in the presence of the EGTA Ca^{2+} chelator since Ca^{2+} is required for GalNAc binding on the carbohydrate recognition domain (CRD) of the receptor [198] as well as in $ASGPr^{-/-}$ knockout cells. Metabolic stabilization of the siRNA payload was shown to be necessary with the trivalent GalNAc system. Increased phosphorothioate (PS) modifications of the antisense (guide strand) backbone, increased *in vivo* potency (5-fold) compared to the lightly PS modified anti-TTR siRNA [195]. 5-vinyl phosphonate (5’-VP) modification of a fully PS modified antisense strand increased the siRNA concentration in liver and improved potency (5-fold) [182]. This synergistic effect – 5’-VP and PS modification of the

GalNAc-siRNA conjugate – is believed to be due to increased phosphatase stability in serum and intracellular XRN nucleases [4]. Interestingly, trivalent GalNAc conjugated siRNAs demonstrated improved *in vivo* performance following subcutaneous (SubQ) *versus* intravenous administration [195]. Knockdown efficiency correlated with siRNA concentration in the liver for each route of administration. Given that the ASGPr has a recycling half-life around 15-30 minutes, potent knockdown could be explained by the interplay between receptor kinetics and the GalNAc conjugate circulation (elimination) time. The SubQ route offers a sustained release model since, injected conjugates have to diffuse, enter lymphatic and capillary circulation before accessing systemic circulation and the ASGP receptor. Preclinical studies in NHPs demonstrated potent antithrombin (AT) knockdown following single and repeated SubQ administration. The comparison between standard template (STC) and the enhanced (ESC) chemistries showed a 10-fold improvement in functional gene knockdown in mouse, normalization of thrombin generation and the time to nadir return in NHP with no adverse events or immune activation [199]. These data demonstrate that the GalNAc system, in combination with stabilized-siRNAs, is an extremely potent system, with long lasting effects, that could be used to treat a variety of liver diseases. Alnylam Pharmaceuticals advanced several GalNAc programs into clinical trials (Table 2-2). As of October 2016, the revusiran program, in Phase III clinical trials, has been terminated due to an imbalanced mortality rate in the treatment *versus* placebo arm [88]. However, the association between observed mortality and components of the payload (i.e. siRNA, or the delivery system) or other factors still need to be mechanistically understood. The revusiran program used an STC modified siRNA and was administered at high doses corresponding to a yearly exposure of 20-25 g [4]. In contrast, the inclisiran program, an ESC modified siRNA, has moved to a phase II clinical trial (NCT 02597127) following positive data [13]. Inclisiran is administered at lower doses than revusiran and is not expected to show adverse events in advanced trials. Alnylam continues to believe in the GalNAc pipeline with other companies following the path.

Table 2-2 GalNAc based clinical candidates in development.

Drug	Sponsor	Chemistry	Target	Disease	Status

Revusiran	Alnylam	STC	Transthyretin	Hereditary ATTR amyloidosis	Retracted
Fitusiran	Alnylam	ESC	Antithrombin	Hemophilia	Phase 2
Inclisiran	Alnylam	ESC	PCSK9	Hypercholesterolemia	Phase 2
ALN-CC5	Alnylam	ESC	Complement protein C5	Complement-mediated diseases	Phase 1/2
ALN-AS1	Alnylam	ESC	Aminolevulinic acid synthase	Liver porphyrias.	Phase 1

Box. 2-1 The hepatic ASGP receptor

In humans, ASGPr is a trimeric receptor assembled of two distinct subunits (i.e. H1 and H2); with the most abundant form consisting of two H1 and one H2 subunit [200]. The receptor is highly expressed on hepatocytes (i.e. 0.5-1 million copies per cell) and is responsible for asialoglycoprotein clearance through clathrin-mediated endocytosis and subsequent trafficking to the lysosomes for elimination [201]. ASGPr has been detected at lower abundance on peritoneal macrophages, in testis (including sperm), human intestinal cells and peripheral blood monocytes. The extracellular domain of each subunit is composed of a calcium-dependent carbohydrate domain (CRD) with three Ca^{2+} binding sites [202]. High-affinity GalNAc binding occurs through cooperative hydrogen and hydrophobic forces between the ligand and amino acids in the CDR; the reader is referred to Huang *et al* for a detailed review on ligand-receptor interaction and the importance of geometry for high-affinity binding [200]. Important information to retain for the delivery of GalNac conjugated nucleic acids include: **1-** Highest avidity achieved with higher valence, **2-** linker (antenna) and spacer length are important for binding, **3-** ligand spacing play a major role for improved binding with 20 Å being optimal [203], and **4-** ASGPr promote clathrin-mediated endocytosis and fast recycling time (~ 15-30 minutes). The importance of the last point (point 4) will be mentioned in section 2.4.3 of this chapter.

2.3.4 **Chitosan for gene delivery**

Chitosan is a linear copolymer composed of glucosamine (D-unit) and N-acetylglucosamine (A-unit) linked by β(1→4) glycosidic bonds (Figure 2-7), and derived by partial deacetylation of chitin. The latter and its derivative chitosan, are the second most abundant polysaccharides on earth after cellulose [204].

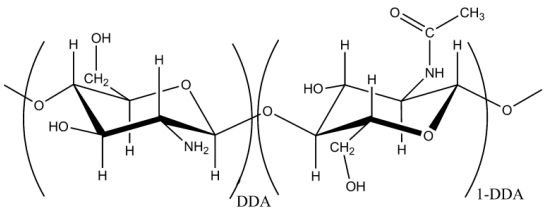

D-unit **A-**unit

Figure 2-7: Chemical structure of chitosan (A and D units represent N-acetyl-D-glucosamine and D-glucosamine, respectively). Adapted from [28] Copyright 2017, with Elsevier's permission.

Chitosan is characterized by its degree of deacetylation (DDA), molecular weight (MW), and polydispersity index (PdI) [28]. The DDA correspond to the molar fraction of D units and plays a major role in controlling the solubility and biodegradability of the polymer as degradation requires a specific pattern of A and D-units. The degree of deacetylation can be accurately measured using ^{1}H-NMR [205] and is calculated using the following equation:

$$DDA = D/((D + A)) \times 100 \qquad \text{Eq. 2-1}$$

The MW, expressed as number ($\overline{M}$n) and/or weight average ($\overline{M}$w), corresponds to the length of the polymer, wherefrom the degree of polymerization (Dp), or the number of monomers, can be derived using the following equation:

$$Dp = \frac{\overline{Mn}\ chitosan}{\overline{Mw}\ monomer\ at\ specific\ DDA} \qquad \text{Eq. 2-2}$$

The molecular weight is generally measured using size exclusion chromatography (SEC) coupled with single, double or triple detectors [19]. The PdI relates to the actual distribution of chain lengths following depolymerization (e.g. chemical or enzymatic) to target molecular weight and is calculated using the following equation:

$$PdI = \frac{\overline{Mw}}{\overline{Mn}} \qquad \text{Eq. 2-3}$$

Chitosan is a weak polybase with an intrinsic pKa of approximately 6.5-6.7, therefore, at lower pH values, the majority of amine containing D-units become protonated enabling interactions with polyanions (Figure 2-8). Electrostatic interaction between chitosan and nucleic acids leads to spontaneous formation of nanoparticles of different sizes and shapes [19, 206]. Additional properties such as mucoadhesive nature, biocompatibility, biodegradability, low toxicity, and

affordable cost of production [19, 207, 208] favored the extensive research and use of chitosan as a nucleic acid delivery system for *in vitro* and *in vivo* applications.

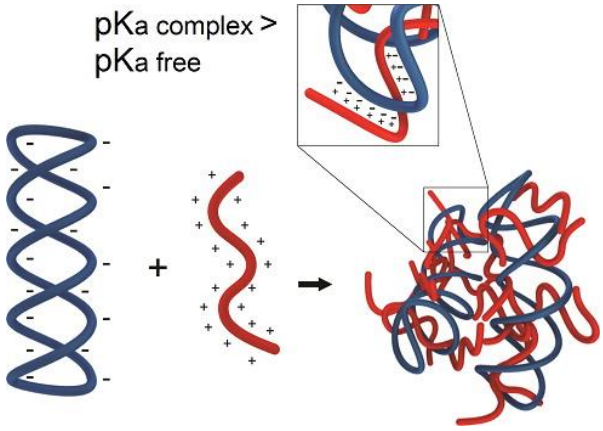

Figure 2-8: Spontaneous assembly of a chitosan-nucleic acid polyelectrolyte complex, or nanoparticle through electrostatic interactions. The nucleic acid depicted in this figure is a circular supercoiled plasmid DNA with a negatively charged phosphate backbone (blue) and the polymer is positively charged (red). The ball of wool or scrambled egg like structure has pKa above the pKa of free polymer (pKa ~6.5). Adapted from [209]. Copyright 2017, with American Chemical Society permission.

In the following sections of this chapter, the influence of chitosan molecular parameters (i.e. DDA, Mn, mixing ratio) on *in vitro* and *in vivo* transfection efficiency will be briefly presented. The effect of chitosan parameters on nanoparticle physicochemical properties i.e. size, surface charge, and shape will not be discussed unless otherwise stated. The reader is referred to Buschmann *et al* [19] for an excellent review on the subject.

2.3.4.1 Chitosan for the delivery of plasmid DNA

The influence of physicochemical parameters on *in vitro* transfection efficiency of chitosan-pDNA nanoparticles was investigated and maximum transgene expression was found to occur for particular combinations of DDA and molecular weights [37]. These results suggested that a fine equilibrium between payload condensation (avidity) and intracellular de-condensation is essential for high transfection efficiency. Isothermal titration calorimetry revealed that an increase in both DDA and Mn was accompanied with augmented binding affinities between the polyelectrolytes

[210]. Intracellular trafficking and nanoparticle de-complexation kinetics were measured using Förster-resonance energy transfer to confirm that nanoparticles with high binding affinity were unable to escape the endosome and release their cargo [39]. In Thibault *et al*, high DDA/low Mn chitosan disassembled at the same time as they escaped the endo-lysosomal vesicles around 12-hours post-transfection [39]. Increasing the Mn, and consequently, the binding affinity resulted in nanoparticles inability to disassemble following endosomal escape. In contrast, a decrease in both the Mn and/or DDA, thus in binding affinity, was shown to limit cell uptake [39] probably due to premature disassembly and reduced cargo protection in the nuclease-rich acidic endosome. In agreement with the above said, Kiang *et al* showed a positive correlation between decreased degrees of deacetylation, at a fixed Mn, and transfection efficiency [211]. Given that chitosan intrinsic pKa is around 6.5-6.7, a decrease in charge density (deprotonation) occurs at higher pH and is expected to decrease the binding affinity between the polyelectrolytes. Several studies have shown that optimal gene delivery is obtained between pH 6.5 and 7.0, efficiency quickly declining at higher pH due to the payload release [37, 38, 212, 213]. Lavertu *et al* showed that the increase in pH displaces the optimal Mn required for efficient transfection toward higher values (longer chains) in order to maintain nanoparticle integrity [37]. The N:P ratio, or chitosan amine-to-nucleic acid phosphate molar ratio, represent important parameter influencing nanoparticle physicochemical and biological properties [28, 206]. The N:P ratio was found to be important to balance nanoparticle stability and affect, along the degree of deacetylation, the net surface charge (ζ-potential) [213]. Ceteris paribus, an increase in N:P ratio is required to compensate for a decrease in Mn and/or DDA [211, 214]. Asymmetric field-flow fractionation (AF4) revealed that a significant fraction of polycations, in chitosan-based systems prepared at N:P above 2, are not associated with the nanoparticles [215]. The importance of this fraction in the promotion of efficient transfection was demonstrated in rescue experiments [216]. Human embryonic kidney cells (HEK-293), were transfected with nanoparticles prepared at N:P 2 and 5, and transgene expression occurred only for the N:P 5 formulation or those that were transfected with N:P 2 and rescued with free polycations. The role of free chitosan was hypothesized to facilitate endosomal swelling and subsequent escape through the proton sponge effect [216]. Low serum concentrations (~5-20%) have been shown, despite their negative effect on colloidal stability, to have a beneficial effect on *in vitro* transfection possibly due to increased cell activity or improved free chitosan uptake [38, 212].

In vivo, chitosan based nanoparticles were administered, mostly using local routes of administration probably due to 1) poor colloidal stability in blood and, 2) adjuvant effect. Intranasal administration showed the successful generation of a systemic Th1/Th2 immune response, with nanoparticles (~350 nm) able to elicit anti-HBsAg IgG levels above the clinical protective levels of 10 mU/mL [217]. Klausner *et al* showed that intra-corneal injection of ultra pure oligomeric chitosan-pDNA nanoparticles led to a 5-fold increase in gene expression compared to PEI [218]. Jean *et al* selected a number of formulations shown to maximize *in vitro* transfection in Lavertu *et al*, and found that maximum *in vivo* gene expression can be obtained with low Mn/High DDA formulations following intramuscular and subcutaneous administration [219, 220]. In contrast, the lower DDA/higher MW formulation (CS 80-80-5) produced high levels of neutralizing antibody resulting in very low detection of the recombinant protein [220] suggesting a differential use of specific formulations for gene delivery or genetic vaccination. In light of these encouraging results, chitosan-plasmid nanoparticles have been increasingly studied for therapeutic gene expression, as well as vaccination and the immunogenicity effect of high Mn/Low DDA elucidated [32].

2.3.4.2 Chitosan for the delivery of small interfering RNAs

The structural differences between pDNA and siRNA are believed to affect nanoparticles complexation/stability and transfection efficiency. In an attempt to investigate the effect of chitosan physicochemical properties, i.e. DDA, Mn and N:P ratio on *in vitro* knockdown nanoparticles were formed, with or without cross-linking agents i.e. tripolyphosphate (TPP), and transfected in different cell lines. *In vitro* knockdown efficiency was found to increase with increasing Mn irrespective of the degree of deacetylation [20, 22, 23, 26, 29, 221]. Liu *et al* showed that low Mn chitosan (10kDa) was unable to form stable nanoparticles and mediate efficient transfection [23]. However, Malmo *et al* showed that low molecular weight chitosan (10kDa) were able to transfect cells and yield efficient knockdown (~ 80%) when formulated at a similar N:P ratio [20]. Chitosan-mediated siRNA delivery has shown more efficient gene silencing at DDA above 80% [23]. However, the effect of the degree of deacetylation seemed minimal on knockdown [20, 22, 23, 26, 29, 221]. Therefore, most of the studies involving chitosan-siRNA nanoparticles were conducted at an intermediate DDA between 80-85 % [21-23, 25, 29] except for Malmo *et al*, where a fully deacetylated chitosan (DDA ~99%) was used to study the effect of Mn and N:P ratio on knockdown efficiency [20]. In contrast to most studies, Ragelle *et al* showed that chitosan was unable to form

stable particles and mediate efficient *in vitro* knockdown when formulated at 80% DDA. Improved knockdown required the addition of TPP, and was maximized when linear polyethyleneimine was incorporated into the nanoparticles to improve endosomal escape [21]. In a remarkable contrast to pDNA, almost all these reports, except for Holzerny *et al*, used very high N:P ratio (>25) into their formulations. Such formulations could pose significant practical problems for *in vivo* delivery such as limited dosing, blood incompatibility and non-specific effects due to large quantities of free excess chitosan. The effect of pH on transfection efficiency was not studied. However, transfection was conducted at pH 7.2 in the presence/absence of serum and showed high knockdown efficiency indicating that siRNA nanoparticles are able to knockdown target genes at physiological pH, further highlighting differences with pDNA [20, 22, 23, 25, 29]. In sum, several discrepancies, and the lack of uniformity in transfection protocols among these studies make overall comparisons difficult and renders the results inconclusive in identifying optimal parameters for siRNA delivery. Therefore a systematic study of siRNA delivery with accurately characterized chitosans that investigates the effect of intrinsic (DDA, Mn and N:P ratio) and extrinsic parameters (serum, pH, ionic strength and mixing conditions) on cell uptake, transfection efficiency, toxicity, genotoxicity, and hemocompatibility is needed before *in vivo* evaluation.

Several studies have demonstrated *in vivo* efficacy following intranasal [22], intratracheal [24], intraperitoneal [44, 222], and intravenous [42] administration. Intranasal administration of chitosan formulation 84-114 (DDA- Mn) at N:P 36 achieved 43% silencing efficiency in an EGFP transgenic mouse model following repeated administration of 1 mg/kg dose [22]. In this study, knockdown was not demonstrated using unbiased stereological methods. However, with a small number of animals (N=2) and the variegated nature of the transgenic model [223], careful conclusions as to objective knockdown should be considered. The same formulation *viz.* 84-114 formulated at N:P 63 was tested in a collagen-induced arthritis model (CIA) [224]. An objective reduction of 43% in plasma TNF-α level was observed with a concomitant improvement in the arthritic score. This study omitted to test inflammatory responses in all animals and to demonstrate *in vivo* mRNA a reduction. Intraperitoneal administration of chitosan 95-150 at 0.5 mg/kg in a unilateral ureteral obstructive model of kidney fibrosis showed an objective decrease in the target gene (cyclooxygenase 2, or COX-2) in macrophages. The decrease in COX-2, measured by qPCR (gene knockdown) and western blot (functional knockdown), correlated with a decrease in prostaglandin 2, pro-inflammatory cytokines, kidney injury molecule (KIM-1) and histological

markers. Interestingly, authors showed that peritoneal macrophages internalized the nanoparticles and preferentially migrated into the UUO kidney [44]. Gao *et al* demonstrated that fully deacetylated chitosan (DDA 99%), at intermediate Mn (40 kDa) and high N:P ratio of 60 accumulate in the kidney cortex following intravenous administration through Megalin-mediated endocytosis. Target gene knockdown was achieved (~50%) at both the mRNA and protein level following three administrations of 1 mg/kg [42]. In contrast, Ghosn *et al* showed that intravenous administration of chitosan and imidazole modified-chitosan accumulates in the liver with functional gene knockdown (GAPDH) achieved at doses ≥ 3 mg/kg [225].

2.4 Mechanisms of cell entry and endosomal escape of siRNA delivery systems

The polyanionic and relatively large molecular weight (~ 14 kDa) of siRNA limit its diffusion into the pharmacological site of action; the cell cytoplasm. Delivery materials, presented above, facilitate siRNA translocation into the cytoplasm by means of endocytosis (Box. 2-2). LNPs have been demonstrated to enter hepatocytes through LDL receptor and LDL receptor-related protein 1 (LRP-1) mediated endocytosis [60, 120]. LNPs undergo ApoE lipoprotein coating in the circulation and recognition by the LDL and LRP-1 receptors [120]. Gilleron *et al* found a biphasic internalization kinetic, with initial LNP uptake (rapid and inefficient) by clathrin-mediated endocytosis (receptor-dependent) followed by further accumulation by means of macropinocytosis (receptor-independent). Knockdown of the LDL receptor, LRP-1, and macropinocytosis regulators (CTBP1, Rac1, Rabankyrin-5) but not Caveolin-1 and CDC-42 (regulator of the clathrin-independent pathway) led to a significant decrease (~ 60%) in LNP internalization [60]. LNPs accumulate in early endosomes (EE)-late endosome (LE) hybrid vesicular structures. These findings were also confirmed by Wittrup *et al* who showed that payload release occurs predominantly at the EE/LE conversion steps instead of release from lysosomes [12].

Cationic polymers such as chitosan and polyethyleneimine have been shown to enter cells using clathrin-mediated endocytosis. However, several reports also showed that polymeric particles composed of either of these polymers showed cell type preferences for specific internalization pathways [226]. In contrast to LNPs, polymeric particles are more polydisperse and subject to rearrangements (aggregation, disintegration, coating, etc.) in the presence of high ionic strength

and protein thus influencing uptake and explain such discrepancies. Lipophilic conjugates have been demonstrated to incorporate LDL and HDLs and enter hepatocyte via the LDL and HDL receptors [175] and are hypothesized to enter cells via LDL and HDL receptor-mediated endocytosis. Cyclodextrin-based polymer decorated with Tf (CDP) use the transferrin receptor (TfR) to enter the cells via clathrin-mediated endocytosis. GlaNAc-conjugated DPCs or siRNA bind to hepatocyte ASGP receptor and enter the cells using clathrin-mediated endocytosis [2, 201].

Box. 2-2 Endocytosis definition, pathways, and dynamics

Endocytosis is an umbrella term of a form of active transport in which cells internalize large macromolecules in an energy dependent process [227]. Endocytosis pathways can be subdivided into two categories *viz.* receptor-dependent and independent pathways. Receptor-dependent pathways involve clathrin (CME), caveolae and Flotillin mediated endocytosis (CvME), and phagocytosis (specific for immune cells). The receptor-independent pathway includes a form of CME and macropinocytosis. Recently, endocytic pathways that do not fall into any of the previously mentioned categories have been discovered and are often referred to as clathrin and caveolae-independent pathways and occur at cholesterol-rich microdomains [228, 229]. Each of these pathways presents a set of features, distinct molecular events and involve complex molecular interactions which are reviewed in great details elsewhere [228, 229]. Regardless of the delivery method, the intracellular trafficking of the siRNA payload and the delivery system begins in the early endosome, progress into late endosomal vesicles, that become acidified (pH 5-6) by membrane-bound proton-pumps (ATPases), and relocates to the lysosomes. Lysosomes are further acidified (pH ~4.5) and contain various nucleases that promote degradation of the material and its payload. To avoid lysosomal degradation, the payload must escape at the early steps of the process (endosome) into the cytosol (see section 2.4).

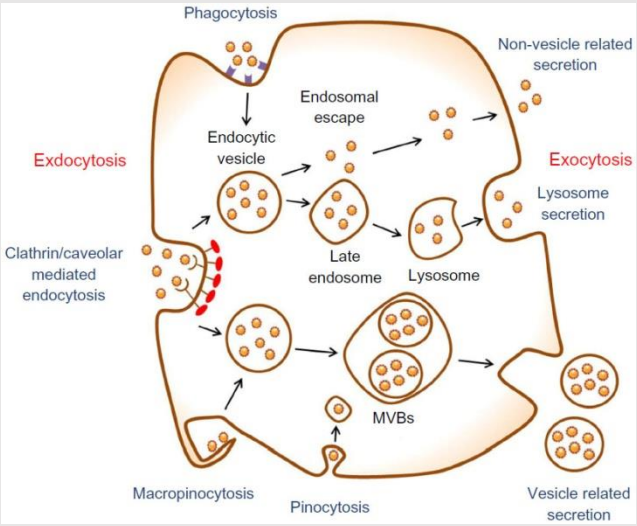

Figure 2-9: Different type of endocytosis. Image adapted from [227]. Copyright 2017, Dove Press

The internalization of the siRNA delivery system discussed above leads to sequestration in the dynamic endosomal compartments. Escape from these vesicles represents the most important barrier affecting the efficacy of the delivery systems and the intended therapeutic effect. The mechanisms of escape are still poorly understood and require future efforts to understand the mechanics and develop novel materials endowed with optimal escape capabilities.

2.4.1 Mechanism of escape of lipid nanoparticles

Lipid nanoparticles composed of cationic or ionizable lipids have intrinsic fusogenic properties [138, 230] that are also augmented when co-lipids with fusogenic properties are included in the formulation [231]. In the endosomes, cationic and ionizable lipids form ion-pairs with endogenous anionic lipids in the endosomal membrane and undergo a phase transition where they shift from the lamellar structure to the hexagonal H2 structure. This transition in shape promotes lipid rearrangement and fusion (Figure 2-10) [140, 232]. Cholesterol, a major component in LNPs (25-50% mol composition), has been found to play a major role in endosomal release by decreasing transition temperature of conical-shaped lipids, therefore aiding the conversion from the lamellar to the hexagonal phase [233]. Cholesterol is incorporated in LNPs to increase membrane rigidity, stability and cell internalization [10].

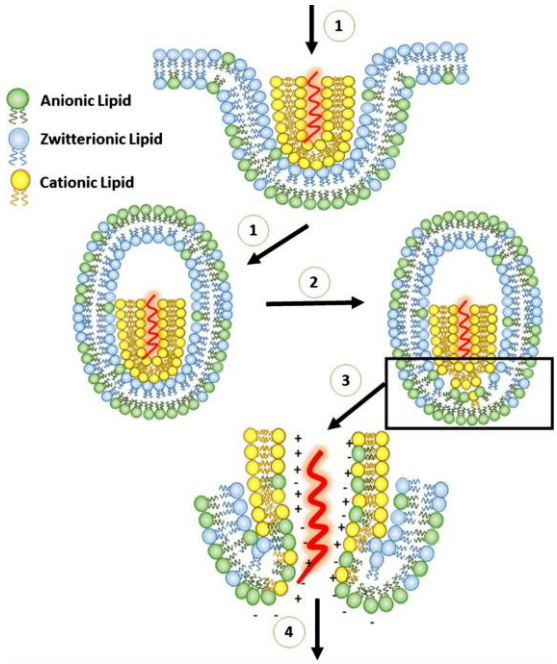

Figure 2-10 Schematic illustration of the uptake pathway and mechanism of endosomal release of cationic lipid nanoparticles. The schematic considers a receptor-independent mechanism of uptake. The same principle is believed to occur for ionizable lipid nanoparticles following PEG hydrolysis and ionization in the acidic environment of the endosome lumen. Adapted [136], Copyright 2017, Elsevier with permission.

2.4.2 Mechanism of escape of cationic polymers and cytoplasmic release

Cationic polymers such as polyethyleneimine, poly-L-lysine, and chitosan are believed to escape the endosome through the proton sponge effect [9]. During endosomal maturation, unsaturated amino groups on cationic polymers in the acidified environment of the endosome are capable of sequestering H^+ ions (protons) that are supplied by the v-ATPase. This process keeps the v-ATPase channels functioning and leads to the retention of one Cl^- ion and one H_2O molecule per proton. Water entering the endosomes creates organelle swelling and rupture leading to particle deposition in the cytoplasm [9, 234]. The exact mechanism that promotes dissociation of self-assembled cationic polymers is not fully understood. It was suggested that competition with cytoplasmic polyanions (i.e. proteins and nucleic acids) could lead to nanoparticle disassembly and payload release [235].

2.4.3 Mechanism of escape of molecular conjugates

The escape mechanism of the DPC system described in section 2.3.3.2 of this chapter is based on the properties of the endosomolytic polymer or protein used (depending on the version used). Mellitin (Mel) is a protein with pore forming properties. At low concentrations mellitin bind to membrane phospholipids and form amphipathic α-helix oriented structure parallel to the membrane, increasing Mel concentration triggers the protein to insert the membrane, forming pores [236] from which delivery materials can escape.

In the absence of escape mechanisms such as fusion, proton sponge, or pore-forming structure, the escape of GalNAc-siRNA conjugates remains to be elucidated. The exact mechanism cannot be elucidated pending the development of techniques allowing the intracellular tracking of low concentration of siRNAs in the endosome [60, 61]. However, Dowdy proposed that such escape could be the result of an extremely rare localized membrane destabilization event that occurs in the ASGPr recycling endosome [2]. The probability of such event increases with the rapid recycling rate of the receptor (~15-30 min) and the millions of siRNAs engaging their receptor consequently a number as low as 5000 siRNA could enter the cytoplasm and promote RNAi [61].

Chapter 3 ORGANIZATION OF ARTICLES

The scientific contribution made through this thesis is presented in this section. **Chapter 4 to 7** represent the core of this thesis and cover the research that was conducted to fulfill the objectives in Section 1.3. The results and their interpretation are presented in the form of published and submitted articles. The last two chapters of this thesis, or **Chapter 8** and **9**, represent a general discussion (**Chapter 8**) summarizing the implications of completed work, followed by a conclusion and future perspective (**Chapter 9**).

In Chapter 4, a simple enzymatic method was developed to overcome a technical challenge encountered during the extraction of total RNA following transfection with chitosan-siRNA nanoparticles. The developed method permitted the extraction of high-quality RNA for subsequent molecular analysis using quantitative real-time PCR. In addition, the developed method was proven to be useful to eliminate bias associated with membrane-bound fluorescently labeled nanoparticles during flow cytometry analysis of uptake. This work has been published in the *International Journal of Nanomedicine; 2010, IF 4.3* as a research manuscript entitled **Chitosanase-based method for RNA isolation from cells transfected with chitosan/siRNA nanocomplexes for real-time RT-PCR in gene silencing.**

In **Chapter 5**, selected formulations were tested for their ability to form nanoparticles with siRNA and characterized for their size, ζ-potential, shape, and evaluated *in vitro* for uptake, toxicity and knockdown efficiency in multiple cell lines. These formulations were selected based on a seminal paper by Lavertu *et al* where molecular properties favoring *in vitro* plasmid DNA delivery were identified. The results presented in this article demonstrate, for the first time, nanoparticles prepared at low N:P ratio had favorable physicochemical characteristics and promote both efficient cell uptake and target gene knockdown in multiple cell lines. These novel findings contrast, most published data where high N:P ratio was a prerequisite to form stable particles and promote *in vitro* knockdown. This work has been published in the *International Journal of Nanomedicine, 2012; IF 4.3* as a research manuscript entitled **Low molecular weight chitosan nanoparticulate system at low N:P ratio for nontoxic polynucleotide delivery.**

In **Chapter 6,** a library of chitosans was produced, accurately characterized and screened to investigate molecular properties favoring efficient *in vitro* and *in vivo* gene knockdown. In the first

part of the study, a full factorial design was used to screen the effect of chitosan molecular parameters such as the degree of deacetylation, molecular weight, N:P ratio on nanoparticle physicochemical characteristics (i.e. size, ζ-potential, payload encapsulation efficiency and integrity), and *in vitro* uptake, toxicity, and target knockdown efficiency. Formulations with the highest knockdown efficiency and low toxicity were further characterized for the effect of Mn and N:P ratio on toxicity, genotoxicity, and the role of increasing serum proteins on knockdown. The study demonstrated that maximization of the response variable was positively correlated with an increase in the degree of deacetylation, Mn and N:P ratio. The interaction effects were studied but not published. In this study, chitosan was demonstrated to perturb reference gene stability highlighting the need to conduct microarray studies. In a second part, the influence of chitosan molecular weight on hemocompatibility, *in vivo* biodistribution using ex-vivo imaging and target knockdown was investigated. Nanoparticles accumulated in kidney cortices, specifically in proximal epithelial tubular cells and induced gene knockdown. This work has been submitted to *Biomacromolecules; 2017, IF 5.83* as a research article entitled **siRNA delivery with chitosan: influence of chitosan molecular weight, degree of deacetylation and amine to phosphate ratio on *in vitro* silencing efficiency, hemocompatibility, biodistribution and *in vivo* efficacy.**

In **Chapter 7**, the toxicity and efficacy of formulations selected in **Chapter 6** were thoroughly assessed following intravenous administration and compared with cationic lipid nanoparticles (Invivofectamine®). First, formulations were characterized for their size, surface charge and polydispersity, and dose-dependent hemocompatibility as per ASTM guidelines. Hemocompatibility and hemagglutination were demonstrated to be dose and molecular weight dependent and could be totally abrogated through hyaluronic acid coating of nanoparticles. These findings allowed us to establish maximum dose to be injected for each type of formulation tested i.e. uncoated and HA coated. Immune stimulating properties, serological and hematological parameters were assessed in single ascending dose toxicity study. In contrast to LNPs, chitosan based formulations were safe and did not induce body weight loss upon single or multiple injections. *In vivo* biodistribution comparing uncoated *versus* HA coated nanoparticle revealed that both types of formulations accumulate in the proximal tubular cells of kidney cortices. However, potent target gene knockdown was only observed for uncoated nanoparticles. The enzymatic activity of GAPDH following knockdown was reduced by 50% further confirmed using multiple

techniques such as western blot and qualitative immunohistochemistry (IHC). In this study, we suggested several explanations for PTEC accumulation and poor performance of HA coated formulations that warrant further investigations. This work has been submitted to the *Journal of Controlled Release; 2017, IF 7.44* as a research article entitled: **Chitosan siRNA nanoparticles produce significant non-toxic functional gene silencing in kidney cortices** and is currently under review.

Chapter 4 ARTICLE 1: CHITOSANASE-BASED METHOD FOR RNA ISOLATION FROM CELLS TRANSFECTED WITH CHITOSAN/SIRNA NANOCOMPLEXES FOR REAL-TIME RT-PCR IN GENE SILENCING

Mohamad Alameh, Myriam Jean, Diogo DeJesus, Michael Buschmann, Abderrazzak Merzouki

Institute of Biomedical Engineering

Department of Chemical Engineering

École Polytechnique

P.O. BOX 6079, Station Centre-ville

Montréal (QC) Canada H3C 3A7

***Corresponding author**

Abderrazzak Merzouki, Ph.D.

Institute of Biomedical Engineering, Department of Chemical Engineering

École Polytechnique

P.O. BOX 6079, Station Centre-ville, Montréal (Québec) Canada H3C 3A7

Tel.: 514-340-5121, ext. 4799;

E-mail: abderrazzak.merzouki@polymtl.ca

Published in the International Journal of Nanomedicine (2010)

Abstract

Chitosan, a well-known natural cationic polysaccharide, has been successfully implemented *in vitro* and *in vivo* as a non-viral delivery system for both plasmid DNA and siRNA. While using chitosan/siRNA polyplexes to knock down specific targets, we have underestimated the effect of nucleic acids binding to chitosan when extracting RNA for subsequent quantitative PCR evaluation of silencing. *In vitro* transfection using chitosan/siRNA-based polyplexes reveals a very poor recovery of total RNA especially when using low cell numbers in 96 well plates. Here, we describe a method that dramatically enhances RNA extraction from chitosan/siRNA treated cells by using an enzymatic treatment with a type III chitosanase. We show that chitosanase treatment prior to RNA extraction greatly enhances the yield and the integrity of extracted RNA. This method will, therefore, eliminate the bias associated with lower RNA yield and integrity when quantifying gene silencing of chitosan-based systems using quantitative real-time PCR.

Keywords: Chitosan, Chitosanase, siRNA, DPP-IV gene silencing, RIN, qPCR

4.1 Introduction

Chitosan is a natural polymer of β (1-4)-glucosamine and N-acetyl-D-glucosamine derived by partial deacetylation of chitin from crustacean shells. [1] Chitosan has a pKa of approximately 6.5, therefore, at lower pH values, the majority of the glucosamine residues on chitosan is cationic due to the protonation of amine groups, which enables the interaction with anionic components such as nucleic acids and cell surface macromolecules. Industrially, the process of partial deacetylation of chitin is controlled to yield specific chitosan types – entities – characterized by their molecular weight (MW) as well as their degree of deacetylation (DDA). These two parameters have a major influence on chitosan biological and physicochemical properties. [2, 3] For example, increasing chitosan's DDA results in reduced biodegradability and biological activity given that acetyl groups promote its degradation by enzymes.

Recent studies have demonstrated the ability of chitosan to efficiently deliver a wide variety of biologics including proteins, [4-6] plasmid DNA [7-11] and siRNA, [12-14] both *in vitro* and *in vivo*. The effectiveness of delivery is generally assessed by evaluating the transfection efficiency for plasmid

DNA or gene silencing for siRNA. Quantitative assessment of gene silencing can be performed by quantitative real-time PCR analysis of targeted genes. The sensitivity and accuracy of the latter method is influenced by many variables including: 1) the quality of tissues/cells, 2) the RNA extraction method, 3) RNA integrity, and 4) the reverse transcription and polymerase chain reaction used in RT-PCR. [15-18] Despite the development of relative quantification techniques like the Pfaffl method [19] and the ΔΔCT method, [20] RNA integrity remains an important issue for generating proper data. While using siRNA-chitosan polyplexes to knock down specific targets, we have underestimated the effect of nucleic acids binding to chitosan when extracting RNA for subsequent quantitative PCR evaluation of silencing. In fact, polysaccharide matrices (ie. agarose and alginate) used for tissue engineering have been shown to interfere with techniques required for protein analysis and with all the procedures currently used for nucleic acid purification. [9, 21, 22] Moreover, our results – described herein– show that chitosan interferes with RNA extraction from low cell numbers. Therefore, we specifically examined this issue by delivering chitosan-siRNA nanoparticles against dipeptidyl peptidase IV (DPP-IV) mRNA in three different cell lines and found that siRNA-chitosan treated cells reveal a very poor recovery of total RNA. The DPP-IV gene encodes a serine protease that cleaves His: Ala: Glu sequence at the N-terminal region of the incretin hormone glucagon-like peptide 1 (GLP-1). GLP-1 regulates glucose homeostasis postprandialy thus decreasing its bioavailability and consequently causing a decrease in glucose level. The inhibition of DPP-IV increases GLP-1 bioavailability hence it represents a potential therapeutic for type II diabetes.

Here, we propose a method to overcome low RNA yield from chitosan/siRNA transfected cells this technical difficulty by enzymatically treating the cell lysate with *Streptomyces griseus* type III chitosanase in order to release mRNA that was bound to chitosan. In addition, we show that our technique is suitable for the removal of membrane-bound chitosan for subsequent analysis by FACS of transfected cells.

4.2 Materials and Methods

4.2.1 Preparation of chitosan/siRNA polyplexes

siRNA sequences targeting the DPP-IV gene sequence were synthesized by Dharmacon (Thermo Scientific, Dharmacon RNAi Technologies, USA) and are available in the On Target Plus® catalogue. The siRNA sequence has a dual strand modification pattern to reduce off-target effects caused by both strands.

A 10 kDa MW chitosan with a degree of deacetylation (DDA) of 92% was prepared and characterized as described previously [11] and dissolved overnight on a rotary mixer at 0.5% (w/v) in hydrochloric acid using a glucosamine: HCl ratio of 1:1. Chitosan solutions were then diluted with deionized water to reach the desired amine (deacetylated groups) to phosphate (of the nucleic acid) ratio (N/P ratio). Chitosan/siRNA polyplexes were formed at three different N/P ratios of 5, 10 and 20. Prior to mixing with siRNA, the diluted chitosan solutions were sterile filtered with a 0.2 µm syringe filter. Chitosan/siRNA nanoparticles were then prepared by adding 100 µl of the sterile diluted chitosan solution to 100 µl of siRNA (100nM) and mixed by rapid pipetting. The polyplexes were allowed to form during 30 min incubation at room temperature before transfection.

Polyplexes were measured independently using Dynamic Light Scattering (DLS) and environmental scanning electronic microscopy (ESEM) and found that polyplexes have a mean diameter of approximately 50 nm.

4.2.2 Cell culture

HT-29, HepG2 and Caco-2 cell lines from American Type Cell Culture (ATCC, Manassas, VA) were cultured in McCoys media (HT-29) and Dulbecco Minimum Essential Media (HepG2 and Caco-2) with 1.85 g/l of sodium bicarbonate and supplemented with 10% FBS (Cedarlane Laboratories, Burlington, ON) at 37˚C and 5% CO_2. These cell types were chosen since they express DPP-IV enzyme and represent models for diabetes research. For transfection, HT-29, HepG2 and Caco-2 cells were plated in 96-well culture plates (Corning, NY, USA) at 25,000 cells/well using 100 µl/well of complete medium. The cells were transfected the following day at ~50% confluency.

4.2.3 Transfection with chitosan/siRNA nanoparticle complexes

Complete transfection media (Dulbecco's Modified Eagle Medium high glucose, 4-Morpholineethanesulfonic acid (MES), pH 6.5) was equilibrated overnight in a 5% CO_2 37˚C incubator. Prior to transfection, pH adjustment to 6.5 was performed with 1 N sterile HCl (Sigma-Aldrich, St.Louis, MO). For transfection, medium over cells was aspirated and replenished with 100 µl transfection medium (DMEM HG, MES, pH 6.5) containing chitosan/siRNA complexes at a concentration of 10 pmol or 50 pmol siRNA/well corresponding to concentrations of 100 nM or 500nM siRNA. Cells were incubated with chitosan/siRNA complexes for 24 hours until analysis. All experiments were done in triplicates, with a minimum of three separate experiments to demonstrate reproducibility.

4.2.4 Transfection with Dharmafect1™

Dharmafect1™/siRNA complexes were prepared with a 1:2 ratio (w/v) of siRNA: Dharmafect1™ according to the manufacturer specifications and were used as a positive control.

Cells were incubated for four hours in presence of Dharmafect 1/siRNA complexes in serum-free medium then replenished with complete media (DMEM HG, 10% FBS, pH 7,4) and incubated for an additional 20 hours before analysis.

4.2.5 Chitosanase treatment of transfected cells and polyplexes degradation

Cells incubated with chitosan/siRNA polyplexes for 24 hours were treated with chitosanase (Sigma-Aldrich, cat # C9830) prior to RNA extraction in order to release anionic mRNA from potential binding sites on chitosan. A final concentration of 6.12 mU of chitosanase per µg of chitosan in DMEM at pH 6.5 (100 µl) or in RA1 lysis buffer (100 µl) + 2 µl of TCEP (Macherey-Nagel™) were used. RA1 lysis buffer containing chitosanase was used to assess the enzyme activity in presence of guanidium thiocyanate. Chitosanase resuspended in DMEM or in lysis buffer was directly applied onto cell monolayer. Cells were then incubated at 37 ˚C for 60 min prior to RNA extraction and quantification for gene expression as described below.

A second set of experiments using chitosan/ DPP-IV_{ODN} nanoparticules – with or without chitosanase treatment – were analyzed electrophoretically for the presence of chitosan and for OligoDeoxyNucleotides (ODN) release. Polyplexes were migrated for 120 min at 100V on a 13 %

polyacrylamide gel (BioRad Laboratories, Mississauga, ON) in 1X MES buffer (20 mM MES, 8 mM sodium acetate, pH 6.5) and stained using coomassie Brillant Blue R250 (BioRad Laboratories, Mississauga, ON) for chitosan visualization or ethidium bromide (0.5 µg/ml) for ODN visualization. Gel documentation and analysis were done using the bio-vision 3000 system and the Vision-Capt software (Vilbert Lourmat, Marne-la-Vallée, France).

4.2.6 FACS analysis

The cellular uptake of 5'6FAM labeled DPP-IV_{ODN} was analyzed using a BD Canto flow cytometer (Becton Dickinson, San Jose, CA) 24 hours post transfection. To determine the level of DNA cellular uptake, cells were transfected with polyplexes formed with 5'6FAM labeled DPP-IV_{ODN} as described above. Following 24 h incubation with polyplexes, cells were incubated with chitosanase for 60 min to dissociate and remove cell surface-associated complexes. For flow cytometry analysis, cells were washed twice in PBS, trypsinized and resuspended in ice-cold PBS. For each sample, 20,000 events were counted and a dot plot of the forward light scatter against the side scatter was used to establish a collection gate to exclude cell debris, dead cells and aggregates of cells. The 5'6FAM-positive cells were excited using a 488-nm laser line and detected using a 530/30-nm band pass filter. To distinguish between autofluorescence and fluorescently labeled cells, we ran non-transfected cells as negative controls. The cellular uptake of the polyplexes was calculated as the percentage of 5'6FAM-DPP-IV_{ODN} labeled cells, and the relative amount of the internalized 5'6FAM-DPP-IV_{ODN} was estimated from the median fluorescence intensity of the 5'6FAM-positive population.

4.2.7 Confocal imaging

Polyplexes internalization was studied by confocal imaging. Chitosans were labeled with fluorescent rhodamine B isothiocyanate (RITC) (Sigma-Aldrich, St-Louis, MO) and DPP-IV_{ODN} (21 nucleic acid) were labeled with 6-FAM on their 5'extremities (Integrated DNA Technologies, inc). Cells were seeded 24 h prior to transfection in 35 mm glass bottom culture dishes (MatTek, Ashland, MA) using 500 µl of complete medium at 40,000 cells/dish. Chitosan/ODN polyplexes were incubated with cells at a concentration of 2.5 µg ODN/wells in media containing 10% serum at pH 6.5 for 24 h. Colocalisation was assessed qualitatively by the occurrence of yellow pixels resulting from the spatial overlap of red (Chitosan pseudocolor) and green pixels (ODN

pseudocolor) from 2 separate channels. Prior to imaging, cell membranes were stained for 5 min at 37°C with 5 ug/ml of Cell Mask™ Deep red (Invitrogen, Carlsbad, CA) in complete media followed by two washes with cold PBS solution and resuspension in complete media. Imaging of live cells was done with a Zeiss LSM 510 META confocal Axioplan 200 microscope (Carl Zeiss AG, Feldbach, Switzerland).

4.2.8 RNA extraction and assessment methods (yield, purity and integrity)

RNA extraction was performed using the RNA XS® extraction kit from Macherey-Nagel (Biolynx, Montréal, QC) according to the manufacturer protocol. For comparison purposes, RNA was also extracted with RNAqueous® from Ambion (Applied Biosystems, Streetsville, ON) according to the manufacturer protocol. Total RNA was quantified and RNA integrity measured using the Agilent BioAnalyzer 2100 (Agilent technologies, Mississauga, ON) following the manufacturer's protocol. RNA integrity was evaluated by the ratio of 28S/18S ribosomal RNA (rRNA) [23] and the RNA integrity number (RIN). Agilent 2100 BioAnalyzer uses automated microfluidics, capillary electrophoresis, and fluorescence to evaluate RNA integrity. The RIN is a related measure of RNA quality that is based on a larger portion of the electrophoretic trace. The BioAnalyzer 2100 automatically computes this parameter, and an ideal non-degraded RNA sample has a RIN of 10.

4.2.9 TaqMan® Gene Expression Assays – Endogenous controls

Gene expression level for endogenous controls was determined using pre-validated Taqman Gene Expression Assays (Applied Biosystems, Streetsville, ON) PCR reactions for 384 well plate formats were performed using 1.5 µl of cDNA samples (25-50 ng), 5 µl of the Fast Universal qPCR MasterMix (Applied Biosystems, Streetsville, ON), 0.5 µl of the TaqMan Gene Expression Assay (20X) and 2.5 µl of water in a total volume of 10 µl. The following genes were used as endogenous control: TBP (TATA binding protein) and HPRT (hypoxanthine guanine phosphoribosyl transferase).

4.2.10 Universal Probe Library (UPL) Assays

Gene expression levels were determined using assays designed with the Universal Probe Library from Roche (www.universalprobelibrary.com). This technology utilizes short hydrolysis probes of 8 or 9 bases. The high melting temperature characteristic of longer probes is retained by using

Locked Nucleic Acid (LNA) nucleotide chemistry in these shorter probes. Since probes are only 8 or 9 bases long, each probe can hybridize to over 7,000 transcripts; thus, a set of only 100 probes can enable the quantification of virtually any transcript in a transcriptome. RNA samples were reverse transcribed into cDNA using the first strand cDNA transcriptor kit following the manufacturer protocol (Roche, Laval, QC). PCR reactions for 384 well plate formats were performed using 2 µL of cDNA samples (25 ng), 5 µl of the Fast Universal qPCR MasterMix (Applied Biosystems, Streetsville, ON), 2 µM of each primer and 1 µM of a UPL probe # 71 (Roche, Laval, QC) in a total volume of 10 µL.

4.2.11 Detection and analysis

The ABI PRISM® 7900HT Sequence Detection System (Applied Biosystems) was used to detect cDNA amplification level and was programmed with an initial step of 3 minutes at 95˚C, followed by 45 cycles of: 5 seconds at 95˚C and 30 seconds at 60˚C. All reactions were run in triplicates and the average values of Ct (cycle threshold) were used for quantification. TBP (TATA binding protein), HPRT (hypoxanthine guanine phosphoribosyl transferase), were used as endogenous controls.

The relative quantification of target genes was determined using the △△CT method. Briefly, the Ct values of target genes were referenced to an endogenous control gene ($\triangle CT = Ct_{target} - Ct_{endoC}$) and compared with a calibrator: $\triangle\triangle CT = \triangle Ct_{Sample} - \triangle Ct_{Calibrator}$. Relative expression (RQ) was calculated using the Sequence Detection System (SDS) 2.2.2 software (Applied Biosystems) using the formula $RQ = 2^{-\triangle\triangle CT}$.

4.2.12 Statistical Analysis

The measurement data were collected and expressed as means values ± standard deviation (SD). And were analyzed with the Statistica 9.0 (STATSOFT; Statistica, Tulsa, OK, USA). The Statistical significance was determined by one-way ANOVA followed by Newman-keuls post hoc test. Differences were considered significant at $p<0.05$ and highly significant at $p<0.01$.

4.3 Results

4.3.1 Cellular Uptake

Transfection efficiency of Chitosan 92-10-5/DPP-IV$_{ODN}$, Chitosan 92-10-10/ DPP-IV$_{ODN}$ and Chitosan 92-10-20/ DPP-IV$_{ODN}$ complexes in HepG2 cells was evaluated using flow cytometry. We found out that polyplexes sedimentation on the cell surface adds a bias to cytometry data when calculating the percentage of positive cells or determining fluorescence intensity levels to assess the amount of internalized oligonucleotide.

Our results show that almost 90% ± 2 of HepG2 cells internalized the polyplexes and no significant difference between the three N/P ratios was observed (Figure 4-1, a). Following chitosanase treatment, approximately a 10% reduction in the positive cell population was observed indicating that trypsinization and thorough washing alone did not fully dissociate surface bound polyplexes (Figure 4-1, a). Furthermore, confocal imaging shows membrane associated polyplexes following thorough washing which supports our FACS data. Although the percentage of 6FAM- DPP-IV$_{ODN}$ positive cells was similar for the three N/P ratios, the amount of the internalized DPP-IV$_{ODN}$, as determined from the fluorescence intensity levels, varied as shown in (Figure 4-1, b).

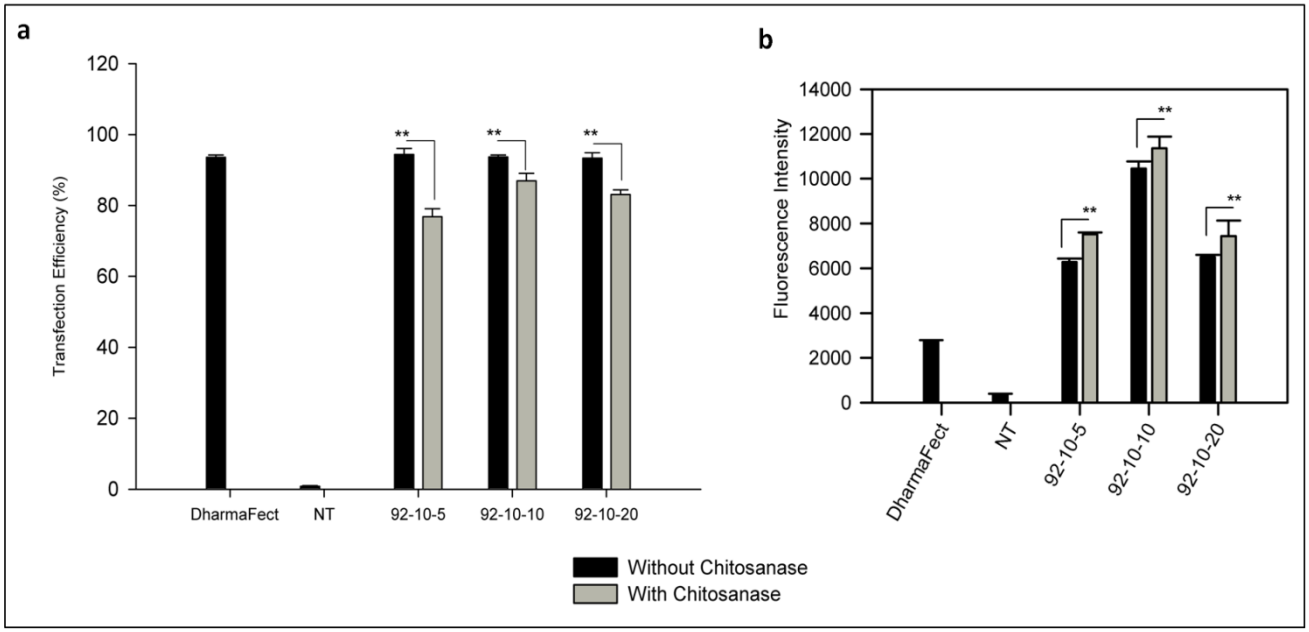

Figure 4-1. FACS analysis of chitosan/DPP-IVODN polyplexes uptake in HepG2 cell line. Uptake of 5'-6FAM labeled DPP-IVODN in chitosanase treated and untreated cells 24 hours post transfection. a) Transfection efficiency was calculated as the percentage of 5'FAM-D

Moreover, cells incubated with formulations that had higher N/P ratios showed lower amounts of internalized DNA. The excessive cellular uptake of polyplexes was further confirmed by confocal imaging, as shown in Figure 4.2. Large internalized assemblies of complexes were observed 2 h post incubation and an optimal dissociation was observed 24 h post transfection (Figure 4-2). The transfection efficiency of each group was evaluated in three independent experiments using flow cytometry.

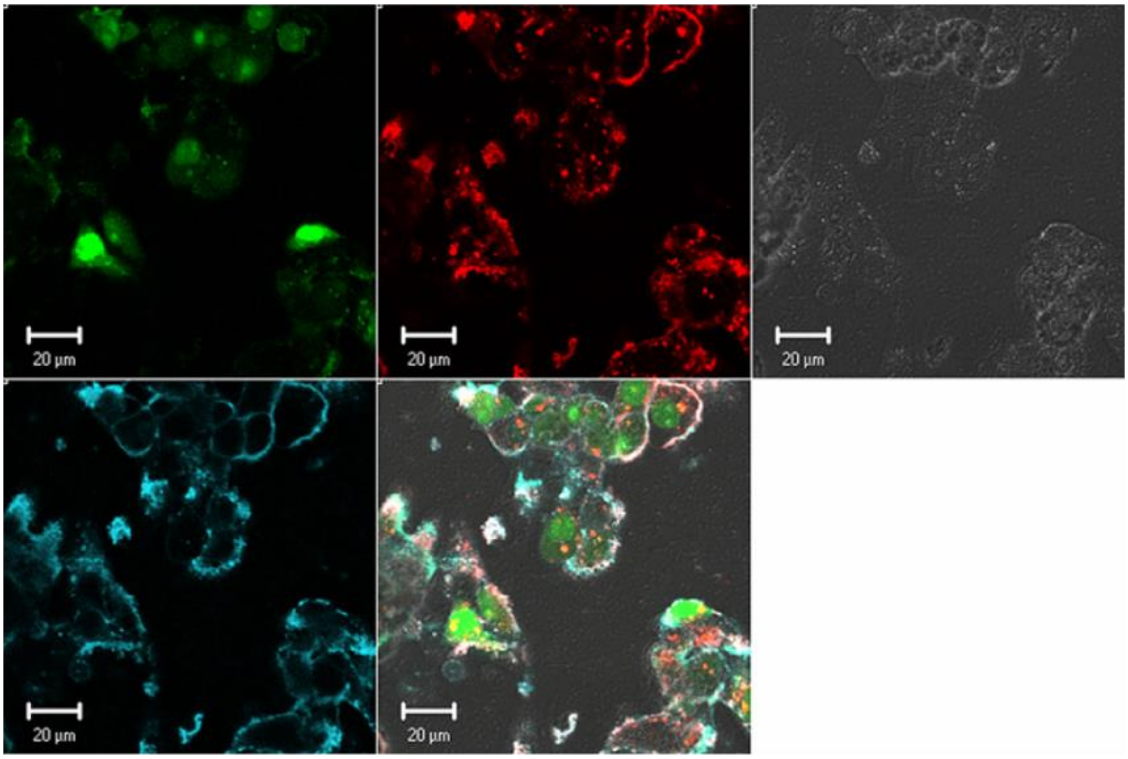

Figure 4-2. Confocal imaging of polyplexes uptake. Confocal microscopy images of HepG2 live cells 24 h post transfection with chitosan/DPP-IV_{ODN} polyplexes (N/P=5). Chitosan 92-10 (DDA, MW) was labeled with Rhodamine (red), the DPP-IV_{ODN} with 6FAM at the 5'extremity (green) and the cell membranes were stained prior to imaging with cell mask (blue). Membrane staining was performed to differentiate between internalized and membrane bound polyplexes.

4.3.1 Effect of low molecular weight chitosan on RNA recovery

The effect of low molecular weight chitosan (DDA=92, MW=10 kDa) at different N/P ratios on RNA extraction was assessed using the Bioanalyzer 2100 system (Figure 4-3). These results show very poor recovery of total RNA from low number cells transfected with chitosan/siRNA polyplexes compared to both DharmaFect®1 treated and non-transfected cells (Figure 4-3). We found that the majority of the samples had a recovery level below the detection threshold (10 ng/µl, RNA Integrity Number (RIN) >7). Additionally, our results indicated that lower N/P ratios or lower amounts of added polyplexes (corresponding to 50 pmol to 10 pmol siRNA per well) did not improve total RNA yield. The extraction efficiency with or without chitosanase treatment was evaluated in three independent experiments with triplicate in each experiment.

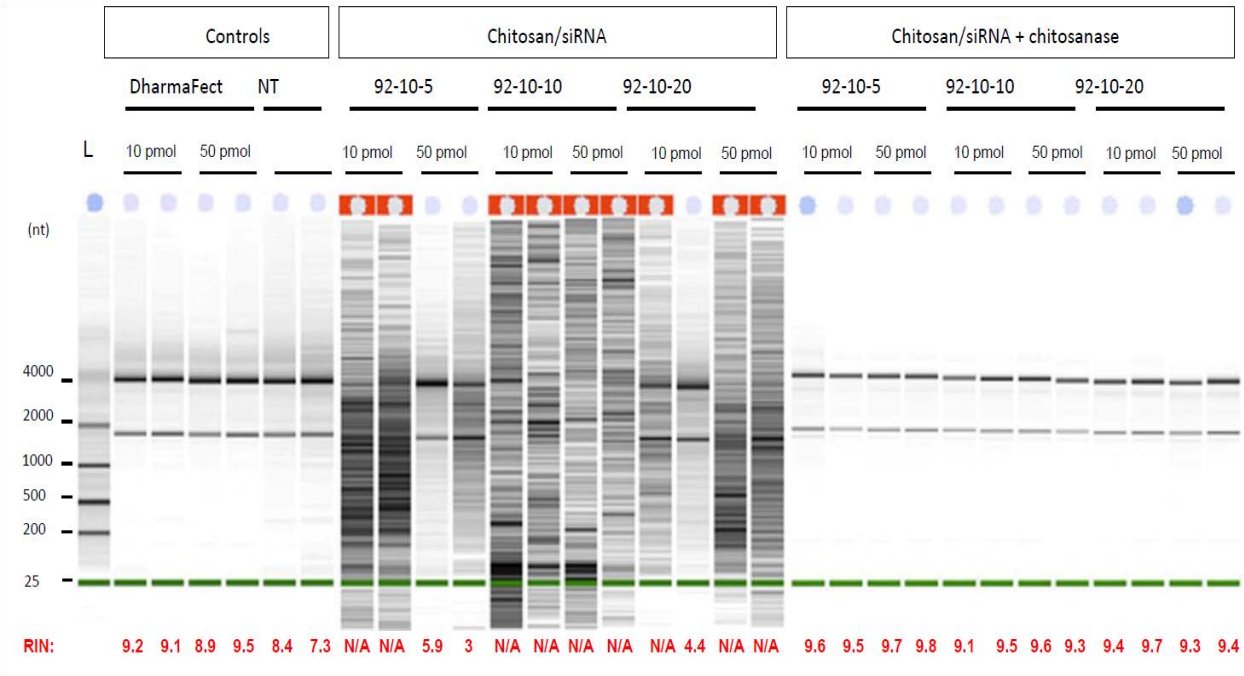

Figure 4-3: Effect of *Streptomyces griseus* chitosanase on yield and integrity of total RNA extraction. Total RNA extraction was performed on HepG2 cells transfected with 10 pmol and 50 pmol of nanoparticles siRNA/chitosan at 3 different N/P ratios indicated by the formulation code 92-10-5, 92-10-10 or 92-10-20 (DDA, MW, N/P). Chitosanase was resuspended in DMEM pH 6.5 and directly applied to cells at a final concentration of 6.12mU/µg of chitosan. Total RNA was extracted from chitosan transfected cell treated with or without chitosanase. The different

extractions were compared to control Dharmafect™ 1 transfected cells and non-transfected (NT) cells. (nt) = nucleotide, L= standard ladder, the green band is a lower marker, which allows sample alignment and permits comparison for RIN calculation. RIN= RNA integrity number, is an algorithm based numbering system that calculate RNA integrity with 10 being the most intact and 1 being fully degraded.

4.3.2 Effect of lysis buffer on Chitosanase activity

We assessed both the effect of guanidium thiocyanate, a chaotropic agent, contained in commercial RA1 lysis buffer and high DDA (92% and 98% respectively) on *S.griseus* chitosanase activity. First, chitosan polyplexes were digested with *S.griseus* chitosanase and were compared to non-digested samples (Figure 4-4).

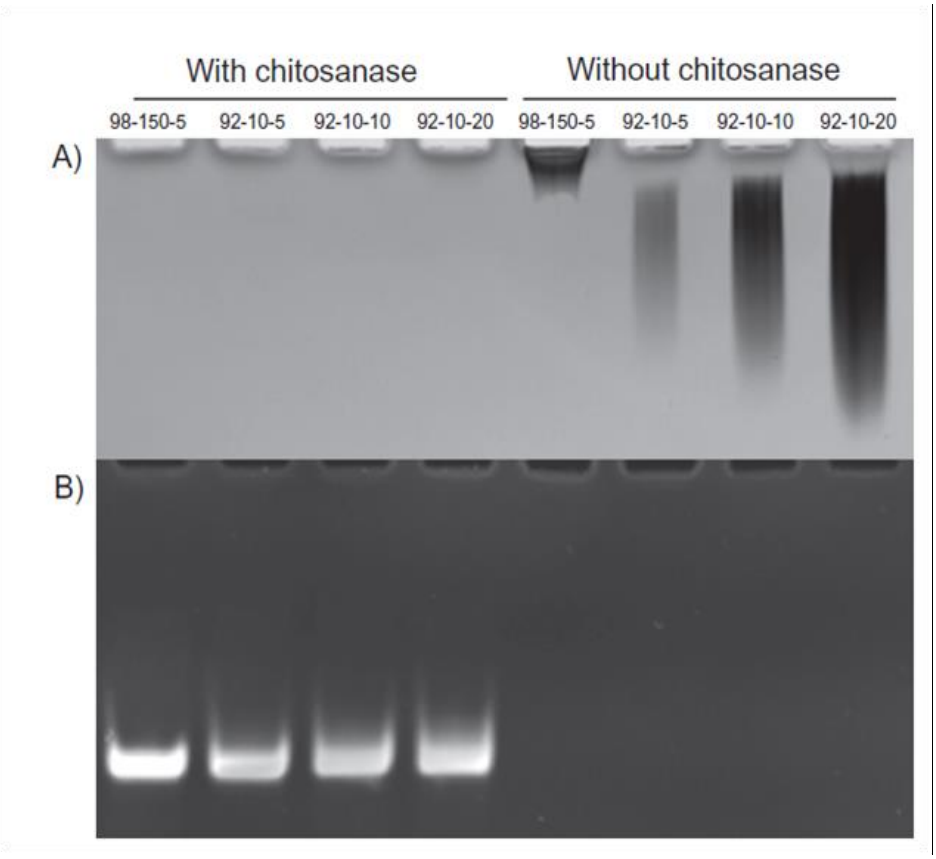

Figure 4-4: Polyacrylamide gel electrophoresis of chitosan/DPP-IV$_{ODN}$ polyplexes bearing different DDAs and N/P ratios, treated with or without Streptomyces griseus chitosanase. a) chitosan migration b) ODN migration. Lane 1 to 4 corresponds to chitosan/DPP-IV$_{ODN}$ directly incubated with chitosanase during 60 minutes at 37ºC. Chitosan digestion allows the ODN

release. Lane 5 to 8 corresponds to chitosan/DPP-IV_{ODN} incubated at the similar conditions without chitosanase. Faster chitosan migration was observed when comparing lanes 5 and 6 due to different MW of theses formulations. Increased band intensity (lane 4-8) results from greater amounts of chitosan at higher N/P ratios

Our results show that chitosan digestion was not affected at high DDA (98%). Moreover, DPP-IV_{ODN} liberated from chitosanase treated polyplexes showed a quasi-total recovery indicating that smaller monomers did not bind nucleic acid. Second, chitosanase activity was assessed in lysis buffer. Our results show that *S.griseus* chitosanase activity is not altered or reduced in lysis buffer (Figure 4-5). These results suggest that the chitosanase digestion can be performed directly in the lysis buffer decreasing the processing time of the sample (Figure 4-5).

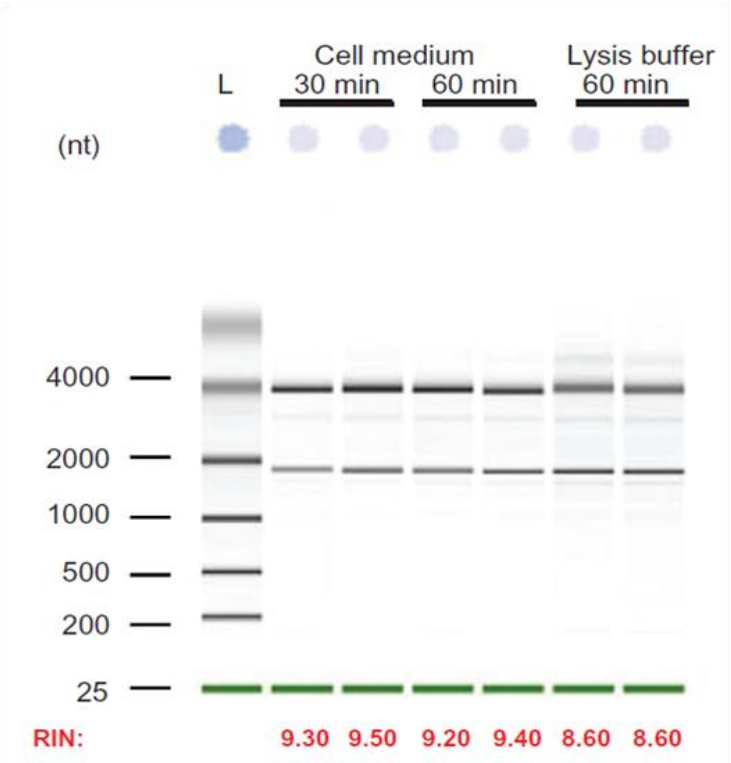

Figure 4-5: Total RNA extraction from HepG2 transfected cells with 10 pmol siRNA. Following transfection, cells were treated with chitosanase for: a) 30 min, b) 60 and c) 60 min in lysis buffer.

4.3.3 Gene silencing

The ability of chitosan 92-10-5 formulation to deliver DPP-IV siRNA in three different cell lines was assessed using qPCR. Our results revealed an 80% and 78% silencing of the DPP-IV gene in HepG2 and Caco-2 cell lines respectively when compared to non-transfected cells. These results are similar to the liposome based positive control, Dharmafect 1™ (Table 4-1). Moreover, total RNA recovery from low cell number without chitosanase treatment was very low with RIN values below the set threshold accounting for the inability to assess gene inhibition using qPCR (Table 4.1). HT-29 cell line was difficult to transfect using this specific chitosan/siRNA formulation due to the absence of cellular uptake as shown by our FACS and confocal microscopy results (data not shown). Although HT-29 cell line was difficult to transfect, recovery of total RNA was poor most probably due to extracellular excess of chitosan and to membrane bound polyplexes. Cellular viability in HepG2, Caco-2 and HT-29 cell lines was maintained after addition of the different chitosan formulations used for transfection, dismissing the likelihood of toxicity effects. Gene silencing was evaluated in two independent experiments with triplicate in each experiment.

Table 4-1: Effect of chitosanase treatment on RNA extraction, Relative Integrity Number (RIN) and real-time PCR (qPCR) analysis in three different DPP-IV expressing cell lines. Inhibition percentages of DPP-IV gene expression in siRNA/polyplexes transfected cells were determined in comparison with non-transfected cells: Effect of chitosanase treatment on RNA extraction, Relative Integrity Number (RIN) and real-time PCR (qPCR) analysis in three different DPP-IV expressing cell lines. Inhibition percentages of DPP-IV gene expression in siRNA/polyplexes transfected cells were determined in comparison with non-transfected cells

Cell line	Chitosan/siRNA			Chitosan/siRNA+ chitosanase		
	RNA extraction		qPCR	RNA extraction		qPCR
	RIN	[total RNA] ng/µl	Inhibition %	RIN	[total RNA] ng/µl	Inhibition %
HepG2	3.0	2.6	N/A	9.0	78	82
HT-29*	2.3	1.7	N/A	9.3	83	20
Caco-2	4.7	3.9	N/A	8.7	76	78

*HT-29 cells were difficult to transfect.
N/A: not applicable, RIN below the set threshold required for qPCR.

4.4 Discussion

Current methods and commercial kits for RNA isolation are based on the use of acid guianidium thiocyanate buffers for cell lysis and protein denaturation. Depending on the methods used, either a phase separation followed by RNA precipitation is performed (TRIzol®) or silica based matrices (RNeasy®; RNA XS®) are used to electrostatically bind and recover RNA through washing and elution steps. These methods present major drawbacks when large polysaccharide fragments are present after sample digestion. These polysaccharide fragments can entrap nucleic acids physically thus reducing RNA after centrifugation. [24] Chitosan is a polymeric cation that has been shown to prevent the efficient purification of nucleic acids from cell entrapped matrices using available procedures and commercial kits. [10, 21] The low efficiency of purification is mainly due to the amine groups, which are protonated in acidic environments [25] such as the guanidinium thiocyanate buffer used in both Trizol® and silica based kits [26] hence promoting nucleic acid entrapment and/or binding. Another explanation to the poor recovery of total RNA when using silica based column is the fact that polysaccharide contaminants have been shown to decrease significantly the efficiency of spin columns. [26] To resolve these issues associated with chitosan protonation, successful attempts have been made to adjust the pH of guanidinium thiocyanate extraction buffers. [27] However, RNA purity ratio could not be measured adequately due to possible polysaccharide contamination. In our study, we showed that chitosan/siRNA transfection of low cell numbers resulted in a poor recovery of total RNA for subsequent transcriptomic analysis. The poor recovery might be due to the high binding affinity of chitosan to nucleic acids as recently quantified. Notably, the majority of the chitosan in these preparations is soluble and not complexed to the polynucleotide according to our recent data using Asymetric Field Flow Fractionation.[28] The main effect of chitosanase treatment may then be to eliminate the free fraction that could clearly bind to polyanionic mRNA and inhibit its extraction from chitosan treated cells. This binding effect would be further accentuated in the cell lysis buffer containing guanidium thiocyanate which has an acidic pH of ~5 and increases ionization of chitosan therefore augments its binding affinity to polynucleotides.

According to their hydrolysis specificity of the β-glycosidic linkages in partially N-acetylated chitosan molecules, chitosanase can be classified into 3 classes. *Streptomyces griseus* chitosanase is a type III enzyme that catalyzes both the endohydrolysis of β-(1-4)-linkage between N-

acetylglucosamine and D-glucosamine (GlcNAc-GlcN) and between D-glucosamine (GlcN-GlcN) residues in chitosane. [29] Sato *et al* found that the relative activity of the enzyme was 80% when degrading chitosan with 90% DDA compared to a 100% activity in the presence of chitosan with 70% DDA. [29, 30] However, despite a lower activity when degrading high DDAs chitosan (>90%), *Streptomyces griseus* chitosanase is a powerful tool for nucleic acid recovery from chitosan nanoparticules bearing different DDAs as shown in this study. Our results show a dramatic enhancement in RNA yield and integrity when treating cells with *S. griseus* chitosanase for 60 minutes prior to extraction. In addition, RNA yields – from transfected cells– are similar to those of non-transfected cells, suggesting a total recovery of RNA from chitosan transfected cells. Furthermore, our results show that a 30 minutes treatment can be sufficient to improve total RNA yield thus reducing sample processing time.

Although guanidium thiocyanate is a potent chaotropic agent that alters dimensional structures of proteins including endonucleases,[31] its concentration in RA1 lysis buffer does not seem to alter the function of this specific chitosanase. This observation is supported by the fact that some chitosanases are resistant to the high concentration of denaturants such as urea or guanidium thiocyanate.[32-34] The chitosanase treatment of DPP-IV_{ODN}/chitosan polyplexes permitted the recovery of ~ 90% of the complexes ODN showing that the digestion of the low MW chitosan – 92-10-5 – into smaller monomers did not interact with ODN release nor with silica based matrices for RNA purification.

This new method has permitted us to obtain enough RNA with high integrity numbers to perform subsequent real-time RT-PCR and analysis. Our results revealed an 80% silencing of the DPP-IV gene with chitosan/siRNA when compared to non-transfected cells. Furthermore, silencing using this specific formulation achieved comparable efficiencies to the positive control Dharmafect™1 liposome, suggesting the potential use of these chitosan formulations to deliver siRNA both i*n vitro* and *in vivo*. HT-29 cell line was found to be more difficult to transfect with the specific chitosan/siRNA formulation, in particular at the cell uptake level as determined by FACS and confocal microscopy (data not shown). This observation is supported by the fact that chitosan has shown cell type dependency when transfecting DNA plasmid. [35]

The silencing effect was also observed at the protein level where we observed a decrease in DPP-IV levels of approximately 55%, 48 hours post transfection (data not shown) demonstrating the

ability of the specific chitosan formulation to efficiently deliver siRNA against DPP-IV mRNA. The FACS analysis of DPP-IV_{ODN} positive cells showed approximately 80% transfection efficiency following chitosanase treatment. The latter permitted a reduction of ~10% in transfection efficiency when compared to the chitosanase untreated cells. The 10% signal bias is possibly due to the membrane bound chitosan as supported by confocal imaging. Therefore, this reduction may account for biased data hence increasing accuracy of transfection efficiency quantification.

4.5 Conclusion

In this study, we have demonstrated that i) mRNA is difficult to extract from chitosan/siRNA transfected cells for subsequent quantification of gene expression, ii) a relatively simple and inexpensive technique based on enzymatic digestion of chitosan permits the extraction and recovery of total RNA for subsequent quantification of messenger levels by qPCR, iii) the method described is suitable for the removal of membrane bound chitosan for FACS analysis of transfection efficiency when using labeled siRNA or ODNs, as a result reducing false positive data. Thus, this new method permits the quantification of gene silencing in chitosan delivery systems and eliminates any bias associated with chitosan binding to polynucleotides.

Acknowledgements

This work was supported by the Canadian Institutes of Health Research (CIHR). The authors thank the members of Pr. Buschmann Research Group for their assistance.

Disclosures

The authors report there are no conflicts of interest relevant to this research.

References

1. Illum L. Chitosan and its use as a pharmaceutical excipient. *Pharm Res.* Sep 1998;15(9):1326-1331.
2. Huang M, Khor E, Lim LY. Uptake and cytotoxicity of chitosan molecules and nanoparticles: effects of molecular weight and degree of deacetylation. *Pharm Res.* Feb 2004;21(2):344-353.
3. Zhang H, Neau SH. In vitro degradation of chitosan by a commercial enzyme preparation: effect of molecular weight and degree of deacetylation. *Biomaterials.* Jun 2001;22(12):1653-1658.
4. Prego C, Torres D, Alonso MJ. Chitosan nanocapsules as carriers for oral peptide delivery: effect of chitosan molecular weight and type of salt on the in vitro behaviour and in vivo effectiveness. *J Nanosci Nanotechnol.* Sep-Oct 2006;6(9-10):2921-2928.
5. Prego C, Fabre M, Torres D, Alonso MJ. Efficacy and mechanism of action of chitosan nanocapsules for oral peptide delivery. *Pharm Res.* Mar 2006;23(3):549-556.
6. Prego C, Torres D, Fernandez-Megia E, Novoa-Carballal R, Quinoa E, Alonso MJ. Chitosan-PEG nanocapsules as new carriers for oral peptide delivery. Effect of chitosan pegylation degree. *J Control Release.* Apr 10 2006;111(3):299-308.
7. Jean M, Smaoui F, Lavertu M, et al. Chitosan-plasmid nanoparticle formulations for IM and SC delivery of recombinant FGF-2 and PDGF-BB or generation of antibodies. *Gene Ther.* Sep 2009;16(9):1097-1110.
8. Centelles MN, Isasi JR, Qian C, Campanero MA, Irache JM. Influence of the chitosan nature on the transfection efficacy of DNA-loaded nanoparticles after hydrodynamic administration in mice. *J Microencapsul.* Feb 15.
9. Zheng F, Shi XW, Yang GF, et al. Chitosan nanoparticle as gene therapy vector via gastrointestinal mucosa administration: results of an in vitro and in vivo study. *Life Sci.* Jan 2 2007;80(4):388-396.

10. Zheng Y, Yang W, Wang C, et al. Nanoparticles based on the complex of chitosan and polyaspartic acid sodium salt: preparation, characterization and the use for 5-fluorouracil delivery. *Eur J Pharm Biopharm.* Nov 2007;67(3):621-631.

11. Lavertu M, Methot S, Tran-Khanh N, Buschmann MD. High efficiency gene transfer using chitosan/DNA nanoparticles with specific combinations of molecular weight and degree of deacetylation. *Biomaterials.* Sep 2006;27(27):4815-4824.

12. Howard KA, Rahbek UL, Liu X, et al. RNA interference in vitro and in vivo using a novel chitosan/siRNA nanoparticle system. *Mol Ther.* Oct 2006;14(4):476-484.

13. Futami K, Kumagai E, Makino H, et al. Anticancer activity of RecQL1 helicase siRNA in mouse xenograft models. *Cancer Sci.* Jun 2008;99(6):1227-1236.

14. Gao S, Dagnaes-Hansen F, Nielsen EJ, et al. The effect of chemical modification and nanoparticle formulation on stability and biodistribution of siRNA in mice. *Mol Ther.* Jul 2009;17(7):1225-1233.

15. Bustin SA. Quantification of mRNA using real-time reverse transcription PCR (RT-PCR): trends and problems. *J Mol Endocrinol.* Aug 2002;29(1):23-39.

16. Ginzinger DG. Gene quantification using real-time quantitative PCR: an emerging technology hits the mainstream. *Exp Hematol.* Jun 2002;30(6):503-512.

17. Fleige S, Walf V, Huch S, Prgomet C, Sehm J, Pfaffl MW. Comparison of relative mRNA quantification models and the impact of RNA integrity in quantitative real-time RT-PCR. *Biotechnol Lett.* Oct 2006;28(19):1601-1613.

18. Fleige S, Pfaffl MW. RNA integrity and the effect on the real-time qRT-PCR performance. *Mol Aspects Med.* Apr-Jun 2006;27(2-3):126-139.

19. Pfaffl MW. A new mathematical model for relative quantification in real-time RT-PCR. *Nucleic Acids Res.* May 1 2001;29(9):e45.

20. Arocho A, Chen B, Ladanyi M, Pan Q. Validation of the 2-DeltaDeltaCt calculation as an alternate method of data analysis for quantitative PCR of BCR-ABL P210 transcripts. *Diagn Mol Pathol.* Mar 2006;15(1):56-61.

21. Tchemtchoua VT, Atanasova G, Aqil A, et al. Development of a procedure to simultaneously isolate RNA, DNA, and proteins for [corrected] characterizing cells invading or cultured on chitosan scaffolds. *Anal Biochem.* Oct 1 2009;393(1):145-147.

22. Gambino G, Perrone I, Gribaudo I. A Rapid and effective method for RNA extraction from different tissues of grapevine and other woody plants. *Phytochem Anal.* Nov 2008;19(6):520-525.

23. Skrypina NA, Timofeeva AV, Khaspekov GL, Savochkina LP, Beabealashvilli R. Total RNA suitable for molecular biology analysis. *J Biotechnol.* Oct 9 2003;105(1-2):1-9.

24. MacRae E. Extraction of plant RNA. *Methods Mol Biol.* 2007;353:15-24.

25. George M, Abraham TE. Polyionic hydrocolloids for the intestinal delivery of protein drugs: alginate and chitosan--a review. *J Control Release.* Aug 10 2006;114(1):1-14.

26. Qiagen, ed. *RNeasy mini handbook.* 4th ed; 2004.

27. Hoemann CD, Sun J, Chrzanowski V, Buschmann MD. A multivalent assay to detect glycosaminoglycan, protein, collagen, RNA, and DNA content in milligram samples of cartilage or hydrogel-based repair cartilage. *Anal Biochem.* Jan 1 2002;300(1):1-10.

28. Ma PL, Lavertu M, Winnik FM, Buschmann MD. New insights into chitosan-DNA interactions using isothermal titration microcalorimetry. *Biomacromolecules.* Jun 8 2009;10(6):1490-1499.

29. Tanabe T, Morinaga K, Fukamizo T, Mitsutomi M. Novel chitosanase from Streptomyces griseus HUT 6037 with transglycosylation activity. *Biosci Biotechnol Biochem.* Feb 2003;67(2):354-364.

30. Jung HS, Son JW, Ji HS, Kim K. Effective Production of Chitinase and Chitosanase by Streptomyces griseus HUT 6037 Using Colloidal Chitin and Various Degrees of Deacetylation of Chitosan. *Biotechnot. Bioprocess Eng.* 1999;4(1):26-31.

31. Mason PE, Neilson GW, Dempsey CE, Barnes AC, Cruickshank JM. The hydration structure of guanidinium and thiocyanate ions: implications for protein stability in aqueous solution. *Proc Natl Acad Sci U S A.* Apr 15 2003;100(8):4557-4561.

32. Cockle SA, Epand RM, Moscarello MA. Resistance of lipophilin, a hydrophobic myelin protein, to denaturation by urea and guanidinium salts. *J Biol Chem.* Nov 25 1978;253(22):8019-8026.

33. Ekowati C, Hariyadi P, Witarto AB, Hwang JK, Suhartono MT. Biochemical characteristics of chitosanase from the Indonesian Bacillus licheniformis MB-2. *Mol Biotechnol.* Jun 2006;33(2):93-102.

34. Yoon HG, Kim HY, Lim YH, et al. Thermostable chitosanase from Bacillus sp. Strain CK4: cloning and expression of the gene and characterization of the enzyme. *Appl Environ Microbiol.* Sep 2000;66(9):3727-3734.

35. Mao HQ, Roy K, Troung-Le VL, et al. Chitosan-DNA nanoparticles as gene carriers: synthesis, characterization and transfection efficiency. *J Control Release.* Feb 23 2001;70(3):399-421.

Chapter 5 ARTICLE 2: LOW MOLECULAR WEIGHT CHITOSAN NANOPARTICULATE SYSTEM AT LOW N:P RATIO FOR NONTOXIC POLYNUCLEOTIDE DELIVERY.

Mohamad Alameh, Diogo DeJesus, Myriam Jean, Vincent Darras, Marc Thibault, Marc Lavertu, Michael D Buschmann, Abderrazzak Merzouki

Institute of Biomedical Engineering, Department of Chemical Engineering, École Polytechnique, Montréal, Canada

Correspondence**:** Abderrazzak Merzouki

Institute of Biomedical Engineering, Department of Chemical Engineering, École Polytechnique, PO Box 6079, Station Centre-ville, Montréal (Québec), Canada H3C 3A7

Tel +1 514 340 5121 ext 4799

Fax +1 514 340 5227

Email abderrazzak.merzouki@polymtl.ca

Published in the International Journal of Nanomedicine (2012)

Abstract

Chitosan, a natural polymer, is a promising system for the therapeutic delivery of both plasmid DNA and synthetic small interfering RNA. Reports attempting to identify the optimal parameters of chitosan for synthetic small interfering RNA delivery were inconclusive with high molecular weight at high amine-to-phosphate (N:P) ratios apparently required for efficient transfection. Here we show, for the first time, that low molecular weight chitosan (LMW-CS) formulations at low N:P ratios are suitable for the *in vitro* delivery of small interfering RNA. LMW-CS nanoparticles at low N:P ratios were positively charged (ζ-potential ~20mV) with an average size below 100 nm as demonstrated by dynamic light scattering and environmental scanning electron microscopy, respectively. Nanoparticles were spherical, a shape promoting decreased cytotoxicity and enhanced cellular uptake. Nanoparticle stability was effective for at least 20 hours at N:P ratios above two in a slightly acidic pH of 6.5. At a higher basic pH of 8, these nanoparticles were unraveled due to chitosan neutralization, exposing their polynucleotide cargo. Cellular uptake ranged from 50% to 95% in six different cell lines as measured by cytometry. Increasing chitosan molecular weight improved nanoparticle stability as well as the ability of nanoparticles to protect the oligonucleotide cargo from nucleases at supraphysiological concentrations. The highest knockdown efficiency was obtained with the specific formulation 92-10-5 that combines sufficient nuclease protection with effective intracellular release. This system attained >70% knockdown of the messenger RNA, similar to commercially available lipoplexes, without apparent cytotoxicity. Contrary to previous reports, our data demonstrate that LMW-CS at low N:P ratios are efficient and nontoxic polynucleotide delivery systems capable of transfecting a plethora of cell lines.

Keywords: siRNA, nonviral delivery system, chitosan, gene silencing, RecQL1, ApoB

5.1 Introduction

RNA interference (RNAi), an evolutionary endogenous gene regulation mechanism based on double-stranded RNA (short hairpin RNA, microRNA, Piwi-interacting RNA, and small interfering RNA [siRNA]), has provided a potential new class of therapeutics.[1] Since its discovery in *Caenorhabditis elegans*,[2] RNAi has been proven effective in mammalian cells[1,3–11] and has reached clinical trials.[1,12–14] However, direct delivery of RNAi-inducing entities such as synthetic siRNA or short hairpin RNA continues to be problematic owing to their rapid extracellular/intracellular degradation by nucleases (i.e. RNAse and DNAse), limited blood stability, poor cellular uptake, and nonspecific targeting.[15–17] As a consequence, the translation of RNAi into a clinical therapeutic reality is still pending resolution of these issues.

Chemical modification of synthetic siRNAs has provided resistance to nuclease degradation and improved blood stability.[18–22] For example, selective addition of a phosphorothioate linkage or substitution with 2′-O-methyl on the C2 position of specific riboses increases nuclease resistance of siRNAs without compromising activity.[14,19,20] Nevertheless, some chemical modifications can increase cytotoxicity, off-target effects and reduce messenger RNA (mRNA) hybridization.[23–27] Despite progress achieved through chemical modification to increase siRNA half-life, transfection efficiency, cellular targeting, and uptake remain as obstacles to effective delivery. Therefore, packaging systems which can both protect and transport chemically unmodified/modified siRNA to target cells are required.

Liposomes/Lipoplexes have been extensively used as non-viral vehicles for plasmid and RNAi entities and pose toxicity concerns. For example, the repeated administration of lipid-based delivery vehicles caused phospholipidosis.[28] Intravenous injection of stable nucleic acid-lipid particles has successfully targeted the liver to silence the *apolipoprotein B* (*ApoB*) gene in mice and nonhuman primates.[10] However, a significant 20-fold transient elevation in serum transaminases (aspartate transaminase, alanine transaminase) indicative of hepatocellular necrosis was identified at the effective dose. Liposomal formulations of nucleic acids are known inducers of inflammatory cytokines including tumor necrosis factor-alpha, interferon-gamma, and interleukin-6 which may be related to liver damage.[29] Polyethylene glycol (PEG)ylation of liposomes, for the purpose of reducing their toxicity, was also demonstrated to elicit acute hypersensitivity after repeated dosing.[30–32] Similarly, the highly studied cationic family of

polymers such as polyethylenimine demonstrated high gene transfer efficiency but was also associated with significant toxicity issues[33,34] limiting their broad use in clinical trials. Polyethylenimine cytotoxicity was characterized as a two-phase process where the polycation–cell interaction induces loss of cell membrane integrity and the induction of programmed cell death. Insights into polyethylenimine toxicity highlight the importance of polycation/organelle interactions – ie, mitochondria and lysosomes – on the induction of toxicity.[35,36] In general, cationic polymers display less toxicity associated with cytokine induction – immune activation – compared to their cationic lipid counterparts.[37]

Chitosan, a family of cationic polymers of β-1-4 N-acetyl-glucosamine and D-glucosamine residues, has been extensively studied for the delivery of plasmid DNA (pDNA) and siRNA both *in vitro* and *in vivo*.[3,8,17,38–44] Chitosan properties include mucoadhesivity,[45] biocompatibility, biodegradability,[46] nontoxicity, and low cost of production. Primary amine residues confer a polycationic nature to chitosan at pH values below its pKa (~6.5) thus enabling it to condense polyanionic compounds such as nucleic acids. Electrostatic interaction between chitosan and nucleic acids leads to the spontaneous formation of nanoparticles of different sizes and shapes.[47] The ability of chitosan-based nanoparticles to transfect cells efficiently depends on several parameters such as: (1) the degree of deacetylation (DDA), which represents the fraction of ionizable monomers; (2) the average molecular weight (M_n), proportional to chain length, and (3) the amine-to-phosphate (N:P) charge ratio represented by the amine-(chitosan)-to-phosphate (DNA or RNA) ratio used to form nanoparticles.

We have previously demonstrated that maximization of *in vitro* transfection efficiency for the delivery of pDNA depends on a fine balance between these tunable parameters of chitosan[39–41] and found maximum transgene expression for DDA:M_n values that run along a diagonal from high DDA/low M_n to low DDA/high M_n.[39] We also have demonstrated that specific chitosan formulations [DDA, M_n, and N:P ratio] efficiently express transgene in vivo.[38,42]

We also demonstrated that specific formulations are able to trigger an anti-transgene immune response;[38] therefore, nanoparticles can be designed based on the fine-tuning of chitosan parameters for application-specific purposes such as genetic vaccination or gene therapy.

The structural differences between pDNA and siRNA are believed to affect the complexation/stability of nanoparticles and optimal parameters required for effective delivery.

Chitosan has also been used for siRNA delivery both *in vitro* and *in vivo*.[1,8,10,17,44] However, and despite attempts to identify optimal physicochemical parameters for siRNA delivery,[44] inconclusive results have been observed in the literature due to experimental discrepancies.[8,17] For example, it was reported that intermediate DDA (80%) and high M_n (64–170 kDa) chitosan were more efficient than low molecular weight chitosan (LMW-CS) (10 kDa) in delivering siRNA.[17,44] However, high molecular weight chitosan are found to be cytotoxic,[48–50] thus potentially limiting their use in future clinical trials. Additionally, most of the reports evaluating the physicochemical parameters of chitosan/siRNA nanoparticles were performed at high N:P ratios (N:P >25).[8,17,44] Such formulations bring significant practical problems including limited dosing due to aggregation and the nonspecific effects of large quantities of soluble chitosan.[51]

Here, we investigate, for the first time, the ability of specific LMW-CS formulations (92-10-5, 80-80-10, 80-40-5, and 80-10-10) [DDA, M_n, and N:P ratio] at low N:P ratios to *in vitro* deliver siRNA targeting: (1) the RecQL1 DNA helicase mRNA in the colon adenocarcinoma RecQL1 overexpressing cell line (LS174T) and (2) ApoB mRNA in the hepatocarcinoma-derived cell line (HepG2). The choice of these two targets resides in their relevance to cancer and atherosclerosis, respectively.[6,7,9,52,53] We also explored the ability of these formulations to transfect multiple cell lines such as A549, AsPC1, HEK293, and Raw264.7 without apparent toxicity. In this study, we hypothesized that, contrary to previous literature,[8,17,43,44] low M_n chitosan (LMW-CS) complexed at low N:P ratios represent suitable formulations for siRNA delivery and gene knockdown; similar to our observations with pDNA.[38–42] Additionally, we hypothesized that low N:P ratios assure sufficient protection and efficient delivery of the siRNA cargo. Moreover, we explore the physicochemical properties of these specific formulations with the prospect of optimizing nanoparticle transfection and silencing efficiencies. Our results demonstrate, for the first time, that LMW-CSs at low N:P ratios are effective and nontoxic delivery systems for polynucleotide and siRNA delivery for *in vitro* gene silencing.

5.2 Materials and methods

5.2.1 Synthesis siRNAs and dsODNs as a structural model of siRNA

siRNAs targeting the RecQL1 DNA helicase and ApoB mRNAs were synthesized using a novel RNA synthesis chemistry, the 5′-silyl-2′-orthoester protecting groups (2′-ACE)[54] combined with a standard phosphoramitide solid-phase technology by Dharmacon (Thermo Scientific, Dharmacon RNAi Technologies, Lafayette, CO). RecQL1 mRNA-specific siRNA (siRNA-RecQL1) contains the sense sequence of 5′-GUUCAGACCACUUCAGCUUdTdT-3′ and antisense 5′-AAGCUGAAGUGGUCUGAACdTdT-3′ whereas ApoB mRNA-specific siRNA (siRNA-ApoB) contains the sense sequence of 5′-GUCAUCACACUGAAUACCAAU-3′ and antisense 5′-AUUGGUAUUCAGUGUGAUGACAC-3′. Mock siRNA were also used as a negative control. Mock siRNA is a non-targeting siRNA (Dharmacon, D-001710-01-05) designed to have minimal targeting of known genes in human, mouse, and rat cells.

Double-stranded oligodeoxynucleotides (dsODNs, 21 bp) encoding the same sequences and mimicking siRNA physicochemical properties were used for nanoparticle characterization. The double-stranded oligodeoxynucleotide (dsODN) sequences were synthesized using the phosphoramidite chemistry (Integrated DNA Technologies Inc, Coralville, IO) and used for size and zeta potential determination, nanoparticle stability, and nuclease protection assays. For confocal microscopy and flow cytometry analysis, 6-carboxyfluorescein (6FAM) 5′-labeled dsODNs were used (Integrated DNA Technologies Inc). The rationale for using dsODN for chitosan nanoparticle physicochemical characterization is their siRNA-mimicking properties. These mimicking properties are due to similarities at the structural level (double-stranded structure, length, and nucleotide overhangs) between siRNA and dsODNs. Additionally, charge densities are similar between siRNA and dsODNs due to identical phosphate residue numbers on their backbone. The main differences between siRNA and dsODNs lie in the substitution of uracil to thymine (U → T) in the dsODN sequences, and in the deoxyribosilation of the dsODN sugar backbone.

5.2.2 Preparation and characterization of depolymerized chitosan

Clinical-grade chitosan at different DDAs was obtained from BioSynthec Inc (Laval, QC, Canada) and depolymerized using nitrous acid to achieve specific number-average molecular weight targets (M_n) of 80, 40, and 10 kDa. Chitosan number- and weight-average molecular weights (M_n and M_w)

were determined by gel permeation chromatography using a Shimadzu LC-20AD isocratic pump, autosampler SIL-20AC HT, oven CTO-20AC coupled with a Dawn HELEOS II multiangle laser light scattering detector (Wyatt Technology Co, Santa Barbara, CA), a Viscostar II (Wyatt Technology Co), an Optilab rEX interferometric refractometer (Wyatt Technology Co), and two Shodex OHpak (SB-806M HQ and SB-805 HQ; Showa Denko America, Inc, New York, NY) columns eluted with a pH 4.5 acetic acid (0.15 M)/sodium acetate (0.1 M)/sodium azide (4 mM) buffer.[55,56] The injection volume was 100 µL, the flow rate 0.8 mL min^{-1} and the temperature 25°C. The dn/dc value was previously calculated for chitosan with a DDA of 92% (for a laser's wavelength of 658 nm) and is equal to 0.208 and 0.201 for chitosan with 80% DDA. The degree of deacetylation was determined by ^{1}H NMR according to our previous reports.[39,57]

5.2.3 Preparation of chitosan nanoparticles

Chitosans with specific M_n and DDA (Table 5.1) were dissolved overnight on a rotary mixer at 0.5% (w/v) in hydrochloric acid using a glucosamine:HCl ratio of 1:1 at a final concentration of 5 mg/mL. Sterile filtered solutions were then diluted with deionized water to obtain the desired ratio (N:P) of amine (chitosan deacetylated groups) to phosphate (dsODNs/siRNA nucleic acids). Nanoparticles (92-10-5, 80-10-10, 80-40-5, and 80-80-5) were then prepared by rapid mixing (pipetting) of 100 µL of diluted chitosan solution to 100 µL of dsODNs or siRNA at a concentration of 0.05 µg/µL or 100 nM.

Table 5-1: Physicochemical characteristics of bulk chitosans

Chitosan	DDA (%)[a]	M_n (kDa)[b]	M_w (kDa)	PDI[c]	N:P ratio[d]
92-10	92	10	11.8	1.5	5
80-10	80	10	14.5	1.3	10
80-40	80	40	53.0	1.3	5
80-80	80	80	110.9	1.6	5

Notes: [a]As determined by 1H NMR; [b]as determined by gel permeation chromatography (GPC); [c]M_w/M_n; [d]nanopartice N:P ratio follwing complexation with either dsODN or siRNA used in this study.
Abbreviations: DDA, degree of deacetylation; M_n, number average molecular weight; M_w, specific molecular weight; PDI, polydispersity index; N:P, amine to phosphate; dsODN, double-stranded oligodeoxynucleotides.

5.2.4 Nanoparticle size and ζ-potential analysis

The size of chitosan/dsODN-RecQL1 and chitosan/dsODN-ApoB nanoparticles – intensity average diameter – was determined by dynamic light scattering at an angle of 173° at room temperature using the Malvern Zetasizer Nano ZS (Malvern, Worcestershire, UK). Following nanoparticle formation, samples were diluted in 10 mM NaCl at a ratio of 1:10 and measured in triplicate. The ζ-potential was measured in triplicate using laser Doppler velocimetry at 25°C on the same instrument with the viscosity and dielectric constant of pure water used for calculations.

5.2.5 High-vacuum scanning electron microscopy (ESEM)

Chitosan/dsODN-RecQL1 and chitosan/dsODN-ApoB nanoparticles were sprayed on silicon wafer substrate then sputter-coated with gold (Agar Manual Sputter Coater; Marivac Inc, Montreal, QC, Canada) and imaged using a Quanta 200 FEG Environmental Scanning Electron Microscope (FEI Inc, Hillsboro, OR). Observations were performed at 20 kV using the high-vacuum mode. The average particle diameter (± standard deviation) was determined using the XT Docu image analysis software (FEI Inc).

5.2.6 Nanoparticle stability assessment by polyacrylamide gel electrophoresis

The stability of chitosan/dsODN nanoparticles at different pHs (6.5 and 8) and for different incubation times (0.5, 4, and 24 hours) was assessed using polyacrylamide gel electrophoresis. Upon formation, nanoparticles were mixed at a ratio of 1:1 with 2-(N-morpholino)ethanesulfonic acid buffer (MES 1X) (20 mM MES, 8 mM sodium acetate, pH 6.5) or Tris-acetate (TAE)-EDTA buffer (TAE 1X) (2 M Tris-acetate, 50 mM EDTA, pH 8). The samples were then migrated on a 13% polyacrylamide gel (BioRad Laboratories, Mississauga, ON, Canada) for 2 hours at 100 mV in either MES or TAE buffer. Gels were stained with 0.5 µg/mL ethidium bromide solution (BioRad Laboratories) to visualize dsODNs. Gel documentation and image analysis were performed using a Bio-Vision 3000 (Vilbert Lourmat, Marne-la-Vallée, France) and the Vision-Capt software, respectively.

5.2.7 Nuclease protection assay

The level of protection against nuclease attack offered by chitosan formulations (92-10-5, 80-80-10, 80-40-5, and 80-80-5) was assessed electrophoretically on a 5% agarose gel. Chitosan/dsODN-RecQL1 and chitosan/dsODN-ApoB nanoparticles at different [DDA, M_w, and N:P ratios] were incubated with 0.5, 1, 2, 5, or 10 units of DNAse I (Sigma-Aldrich, Oakville, ON, Canada) per µg of dsODNs in 20 µL of MES-$MgCl_2$ buffer (20 mM MES, 1 mM $MgCl_2$, pH 6.5) for 30 minutes at 37°C. The reaction was stopped by adding 2 µL of EDTA (50 mM) (Sigma-Aldrich). To ensure proper migration of the nondigested dsODNs, samples were treated with *Streptomyces griseus* type III chitosanase (Sigma-Aldrich) at 10 mU/µL for 1.5 hours at 37°C and stopped by placing the samples at –20°C for 15 minutes as previously described.[3] Samples were migrated at 90 V during 1 hour then stained with 0.5 µg/mL ethidium bromide solution before visualization. Captured images were analyzed using Vision-Capt software (v 15.06; Vilber Lourmat, Paris, France). Relative amounts of dsODN-RecQL1 or dsODN-ApoB (%) were determined by comparison of the integrated signal intensity of nuclease-treated samples *versus* nontreated samples.

5.2.8 *In vitro* cell transfection

5.2.8.1 Cell culture

All cell lines were purchased from American Type Cell Culture (Manassas, VA). The HepG2 cell line was cultured in minimal essential medium (MEM). The HEK293, Raw294.7, and LS174T cell lines were cultured in high-glucose Dulbecco's modified eagle's media (DMEM-HG). The A549 and AsPC1 cell lines were cultured in F12-K and *Roswell Park Memorial Institute medium* media, respectively. All cell culture media contained 1.85 g/L of sodium bicarbonate ($NaHCO_3$) and were supplemented with 10% fetal bovine serum (Cedarlane Laboratories, Burlington, ON, Canada). All cell lines were cultured at 37°C in a 5% CO_2 incubator. For transfection, cells were plated in 96-well or 24-well culture plates (Corning, Lowell, MA) to obtain a ~50% confluence the day of transfection using 100 µL/well or 500 µL/well, respectively, of complete culture medium.

5.2.8.2 Cell transfection

For *in vitro* transfection, DMEM-HG was prepared with 0.976 g/L of MES and 0.84 g/L of $NaHCO_3$ at a pH of 6.5. Transfection media containing 10% fetal bovine serum was equilibrated overnight at 37°C in a 5% CO_2 incubator and the pH was adjusted to 6.5 using sterile HCl (1N) prior to transfection. For siRNA transfection performed in a 96-well plate, chitosan/siRNA nanoparticles were prepared as described above, 30 minutes before use. A 100 µL siRNA solution at a concentration of 0.05 µg/µL was used for siRNA complexation with chitosan at a 1:1 ratio (v/v). Following complexation, nanoparticles were incubated in a ghost plate containing the transfection media (DMEM-HG + fetal bovine serum) at a final concentration of 1.35 ng/µL; equivalent to 10 pmol per well of siRNA. For dsODN transfection performed in a 24-well plate, nanoparticles were complexed as described above and incubated at a final concentration of 8.07 ng/µL, equivalent to 60 pmol per well of dsODNs. Plates containing nanoparticles were equilibrated for 10 minutes at 37°C, 5% CO_2. Medium over cells was aspirated and replenished with either 500 µL (24-well plate) or 100 µL per well (96-well plate) of the transfection medium containing dsODN- or siRNA-based nanoparticles. Cells were incubated with chitosan/siRNA or chitosan/dsODN nanoparticles until analysis 24 hours post transfection. The commercially available liposome, DharmaFECT™ (Dharmacon RNAi Technologies), was used as a positive control and both untreated cells and uncomplexed siRNA/dsODN-treated cells were used as negative controls.

5.2.8.3 Transfection with DharmaFECT

DharmaFECT was used as a positive control for transfection efficiency in all tested cell lines. DharmaFECT/dsODN (flow cytometry and confocal microscopy) or DharmaFECT/siRNA (qPCR and viability assay) lipoplexes (1:2 [w/v] ratio) were prepared following the manufacturer's protocol.

5.2.9 *In vitro* cell viability assay

Nanoparticle toxicity was evaluated using the alamarBlue® proliferation assay (Invitrogen, Carlsbad, CA). The principle of the assay is based on the natural reducing power of viable cells to

convert resazurin, a blue and nonfluorescent compound, into resofurin; a red and fluorescent molecule. Viable cells continuously convert resazurin to resofurin, thereby providing a quantitative measure of viability. Transfection was performed as described above using chitosan-siRNA nanoparticles. Five thousand cells/well were seeded 24 hours before transfection. To alleviate the experimental bias from the effect of RecQL1 gene silencing on cell viability, nontargeting siRNA (siRNA mock) was used instead. Twenty-four hours post transfection with chitosan-based nanoparticles, 20 µL of alamarBlue reagent, pre-warmed at 37ºC was added to each well and incubated for another 4 hours. At the end of the incubation 100 µL of media containing reduced alamarBlue dye was transferred to a black Corning 96-well plate and read on an infinite 200 fluorescence plate reader (Tecan Systems, San Jose, CA) with excitation 560 nm, emission 590 nm and a cut-off of 570 nm. Cells without the addition of alamarBlue were used as blank and dimethyl sulfoxide was used as a positive control of toxicity. The viability of nontransfected control cells was arbitrarily defined as 100%. The relative cell viability was calculated using the following formula: (fluorescence $\text{intensity}_{\text{sample}}$/fluorescence $\text{intensity}_{\text{control}}$) × 100.

5.2.10 Uptake analysis by flow cytometry and confocal microscopy

5.2.10.1 Fluorescence-activated cell sorting (FACS) analysis

The cellular uptake of dsODNs was determined by transfecting AsPC1, A549, LS174T, HepG2, HEK293, and Raw264.7 cell lines with nanoparticles formed with (6FAM) 5′labeled dsODNs. Twenty-four hours post-transfection, cells were chitosanase treated for 60 minutes to eliminate any cell surface-associated nanoparticles left from the transfection as described previously.[3] Afterward, cells were washed twice with phosphate-buffered saline, trypsinized, and resuspended in phosphate-buffered saline. The analysis of cell uptake was made using a BD Canto flow cytometer (Becton Dickinson, San Jose, CA). For each sample, 20,000 events were counted and to exclude cell debris, dead cells, and aggregated cells, a collection gate was established using a dot plot of the forward light scatter against the side scatter. Nontransfected cells were used as negative controls to discriminate (6FAM) positive cells from auto-fluorescence.

5.2.10.2 Confocal microscopy

For nanoparticle internalization analysis, the LS174T, HepG2, HEK293, and Raw264.7 cell lines were seeded on 35 mm glass-bottom culture dishes (MatTek, Ashland, MA) at 40,000 cells/dish using 500 µL of complete culture medium. Nanoparticles were formed with fluorescent rhodamine B isothiocyanate-labeled chitosan and dsODNs labeled with 6FAM on their 5′ extremities (Integrated DNA Technologies). Prior to imaging, cell membranes were stained with 5 µg/mL of Cell Mask™ Deep Red (Invitrogen, Burlington, ON, Canada). Images were taken in multitrack mode using a Zeiss LSM 510 META confocal Axioplan 200 microscope (Carl Zeiss AG, Feldbach, Switzerland). Chitosan and dsODNs were visualized as red and green pseudocolors, respectively. The spatial overlap of these two colors produced yellow which permitted a qualitative assessment of colocalization.

5.2.11 Quantitative PCR (qPCR) analysis of RecQL1 and ApoB mRNA knockdown

5.2.11.1 RNA extraction and assessment methods (yield, purity, and integrity)

RNA extraction was performed using the RNA XS® extraction kit from Macherey-Nagel (Biolynx, Montréal, QC, Canada) according to the manufacturer's protocol following chitosanase treatment, as described previously.[3] Total RNA was quantified and RNA integrity was measured using the Agilent BioAnalyzer 2100 (Agilent Technologies, Mississauga, ON, Canada) following the manufacturer's protocol. RNA integrity was evaluated by the ratio of 28S/18S ribosomal RNA[58] and the RNA integrity number (RIN). The Agilent 2100 BioAnalyzer uses automated microfluidics, capillary electrophoresis, and fluorescence to evaluate RNA integrity. The RIN is a relative measure of RNA quality that is based largely on electrophoretic trace analysis. The BioAnalyzer 2100 automatically computes RIN, where an ideal nondegraded RNA sample has RIN = 10.

5.2.11.2 Reverse transcription

Total RNA was reverse transcribed in a final volume of 20 µL using the First Strand cDNA Transcriptor Kit (Roche Diagnostics, Laval, QC, Canada) with oligodT primers as described by the manufacturer's protocol. Samples were stored at –20°C.

5.2.11.3 Gene expression assays

The RecQL1 and ApoB mRNA expression level was determined using assays designed with the Universal Probe Library (UPL) from Roche (Roche Applied Science, Laval, QC, Canada). Endogenous control (hypoxanthine guanine phosphoribosyl transferase) and glyceraldehyde 3-phosphate dehydrogenase expression levels were determined using pre-validated TaqMan® Gene Expression Assays (Applied Biosystems, Carlsbad, CA). RecQL1 and ApoB mRNA (target detection) reactions for 384-well plate formats were performed using 1.5 µL of cDNA samples (25–50 ng), 5 µL of the Fast Universal qPCR MasterMix (Applied Biosystems) 2 µM of each primer, and 1 µM of a Universal Probe Library probe (RecQL1 [probe #29]/ApoB [probe #55]) in a total volume of 10 µL. For endogenous control assessment, reactions were performed using identical volume of cDNA, Fast Universal qPCR Master Mix, 0.5 µL of the TaqMan Gene Expression Assay (20X) and 2.5 µL of water in a total volume of 10 µL.

5.2.11.4 Detection and analysis

The ABI PRISM® 7900HT Sequence Detection System (Applied Biosystems) was used to detect the amplification level and was programmed with an initial step of 3 minutes at 95°C, followed by 45 cycles of 5 seconds at 95°C and 30 seconds at 60°C. All reactions were run in triplicate and the average values of Cts (threshold cycle) were used for quantification. Glyceraldehyde 3-phosphate dehydrogenase and hypoxanthine guanine phosphoribosyl transferase were used as endogenous controls. The relative quantification of target genes was determined using the △△CT method. Briefly, the Ct values of target genes were normalized to an endogenous control gene (endogenous control) ($\triangle CT = Ct_{target} - Ct_{endoC}$) and compared with a calibrator: $\triangle\triangle CT = \triangle Ct_{target} - \triangle Ct_{calibrator}$. Relative expression (RQ) was calculated using the Sequence Detection System 2.2.2 software using the $RQ = 2^{-\triangle\triangle CT}$ formula.

5.2.12 Statistical analysis

The statistical analysis was performed using Statistica 9.0 Software (STATSOFT; Statistica, Tulsa, OK). Data are expressed as mean ± standard deviation. Statistical significance was determined with one-way analysis of variance, followed by Tukey's post hoc test. The results were considered significant and highly significant ($P < 0.05$ and $P < 0.01$, respectively).

5.3 Results

5.3.1 Size and ζ-potential of chitosan nanoparticles

All formulations of chitosan/dsODN nanoparticles were in the range of 41–109 nm as measured by environmental scanning electron microscopy (ESEM) and dynamic light scattering (Figure 5.1 and Table 5.2).

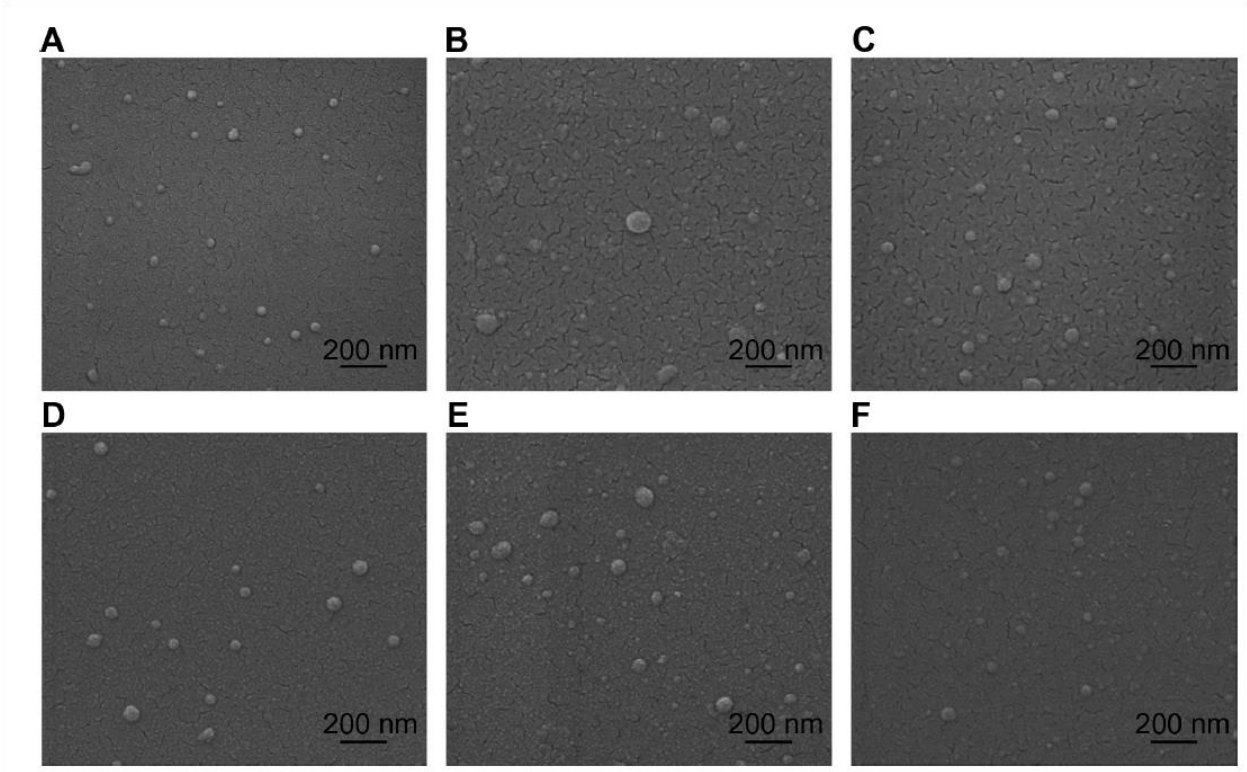

Figure 5-1: Environmental scanning electron microscopy images of spherical chitosan/dsODN nanoparticles. (A) 92-10-5 chitosan/dsODN-RecQL1 nanoparticles; (B) 80-40-5

chitosan/dsODN-RecQL1 nanoparticles; (C) 80-10-10 chitosan/dsODN-RecQL1 nanoparticles; (D) 92-10-5 chitosan/dsODN-ApoB nanoparticles; (E) 80-80-5 chitosan/dsODN-ApoB nanoparticles, and (F) 80-10-10 chitosan/dsODN-ApoB nanoparticles.

Abbreviation: ApoB, apolipoprotein B; dsODN, double-stranded oligodeoxynucleotide

Chitosan/dsODN nanoparticles showed higher size values with increasing M_n. No statistically significant differences were observed when comparing DDAs for these specific formulations. The excess chitosan in all formulations resulted in positively charged nanoparticles as shown by ζ-potential measurements (Table 5-2).

Table 5-2: Size and zeta potential values obtained by dynamic light scattering for chitosan/dsODN-RecQL1 and chitosan/dsODN-ApoB nanoparticles

ODN	Chitosan	Size DLS (nm)	Size ESEM (nm)	Zeta potential (mV)
RecQL1	92-10-5	63 ± 8	54 ± 6	23 ± 1
RecQL1	80-40-5	86 ± 9	97 ± 12	18 ± 1
RecQL1	80-10-10	91 ± 7	73 ± 9	18 ± 2
ApoB	92-10-5	45 ± 4	66 ± 5	21 ± 2
ApoB	80-80-5	100 ± 8	75 ± 13	16 ± 1
ApoB	80-10-10	64 ± 6	67 ± 7	19 ± 2

Notes: Values are mean ± SD; n = 3.
Abbreviations: ApoB, apolipoprotein B; dsODN, double-stranded oligodeoxynucleotides; DLS, dynamic light scattering; ESEM, environmental scanning electron microscopy; SD, standard deviation.

5.3.2 Chitosan/dsODN nanoparticle stability

Chitosan-based nanoparticles were incubated for 0.5, 4, and 20 hours in two different buffers (pH 6.5 and 8) to assess the effect of time and pH on nanoparticle stability (Figure 5-2). Nanoparticles were stable up to 20 hours at an N:P ratio above 2 in slightly acidic buffers (pH 6.5). At 4 hours following nanoparticle formation, and under slightly acidic conditions, no detectable dsODNs were

observed at N:P ratios of 2 or higher (Figure 5-2 A and 5-2 C). On the contrary, dsODN release was observed for the same N:P ratios at a pH of 8 (Figure 5-2 B and 5-2 D). Longer exposure time – 20 hours – at a pH of 6.5 resulted in increased dsODN-ApoB release at an N:P ratio of 2. This pattern was not observed for the dsODN-RecQL1 sequence. This may be due to sequence/structural differences between the two dsODNs. Furthermore, our results at a pH of 8 show a rapid partial-to-complete dsODN release after 0.5 hour at an N:P ratio of 2 (Figure 5-2 B and 5.2D). At N:P ratio 10 and for the same pH of 8, chitosan showed a partial release of dsODNs indicating the effect of excess chitosan on preserving stability. Overall, our specific chitosan formulations assured nanoparticle stability for a minimum period of 20 hours at an N:P ratio above 2 in slightly acidic near-neutral pH environments.

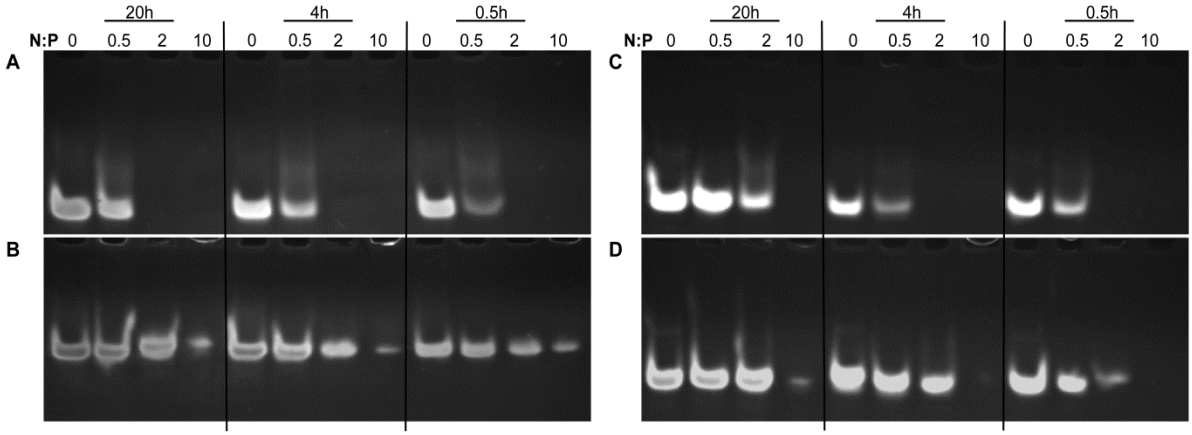

Figure 5-2: Chitosan nanoparticle temporal stability. Stability was assessed at 0.5, 4, and 24 hours after complex formation using polyacrylamide gel electrophoresis at a pH of 6.5 (MES 1X) and pH8 (TAE 1X). Chitosan 92-10 at different N:P ratios (0.5, 2, and 10) was complexed with (A) dsODN-RecQL1 at pH of 6.5; (B) dsODN-RecQL1 at a pH of 8; (C) ds-ODN-ApoB at a pH of 6.5, and (D) ds-ODN-ApoB at a pH of 8. Unstable nanoparticles release dsODNs which become visible following EtBr staining on polyacrylamide gel following eethidium bromide staining of the polyacrylamid gel.

Abbreviations: ApoB, apolipoprotein B; dsODN, double-stranded oligodeoxynucleotide; N:P, amine to phosphate.

5.3.3 Nanoparticle protection assay

For effective gene expression and/or inhibition, nucleic acids entrapped in the delivery vehicle must be protected from degradation by enzymes such as serum nucleases.[59] The ability of chitosan-based nanoparticles to protect siRNA mimicking dsODN sequences was assessed using a DNAse I protection assay against different chitosan formulations complexed with dsODN-RecQL1 or dsODN-ApoB. Upon incubation with DNAse I, naked dsODN-RecQL1 and dsODN-ApoB (controls) were completely degraded (Figure 5-3 A–D, lane 3). In contrast, DNAse I protection assay showed that all chitosans tested protected dsODNs from degradation at DNAse I concentrations <2 units DNAse I per µg dsODN (Figure 5-3). Chitosan formulations demonstrated an average of ~80% protection of dsODNs at DNAse I concentrations of 0.5 U/µg (Figure 5-3). The ability of LMW-CS (92-10, 80-40, 80-80, and 80-10) to protect dsODNs from nuclease degradation decreased with increased concentrations of DNAse I. Our results show that protection decreased from ~50% at a DNAse I concentration of 1 U/µg to less than ~20% at 2 U/µg (92-10 and 80-10). Moreover, our results suggest that higher M_n chitosan (80-40 and 80-80) offers a slightly better protection of dsODNs as compared to lower M_n chitosan (92-10 and 80-10) at high DNAse I concentrations (2 U/µg) (Figure 5-3 A–D). The enhanced cargo protection observed with higher molecular weight chitosans is consistent with previous studies where higher binding affinities between high Mw chitosans and nucleic acids was demonstrated.[60] Altogether, our results show that DNAse I protection is considerable when using intermediate to low DDA/M_n and preserves approximately 60% of nucleic acid when using 1 unit of DNAse I per µg of dsODNs.

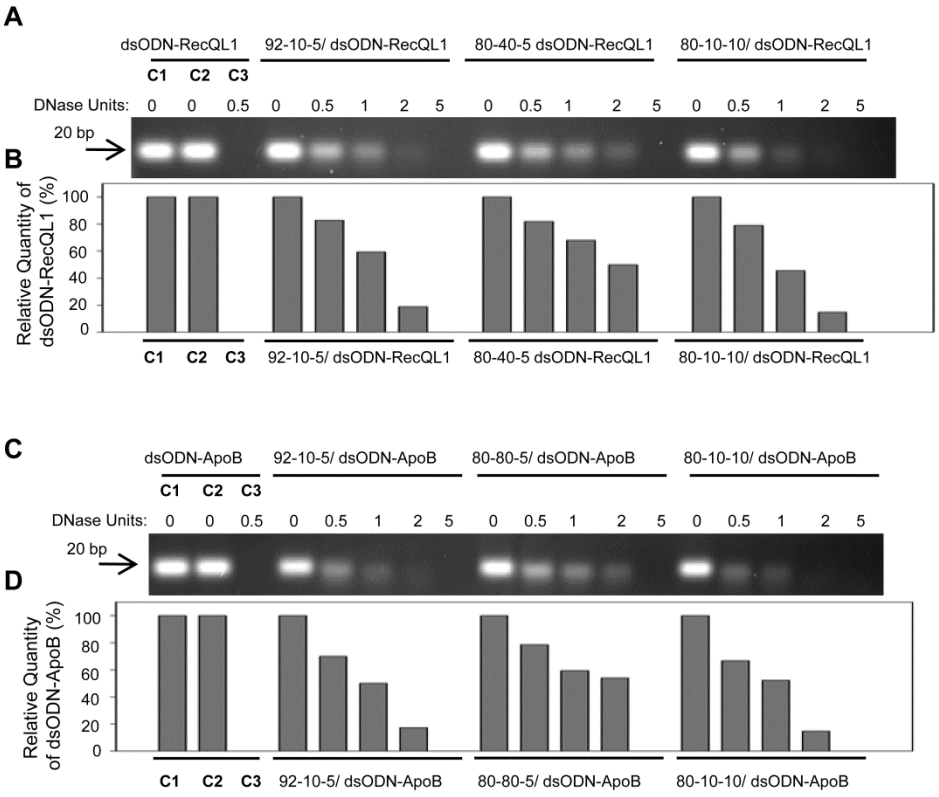

Figure 5-3: Nuclease protection assays of chitosan/dsODN nanocomplexes. (A) Chitosan (92-10-5, 80-40-5 or 80-10-10) complexed with dsODN-RecQL1. (B) dsODN-RecQL1 remaining after the DNAse I digestion was assessed using the signal intensity of the treated samples with the control (ie, 0 U DNAse I = 100% intensity). This comparison was made between the samples of the same chitosan formulation. (C) Chitosan (92-10-5, 80-80-5 or 80-10-10) complexed with dsODN-ApoB. (D) dsODN-ApoB remaining after the DNAse I digestion was similarly assessed as in (B).

Abbreviations: ApoB, apolipoprotein B; dsODN, double-stranded oligodeoxynucleotide.

5.3.4 *In vitro* cell uptake analysis by flow cytometry and confocal microscopy

Nanoparticle internalization into cells can be another rate-limiting step for effective drug delivery systems. In general, efficient nanoparticle internalization depends on several factors, such as the cell type, the physicochemical surface properties of the nanoparticles, and the bio–nano interface.[61] The internalization of RecQL1- and ApoB-bearing nanoparticles was assessed in two different sets

of relevant cell lines using flow cytometry (FACS). For the assessment of (6FAM) 5′-labeled RecQL1dsODN uptake, transfection and FACS analysis were performed on AsPC1, A549, and LS174T cancer cell lines whereas (6FAM) 5′ labeled ApoB dsODN uptake was performed on HEK293, HepG2, and Raw269.7 cell lines. Our FACS results show that cell uptake using chitosan/(6FAM) 5′-labeled dsODN nanoparticles achieved levels comparable to the commercially used lipoplex (DharmaFECT) (Figure 5-4 and 5-5), demonstrating the internalization efficiency of LMW-CS formulations in different cell lines. Moreover, our results indicate that different chitosan formulations show statistically significant differences in their cell uptake efficiency, with LMW-CSs 92-10-5 and 80-10-10 more easily internalized compared to the higher molecular weight 80-80-5 and 80-40-5, in a cell-line-dependent manner. Interestingly, the A549 and HEK293 cell lines demonstrated no statistical differences in uptake efficiency between the different chitosan formulations (Figure 5-4 and 5.5A).

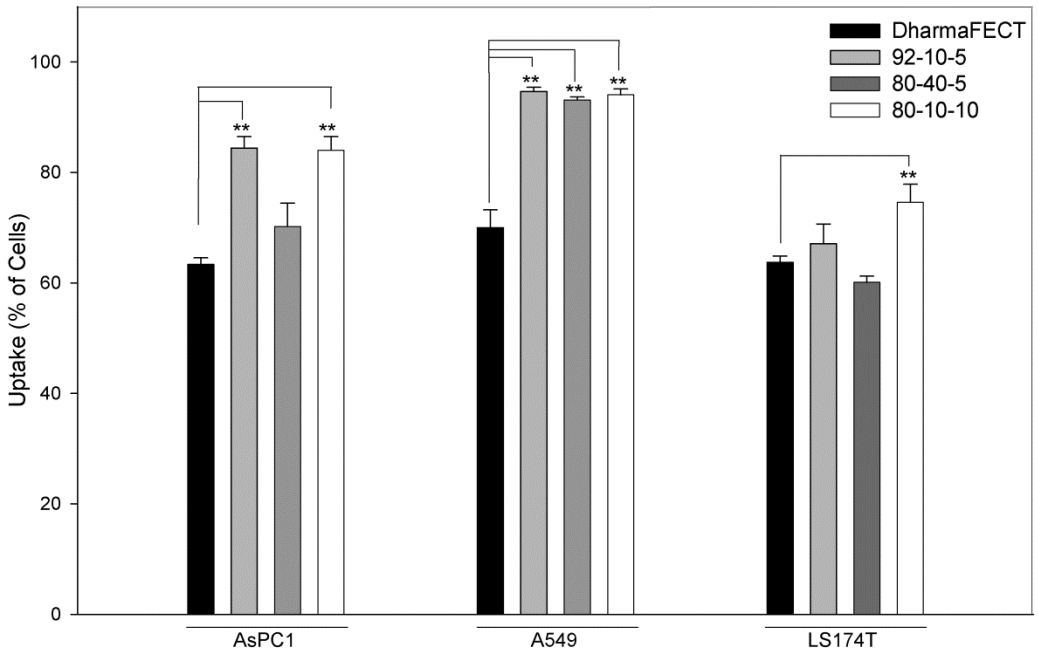

Figure 5-4. Polyacrylamide gel electrophoresis of chitosan/DPP-IV$_{ODN}$ polyplexes bearing different DDAs and N/P ratios, treated with or without Streptomyces griseus chitosanase. a) chitosan migration b) ODN migration. Lane 1 to 4 corresponds to chitosan/DPP-IV$_{ODN}$ directly incubated with chitosanase during 60 minutes at 37ºC. Chitosan digestion allows the ODN release. Lane 5 to 8 corresponds to chitosan/DPP-IV$_{ODN}$ incubated at the similar conditions

without chitosanase. Faster chitosan migration was observed when comparing lanes 5 and 6 due to different MW of theses formulations. Increased band intensity (lane 4-8) results from greater amounts of chitosan at higher N/P ratios

However, the A549 and HEK293 cell lines showed statistically significant increases in uptake when compared to the LS174T and Raw264.7 cell lines, again highlighting some important cell-type dependencies. In general, LMW-CS (92-10-5 and 80-10-10) showed higher uptake efficiency, ranging from approximately 65% to 95% depending on the transfected cell line (Figure 5-4 and 5-5A).

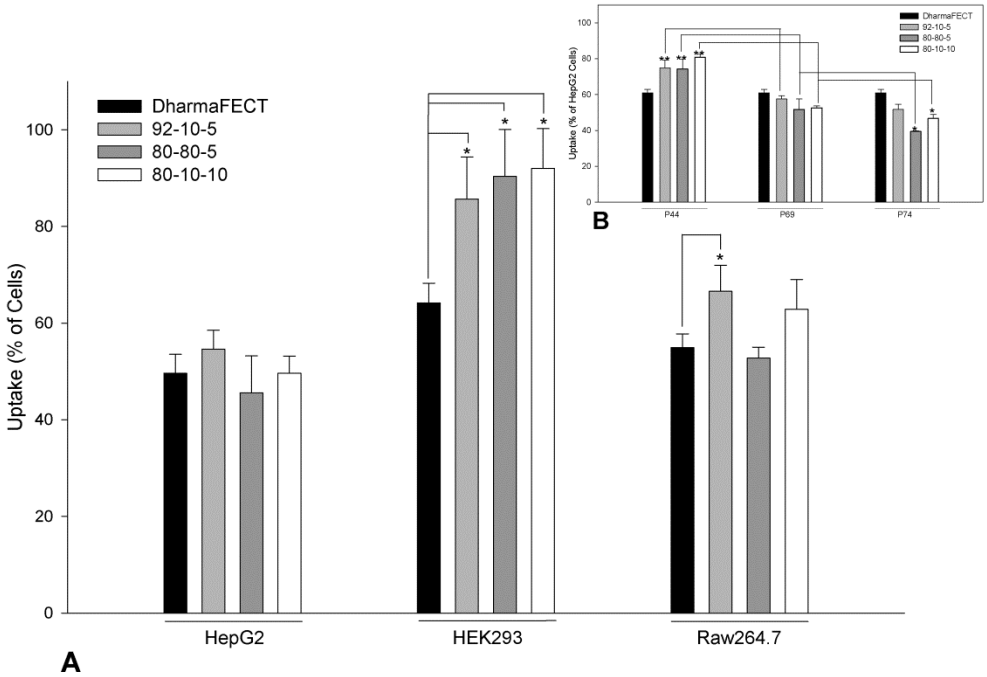

Figure 5-5: Cellular uptake of dsODN-ApoB nanoparticles 24 hours post transfection in HEK293, Raw269.7, and HepG2 cell lines. Chitosan formulations 92-10-5, 80-80-5, and 80-10-10 were complexed to (6FAM) 5′ labeled dsODN-ApoB and transfected at 60 pmol/well 24 hours prior to fluorescence-activated cell sorting analysis. (A) Uptake efficiency of ApoB dsODN in percentage (%). (B) Uptake efficiency of ApoB dsODN in HepG2 cells at different passage number. DharmaFECT was used as the positive uptake control.

Notes: Values are mean ± SD; n = 3; *P >0.05; **P > 0.01.

Abbreviations: ApoB, apolipoprotein B; dsODN, double-stranded oligodeoxynucleotide; SD, standard deviation.

These results are in accordance with confocal microscopy data, where images representative of the whole population show that the vast majority of cells for each of the four cell types imaged show nanoparticle internalization (Figure 5-6). The lack of colocalization at 24 hours between dsODNs and chitosan indicates that complete release of the dsODN cargo was achieved 24 hours post transfection. Furthermore, the diffuse staining pattern of dsODNs seen in most transfected cells suggests that complexes have escaped endocytic vesicles (Figure 5-6), consistent with previous live cell imaging work using chitosan–plasmid DNA nanoparticles.[41]

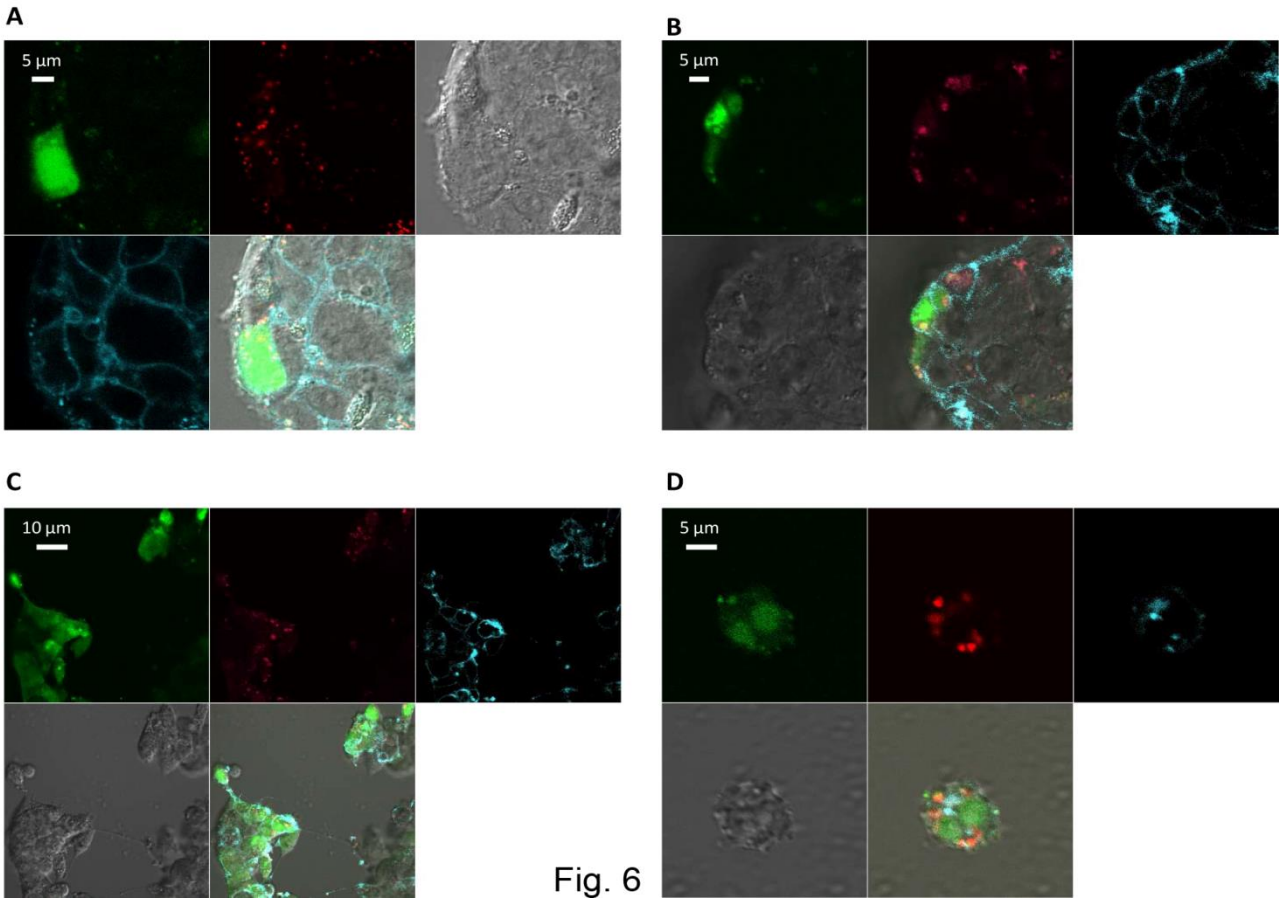

Figure 5-6: Confocal imaging of chitosan/dsODN nanocomplex uptake 24 hours post transfection. Chitosan 92-10 (DDA, M_n) was labeled with rhodamine (red) and dsODNs were 5′ labeled with (6FAM) (green). Chitosan 92-10 was complexed to dsODNs at an N:P ratio of 5.

Cell membranes were stained prior to imaging with CellMask™ (blue) to differentiate between internalized and membrane-bound nanoparticles. Images shown represent each separate channel, with dsODNs in green, chitosan in red, membrane in blue, differential interference contrast image in grey, and the merged images shown on the bottom left quadrant. (A) LS174T cells transfected with chitosan/ dsODN-RecQL1 nanoparticles. (B) HepG2 cells transfected with chitosan/dsODN-ApoB nanoparticles. (C) HEK293 cells transfected with chitosan/dsODN-ApoB nanoparticles. (D) Raw 294.7 cells transfected with chitosan/dsODN-ApoB nanoparticles.

Abbreviations: ApoB, apolipoprotein B; dsODN, double-stranded oligodeoxynucleotide; N:P, amine to phosphate.

5.3.5 Specific gene silencing and cell cytotoxicity evaluation of chitosan nanoparticles in different cell lines

Gene silencing occurs when complementarity is achieved between the siRNA seed region and target mRNA.[1] Chitosan-specific formulations (92-10-5, 80-40-5, 80-10-10, and 80-80-5) were assessed for mRNA knockdown in two different cell lines relevant to cancer and atherosclerosis, targeted by RecQL1 and ApoB siRNA, respectively. qPCR analysis revealed inhibition of RecQL1 and ApoB since their coding mRNAs were downregulated more than twofold (Figure 5-7). More specifically, in LS174T cells, chitosan 92-10-5 showed a high level of silencing (~80%) of RecQL1, similar to the current commercial gold standard liposomal formulation (~80%), used here as a positive control. Formulations 80-40-5 and 80-10-10 also induced significant silencing but to a lower degree than 92-10-5 and also with an increase of non-specific mock silencing, especially for formulation 80-10-10, for reasons that remain to be elucidated.

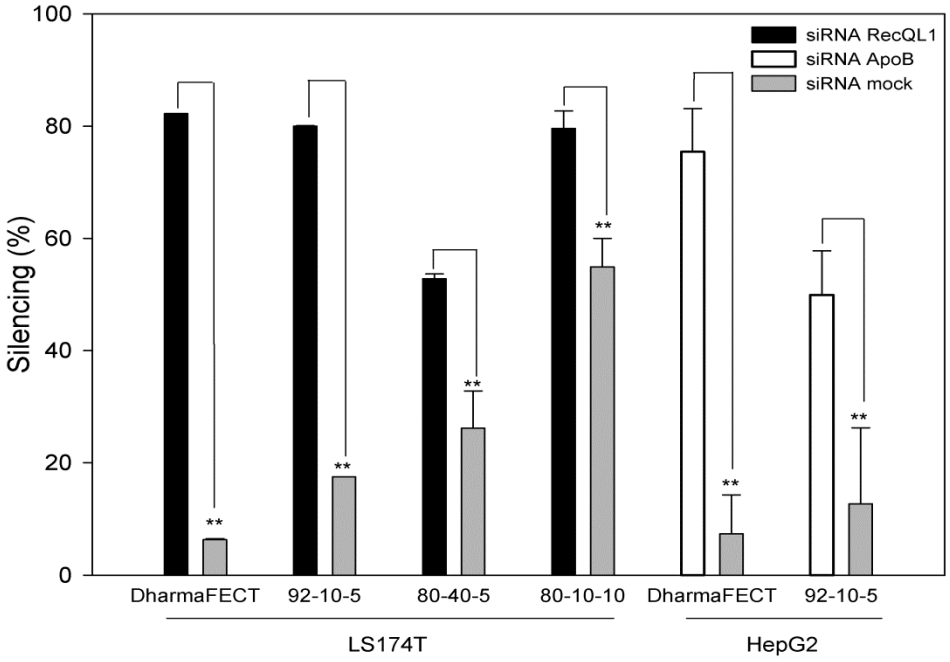

Figure 5-7: Real-time polymerase chain reaction analysis of the inhibition of RecQL1 and ApoB gene expression in specific cell lines. LS174T cells were transfected with chitosan (92-10-5, 80-40-5, and 80-10-10)/siRNA-RecQL1 nanoparticles, whereas HepG2 cells were transfected with chitosan (92-10-5)/siRNA-ApoB nanoparticles. The inhibition percentage was obtained by comparing the transfected and nontransfected cells, using the ΔΔCT method.

Notes: Values are mean ± SD; n = 3; *$P > 0.05$; **$P > 0.01$.

Abbreviations: ApoB, apolipoprotein B; siRNA, small interfering RNA; SD, standard deviation.

For the HepG2 cell line, only the best performing 92-10-5 was tested and induced significant silencing (~55% *versus* ~80% for positive control) of ApoB but slightly lower than RecQL1 for LS174T. Importantly, our results showed that silencing efficiency with chitosan reached similar levels to the positive control, with a markedly reduced cytotoxicity from the delivery system as assessed using the alamarBlue assay (Figure 5-8).

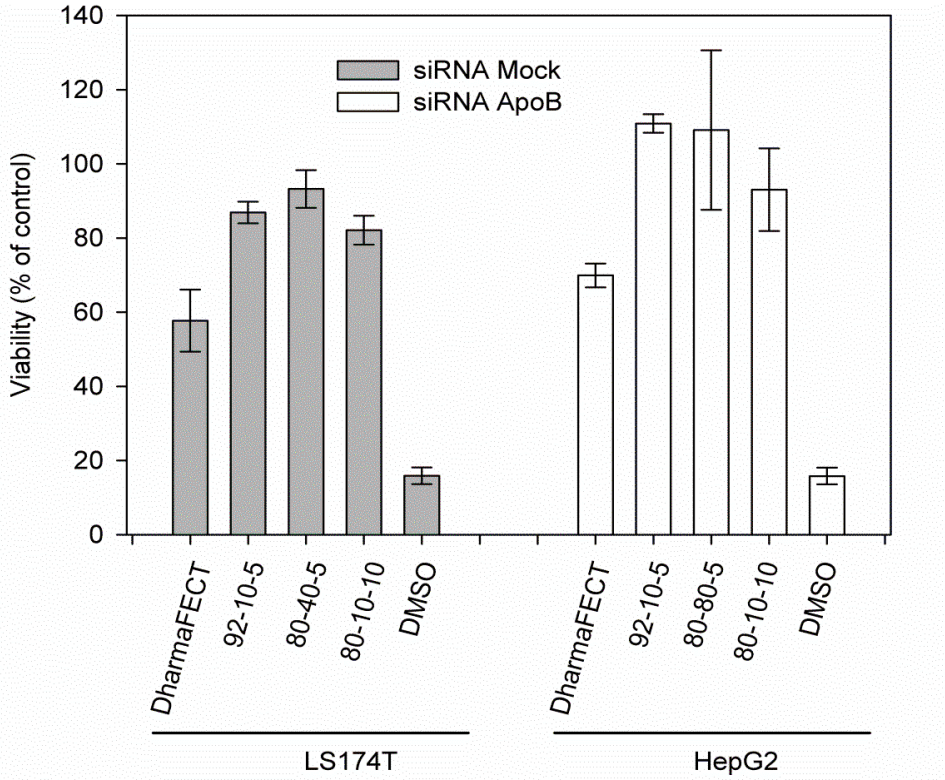

Figure 5-8: Cell viability assessment using the alamarBlue® assay 24 hours post transfection with different chitosan/siRNA formulations. To alleviate the apoptotic effect of RecQL1 gene silencing for a proper assessment of chitosan-siRNA toxicity, mock siRNA was used for transfection in the LS174T cell line. The HepG2 cell line was transfected with ApoB siRNA. DharmaFECT was used for comparison purposes whereas dimethyl sulfoxide was used as a positive control of toxicity.

Notes: Values are presented as mean ± SD; n = 3.

Abbreviations: ApoB, apolipoprotein B; siRNA, small interfering RNA.

5.4 Discussion

In this study, we evaluated the efficiency of specific low molecular weight chitosan (LMW-CS) formulations at low N:P ratios for the *in vitro* delivery of siRNA targeting either RecQL1 or ApoB genes. RecQL1 is a DNA helicase playing a major role in homologous recombination, maintenance of genomic stability, and DNA repair at damaged replication forks.[53,62] Overexpression of RecQL1

has been implicated in cancer by preventing cell apoptosis.[6,7,63] As for ApoB, it is a major gene involved in atherosclerosis through its essential role in the formation of very low density lipoprotein which will therefore generate low density lipoproteins following triacylglycerol hydrolyzation in the circulation.[52,64,65]

Nanoparticle size is one parameter affecting uptake and intracellular trafficking, both considered as potential rate-limiting steps for effective gene therapy.[42,43] For instance, nano-sized particles have been shown to be internalized more efficiently than micro-sized particles.[66–68] In this study, LMW-CS-based nanoparticles ranged in size from 41–110 nm, a size range promoting uptake, prolonged blood circulation, higher tissue penetration, and a relatively free passage from the mononuclear phagocyte system.[47,69–71] Therefore, our results show that these specific LMW-CS nanoparticles at low N:P ratios meet performance criteria (Table 5-3) and are potentially relevant for *in vivo* administration.

Table 5-3: Safety and performance criteria for the development of effective nonviral gene delivery systems

Categories	Performance criteria**
Physical and chemical properties	• Nanoparticle formation/assembly at a nucleic acid scale of 10 mg, from the perspective of size, shape, aggregation, and charge, as well as from an efficacy standpoint (such as toxicity and transfection efficacy), should be similar/reproducible each time nanoparticles are formed at this and lower concentrations • Assemblies less than 300 nm, PDI (<0.3) and no less than 80% incorporation efficiency • No aggregation in 50% mouse/human serum • Chemical stability of the assembly for >30 days • Preferably amenable to freeze-drying without any loss of its performance criteria
Activity in cell based assays*	• >50% reducation in target mRNA by target specific siRNA at concentrations <100 nm in 10% serum containing media • <10% reduction in target mRNA by control siRNA at concentrations <100 nm in 10% serum containing media • >5-fold window between target gene silencing IC50 and IC50 for reduction in viability • Activity in at least relevant 3 cell lines to the delivery system under evaluation
Performance and safety in animal models	• >50% reduction in target mRNA levels by target siRNA and <10% reduction in target mRNA levels in target tissue at 1 mg/kg dose by control siRNA by 24–48 hr • Demonstration of RNAi-mediated target mRNA cleavage by 5'-RACE • <10-fold cytokine induction (TNFα, IFNβ, IL6) and <10-fold increase in ALT and AST at 3 mg/kg siRNA dose • No effect on body weight and normal blood clinical chemistry and hematology data • Lack of immunogenicity • Lack of auto-antibodies and anti-DNA antibodies • Lack of systemic toxicity • No effect on body weight and normal blood clinical chemistry and hematology data

Notes: *If the delivery platform incorporates a targeting moiety evidence should be provided for targeting by (a) using cell lines with differential expression of targeted receptor and (b) using assemblies with "active" and "inactive or mutant" targeting moieties; **performance criteria described here are for both siRNA and plasmid DNA delivery systems. The criteria in this table has been adapted from information in US FDA[84,85] and US Pharmacopeia.[86]

Abbreviations: PDI, polydispersity index; mRNA, messenger RNA; siRNA, small interfering RNA; IC50, half maximal inhibitory concentration; RACE, rapid amplification of cDNA ends; ALT, alanine transaminase; AST, aspartate transaminase.

The different chitosan parameters – DDA, M_n, and N:P ratios – used in this study did not significantly affect nanoparticle size, with higher molecular weight chitosan promoting a slightly

increased size (Table 5-2). Our results are in contrast to previously published reports where the authors found increased nanoparticle size for lower molecular weight chitosan.[44] This discrepancy may be due to differences in experimental conditions and to the high N:P ratio used in Liu et al and Howard et al reports[8,44] *versus* low N:P ratios reported in our study. ESEM analysis revealed that these small nanoparticles were of spherical shape consistent with previous findings for pDNA,[38] siRNA,[8] and dsODNs.[72] The effect of nanoparticle shape on internalization efficiency showed spherical particles of similar size being internalized 500% more efficiently than rod-shaped particles.[73–75] This is mainly explained by increased membrane-wrapping time required for elongated particles and greater thermodynamic forces required for their engulfment.[61,75] It was previously demonstrated that the morphology of chitosan-pDNA nanoparticles is strongly dependent upon their charge ratios, and the variation of the latter resulted in nanoparticles with different topological conformations including spherical,[76] toroidal,[77,78] and globular morphologies.[77,79] Chitosan-based nanoparticle shape may also seem to be affected by the type of nucleic acid – pDNA or siRNA/dsODN – used for complexation and the process of nanoparticle formation; ie, ionic gelation. The fact that these LMW-CS nanoparticles demonstrated a reproducible pattern of spherical particles at low N:P ratios may be indicative of higher internalization efficiency than nanoparticles of different topological conformations.

Nanoparticle stability and nucleic acid protection are important parameters for efficient nucleic acid delivery. Our results of nuclease protection indicate that all LMW-CS formulations tested were able to protect dsODNs at supraphysiological concentrations of nucleases. Nuclease protection is of great importance for nucleic acid delivery systems through maintenance of cargo bioavailability and improved pharmacokinetic profile, thereby increasing the therapeutic potential of these nanoparticles. Increasing chitosan molecular weight resulted in an enhanced cargo protection (Figure 5-3) in agreement with previous findings.[17,39,43,44,47] Nevertheless, enhancing the ability of nanoparticles to protect their siRNA from degradation may render their intracellular disassembly more difficult, as demonstrated with high molecular weight chitosan-pDNA nanoparticles.[41] Further characterization of nanoparticle stability by gel retardation assays show that low M_n chitosan used at low N:P ratios can effectively complex and compact dsODNs into stable particles. We found LMW-CS nanoparticles at N:P ratios above 2 to be stable in slightly acidic buffers for at least 20 hours. These interesting findings are in contrast with most previous studies using chitosan-siRNA nanoparticles, where high M_n and high N:P ratios are usually

required to achieve particle stability.[8,17,43,44,80] This discrepancy can be explained by the lower pH (pH 6.5) of the electrophoresis buffer in our study compared to the commonly used TAE buffer at a pH of 8 for chitosan-based nanoparticle characterization,[8,17,43,44,81] a difference that was clearly highlighted by our gel retardation assay performed at both pHs (Figure 5-2). The use of a lower pH in the electrophoresis buffer results in higher degrees of chitosan ionization which translates to stronger electrostatic attraction to the polyanionic nucleic acid and hence more stable nanoparticles. This simple modification of the pH permits lower N:P ratios than those observed previously[8,17,43,44,81] to achieve nanoparticle stability. A direct consequence of this modification translates into reduced dosing, aggregation, and other undesirable nonspecific effects of large quantities of soluble chitosan for *in vivo* delivery where nanoparticles are to be injected at physiological pH values close to the chitosan pK_a of 6.5.

In general, efficient nanoparticle internalization depends on factors such as cell type, physicochemical surface properties of the nanoparticles, and the bio-nano interface.[61] In this report, we demonstrated that LMW-CS nanoparticles were efficiently internalized in multiple cell lines. The uptake efficiency as measured by flow cytometry ranged from 50% (Raw269.7) to 95% (A549 and HEK293), depending on the cell line. Statistical analysis of uptake efficiency inter-cell lines showed meaningful differences when comparing the A549 and HEK293 (high uptake) to the LS174T and Raw 269.7 (medium uptake), indicating a cell-line dependency of chitosan uptake. The cell-line dependency of chitosan nanoparticles uptake was previously suggested to be associated with different endocytic pathways.[82,83] Flow cytometry data showed LMW-CS nanoparticles to be efficiently internalized to levels similar or higher than commercially available liposomal systems such as DharmaFECT.

Finally, the transfection efficiency of LMW-CS nanoparticles as measured by gene-silencing efficacy was evaluated in two different cell lines: RecQL1 in LS174T cells and ApoB in HepG2 cells. The ability of these chitosan formulations to efficiently silence gene expression reached more than a twofold specific mRNA knockdown; with chitosan 92-10-5 being the most efficient and specific in the LS174T cell line. Other low molecular weight formulations also achieved good levels of gene silencing in the LS174T cell line. Interestingly, chitosan 80-10-10 achieved a high level of silencing with a concomitant increase in silencing when delivering mock siRNA. This intriguing observation is currently under investigation in our laboratory. The chitosan formulation 92-10-5 complexed to ApoB siRNA showed lower target mRNA knockdown in HepG2 when

compared to the LS174T cell lines targeted with the RecQL1 siRNA. The silencing efficiency correlated well with uptake efficiency as observed by flow cytometry where chitosan 92-10-5 showed both high uptake and high silencing efficiencies. Despite structural differences between pDNA and siRNA,[47] the chitosan formulation 92-10-5 has shown the highest transfection efficiencies for both siRNA and pDNA to date.[38–42] Taken together, our results show that LWM-CS nanoparticles at low N:P ratios can achieve efficient uptake and gene silencing *in vitro,* serving as a proof of concept for their use as efficient siRNA delivery vectors in cancer and atherosclerotic animal models. Although *in vitro* and *in vivo* performance criteria differ, no consensus on such performances has been established. For *in vivo* performance, safety remains the major issue, with guidance available from the US Food and Drug Administration for the development of gene and cell therapy products.[84] Therefore, the development of non-viral drug delivery systems for *in vivo* use should take into account physicochemical criteria, cell-based criteria, and, most importantly, *in vivo* performance and safety criteria (Table 5.3). The low-molecular-weight low-NP system presented here meets many of these criteria and has already been demonstrated as efficient *in vivo* for plasmid DNA delivery.[38,42] Thus a complete characterization of the safety and *in vivo* performance of our LMW-CS system delivering RecQL1 and ApoB targeting siRNA is currently under investigation in animal models of cancer and atherosclerosis.

Acknowledgments

This work was supported by the National Science and Engineering Research Council (NSERC) and by the Groupe de Recherche en Sciences et Technologies Biomédicales of the Fonds de la Recherche en Santé Quebec. We are grateful to Dr Monica Nelea for the ESEM analyses.

Disclosure

The authors declare no conflicts of interest in this work.

References

1. de Fougerolles A, Vornlocher HP, Maraganore J, Lieberman J. Interfering with disease: a progress report on siRNA-based therapeutics. *Nat Rev Drug Discov.* 2007;6(6):443–453.
2. Fire A, Xu S, Montgomery MK, Kostas SA, Driver SE, Mello CC. Potent and specific genetic interference by double-stranded RNA in Caenorhabditis elegans. *Nature.* 1998;391(6669):806–811.
3. Alameh M, Jean M, DeJesus D, Buschmann MD, Merzouki A. Chitosanase-based method for RNA isolation from cells transfected with chitosan/siRNA nanocomplexes for real-time RT-PCR in gene silencing. *Int J Nanomedicine.* 2010 2010;5:473.
4. Bantounas I, Phylactou LA, Uney JB. RNA interference and the use of small interfering RNA to study gene function in mammalian systems. *J Mol Endocrinol.* 2004;33(3):545–557.
5. Castanotto D, Rossi JJ. The promises and pitfalls of RNA-interference-based therapeutics. *Nature.* 2009;457(7228):426–433.
6. Futami K, Kumagai E, Makino H, et al. Induction of mitotic cell death in cancer cells by small interference RNA suppressing the expression of RecQL1 helicase. *Cancer Sci.* 2008;99(1):71–80.
7. Futami K, Kumagai E, Makino H, et al. Anticancer activity of RecQL1 helicase siRNA in mouse xenograft models. *Cancer Sci.* 2008;99(6):1227–1236.
8. Howard KA, Rahbek UL, Liu X, et al. RNA interference in vitro and in vivo using a novel chitosan/siRNA nanoparticle system. *Mol Ther.* 2006;14(4):476–484.
9. Soutschek J, Akinc A, Bramlage B, et al. Therapeutic silencing of an endogenous gene by systemic administration of modified siRNAs. *Nature.* 2004;432(7014):173–178.
10. Zimmermann TS, Lee AC, Akinc A, et al. RNAi-mediated gene silencing in non-human primates. *Nature.* 2006;441(7089):111–114.
11. Elbashir SM, Harborth J, Lendeckel W, Yalcin A, Weber K, Tuschl T. Duplexes of 21-nucleotide RNAs mediate RNA interference in cultured mammalian cells. *Nature.* 2001;411(6836):494–498.
12. Whelan J. First clinical data on RNAi. *Drug Discov Today.* 2005;10(15):1014–1015.
13. Corey DR. RNA learns from antisense. *Nat Chem Biol.* 2007;3(1):8–11.

14. Corey DR. Chemical modification: the key to clinical application of RNA interference? *J Clin Invest.* 2007;117(12):3615–3622.
15. Stein CA. Phosphorothioate antisense oligodeoxynucleotides: questions of specificity. *Trends Biotechnol.* 1996;14(5):147–149.
16. Urban-Klein B, Werth S, Abuharbeid S, Czubayko F, Aigner A. RNAi-mediated gene-targeting throught systemic application of polyethylenimine (PEI)-complexed siRNA in vivo. *Gene Ther.* 2004;12(5):461–466.
17. Katas H, Alpar HO. Development and characterisation of chitosan nanoparticles for siRNA delivery. *J Control Release.* 2006;115(2):216–225.
18. Elmen J, Thonberg H, Ljungberg K, et al. Locked nucleic acid (LNA) mediated improvements in siRNA stability and functionality. *Nucleic Acids Res.* 2005;33(1):439–447.
19. Judge AD, Bola G, Lee AC, MacLachlan I. Design of noninflammatory synthetic siRNA mediating potent gene silencing in vivo. *Mol Ther.* 2006;13(3):494–505.
20. Whitehead KA, Langer R, Anderson DG. Knocking down barriers: advances in siRNA delivery. *Nat Rev Drug Discov.* 2009;8(2):129–138.
21. Bramsen JB, Laursen MB, Nielsen AF, et al. A large-scale chemical modification screen identifies design rules to generate siRNAs with high activity, high stability and low toxicity. *Nucleic Acids Res.* 2009;37(9):2867–2881.
22. Layzer JM, McCaffrey AP, Tanner AK, Huang Z, Kay MA, Sullenger BA. In vivo activity of nuclease-resistant siRNAs. *RNA.* 2004;10(5):766–771.
23. Weyermann J, Lochmann D, Georgens C, Zimmer A. Albumin-protamine-oligonucleotide-nanoparticles as a new antisense delivery system. Part 2: cellular uptake and effect. *Eur J Pharm Biopharm.* 2005;59(3):431–438.
24. Amarzguioui M, Holen T, Babaie E, Prydz H. Tolerance for mutations and chemical modifications in a siRNA. *Nucleic Acids Res.* 2003;31(2):589–595.
25. Parrish S, Fleenor J, Xu S, Mello C, Fire A. Functional anatomy of a dsRNA trigger: differential requirement for the two trigger strands in RNA interference. *Mol Cell.* 2000;6(5):1077–1087.
26. Braasch DA, Jensen S, Liu Y, et al. RNA interference in mammalian cells by chemically-modified RNA. *Biochemistry.* 2003;42(26):7967–7975.

27. Harborth J, Elbashir SM, Vandenburgh K, et al. Sequence, chemical, and structural variation of small interfering RNAs and short hairpin RNAs and the effect on mammalian gene silencing. *Antisense Nucleic Acid Drug Dev.* 2003;13(2):83–105.
28. Reasor MJ, Kacew S. Drug-induced phospholipidosis: are there functional consequences? *Exp Biol Med (Maywood).* 2001;226(9):825–830.
29. Tousignant JD, Gates AL, Ingram LA, et al. Comprehensive analysis of the acute toxicities induced by systemic administration of cationic lipid:plasmid DNA complexes in mice. *Hum Gene Ther.* 2000;11(18):2493–2513.
30. Ishida T, Ichihara M, Wang X, et al. Injection of PEGylated liposomes in rats elicits PEG-specific IgM, which is responsible for rapid elimination of a second dose of PEGylated liposomes. *J Control Release.* 2006;112(1):15–25.
31. Judge A, McClintock K, Phelps JR, MacLachlan I. Hypersensitivity and loss of disease site targeting caused by antibody responses to PEGylated liposomes. *Mol Ther.* 2006;13(2):328–337. Epub 2005 Nov 7.
32. Semple SC, Harasym TO, Clow KA, Ansell SM, Klimuk SK, Hope MJ. Immunogenicity and rapid blood clearance of liposomes containing polyethylene glycol-lipid conjugates and nucleic acid. *J Pharmacol Exp Ther*. 2005;312(3):1020–1026. Epub 2004 Nov 3.
33. Boeckle S, von Gersdorff K, van der Piepen S, Culmsee C, Wagner E, Ogris M. Purification of polyethylenimine polyplexes highlights the role of free polycations in gene transfer. *J Gene Med.* 2004;6(10):1102–1111.
34. de Fougerolles A, Vornlocher HP, Maraganore J, Lieberman J. Interfering with disease: a progress report on siRNA-based therapeutics. *Nat Rev Drug Discov*. 2007;6(6):443–453.
35. Moghimi SM, Symonds P, Murray JC, Hunter AC, Debska G, Szewczyk A. A two-stage poly(ethylenimine)-mediated cytotoxicity: implications for gene transfer/therapy. *Mol Ther.* 2005;11(6):990–995.
36. Hunter AC, Moghimi SM. Cationic carriers of genetic material and cell death: a mitochondrial tale. *Biochim Biophys Acta.* 2010;1797(6–7):1203–1209.
37. Al-Dosari MS, Gao X. Nonviral gene delivery: principle, limitations, and recent progress. *AAPS J.* 2009;(4):671–681. Epub 2009 Oct 16.

38. Jean M, Smaoui F, Lavertu M, et al. Chitosan-plasmid nanoparticle formulations for IM and SC delivery of recombinant FGF-2 and PDGF-BB or generation of antibodies. *Gene Ther.* 2009;16(9):1097–1110.
39. Lavertu M, Méthot S, Tran-Khanh N, Buschmann MD. High efficiency gene transfer using chitosan/DNA nanoparticles with specific combinations of molecular weight and degree of deacetylation. *Biomaterials.* 2006;27(27):4815–4824.
40. Nimesh S, Thibault MM, Lavertu M, Buschmann MD. Enhanced gene delivery mediated by low molecular weight chitosan/DNA complexes: effect of pH and serum. *Mol Biotechnol.* 2010;46(2):182–196.
41. Thibault M, Nimesh S, Lavertu M, Buschmann MD. Intracellular trafficking and decondensation kinetics of chitosan-pDNA polyplexes. *Mol Ther.* 2010;18(10):1797–1795.
42. Jean M, Alameh M, Buschmann MD, Merzouki A. Effective and safe gene-based delivery of GLP-1 using chitosan/plasmid-DNA therapeutic nanocomplexes in an animal model of Type 2 Diabetes. *Gene Ther.* 2011 18(8):807–816.
43. Howard KA, Kjems J. Polycation-based nanoparticle delivery for improved RNA interference therapeutics. *Expert Opin Biol Ther.* 2007;7(12):1811–1822.
44. Liu X, Howard KA, Dong M, et al. The influence of polymeric properties on chitosan/siRNA nanoparticle formulation and gene silencing. *Biomaterials.* 2007;28(6):1280–1288.
45. de Campos AM, Diebold Y, Carvalho EL, Sanchez A, Alonso MJ. Chitosan nanoparticles as new ocular drug delivery systems: in vitro stability, in vivo fate, and cellular toxicity. *Pharm Res.* 2004;21(5):803–810.
46. Onishi H, Machida Y. Biodegradation and distribution of water-soluble chitosan in mice. *Biomaterials.* 1999;20(2):175–182.
47. Mao S, Sun W, Kissel T. Chitosan-based formulations for delivery of DNA and siRNA. *Adv Drug Deliv Rev.* 2010;62(1):12–27.
48. Richardson SC, Kolbe HV, Duncan R. Potential of low molecular mass chitosan as a DNA delivery system: biocompatibility, body distribution and ability to complex and protect DNA. *Int J Pharm.* 1999;178(2):231–243.
49. Huang M, Khor E, Lim LY. Uptake and cytotoxicity of chitosan molecules and nanoparticles: effects of molecular weight and degree of deacetylation. *Pharm Res.* 2004;21(2):344–353.

50. Wiegand C, Winter D, Hipler UC. Molecular-weight-dependent toxic effects of chitosans on the human keratinocyte cell line HaCaT. *Skin Pharmacol Physiol.* 2010;23(3):164–170.
51. Ma PL, Buschmann MD, Winnik FM. One-step analysis of DNA/chitosan complexes by field-flow fractionation reveals particle size and free chitosan content. *Biomacromolecules.* 2010;11(3):549–554.
52. Olofsson SO, Boren J. Apolipoprotein B: a clinically important apolipoprotein which assembles atherogenic lipoproteins and promotes the development of atherosclerosis. *J Intern Med* 2005;258(5):395–410.
53. Sharma S, Doherty KM, Brosh RM, Jr. Mechanisms of RecQ helicases in pathways of DNA metabolism and maintenance of genomic stability. *Biochem J.* 2006;398(3):319–337.
54. Scaringe SA, Wincott FE, Caruthers MH. Novel RNA synthesis method using 5'-silyl-2'-orthoester protecting groups. *J Am Chem Soc.* 1998(120):11820–11821.
55. Nguyen S, Hisiger S, Jolicoeur M, Winnik FM, Buschmann MD. Fractionation and characterization of chitosan by analytical SEC and ^{1}H-NMR after semi-preparative SEC. *Carbohydr Polym.* 2009(75):636–646.
56. Nguyen S, Winnik FM, Buschmann MD. Improved reproducibility in the determination of the molecular weight of chitosan by analytical size exclusion chromatography. *Carbohydr Polym.* 2009(75):582–533.
57. Lavertu M, Xia Z, Serreqi AN, et al. A validated ^{1}H-NMR method for the determination of the degree of deacetylation of chitosan. *J Pharm Biomed Anal.* 2003;32(6):1149–1158.
58. Skrypina NA, Timofeeva AV, Khaspekov GL, Savochkina LP, Beabealashvilli R. Total RNA suitable for molecular biology analysis. *J Biotechnol.* 2003;105(1–2):1–9.
59. Quong D, Neufeld RJ. DNA protection from extracapsular nucleases, within chitosan- or poly-L-lysine-coated alginate beads. *Biotechnol Bioeng.* 1998;60(1):124–134.
60. Ma PL, Lavertu M, Winnik FM, Buschmann MD. New insights into chitosan-DNA interactions using isothermal titration microcalorimetry. *Biomacromolecules.* 2009;10(6):1490–1499.
61. Nel AE, Madler L, Velegol D, et al. Understanding biophysicochemical interactions at the nano-bio interface. *Nat Mater.* 2009;8(7):543–557.
62. Wu L, Hickson ID. DNA helicases required for homologous recombination and repair of damaged replication forks. *Annu Rev Genet.* 2006;40:279–306.

63. Kawabe T, Tsuyama N, Kitao S, et al. Differential regulation of human RecQ family helicases in cell transformation and cell cycle. *Oncogene.* 2000;19(41):4764–4772.
64. Schaefer JR, Scharnagl H, Baumstark MW, et al. Homozygous familial defective apolipoprotein B-100. Enhanced removal of apolipoprotein E-containing VLDLs and decreased production of LDLs. *Arterioscler Thromb Vasc Biol.* 1997;17(2):348–353.
65. Itabe H. Oxidative modification of LDL: its pathological role in atherosclerosis. *Clin Rev Allergy Immunol.* 2009;37(1):4–11.
66. Gref R, Domb A, Quellec P, et al. The controlled intravenous delivery of drugs using PEG-coated sterically stabilized nanospheres. *Adv Drug Deliv Rev.* 1995;16:215–233.
67. Bivas-Benita M, Romeijn S, Junginger HE, Borchard G. PLGA-PEI nanoparticles for gene delivery to pulmonary epithelium. *Eur J Pharm Biopharm.* 2004;58(1):1–6.
68. Panyam J, Labhasetwar V. Biodegradable nanoparticles for drug and gene delivery to cells and tissue. *Adv Drug Deliv Rev.* 2003;55(3):329–347.
69. Guy J, Drabek D, Antoniou M. Delivery of DNA into mammalian cells by receptor-mediated endocytosis and gene therapy. *Mol Biotechnol.* 1995;3(3):237–248.
70. Desai MP, Labhasetwar V, Amidon GL, Levy RJ. Gastrointestinal uptake of biodegradable microparticles: effect of particle size. *Pharm Res.* 1996;13(12):1838–1845.
71. Seymour LW. Passive tumor targeting of soluble macromolecules and drug conjugates. *Crit Rev Ther Drug Carrier Syst.* 1992;9(2):135–187.
72. Jean M, Alameh M, De Jesus D, et al. Chitosan-based therapeutic nanocomplexes for combination gene therapy and gene silencing of in vitro cell lines relevant to type 2 diabetes. *Eur J Pharm Sci.* 2011;45(1–2):138–149. Epub 2011 Nov 9.
73. Chithrani BD, Chan WC. Elucidating the mechanism of cellular uptake and removal of protein-coated gold nanoparticles of different sizes and shapes. *Nano Lett.* 2007;7(6):1542–1550.
74. Chithrani BD, Ghazani AA, Chan WC. Determining the size and shape dependence of gold nanoparticle uptake into mammalian cells. *Nano Lett.* 2006;6(4):662–668.
75. Verma A, Stellacci F. Effect of surface properties on nanoparticle-cell interactions. *Small.* 2010;6(1):12–21.
76. Liu W, Sun S, Cao Z, et al. An investigation on the physicochemical properties of chitosan/DNA polyelectrolyte complexes. *Biomaterials.* 2005;26(15):2705–2711.

77. Erbacher P, Zou S, Bettinger T, Steffan AM, Remy JS. Chitosan-based vector/DNA complexes for gene delivery: biophysical characteristics and transfection ability. *Pharm Res.* 1998;15(9):1332–1339.
78. Danielsen S, Strand S, de Lange Davies C, Stokke BT. Glycosaminoglycan destabilization of DNA-chitosan polyplexes for gene delivery depends on chitosan chain length and GAG properties. *Biochim Biophys Acta.* 2005;1721(1–3):44–54. Epub 2004 Nov 2.
79. Köping-Höggård M, Mel'nikova YS, Vårum KM, Lindman B, Artursson P. Relationship between the physical shape and the efficiency of oligomeric chitosan as a gene delivery system in vitro and in vivo. *J Gene Med.* 2003;5(2):130–141.
80. Gao S, Dagnaes-Hansen F, Nielsen EJ, et al. The effect of chemical modification and nanoparticle formulation on stability and biodistribution of siRNA in mice. *Mol Ther.* 2009;17(7):1225–1233.
81. Ji AM, Su D, Che O, et al. Functional gene silencing mediated by chitosan/siRNA nanocomplexes. *Nanotechnology.* 2009;20(40):405103.
82. Bishop NE. An Update on Non-clathrin-coated Endocytosis. *Rev Med Virol.* 1997;7(4):199–209.
83. Huang M, Ma Z, Khor E, Lim LY. Uptake of FITC-chitosan nanoparticles by A549 cells. *Pharm Res.* 2002;19(10):1488–1494.
84. Center for Biologics Evaluation and Research, US Food and Drug Administration. Guidance for industry: considerations for plasmid dna vaccines for infectious disease indications. Rockville, MD; 2007. Available from: http://www.fda.gov/BiologicsBloodVaccines/GuidanceComplianceRegulatoryInformation/Guidances/Vaccines/ucm074770.htm. Accessed January 1, 2012.

Chapter 6 ARTICLE 3: SIRNA DELIVERY WITH CHITOSAN: INFLUENCE OF CHITOSAN MOLECULAR WEIGHT, DEGREE OF DEACETYLATION AND AMINE TO PHOSPHATE RATIO ON IN VITRO SILENCING EFFICIENCY, HEMOCOMPATIBILITY, BIODISTRIBUTION AND IN VIVO EFFICACY

Mohamad Alameh[2], Marc Lavertu[1,2], Nicolas Tran-Khan[1], Chi-Yuan Chang[1], Frederic Lesage[3], Vincent Darras[1], and Michael D Buschmann[1,2**].

[1] Polytechnique Montreal, Department of Chemical engineering, Montreal, QC, Canada. [2] Polytechnique Montreal, Institute of Biomedical engineering, Montreal, QC, Canada. [3] Polytechnique Montreal, Department of Electrical engineering, Montreal, QC, Canada

**Corresponding author.

Submitted to Biomacromolecules (2017)

Graphical abstract:

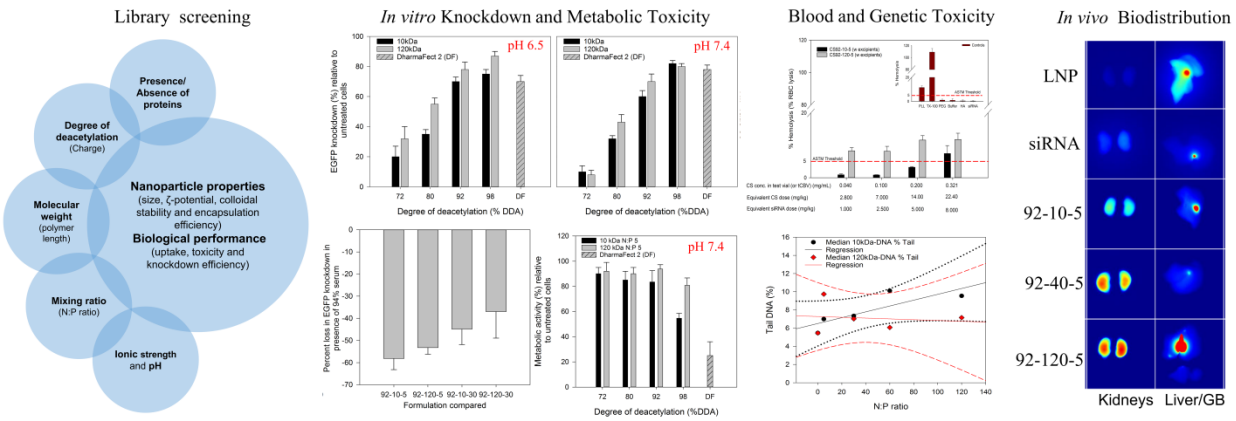

Abstract: Chitosan is a natural non-toxic and biodegradable polymer that has shown *in vitro* and *in vivo* efficacy for siRNA delivery. Previous reports investigating the effect of chitosan parameters, including the degree of deacetylation (DDA) and molecular weight (Mn), on nanoparticle performance have resulted in contradictory findings. To understand the influence of these parameters on *in vitro* transfection efficiency, toxicity, genotoxicity, hemocompatibility and *in vivo* bio-distribution, a library of precisely characterized chitosans was produced at different DDAs (98%, 92%, 80% and 72%) and Mn (5, 10, 40, 80 and 120 kDa). 8 chitosans were manually mixed with siRNA at amine to phosphate ratios of 5:1 and 30:1, and resulting nanoparticles characterized for their size and surface charge (ζ-potential) in the presence of 10 and 150 mM salt. Encapsulation efficiency (EE) and transfection efficiency were characterized at pH 6.5 and 8 for EE and pH 6.5 and 7.4 for *in vitro* transfection. Optimized formulations were selected for further characterization of the influence of Mn and N:P ratio on nanoparticle uptake, resulting metabolic activity, genotoxicity, and *in vitro* transfection in the presence of increasing concentrations of serum. Hemocompatibility and *in vivo* biodistribution were also investigated for different Mn, N:P ratio and dose. Nanoparticle uptake and gene silencing positively correlated with increased surface charge, which in turn was obtained at high DDA and high Mn. A minimum polymer length of ~60-70 monomers, or Mn of ~10kDa, was required for stability and *in vitro* knockdown in the presence or absence of serum. *In vitro* knockdown reached levels equivalent to the lipid control (DharmaFect® 2) with no metabolic toxicity or genotoxicity, the former in contrast to the lipid which severely impaired metabolic activity. The negative effect of serum on biological performance was dependent on DDA, Mn and N:P . The poor *in vitro* performance above 50%

serum is believed to be multifactorial in cause. *In vivo* biodistribution in mice show accumulation of nanoparticles in the proximal epithelial tubules of the kidney, where 40-50% functional knockdown was observed, suggesting potential applications in kidney diseases.

Key words: Chitosan, siRNA, Degree of deacetylation, Molecular weight, Library screening, Biodistribution.

6.1 Introduction

Oligonucleotide (ON) therapeutics represent a novel class of molecules designed to modulate gene expression through direct interference with ribonucleic acids (RNA) or proteins [1]. Clinical translation depends on the efficient delivery and cellular uptake of large and negatively charged ON [2]. Advances in understanding ON biology, mechanism of action, physico-chemistry and their interactions with molecular machines (i.e. RNAi Inducing Silencing Complex) and/or sensors (i.e. Toll-Like Receptors) has allowed the introduction of design rules and chemical modifications that improve nuclease resistance and reduce immune activation and sequence-dependent off-target effects. For instance, chemical modifications of the phosphate backbone and the 2'position of the ribose protect small interfering RNA (siRNA) from nuclease digestion and thus modulate its pharmacokinetics (PK) and dynamics (PD) by improving serum half-life [3, 4]. In addition, modifications such as 2'OMe were demonstrated to prevent immune activation [5, 6] and limit off-target effects due to improved thermodynamic stability (hybridization complementarity between anti-sense sequence and target mRNA) [7]. Although modifications improve serum half-life ($t_{1/2}$) and promote siRNA binding to proteins, intracellular translocation to the pharmacological site of action and renal elimination cannot be circumvented by this strategy nor can improvement of sequence design. As a consequence, chemical conjugation with ligands or encapsulation in delivery systems constitute the two predominant strategies used in clinical development of siRNA delivery. Trivalent N-acetylgalactosamine (GalNAc) conjugation on the sense strand results in highly potent hepatocyte targeted siRNA able to escape endosomal compartments and achieve meaningful knockdown in phase II/III clinical trials [2]. Dynamic Poly-Conjugates (DPC), employ a similar strategy where cholesterol-conjugated siRNA is coadministered with a GalNAc targeted and polyethylene glycol masked endosomolytic peptide or polymer [8]. These two conjugation approaches continue to demonstrate potency in pre-clinical and clinical studies but face serious challenges with the recent discontinuation of the Revusiran and ARC-520/521 programs [9, 10].

Discontinuation followed findings of imbalanced mortality in the Revusiran arm compared to placebo [9] and the death of a non-human primate administered with high doses of DPCs [10]. However, mechanistic insight leading to the observed mortality needs to be determined before being associated with the siRNA payload or the delivery system or other factors [9].

Encapsulation of siRNA into delivery systems physically protect the siRNA from serum nucleases, increase bioavailability and allow efficient delivery to certain targeted organs and cells using lipid nanoparticles (LNP) that have reached clinical trials [8, 9, 11]. However, LNPs are associated with serious side effects such as immune activation and their clinical administration is preceded by and/or accompanied with prophylactic anti-inflammatory steroids [12, 13]. The shortcomings of LNP based vectors are not limited to the above-mentioned issues but also include their limited capability to deliver nucleic acid cargos beyond the liver [14]. Therefore, delivery systems that meet criteria such as colloidal stability, high encapsulation efficiency, low toxicity, reduced renal clearance, and deliver siRNA efficiently to extrahepatic organs are critically needed.

Chitosan is a family of cationic bio-copolymers composed of β (1-4) linked N-acetyl glucosamine (GlcNAc) and D-glucosamine (Glc) that has gained considerable attention for ON delivery. Chitosan is characterized by low *in vitro* and *in vivo* toxicity, ease of production/chemical conjugation, and is generally recognized as safe (GRAS) [15]. Chitosan can be easily fine-tuned to reach specific degrees of deacetylation (DDA), or fractions of protonatable amine (charge), and average molecular weights (Mw or Mn). The high degree of protonation of amino groups (NH_2) occurring at a pH below chitosan pKa (~6.5-6.9) favors the spontaneous formation of nanosized polyelectrolyte complexes through electrostatic interaction with polyanionic molecules such as ON.

Early work showed that transfection efficiency (TE) of plasmid-containing chitosan nanoparticles depended on a fine equilibrium between chitosan tunable parameters of DDA, Mn and the molar ratio of chitosan amine to plasmid phosphate (N:P) as well as other extrinsic factors such as pH and the presence of serum proteins [16-20]. Chitosan has also been used to deliver short double-stranded siRNAs both *in vitro* [21-32] and *in vivo* [28, 32-37]. Most reports evaluating physicochemical parameters for efficient *in vitro* siRNA delivery were performed using partly deacetylated (DDA ~ 80-85%) chitosan formulated at high N:P ratio (>25) [26-31, 33]. Such formulations could pose significant practical problems for *in vivo* delivery such as premature

dissociation, limited dosing, blood incompatibility and non-specific effects due to large quantities of free excess chitosan. Although gene knockdown (KD) has been achieved, experimental discrepancies, differences in chitosan sources, and lack of characterization rendered results inconclusive in identifying optimal parameters for siRNA delivery [15]. Reports correlating transfection efficiency (TE) as a function of chitosan DDA, Mn and N:P ratio have been contradictory [24-27, 29]. Therefore a systematic study of siRNA delivery with accurately characterized chitosans that investigates the effect of intrinsic (DDA, Mn and N:P ratio) and extrinsic parameters (serum, pH, ionic strength and mixing conditions) on cell uptake, transfection efficiency, toxicity, genotoxicity, hemocompatibility and *in vivo* bio-distribution is needed.

To understand the correlation between nanoparticle physicochemical properties and knockdown efficiency (KD), we produced a library of chitosans precisely characterized by gel permeation chromatography for molecular weight and ^{1}H NMR for DDA. The effect of DDA, polymer length (Mn), mixing ratio (N:P) and pH was systematically examined and correlated with nanoparticle physicochemical properties including size, surface charge (ζ-potential), encapsulation efficiency (EE), and *in vitro* delivery. Potent formulations were selected for further characterization and tested in the presence of increased serum concentrations and correlated to knockdown efficiency. In addition, off-target effects and nanoparticle mediated toxicity were examined using a metabolic assay coupled with genotoxicity testing. The influence of experimental conditions on reference gene stability was determined using an MIQE [38] compliant assessment of mRNA knockdown. We also show that selected formulations may be intravenously administered at doses up to 14 mg/kg of chitosan, accumulate in the kidney specifically in the proximal tubule epithelial cells (PTEC) and induce functional target knockdown in the kidney.

6.2 Materials and methods

6.2.1 siRNA sequences and chitosan characterization

siRNA sequences were custom synthesized by Dharmacon Inc (GE Dharmacon, Lafayette, CO, USA) except for the non-targeting siRNA (siNT) which was purchased as a predesigned product from the same supplier (D-001710-01-50). All siRNA sequences used *in vitro* were provided by the manufacturer in a lyophilized format following standard desalting. The anti-EGFP siRNA sense sequence was 5’-GAC GUA AAC GGC CAC AAG UUC-3’ and the antisense sequence was 3’-

CGC UGC AUU UGC CGG UGU UCA-‘5, duplex Mw 13,360 g/mol. The siRNA sequence has been used in two chitosan-siRNA studies [28, 29]. The DY^{647} siRNA sequence was modified at the 5’ end of the sense strand and purified by HPLC for *in vivo* administration.

Chitosans (**Table 7-1**) at different DDAs were obtained from Marinard, (Laval, QC, Canada) and depolymerized in our laboratory using nitrous acid to achieve specific number-average molecular weight targets (Mn) of 5, 10, 40, 80 and 120 kDa (**Table 7-1**). Chitosan number and weight-average molecular weights (Mn and Mw) were determined by gel permeation chromatography (GPC) using a Shimadzu LC-20AD isocratic pump coupled with a Dawn HELEOS II multi-angle laser light scattering detector (Wyatt Technology Co, Santa Barbara, CA), an Optilab rEX interferometric refractometer (Wyatt Technology Co), and two Tosoh TSKgel (G6000PWxl-CP and G5000PWxl-CP; Tosoh Bioscience LLC, King of Prussia, PA) columns. Chitosans were eluted at pH 4.5 using an acetic acid (0.15 M)/sodium acetate (0.1 M)/sodium azide (4 mM) buffer. The injection volume was 100µL, the flow rate 0.8 mL min^{-1} and temperature 25°C. The dn/dc values for chitosan with a 92 and 80% DDA were determined at 0.208 and 0.201 using a laser’s wavelength of 658 nm. The degree of deacetylation was determined by ^{1}H NMR as per *in house* published methods [39].

Table 6-1 Characterization of chitosans tested in this study. Different chitosans are denoted according to their chemical composition using the nomenclature [DDA-Mn] and are represented in the first column of the table. The degree of deacetylation (DDA) was determined by ^{1}H NMR. The number and weight average molecular weight (Mn and Mw) were determined by gel permeation chromatography (GPC). The polydispersity index (PdI) was calculated as M_w/M_n. The degree of polymerization (Dp) or chain length was computed using the following equation

$$Dp = (Mn\ chitosan)/(Mw\ monomer\ at\ specific\ DDA)$$

Chitosan	DDA (%)	Mn (kDa)	Mw (kDa)	PdI	Dp
72-10	75.4	11.8	17.9	1.60	69
72-120	71.7	140.4	182.5	1.30	811
80-10	84.4	10.8	14.5	1.34	64
80-120	82.9	177.4	290.4	1.64	1,054
92-5	91.7	4.3	6.4	1.51	26
92-10	92.0	9.0	13.7	1.52	55
92-40	92.5	40.7	54.9	1.35	248
92-80	92.7	81.1	267.6	3.30	494
92-120	91.9	137.6	180.7	1.31	836
98-10	98.9	8.8	11.4	1.29	54
98-120	98.5	127.5	188.3	1.47	788

6.2.2 Preparation of nanoparticles by manual mixing

Chitosans were dissolved overnight in nuclease free water (Life Technologies, Burlington, ON, Canada) and 1N HCl (Sigma-Aldrich, Oakville, ON, Canada), using a glucosamine to HCl ratio of 1:1, to a final concentration of 5 mg/mL. The stock solutions were sterile filtered using a 0.22 µm PVDF filter and used to prepare solutions at specific N:P ratio by dilution in nuclease-free water. Before complexation, siRNA was diluted to a working concentration of 0.1 mg/mL. Unless otherwise stated, nanoparticles were formed by simple electrostatic complexation following manual addition of chitosan to siRNA at a 1:1 ratio (v/v). The final volume never exceeded 250 µL and chitosan was pipetted into siRNA. Nanoparticles were kept at room temperature for 20-30 minutes before further use.

6.2.3 Determination of nanoparticle size and surface charge

Size and surface charge (ζ-potential) of nanoparticles were determined by Dynamic Light Scattering (DLS) and Laser Doppler velocimetry using a ZetaSizer Nano ZS device (Malvern Instruments Ltd, Malvern, UK). The scattering angle of the detector was fixed at 173° and measurements were performed at 25°C using the viscosity of water as sample diluent. Nanoparticles were diluted 1:4 and 1:8 using sterile filtered NaCl solution (20 or 150mM) before determination of size and ζ-potential respectively. For data in Figure 6-1, size and ζ-potential were measured immediately post incubation in buffer (~2.5 min for size and 5 min for ζ-potential). For data in Figure S. 6-1 size and ζ-potential were measured at the respective time point post incubation in buffer. The Smoluchowski equation was used to calculate ζ-potential from the measured electrophoretic mobility. All measurements were done in duplicate and replicated twice (N=3, n=6).

6.2.4 Encapsulation efficiency and siRNA release

The encapsulation efficiency (EE) of siRNA was determined using the Quant-iT™ Ribogreen® RNA reagent (Life Technologies, Burlington, ON, Canada) to assess siRNA free in solution after mixing with chitosan. Encapsulation efficiency (EE) was calculated as percentage fluorescence intensity relative to non-formulated siRNA.

6.2.4.1 siRNA release at different pH

Nanoparticles were incubated in buffers with different pH, 25 mM MES (pH 6.5), 1X PBS (pH 7.2) or 1X TAE (pH 8.0) and aliquots were taken at 24 hours post incubation. Aliquots were further diluted 1:200 in respective buffers, mixed with an equal volume of Quant-iT™ RiboGreen® reagent to detect free siRNA, incubated for 5 minutes at room temperature and fluorescence measured using the TECAN Infinite® M200 PRO microplate system (Tecan Systems, Mannedorf, Switzerland).

6.2.4.2 siRNA release in the presence of heparin

The effect of physiological concentrations of heparin on siRNA release was tested. Heparin (Sigma-Aldrich, Oakville, ON, Canada) solution at 1 mg/mL was prepared in nuclease free water, sterile filtered and diluted to 5 µg/mL. Nanoparticles were prepared as mentioned above and diluted 1:2 in heparin, incubated for 1h and then diluted 1:100 in Tris-EDTA (TE 1X, pH 7.2) and a volume of 100 µL transferred into black plates (Corning, NY, USA). Quant-iT™ RiboGreen® reagent (1:200) was prepared in TE 1X (pH 7.2) and an equal volume (100µL) was added to the nanoparticles. Plates were incubated on a rotary mixer for 5 minutes in the dark and fluorescence measured using a TECAN Infinite® M200 PRO microplate system (Tecan Systems, Mannedorf, Switzerland). The excitation and emission wavelengths were 480 and 530 nm respectively. Naked siRNA, heparin alone, TE 1X, chitosan/heparin and siRNA/heparin were used as controls to assess background, assay interference and as subtraction blank.

6.2.4.3 siRNA release in the presence of serum albumin

The effect of physiological concentrations of bovine serum albumin (BSA) on siRNA release was tested. BSA stock solution (125 mg/mL) was prepared in nuclease free water, quantified using the microBCA assay (Life Technologies, Burlington, ON, Canada) and diluted to reach 50 mg/mL respectively. The Quant-iT™ RiboGreen® assay was identical to the heparin competition assay described above with the only difference that nanoparticles challenged with BSA were diluted 1:2000 in TE 1 X (pH 7.2). This high dilution was used to overcome assay inhibition. Naked siRNA, BSA alone, TE 1X, chitosan-BSA and siRNA-BSA were used as controls to assess background, assay interference, and as subtraction blank.

6.2.5 Cell culture

The $EGFP^+$ H1299 cell line (human lung carcinoma) was provided by Prof. Jorgen Kjems (Aarhus University, Denmark) and has been used in several chitosan-siRNA studies [26, 28, 29, 31, 33]. This cell line was generated by Dr Anne Chauchereaux (Gustave Roussy Institute, Paris, France) by transducing the parental H1299 cell line (ATCC, Manassas, VA, USA) with pd2EGFP-N1 (Clonetech, Mountain View, CA, USA). The plasmid encodes a modified version of EGFP with a turnaround rate of 2 h ($t_{1/2}$ ~2h). Cells were cultured in RPMI-1640 (ATCC, Manassas, VA, USA) supplemented with 10% heat-inactivated FBS (Life Technologies, Burlington, ON, Canada), 1% GlutaMAX™ (Life Technologies, Burlington, ON, Canada) and 500 µg/mL of G418 antibiotic at 37°C in a 5% CO_2 environment.

6.2.6 *In vitro* transfection

For target gene knockdown and siRNA uptake, cells were seeded in 24 well plates at a density of 45,000 cells/well to reach ~75-80% confluence on the day of transfection. Prior to transfection, cells were washed once with 500 µL of warm Ca^{2+}/Mg^{2+} free PBS and replenished with fresh RPMI-1640 which contained varying amounts of FBS (0-94%). Nanoparticles were prepared as described above and a specific volume added to cells to reach the target siRNA concentration 25-400 nM per well. Cells were incubated for either 4h (toxicity), 8h (genotoxicity) or 48 hours (knockdown, toxicity, and genotoxicity). For the serum challenge experiment, medium containing increasing amounts of FBS (0-94%) was aspirated and replaced with complete RPMI-1640 medium 4 hours post transfection.

DharmaFect® 2-siRNA nanoparticles were prepared by diluting siRNA stock solution to 0.025 mg/mL (4 µM) in Opti-MEM® serum free media and complexed to the lipid component as per manufacturer recommendation; a volume of 6.4 µL of DharmaFect® 2 in 153.6 µL Opti-MEM® was used for complexation.

6.2.7 Assessment of EGFP knockdown and nanoparticle uptake using flow cytometry

EGFP knockdown was measured using a MoFLo™ flow cytometer (Beckman Coulter, Mississauga, ON, Canada) equipped with a 488 nm argon laser for excitation (model ENTCII-621,

Coherent, Santa Clara, CA, USA) and a 510/20nm (FL1) band pass filter to detect fluorescence. Nanoparticle uptake was measured on a BD FACSAria™ equipped with a 633 laser and a 660/20nm (FL1) band pass filter to detect fluorescence of internalized DY^{647} labeled siRNA. Before analysis, $EGFP^+$ H1299 cells were washed twice with ice-cold Ca^{2+}/Mg^{2+} free PBS, trypsinized and suspended in complete RPMI-1640 medium. For uptake, cells were incubated with *Streptomyces griseus* type III chitosanase as per [21] before washing and trypsinization. A dot plot of forward scatter (FSC) *versus* side scatter (SSC) was created and a collection gate established using the Summit 3.0 software (Beckman Coulter, Mississauga, ON, Canada) to exclude cell debris, dead and aggregated cells. 20,000 events per sample were recorded and non-transfected cells (untreated) were used to establish baseline EGFP expression in terms of absolute fluorescence intensity (FI). EGFP knockdown in treated samples was calculated as mean FI relative to non-transfected cells ($KD\ (\%) = \frac{mean\ FI\ (treated)}{mean\ FI\ (untreated)} \times\ 100$).

6.2.8 MIQE compliant quantitative real-time PCR (qPCR)

The secondary structure of endogenous and target genes used in this study was *in silico* assessed using the mFold freeware [40]. The position of the primer and probe sequences relative to the structure was determined prior to qPCR analysis. Before extraction, transfected $EGFP^+$ H1299 cells were treated with *Streptomyces griseus* type III chitosanase (Sigma-Aldrich, Oakville, ON, Canada) as described in [21]. Total RNA extraction was performed 48 hours post transfection using the RNeasy® Plus Mini extraction kit (Qiagen, Toronto, ON, Canada) as per manufacturer protocol. Following extraction, samples were digested with 2 µL TURBO™ DNA-free kit (Life Technologies, Burlington, ON, Canada) for 30 minutes to remove potential genomic DNA contamination and then inactivated with 5 µL DNase inactivation reagent, spun down for 1.5 minutes at 10,000 g and the supernatant collected. The purity of total RNA was determined by measuring A_{230}/A_{260}, A_{260}/A_{280} and A_{340} using a Jenway spectrophotometer. The integrity of total RNA (RIN) was determined using the Agilent 2100 Bioanalyzer system (Agilent Technologies, Mississauga, ON, Canada). Total RNA concentration was determined using the Quant-iT™ RiboGreen® Assay (Life Technologies, Burlington, ON, Canada). RiboGreen® reagent and extracted RNA samples were diluted 1:200 and 1:100 respectively using the supplied nuclease free TE 1X buffer (pH 8.0), mixed at 1:1 ratio (v/v) and a volume of 200 µL pipetted into 96 well black plates (Corning, NY, USA). Plates were incubated at room temperature in the dark for 5 minutes

before measuring fluorescence using a TECAN Infinite® M200 PRO microplate system (Tecan Systems, Mannedorf, Switzerland). The excitation and emission wavelengths were 485 and 530 nm respectively and concentrations (ng/mL) were derived from a ribosomal RNA (rRNA) standard curves prepared on the same plate as per manufacturer recommendations. A total 1 µg of extracted RNA was reverse transcribed at 42ºC for 60 min using the SuperScript® VILO™ cDNA synthesis kit (Life Technologies, Burlington, ON, Canada). For qPCR, 10 ng cDNA was amplified using TaqMan Fast Advanced Master Mix® (Life Technologies, Burlington, ON, Canada) on an ABI HT-7900 real-time PCR system (Applied Biosystems, Mississauga, ON, Canada). All reactions were performed in a 384 well plate in a final volume of 10 µL. Quantitative real-time PCR (qPCR) was performed using the following cycle conditions: 2-minute hold at 55ºC, 10-minute hold at 95ºC followed by 40 cycles at 95ºC for 15 s and 60ºC for 1 min. Primer-probe efficiency was determined using the standard curve method. For each assay tested, a 6 log 10-fold dilution curve was constructed by plotting the quantification cycle (Cq) *versus* Log cDNA concentration and linearly regressed to fit the data. The PCR reaction efficiency was estimated using $E = 10^{(-\frac{1}{slope})}$. The list of assays (primer-probe pairs) used in this study and their respective efficiencies can be found in the supplementary methods section. Reference gene stability was assessed using the geNorm statistical package (Biogazelle NV, Zwijnaarde, Belgium) with a panel of 10 reference genes under 10 experimental conditions including non-treated, lipid-treated, high and low N:P ratio, high and intermediate DDA and high and low Mn). The experiment was replicated once and the M (stability parameter) and V (pair wise variation of normalization factors) scores determined [41].

6.2.9 Assessment of nanoparticle toxicity using the alamarBlue® assay

The effect of nanoparticle on metabolic activity was measured using alamarBlue® (Life Technologies, Burlington, ON, Canada). Preliminary experiments were performed as per manufacturer protocols to define optimal cell density, incubation time and assess assay interference with chitosan. $EGFP^+$ H1299 cells were seeded in 96 well plates (CellBIND®, Fisher Scientific, Mississauga, ON, Canada) at a density of 5,000 cells/well 20-24 hours prior to transfection. Cells were transfected as previously described at a final anti-EGFP siRNA concentration of 100 nM. Metabolic activity was measured at 4 hours and 44 hours post transfection by replacing medium over cells with 200 µL of complete RPMI-1640 medium supplemented with 10% alamarBlue®

reagent. Absorbance was measured at 570 and 600 nm using a TECAN Infinite® M200 PRO microplate system (Tecan Systems, Mannedorf, Switzerland) 4 hours after the addition of assay reagent. Metabolic activity of cells was evaluated as the percentage reduction of alamarBlue® relative to untreated cells.

6.2.10 Assessment of nanoparticle genotoxicity using the comet or single cell gel electrophoresis assay.

The assessment of nanoparticle genotoxicity was performed using the Trevigen alkaline cometAssay® kit (Trevigen Inc, Gaithersburg, MD, USA) at 8 and 48 hours post-transfection. The 8-hour time point was assessed to mimic the alamarBlue® time point (4 h transfection + 4 hours incubation with reagent). $EGFP^+$ H1299 cells were transfected as described above, trypsinized, resuspended in complete RPMI-1640 media and counted using the Countess automated cell counter system (Life Technologies, Burlington, ON, Canada). Cells were centrifuged at 100 g for 3 minutes, and the pellet suspended in ice cold PBS (Ca^{2+}/Mg^{2+} free) at a concentration of 100,000 cells/mL. Agarose embedding, lysis, and electrophoresis were performed according to the manufacturer protocol. Slides were stained with 100 µL of (1:10,000) SYBR gold® nucleic acid stain (Life technologies, Burlington, ON, Canada), dried at 37ºC and imaged following excitation at 488 nm using an Axiovert epi-fluorescent microscope (Carl Zeiss, Toronto, ON, Canada). Images were analyzed using the Open Comet plugin [42] installed in the ImageJ freeware (NIH, Besthada, CA, USA). The experiment was replicated once and at least 100 comets were counted per experiment (N=2, n≥ 200).

6.2.11 Assessment of nanoparticle hemocompatibility at doses relevant for *in vivo* administration

Hemolytic and hemagglutination properties of nanoparticles were tested according to ASTM E2524 [43] and Evani et al [44] respectively. Human blood was collected from consenting and healthy donors following protocol approval by the University Ethics Committee. Nanoparticles were prepared using an in-house automated in-line mixing system [45] and freeze-dried (FD) in the presence of 0.83% w/v trehalose (Sigma-Aldrich, Oakville, ON, Canada), and 5.8 mM histidine (pH 6.5) (Sigma-Aldrich, Oakville, ON, Canada). FD samples were rehydrated to 12X using

nuclease free water to reach the highest tested concentration (or dose) and iso-osmolality then serially diluted using 10% w/v trehalose buffer (300 mOsm) to a final siRNA concentration of 0.1, 0.25, 0.5, and 0.8 mg/mL. The plasma-free hemoglobin (PFH) in the blood was measured at 0.49 mg/mL prior to initiating the assay. Total blood hemoglobin (TBH) was adjusted with PBS to a concentration of 10 ± 1 mg/mL. Nanoparticles were mixed with PBS and diluted TBH blood (TBHd) at a 1:7:1 volumetric ratio, with 100 µL of nanoparticles at the target concentration pipetted into an Eppendorf tube containing 700µL PBS and 100 µL of blood (TBHd 10 ± 1 mg/mL). For colorimetric determination of hemolysis, samples (700 µL) were incubated for 3 h in a water bath at 37 °C and visually inspected every 30 minutes for nanoparticle flocculation, dispersion, sinking or floating. The supernatant was collected following centrifugation at 800 g for 15 min and absorbance measured at 540 nm on a TECAN Infinite® M200 PRO microplate system (Tecan Systems, Mannedorf, Switzerland. A four-parameter regression algorithm (4PL) was used to obtain the calibration curve required to calculate the hemoglobin concentration in the supernatant of each sample (PFHsample). The percentage of hemolysis was computed as: $Hemolysis\ (\%) = 100 \times (PFH_{sample}/TBHd)$. For hemagglutination, the remaining 200 µL of each sample prepared above were pipetted in 96 well assay plates, incubated for 3h, visualized using an Axiovert light microscope and the area covered by red blood cells (RBCs) estimated and scored.

6.2.12 *In vivo* biodistribution and efficacy studies

All *in vivo* experiments described in this manuscript were randomized double blinded and approved by the University of Montreal Ethics Committee (CDEA) and the Montreal Heart Institute Research Center Ethics Committee. Mice were purchased from Charles Rivers (Charles River, Quebec, Canada), housed and acclimatized in a specific pathogen-free facility with unrestricted access to water and food. Mice had body condition scores (BCS) of 3 [46] and their body weights (BW) were in the range of 20-25 g at the time of injection. All injection volumes were calculated as 10 µL/g of BW and injections performed within 10-15 seconds. Mice were euthanized under anesthesia (mixture of 3% Forane™ and 20-80% oxygen-air vol/vol) by cardiac puncture followed by cervical dislocation

6.2.12.1 Determination of chitosan-siRNA biodistribution using *ex-vivo* whole organ imaging

Balb/c nude female (♀) mice aged 6 weeks and weighing 20-22 g were injected for the biodistribution experiments All test articles i.e. Naked siRNA, Invivofectamine® 2.0 and chitosan based nanoparticles formulated at N:P 5 (Mn 10, 40 and 120 kDa) were intravenously injected (I.V.) at a dose of 0.5 mg/kg DY^{647} labeled siRNA. The DY^{647} fluorophore was injected at a dose of 0.5 mg/kg. Mice were euthanized 4 hours post administration and immediately perfused using PBS (1 X 20 mL) and 10% Neutral Buffer Formalin (NBF, 1 X 40 mL). *Ex-vivo* imaging on collected organs was performed using a whole animal imaging system mounted with an EMCCD EM N2 camera (NUVU Cameras, Montreal, QC, Canada). Controls included PBS, naked DY^{647} labeled siRNA, DY^{647} alone, and commercially available lipid control Invivofectamine® 2.0 (Life Technologies, Burlington, ON, Canada). The latter was prepared as per manufacturer recommendation.

6.2.12.2 Determination of *in vivo* functional gene knockdown

6.2.12.2.1 Preparation, lyophilization, reconstitution, and characterization of injected nanoparticles for *in vivo* efficacy

Low (10kDa) and high (120kDa) molecular weight chitosans with a degree of deacetylation of 92 and 98% (Table 6-1) were dissolved as described above to a final concentration of 5 mg/mL. The stock solutions were sterile filtered using a 0.22 µm PVDF filter (EMD Millipore, Etobicoke, ON, Canada) and used to prepare solutions, containing 1% trehalose and 3.8 mM histidine, at an N:P ratio of 5 by dilution in nuclease-free water, 4% w/v trehalose and 28 mM histidine (pH 6.5). Before complexation, anti-GAPDH siRNA stock solutions (4 mg/mL) were diluted to 0.2 mg/mL in the same buffer as chitosan. Nanoparticles were prepared at a final N:P ratio of 5:1 using simple manual mixing. All nanoparticles were incubated for 30 min at room temperature upon preparation before analyses or freeze-drying. Anti-GAPDH nanoparticles were lyophilized under sterile conditions using a Laboratory Series Freeze-Dryer PC/PLC (Millrock Technology, Kingston, NY, USA). An optimized 1-day cycle comprising the following program: rapid cooling to 5 °C, 30 min hold, rapid cooling to -5 °C, 30 min hold, temperature decrease from -5 to -40 ^{o}C, at a rate of 1 °C/min, 2 hours hold, initiation of primary drying for 10 h at -32 ^{o}C and 60 mTorr; followed by secondary drying cycle at 60 mTorr, increase in shelf temperature to 30°C, at rate of 0.2°C/min, and a 6 hours hold

was used. Nanoparticle volumes of 3.84, or 7 mL were freeze-dried in 10 or 20 mL serum vials respectively, using 20 mm butyl-lyophilization stoppers. Samples were backfilled with argon, stoppered, crimped, and stored at 4°C until reconstitution. All FD samples were reconstituted at the animal facility to 10-times their initial concentration using water for injection and their concentration adjusted by diluting with a nearly-isotonic aqueous solution comprising 10% w/v trehalose, so that the desired dosage (mg siRNA/kg animal body weight) would be reached upon injection of 10 µL of nanoparticles per gram of animal body weight. Immediately after injection, reconstituted nanoparticles were characterized for their size and polydispersity as described above.

6.2.12.2.2 *In vivo* efficacy and monitoring of clinical signs and body weight

Balb/c male (♂) mice aged 6-7 weeks and weighing 22-25g were used for the efficacy study (3 animals/group). Uncoated anti-GAPDH NPs were prepared as described above and administered at 2.5 mg/kg every other day for a total of three injections and mice were sacrificed 72 hours following the last injection. Naked anti-GAPDH siRNAs (siGAPDH) were administered at 2.5 mg/kg following the same schedule. Clinical signs were determined for a period of 4-hours post-administration of test articles and at euthanasia. The clinical signs were recorded by trained personnel and qualified animal care technicians. Clinical signs were scored for body condition, general aspect, natural behavior, and provoked behavior. Body weight was recorded prior to each injection and at euthanasia using an Avery Berkel scale (Avery Berkel, Fairmont, MN, USA). Body weight was expressed as percent change relative to the previous injection. Mice were euthanized, under anesthesia, using cardiac puncture, followed by cervical dislocation, total circulating blood volume (tCBV) and organs collected. tCBV was serum separated and immediately stored at -80ºC, and organs split into halves and stored in LiqN and fixed in 10% NBF before protein extraction and determination of GAPDH enzymatic activity.

6.2.12.2.3 *In vivo* assessment of functional knockdown using the KDalert® assay

Following collection, organs were snap frozen in liquid nitrogen and stored at -80ºC until use. Frozen tissues were cut on dry ice, weighed (~20 mg), and disrupted using the TissueLyzer® II

system (Qiagen Inc, Toronto, ON, Canada). Tissues were disrupted using the 5 mm steel beads (Qiagen Inc, Toronto, ON, Canada) under the following conditions: 2 x 30 Hz, 20 seconds per cycle. Homogenized tissues were resuspended in 750 µL of KDalert™ lysis buffer (Life Technologies, Burlington, ON, Canada), and incubated on ice for 30 minutes with inversions every 10 minutes. Lysates were clarified by centrifugation (2270 g, 30 minutes, 4°C), transferred to new tubes, and diluted (1:20), in KDalert™ lysis buffer. The standard curve was prepared by diluting GAPDH stock solution (26 U/mL) with lysis buffer at a 1:100 ratio (GAPDH: Lysis), followed by 2-fold serial dilutions from 1:5 to 1:320. Twenty microliters of diluted samples and standards were transferred into 96 well plates (Corning, NY, USA), and 180µL of the KDalert™ Master Mix (Life Technologies, Burlington, ON, Canada) was pipetted into each well. Plates were incubated for 15 minutes at room temperature and absorbance measured at 610 (10) nm using a TECAN Infinite® F-500 microplate system (Tecan Systems, Mannedorf, Switzerland). GAPDH activity in units (U) was computed from the standard curve and normalized to total protein content (mg) of the lysate sample as determined using the BioRad DC Protein assay kit (Bio-Rad Laboratories, Mississauga, ON, Canada).

6.2.13 Assessment of *in vitro* knockdown and nanoparticle biodistribution using confocal microscopy

Visual confirmation of *in vitro* knockdown was performed using live cell imaging. $EGFP^{+}$ H1299 cells were seeded at a density of 25,000 cells/well onto an 8-chamber Lab-Tek® (MatTek, Ashland, MA, USA) and imaged in multitrack mode using a Zeiss LSM 510 META confocal Axioplan 200 microscope (Carl Zeiss AG, Feldbach, Switzerland). For *in vivo* biodistribution and subcellular localization of DY^{647} labeled siRNA, organs were cryosectioned (5 µm), actin stained using phalloidin red and counterstained with Hoechst (Life Technologies, Burlington, ON, Canada).

6.2.14 Statistical analysis

Data were collected and expressed as average ± standard deviation (stdev). Statistical analysis was conducted using STATISTICA® 12.0 (Dell Statsoft, Tulsa, OK, USA) and SigmaPlot® 13.0 (Systat software, San Jose, CA, USA) software packages. Unless otherwise stated, the General Linear

Model, One/Two-Factor ANOVA, and multiple regression analysis were performed on collected data. The design of experiment module in STATISTICA® 12.0 was used to generate full or fractional factorial designs and generate multifactorial modeling. Data from the comet experiments was also subjected to non-parametric analysis.

6.3 Results

6.3.1 Chitosan dictate nanoparticle uptake, target knockdown, ζ-potential and encapsulation efficiency at physiological pH while increasing Mn and N:P ratio have positive effects

A library of chitosans was produced, precisely characterized (Table 6-1), and assessed under different experimental conditions (pH, ionic strength and presence/absence of serum) to understand molecular parameters favoring adequate physicochemical properties (size, surface charge, colloidal stability, and encapsulation efficiency) and efficient non-toxic *in vitro* knockdown (target knockdown and metabolic toxicity). As illustrated in Figure 6-1, nanoparticle size, measured 2.5 minutes post-incubation in the buffer, increased with both polymer length (Mn) and ionic strength. In both low and high ionic strength, size increased 2-3 -fold due to an increase in Mn from 10 to 120kDa. The effect of chitosan DDA and amine to phosphate ratio (N:P) on size was minimal. Nanoparticle surface charge (ζ-potential) decreased with increasing ionic strength, as expected due to salt-induced electrostatic screening. At low ionic strength, ζ-potential increased with increased DDA, Mn and N:P ratio. As shown in Figure 6-1C, and confirmed using multiple regression analysis, DDA had the strongest effect on ζ-potential followed by N:P ratio and Mn, respectively. Although ζ-potential was around 2-3 fold lower at high ionic strength, the tendency of increased ζ-potential with a concomitant increase in DDA, Mn and N:P ratio was conserved (Figure 6-1C and D).

Given that DDA and the N:P ratio did not significantly alter size, colloidal stability was investigated using low and high Mn chitosan-formulated at an N:P ratio of 5 (92-10-5 and 92-120-5). As shown in Figure S. 6-1, nanoparticle size and polydispersity was independent of Mn in 10 mM NaCl and stable up to at least 1-hour post complexation. Increasing the ionic strength to 150 mM had a significant impact on colloidal stability with nanoparticles aggregating rapidly to reach the µm scale. The polydispersity index (PdI), a dimensionless measure of dispersion around the mean, reached its maximum value of 1 in 150 mM NaCl around 15 min post complexation indicating severe aggregation/high heterogeneity. Interestingly, colloidal instability increased with the increase of molecular weight.

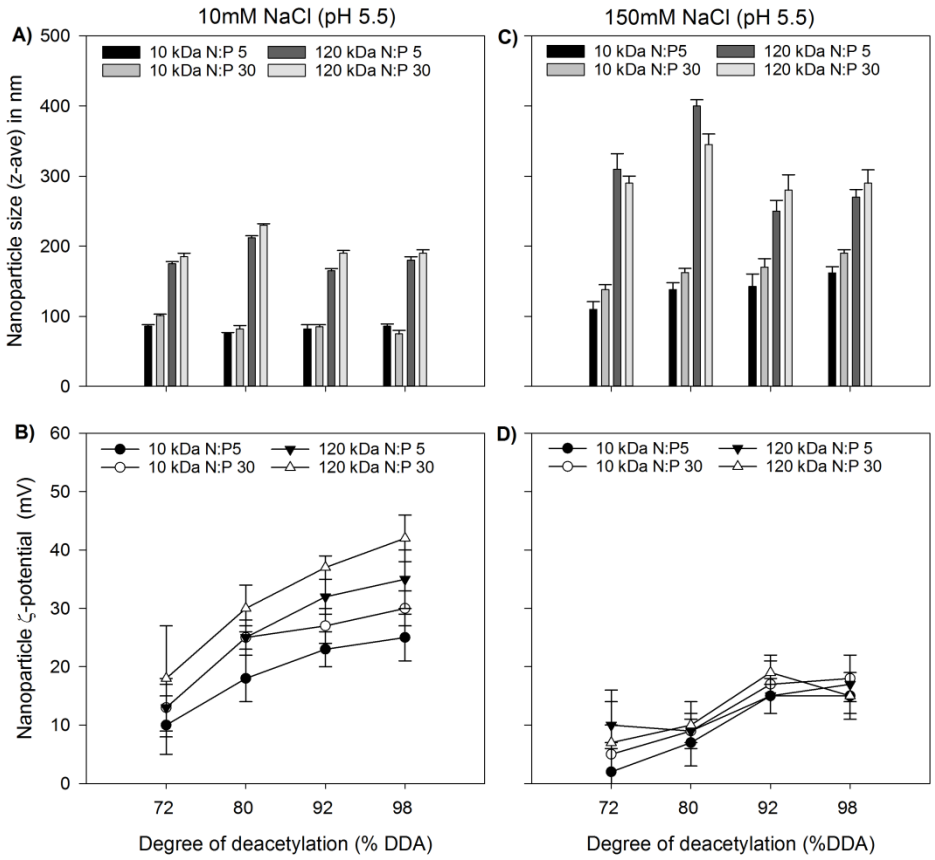

Figure 6-1 Nanoparticle size and ζ-potential as a function of DDA, Mn, and amine to phosphate ratio (N:P) measured in the presence of 10 and 150 mM NaCl. A) Nanoparticle size (Z-ave diameter) vs DDA, Mn and N:P ratio in the presence of low ionic strength (10 mM NaCl, pH 5.5, measurement at 2.5 min post incubation in medium). B) Nanoparticle surface charge (ζ-potential) vs DDA, Mn and N:P ratio in the presence of low ionic strength (10 mM NaCl, pH 5.5). C) Nanoparticle size vs DDA, Mn and N:P ratio in the presence of high ionic strength (150 mM NaCl, pH 5.5). D) Nanoparticle surface charge (ζ-potential) vs DDA, Mn and N:P ratio in the presence of high ionic strength (150 mM NaCl, pH 5.5). Data represent the average ± standard deviation of 3 independent experiments with 2 technical replicates per experiment (N=3, n=6). Measurements in 150 mM NaCl were taken immediately after adding 150 mM NaCl. Measurements in 10 mM NaCl were stable over time (see Supp Info Figure S. 6-1)

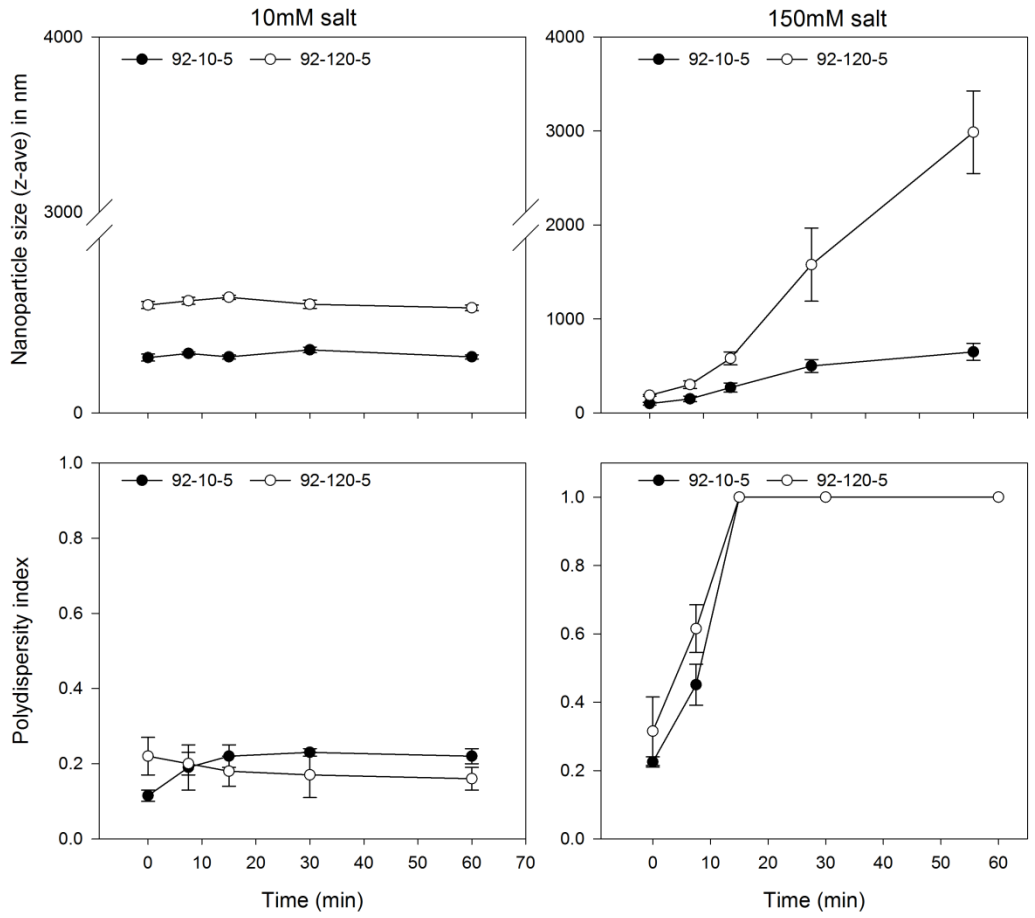

Figure S. 6-1 Nanoparticle colloidal stability versus time. The effect of polymer length on nanoparticle size was investigated in medium containing 10 and 150mM salt (NaCl) over a period of 1h. Nanoparticles were prepared in water by manual mixing of chitosan and siRNA (0.1mg/mL) at 1:1 v/v to reach an N:P ratio of 5, diluted 1:8 in media and size measured over time. Measurements were conducted at 0, 7.5, 15, 30 and 60 minutes post dilution. Data represent the average of 2 independent experiments. Each DLS measurement consisted of 15 repeats.

siRNA compositions should be able to protect the nucleic acid cargo in physiological fluids through a material specific mechanism of payload entrapment. As a consequence, encapsulation efficiency (EE), or the percentage of siRNA incorporated into the nanoparticle, was measured as a function of DDA, Mn, N:P ratio and pH using dye exclusion. In order to eliminate the effect of colloidal instability on dye exclusion, the assay was performed at low ionic strength. As shown in Figure 6-2, all formulations were able to achieve complete payload encapsulation at pH 6.5. Increasing the pH from 6.5 to 8.0 resulted in dye accessing siRNA payload indicating release and highlighting

the importance of DDA, Mn and N:P ratio, and their interaction, on the integrity/stability of the particles and payload protection. Maximization of nanoparticle integrity at high pH could be achieved by increasing DDA, Mn and N:P ratio.

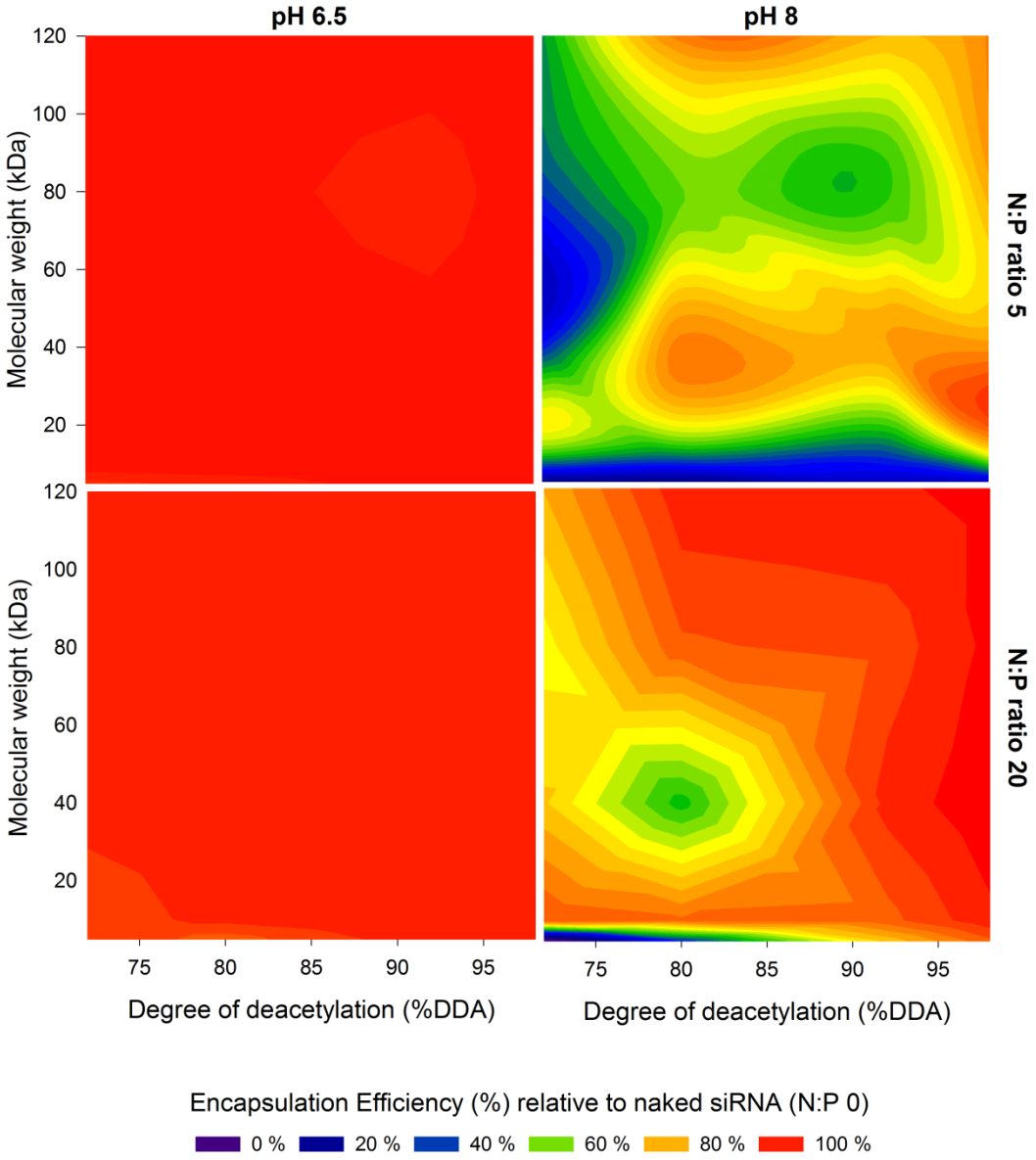

Figure 6-2 Effect of DDA, Mn and N:P ratio on the encapsulation efficiency at two different pH. Nanoparticles were formed in water and incubated either in 25 mM MES (pH 6.5) or 1X TAE (pH 8.0) for 24 hours then assayed for siRNA release using the Quant-iT™ RiboGreen® assay. The percentage of siRNA release provided the percent encapsulation efficiency (% EE) computed relative to naked siRNA (N:P 0). Red color corresponds to 100% encapsulation efficiency (no release) while magenta corresponds to 0% encapsulation efficiency (all released). Average values

from 2 independent experiments with 3-4 technical replicates per experiment. At pH 6.5, complete encapsulation (0% release) of the payload is observed at all DDA, Mn and N:P ratio used to form nanoparticles. However, at pH 8.0, chitosan glucosamine units become deprotonated and their interaction with siRNA phosphate groups decreases promoting payload release. At pH 8, an increase in DDA, Mn and N:P ratio is required to maintain nanoparticle integrity.

In vitro performance of these formulations in the presence of 10% serum was assessed using the EGFP $^{+}$ H1299 cell line and correlated with nanoparticle physicochemical properties. As illustrated in Figure 6-3, EGFP knockdown significantly increased with increasing charge density (DDA), and to a lesser extent with increasing polymer length (Mn) and N:P ratio. The effect of pH on the biological performance of nanoparticles was minimal with a slight decrease in knockdown efficiency at higher pH observed for formulations with low-to-intermediate DDA (i.e. 72-10, 72-120, 80-10 and 80-120). No pH dependent performance could be detected for formulations with high charge density (92-10, 92-120, 98-10 and 98-120) when transfection pH increased from 6.5 to 7.4 (Figure 6-3). In contrast, a statistically insignificant improvement in knockdown at acidic pH was observed for formulations with low-to-intermedia charge density. Although the effect of N:P ratio was minimal in contrast to DDA, increasing N:P ratio could increase knockdown efficiency of formulations with low-to-intermediate DDA (Figure 6-3).

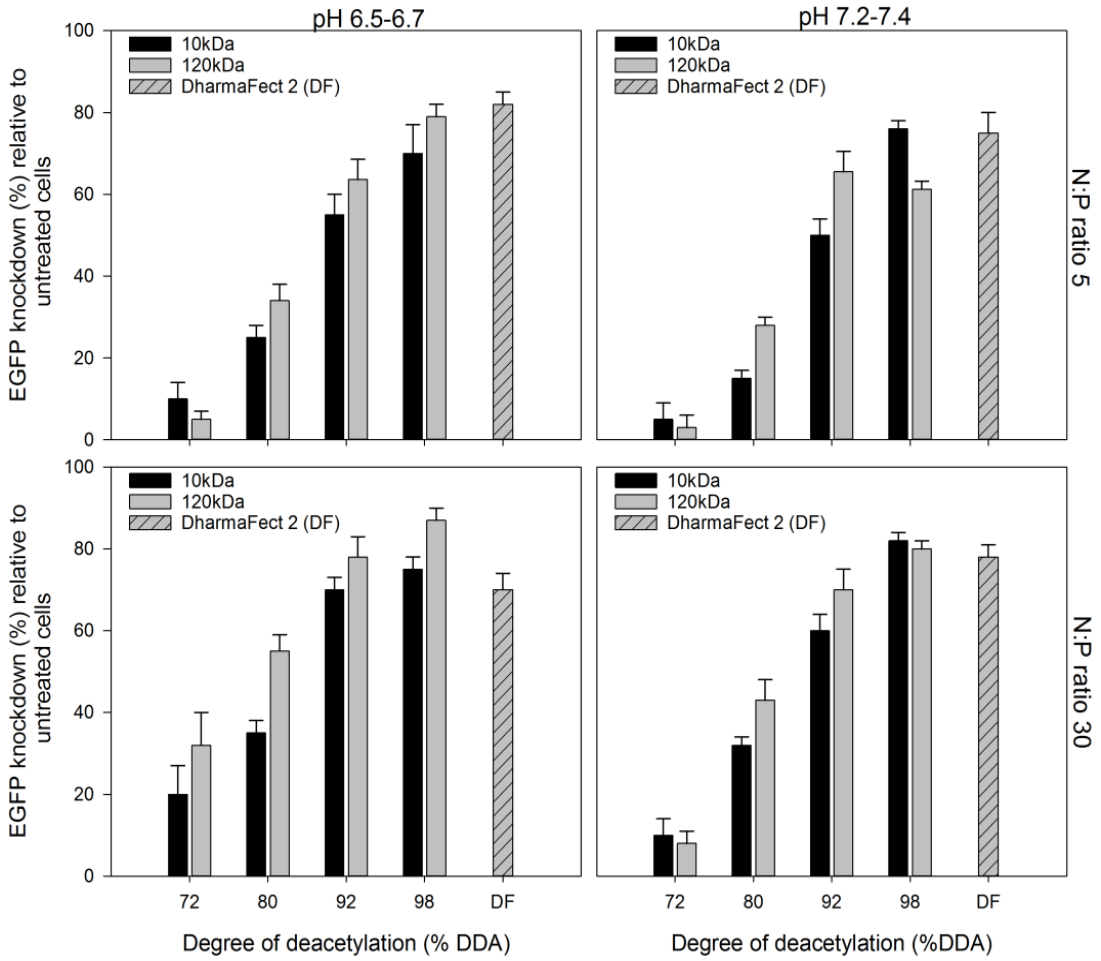

Figure 6-3 Effect of DDA, Mn, N:P ratio and pH on the biological performance of chitosan-siRNA nanoparticles. Nanoparticles were formed in water following 1:1 (v/v) mixing of chitosan to siRNA (0.1 mg/mL). $EGFP^+$ H1299 cells were transfected at a final siRNA concentration of 100 nM. Data represent average ± standard deviation of at least 3 independent experiments with at least 2-3 technical replicates in each experiment (N=3, n=6-9).

The effect of DDA, Mn and N:P ratio on nanoparticle internalization was investigated at physiological pH (7.2-7.4, 290mOsm) and in the presence of serum. As depicted in Figure 6-4A, nanoparticle internalization increased with increasing DDA, Mn and N:P ratio reminiscent of the trend observed in Figure 6-3.

To understand the relationship between nanoparticle physicochemical characteristics and their biological activity, physiochemical parameters were correlated and regressed with respect to

knockdown efficiency. Figure 6-4 shows the relationship between size, surface ζ-potential, and knockdown efficiency. No correlation between size measured in 10 or 150 mM NaCl and knockdown was observed (Figure 6-4, B). However, nanoparticle ζ-potential, a parameter found to be strongly dependent on DDA, Mn and N:P ratio (Figure 6-1), showed strong correlation with EGFP knockdown with Pearson product moment correlation coefficient (PPMCC) reaching 0.74-0.88.

In order to demonstrate that observed knockdown is independent of metabolic disturbances, the viability of treated cells was determined relative to untreated controls using the alamarBlue® assay. The principle of the assay is based on the mitochondrial reduction of resazurin, a blue and non-fluorescent molecule, into resorufin, a red and fluorescent molecule. As such, the number of cells and the incubation time were optimized before performing the assay since seeding density and population doubling time are critical parameters for accurate results.

Figure S. 6-2 shows complete depletion of resazurin four hours post incubation at a cell density of 65,000 cells/cm^2. The optimal number of cells for viability testing was thereby determined to be 15,625 cell/cm2, a cell density equivalent to 5,000 cells/well (96 well plate).

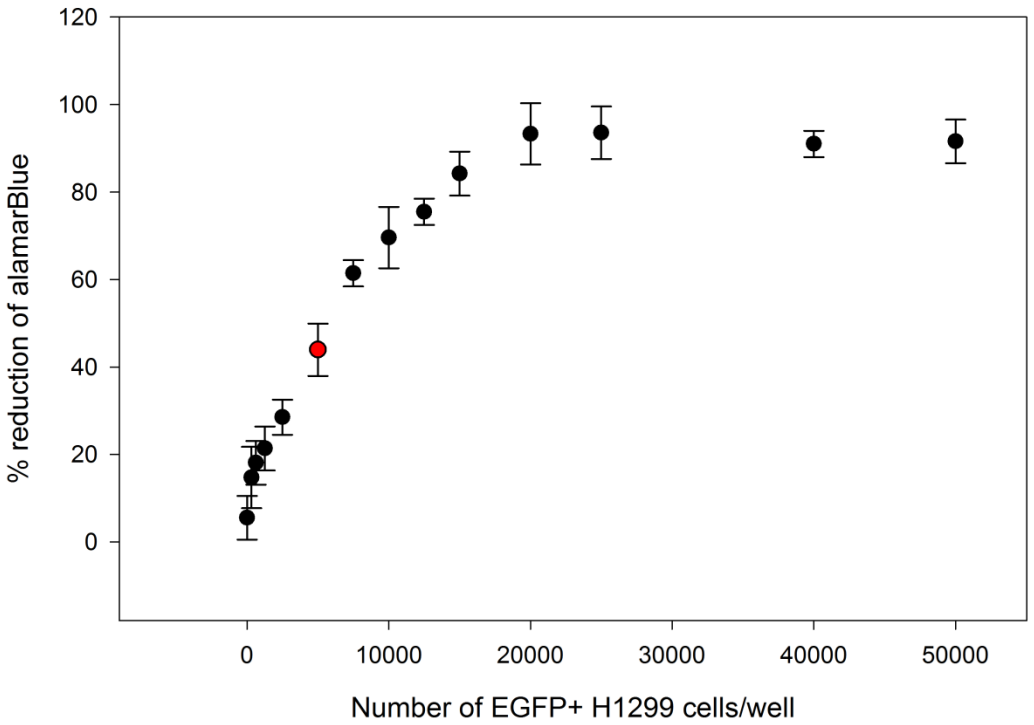

Figure S. 6-2 Effect of EGFP^{+} H1299 cell number on the reduction of alamarBlue®. Increasing cell numbers were seeded in 96 well plate, one day prior to the addition of alamarBlue®. Absorbance at 570 and 600nm was read 4 hours post-incubation and % reduction calculated using the following equation: $\%\ reduction = \frac{((e_{OX})\lambda_2 A\lambda_1)-((e_{OX})\lambda_1 A\lambda_2)}{((e_{RED})\lambda_1 A'\lambda_2)-((e_{RED})\lambda_2 A'\lambda_1)}$ where the ε_{ox} is the molar extinction coefficient (ε) of alamarBlue® oxidized form, ε_{RED} is the molar extinction coefficient of the reduced form, A absorbance of test well, A' absorbance of negative well (media+ alamarBlue® only), λ_1 is 570nm and λ_2 is 600nm. The optimal number of cells to be seeded 24 hours post transfection and tested for toxicity 48 hours post transfection with nanoparticles was determined to be 5,000 cells/well.

As illustrated in Figure 6-4 D, a slight decrease of 5-15% in metabolic activity was recorded for all formulations tested except for the larger decrease observed with 98-10-5. Under identical transfection conditions where polymer and lipid-based nanoparticles are in contact with cells for 48 hours, all formulations outperformed the lipid control. Under such conditions, DharmaFect® 2 showed strong toxicity with around 60-80% cell death. However, it is noteworthy to mention that media replacement 5 hours post transfection abrogated changes in metabolic activity relative to

untreated cells for both chitosan and the lipid formulations and that no toxicity was observed when evaluated 4 hours post-transfection (data not shown).

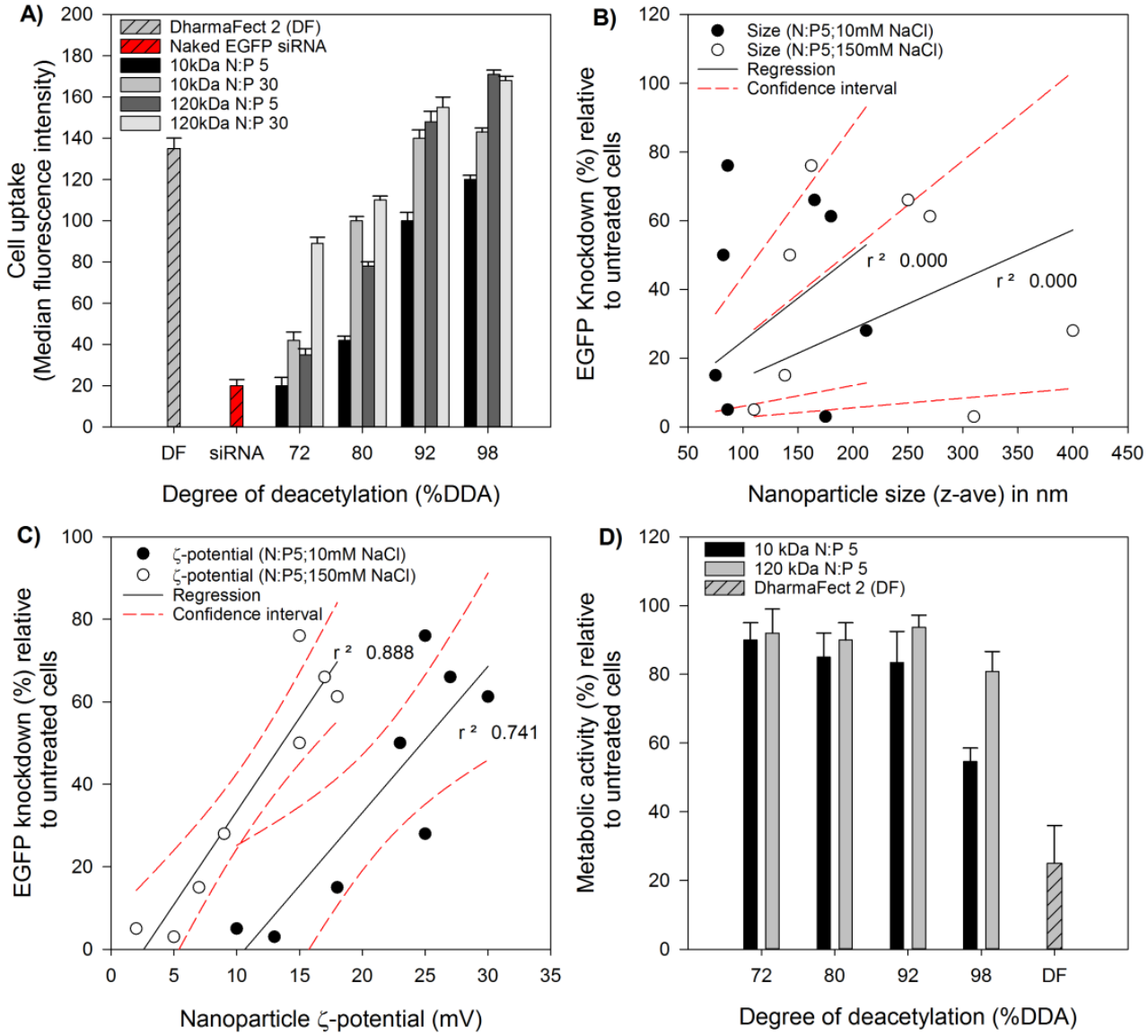

Figure 6-4 Cell uptake, knockdown, correlations to size and charge, cell toxicity. A) The effects of DDA, Mn and N:P ratio on uptake were measured in the EGFP^{+} H1299 cell line 48 hours post transfection at 100 nM siRNA B) Lack of correlation between EGFP knockdown and nanoparticle size measured at low and high ionic strength. C) Strong correlation between EGFP knockdown and nanoparticle surface charge (ζ-potential) measured at low and high ionic strength. D) Effect of different formulations prepared at N:P 5 on metabolic toxicity. All experiments in these figures were performed at pH 7.2-7.4 in the absence of serum. Media over

cells was aspirated and replenished with complete media 44 hours before analysis. All data shown represent average of at least 3 independent experiments with 2-3 technical replicates per experiment (N=3, n=6-9). Correlation graphs represent average values of size or ζ-potential correlated with average values of EGFP knockdown.

6.3.2 In *vitro* knockdown efficiency is Mn independent above a certain threshold with chitosan found to disturb global gene expression.

Based on the above results obtained from *in vitro* knockdown and the correlation between chitosan DDA, Mn and N:P ratio and physicochemical properties (size, ζ-potential and EE) and/or biological performance (EGFP knockdown and viability), the family of polymers with a degree of deacetylation of 92% was selected for further characterization of the effect of Mn, N:P ratio and serum proteins on siRNA uptake and knockdown. As depicted in Figure 6-5 A, *in vitro* uptake, or internalization, of DY^{647} labeled siRNA requires a threshold of polymer length of 10 kDa, above which internalization appears to be independent of both Mn and N:P ratio. Below this Mn threshold of 10 kDa, the role of N:P ratio appears critical with a two-*fold* increase in siRNA uptake when increasing N:P ratio from 5 to 30 (Figure 6-5 A). As expected, EGFP knockdown followed a similar pattern since uptake and knockdown are generally correlated, given the ability of these nanoparticles to escape endosomal compartments [17, 47]. Knockdown efficiency was independent of Mn and N:P ratio above 40 kDa (Figure 6-5). To demonstrate that the decrease in EGFP fluorescence intensity was not related to toxic or non-specific effects of chitosan itself, mock transfections with naked chitosan (M) and transfections using non-targeting siRNA (siNT) were included as controls. As shown Figure 6-5 C and D, the delivery of siNT resulted in minimal EGFP knockdown, reaching a maximum of 10±2% with 92-40. In contrast, mock transfections mediated a modest 5-10% increase in EGFP expression for some chitosans. The pattern of EGFP knockdown and/or expression for both siNT and mock seem to follow a trend where longer chain chitosans appears to have a slight positive effect on EGFP expression.

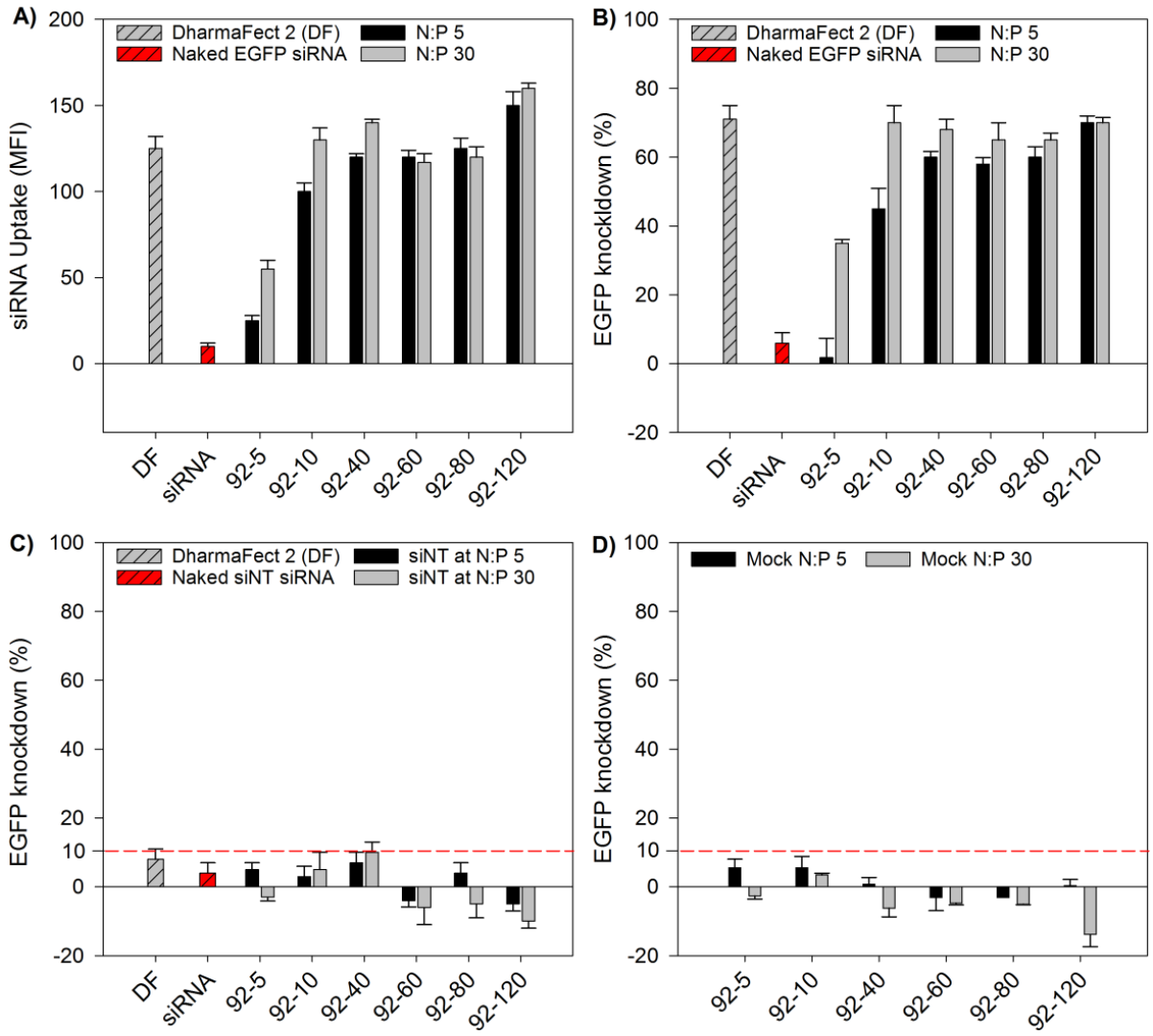

Figure 6-5 Effect of Mn at 92% DDA (92-Mn) and N:P ratio on uptake and knockdown. The $EGFP^{+}$ H1299 cell line was transfected in the presence of 10% serum at a final siRNA concentration of 100 nM. A) Uptake of DY^{647} labeled siRNA expressed as median fluorescence intensity (MFI). B) EGFP knockdown post transfection with anti EGFP nanoparticles. C) Lack of EGFP knockdown post transfection with non-targeting siNT nanoparticles; siNT represents a scrambled siRNA and is an indicator of specificity to the target siRNA sequence. D) Lack of EGFP knockdown following transfection with chitosan only. Data represent the average ± standard deviation of 3 independent experiments with 2 technical replicates per experiment (N=3, n=6).

Since siRNA is a small and rigid molecule compared to other nucleic acids previously studied with chitosan, we hypothesized that chitosan chain length below a threshold of ~ 60-70 monomers (10 kDa) have a lower affinity for siRNA and therefore release siRNA in complex media (pH 7.4, high ionic strength and presence of serum). As shown in Figure S. 6-3, an increase in Mn from 5 to 10 kDa or 10 to 120 kDa dramatically improves siRNA encapsulation at low N:P ratios. Although the effect of physiological pH on nanoparticle stability, below the Mn 10kDa threshold, is clear (Figure S. 6-3), it does not seem to totally account for the loss of internalization and knockdown efficiencies observed in Figure 6-5**.**

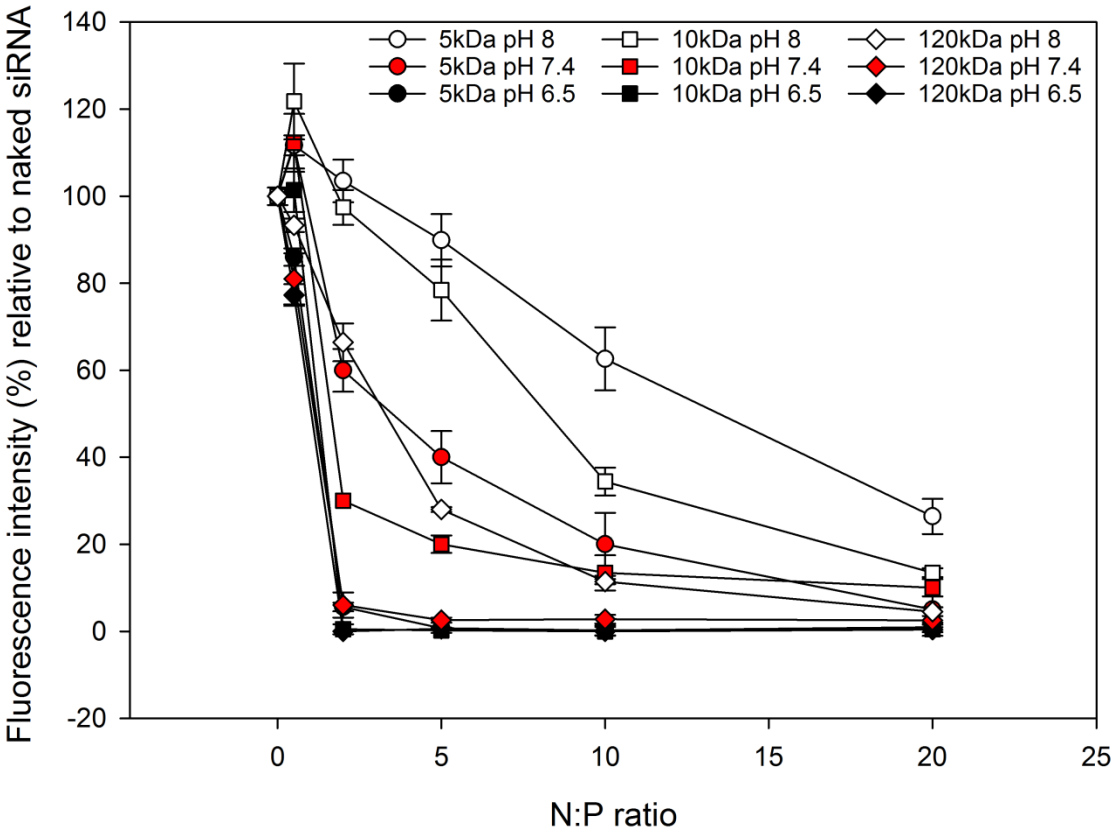

Figure S. 6-3 siRNA encapsulation efficiency of low and high Mn chitosan. Nanoparticles were formed in water by manual mixing of siRNA (0.1mg/mL) with chitosan at different N:P ratio, incubated in low ionic strength pH controlled buffers (MES pH 6.5, TE pH 7.4 and TAE pH 8.0) for 24 hours and siRNA release quantified using the Quant-iT™ RiboGreen® Assay. The percent siRNA release was quantified relative to naked siRNA or N:P 0. At pH 6.5, complete siRNA encapsulation was observed regardless of the Mn and N:P ratio used. At pH 7.4 and 8.0, siRNA release shows a Mn and N:P dependence with higher Mn and N:P ratio required for efficient

encapsulation. However, at physiological pH and at N:P ratio of 5, the 5 and 10kDa chitosans were able to encapsulate siRNA 60 and 80% respectively.

We subsequently verified the effect of serum on EGFP knockdown with low *versus* high Mn chitosans (10 *vs* 120 kDa). Figure 6-6 shows a decrease in performance in the presence of 10% serum for the 10 kDa chain which was rescued by increasing the N:P ratio from 5 to 30 indicating that a threshold of at least 10 kDa is needed to counter the negative effects of both pH and serum (Figure S. 6-3 and Figure 6-6).

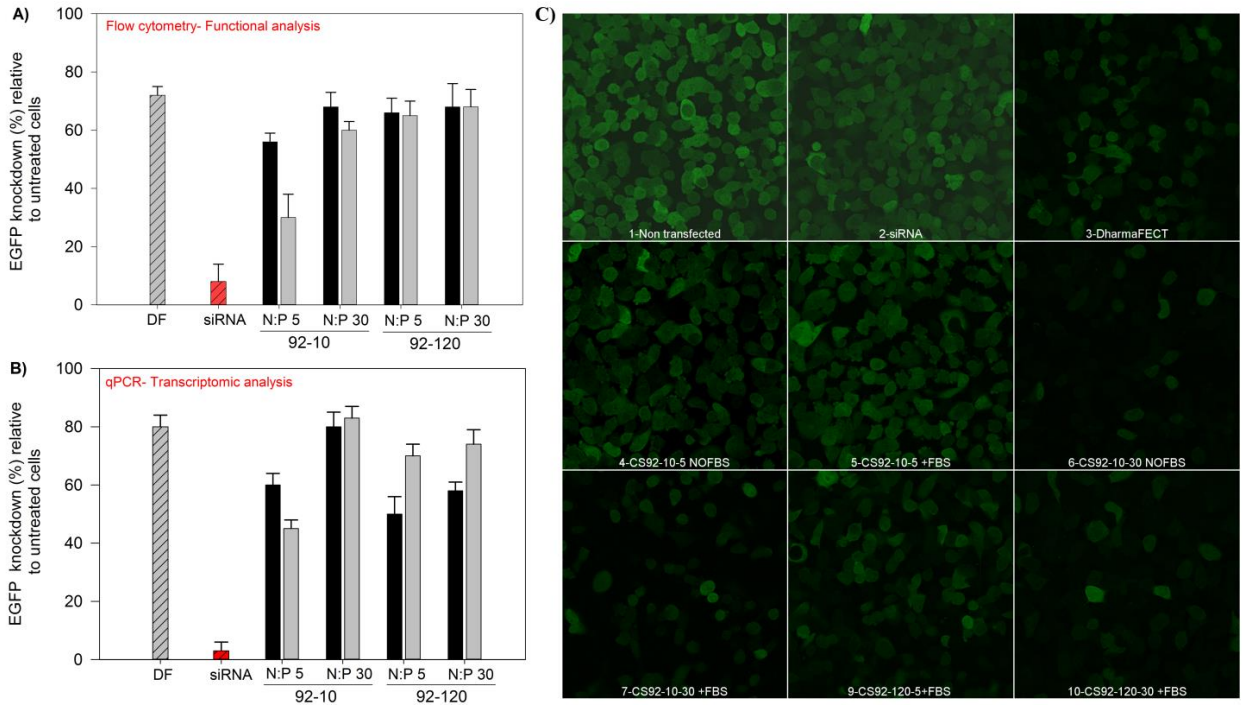

Figure 6-6 Effect of FBS, chitosan Mn and N:P ratio at 92% deacetylation on EGFP knockdown in H1299 cells. A) EGFP knockdown measured as the average fluorescence intensity (FI) relative to untreated cells 48 h post transfection with siEGFP. $EGFP^+$ H1299 cells were transfected in the absence or presence of 10% serum for a period of 5 hours, media aspirated and replenished with complete RPMI-1640 media (pH 7.2-7.4, 290 mOsm) and incubated for 44 hours before analysis. B) EGFP mRNA knockdown measured using qPCR, normalized using the geometric average of EIF, PUM-1, and GAPDH and calibrated to untreated cells. $EGFP^+$ H1299 cells were treated as described in A. C) Representative confocal laser scanning microscopy (CLSM) images. EGFP is indicated in green. In all experiments, siRNA was delivered at a final concentration of 100 nM

and data in A and B expressed as the average value of 3 independent experiments with 2-3 technical replicates per experiment (N=3, n=6-9), *p-value < 0.01.

Next, we confirmed assessed knockdown on the transcriptomic level by quantifying EGFP messenger RNA (mRNA) using MIQE compliant quantitative real-time PCR (qPCR). qPCR is a very sensitive and powerful technique but can generate biased results in several cases where a single or a combination of factors such as normalization strategy, validation of primer efficiency and/or RNA integrity are not properly controlled [38, 41, 48-53]. As a consequence, the stability of reference genes following treatments was validated in parallel with the validation of primer-probe efficacy (Error! Reference source not found.). As seen in Figure 6-7, common reference genes i.e. β-actin and HPRT were highly unstable with M scores above 0.5. Treatment dependent fluctuations were also observed during modeling of treatment effect, with the removal of DharmaFect® 2 altering the classification of reference genes (Figure 6-7**,** B). This observation confirms that treatments with either lipid or chitosan-based nanoparticles have, in principle, a certain impact on the transcriptome or at least on these tested reference genes.

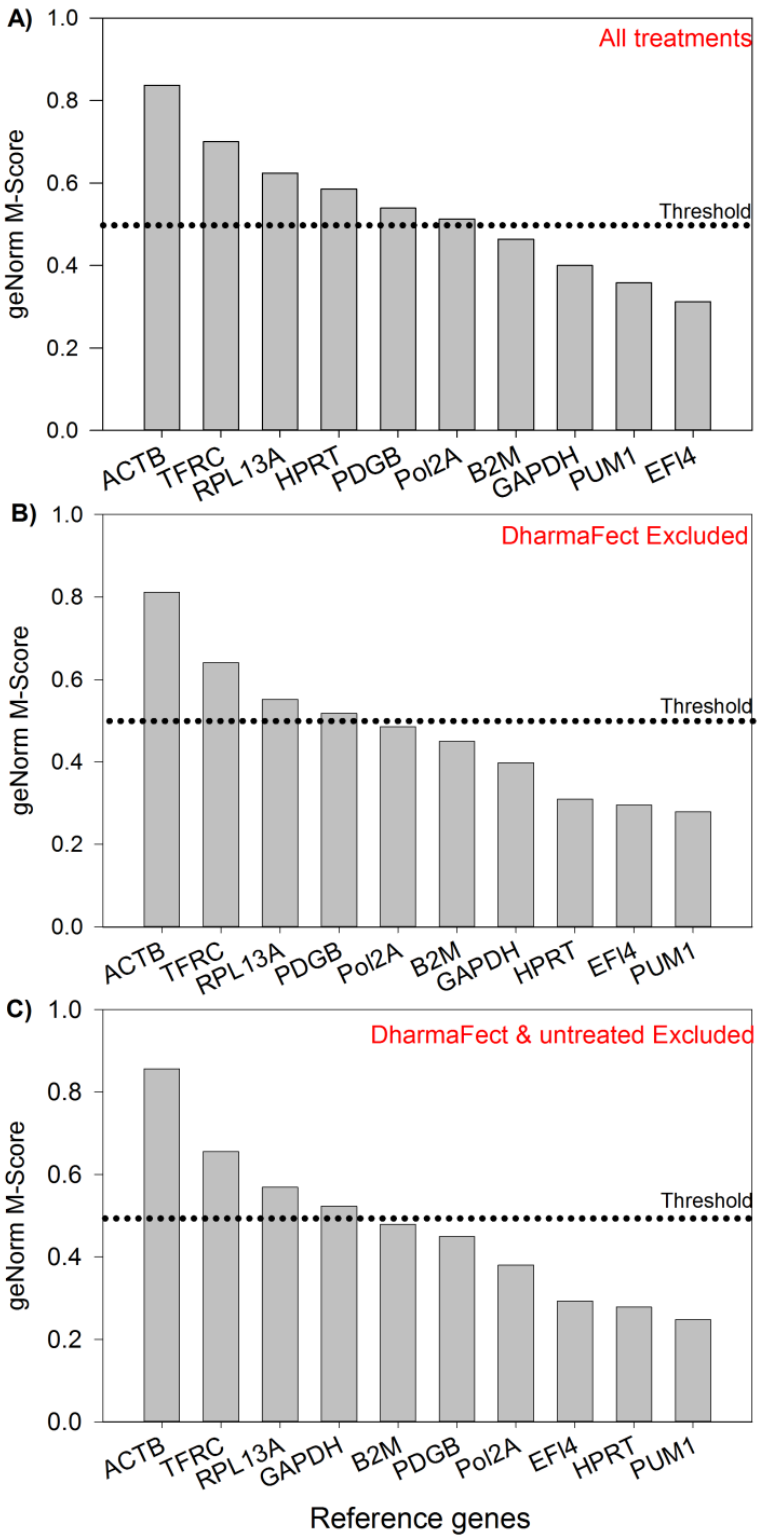

Figure 6-7 Effect of chitosan and DharmaFect® 2 treatment on reference gene stability. A panel of 10 reference genes was tested for expression stability under diverse experimental conditions. EGFP^{+} H1299 cells were transfected with the following formulations i.e. 92-10-5, 92-10-30, 92-

120-5, 92-120-30, 98-10-5, 98-10-30 and DharmaFect® 2 at a final siRNA concentration of 100 nM. Untreated cells were included in the analysis. A) panel shows the classification of the least to most stable (left to right) reference gene based on the average expression stability values, or geNorm M-Score, computed on the remaining control genes during stepwise exclusion of the least stable control gene, for samples from all treatments. B) panel shows the effect of the exclusion of DharmaFect® 2 from the statistical analysis. C) Panel shows the effect of the exclusion of both DharmaFect® 2 and untreated cells from the analysis. The M-Scores were computed using the geNorm statistical package on the average Cq of two independent experiments

The high variability of β-actin could be attributed to poor assay efficiency (84%), which was confirmed to be treatment independent as assays had the same amplification efficiency on cDNA amplified from total RNA extracted from treated *vs* untreated samples (**Error! Reference source not found.**).

Table S 6-1 Efficiency of the primer-probe pairs used in this study. Reference gene specific primer-probe pairs were tested for their amplification efficiency on complementary DNA (cDNA) prepared from total RNA extracted from non-treated $EGFP^+$ H1299 cells. In order to validate that chitosan treatment does not affect reaction efficiency, primer-probe pairs specific to β2M and RPL13A were also tested on cDNA prepared from total RNA extracted from cells treated (transfected) with 92-10-30. Formulations were designated [DDA(%)-Mn (kDa)-N:P ratio]. High N:P was chosen to ensure maximum potential contamination of total RNA with chitosan. Data show that almost all primer-probe pairs passed, except for ACTB, and that chitosan does not affect amplification efficiency

Treatment	Assay name	ABI Assay ID	Efficiency (%)	R^2	Fail/Pass
Non-treated	PUM1	Hs00472881_m1	96.0	0.998	Pass
	RPL13A	Hs04194366_g1	92.0	0.995	Pass

	Pol2A	Hs00172187_m1	96.5	0.999	Pass
	β2M	Hs00984230_m1	95.0	1.000	Pass
	TFRC	Hs00951083_m1	95.0	0.999	Pass
	HPRT	Hs01003267_m1	102.0	0.997	Pass
	ELF1	Hs00152844_m1	94.0	0.999	Pass
	GAPDH	Hs02758991_g1	94.0	0.997	Pass
	ACTB	Hs01060665_g1	84.0	0.998	Fail
	PBGD	Hs00609297_m1	94.5	1.000	Pass
	RecQL1	Hs00262956_m1	92.0	0.999	Pass
	eGFP	Mr03989638	98.5	0.998	Pass
CS treated	β2M	Hs00984230_m1	95.0	1.000	Pass
	RPL13A	Hs04194366_g1	92.0	0.995	Pass

The V-score, or the pairwise variation between the normalization factors NF_n and NF_{n+1}, showed that accurate normalization could be achieved by using the geometric mean of the 2-3 most stable reference genes (Figure S. 6-4). Under optimal normalization conditions and following MIQE guidelines, a similar trend for the effect of Mn and N:P ratio in the presence/absence of serum was observed using quantitative PCR (Figure 6-6, B). The knockdown of EGFP in the H1299 cells was qualitatively confirmed by confocal laser scanning microscopy (CLSM), as shown in Figure 6-6 C.

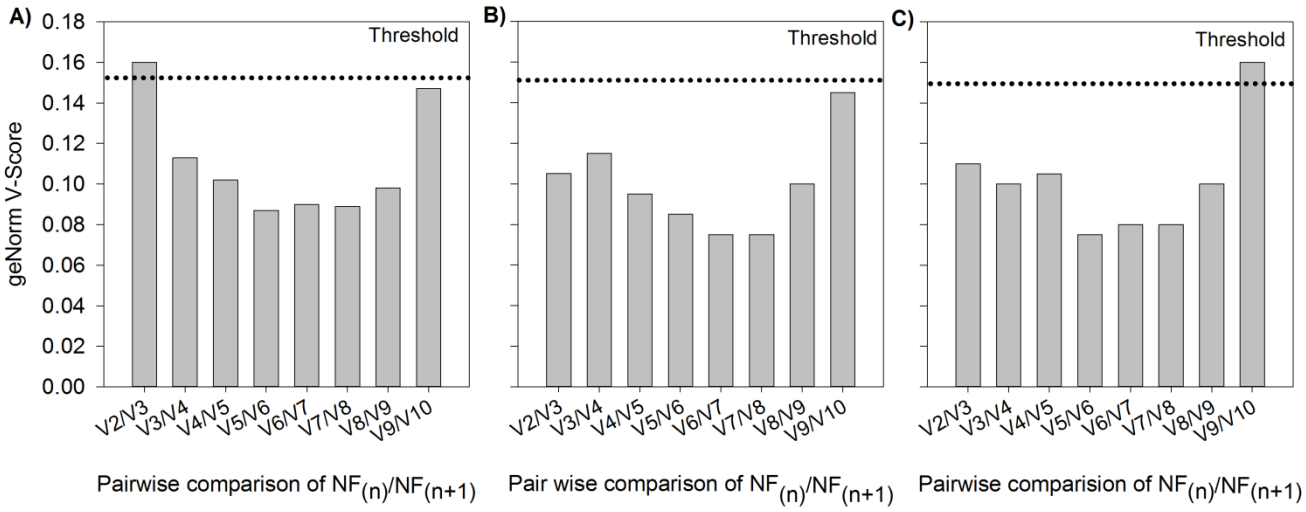

Figure S. 6-4 Pairwise comparison on normalization factors to determine the minimum number of reference genes needed for accurate normalization using the Vandsompele model. A) All treatments, B) Excluding DharmaFect® 2, C) Excluding DharmaFect® 2 and untreated cells. A minimum of 3 reference genes needs to be used for accurate normalization when comparing all treatments.

6.3.3 *In vitro* lipid nanoparticle (LNP) like potency (EC_{50}) can be achieved, in the presence of serum, using chitosans with increasing Mn and N:P ratio

The effect of Mn and N:P ratio on the minimum effective dose needed for EGFP knockdown in the H1299 cell line was determined in the presence of serum. The half maximal effective concentration (EC_{50}), a measurement of nanoparticle potency, was computed from a 4-parameter sigmoidal curve (4-PL) 48 hours post-transfection. Table 6-2 shows that potency increased with increased Mn and N:P ratio. DharmaFect® 2, a lipid control developed for siRNA delivery in H1299 cells, had the lowest EC_{50} (Table 6-2) and was able to induce meaningful knockdown at an EC_{50} of 23 nM. Similar potency was obtained with the 92-120-30 formulation (EC_{50} of 29.3 nM).

Table 6-2 Effect of Mn and N:P ratio on in vitro dose-dependent knockdown. EC_{50} values were derived from a 4-parameter sigmoid curve fitted to data derived from 2 independent experiments with 2 technical replicates per experiment; Figure S. 6-5 in supplemental data for more information, p-value <0.05.

Formulation	N:P ratio	EC_{50}(nM)	EC_{50} Standard error	p-value	Curve fit R^2
92-10	5	77.2	9.88	0.01	0.99
92-10	30	42.8	4.32	0.00	0.99
92-120	5	46.3	1.71	0.00	0.99
92-120	30	29.4	4.52	0.02	0.99
DharmaFect® 2	NA	23.8	3.28	0.02	0.99

As shown in Figure S. 6-5, all formulations reached a plateau around 200 nM with a marginal increase in EGFP knockdown observed at higher concentrations. The delivery of non-targeting siRNA (siNT) at higher doses (Figure S. 6-5) compared to Figure 6-5, C, did not cause a meaningful increase in off-target effects. Again, siNT induced a small decrease/increase in EGFP expression with low and high Mn chitosan respectively indicating that off-target effects are probably due to reduced metabolic activity observed with low Mn chitosan (Figure 6-9, A).

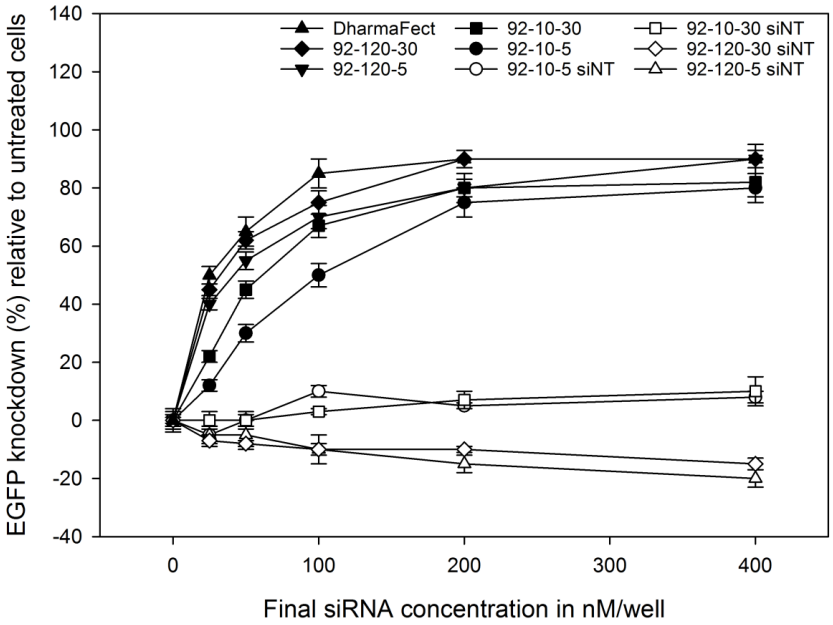

Figure S. 6-5 Effects of charge density, chain length and N:P ratio on dose-dependent EGFP knockdown. Nanoparticles were formulated with either siEGFP (anti-EGFP) or siNT (non-targeting) and EGFP^{+} H1299 cells transfected in the presence of 10% FBS at increasing siRNA concentrations. DharmaFect® 2 was used a positive control to benchmark efficacy. EGFP knockdown was analyzed 48 hours post transfection using flow cytometry. Data represent average values ± standard deviation of 2 independent experiments with 2 technical replicates per experiment.

6.3.4 Reduction in knockdown efficiency due to serum can be mitigated by increasing Mn and N:P ratio

Following observations regarding the effect of serum on the performance of low molecular weight chitosan, coupled with the fact that one use of nanoparticle is systemic administration *in vivo*, the effect of increasing serum concentration on biological performance was studied. In particular, the effect of Mn and N:P ratio on EGFP knockdown was investigated in the presence of increasing serum concentrations. As shown in Figure 6-8 A, nanoparticles rapidly lost their performance in the presence of increasing serum concentration. This loss of performance could be mitigated by higher Mn and/or N:P ratio. The latter seems to play an important role in promoting transfection in the presence of high concentration of serum (i.e. 94%). The effect of physiological concentrations

of heparin (2.5 µg/mL) [54] and albumin (25-40 mg/mL) at pH of 7.2-7.4 on payload release was studied by means of dye exclusion. As shown in Figure 6-8, C, a physiological concentration of heparin, equivalent to concentrations found in 94% serum, was able to displace the payload. Increasing both Mn and N:P ratio improved encapsulation efficiency but could not abrogate payload release. In contrast, serum albumin seems to have a protective effect (Figure 6-8, D) with no payload release observed following incubation of nanoparticles with physiological concentrations of the protein.

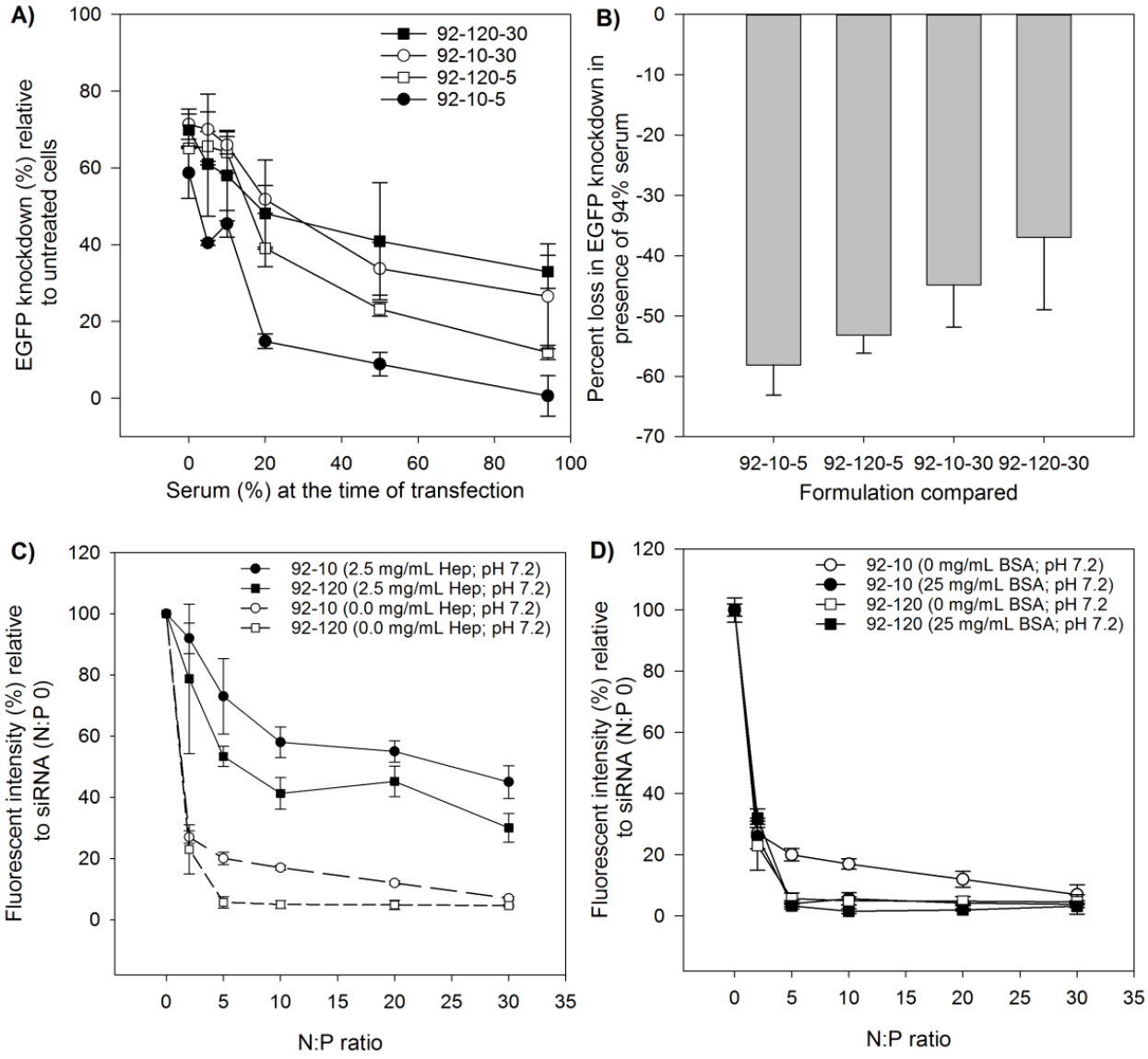

Figure 6-8 Effect of increasing concentration of serum on the biological performance of nanoparticles. A) Effect of increasing serum concentration on EGFP knockdown. B) Percent loss of EGFP knockdown in the presence of 94% serum compared to transfection without serum. C)

Effect of physiological concentration of heparin sulfate (2.5 µg/mL) on payload release. Low (10 kDa) and high (120 kDa) 92% deacetylated chitosan was formulated with siRNA at different N:P ratio and incubated for 1 hour in the absence and presence of heparin sulfate (pH 7.4). Increased fluorescence indicates increased payload release D) Effect of physiological concentration of BSA (25 mg/mL) on payload release. Low (10 kDa) and high (120 kDa) 92% DDA chitosan was formulated with siRNA at different N:P ratio and incubated for 1 hour in the absence and presence of BSA (pH 7.4).

6.3.5 Metabolic and genotoxic testing demonstrate the safety of chitosan-siRNA nanoparticles at low/high Mn and N:P ratios

The effect of chitosan chain length and N:P ratio on metabolic activity and genomic integrity was assessed using the alamarBlue® and comet assays respectively. Figure 6-9 A shows a small decrease in metabolic activity with low molecular weight chitosan at both N:P ratio of 5 and 30. In contrast, no reduction in metabolic activity was observed for the high molecular weight chitosan. Increasing N:P ratio had no effect on metabolic activity, or cell viability, as revealed by the comparison of low *vs* high N:P ratio for the two Mn tested, 10 and 120 kDa (Figure 6-10A). Sequence-dependent activation of IFN, PKR, and TLRs, among others, has been demonstrated for other delivery systems and could potentially affect *in vitro* metabolic activity through translation inhibition or other mechanisms. As a consequence, mock transfections were performed in parallel to rule out sequence-dependent effects and showed no significant differences between mock and nanoparticles treated cells suggesting chitosan as the principal factor affecting metabolic activity (Figure 6-9, A).

The effect of molecular weight and increasing N:P ratios, where the latter increases the amount of free chitosan not complexed to nanoparticles, on genotoxicity was measured by the comet assay at 8 and 48 hours post transfection. The percentage DNA in the tail (PDT), or the proportion of damaged DNA, and the Olive Tail Moment (OTM), or the product of the tail length and the fraction of total DNA in the tail, were computed for all comets obtained for each treatment (Figure 6-9, B and C). Interestingly, opposing trends were observed for low *vs* high Mn (Figure 6-9, B). An identical, but less pronounced, pattern was observed for OTM (Figure 6-9, C). The significance of the observed increase, for either parameter recorded, was evaluated using the Kruskal-Wallis (KW) non-parametric statistics. Significant differences between treatments were only detected for percent

DNA in tail (PDT) (Figure 6-9, B) and is probably due to approximation bias in tail length assessment. Therefore, and due to lack of agreement between the two parameters (PDT *vs* OTM), the KW test was deemed questionable to demonstrate genotoxic effects. As a consequence, an analytical approach based on [55] was used. Each series of measures was reduced to the median and the 75th percentile, two representative parameters of comet distribution, and a regression analysis followed by an ANCOVA performed. Figure 6-9D, show no significant effect of the molecular weight or the N:P ratio suggesting no genotoxic effect of chitosan.

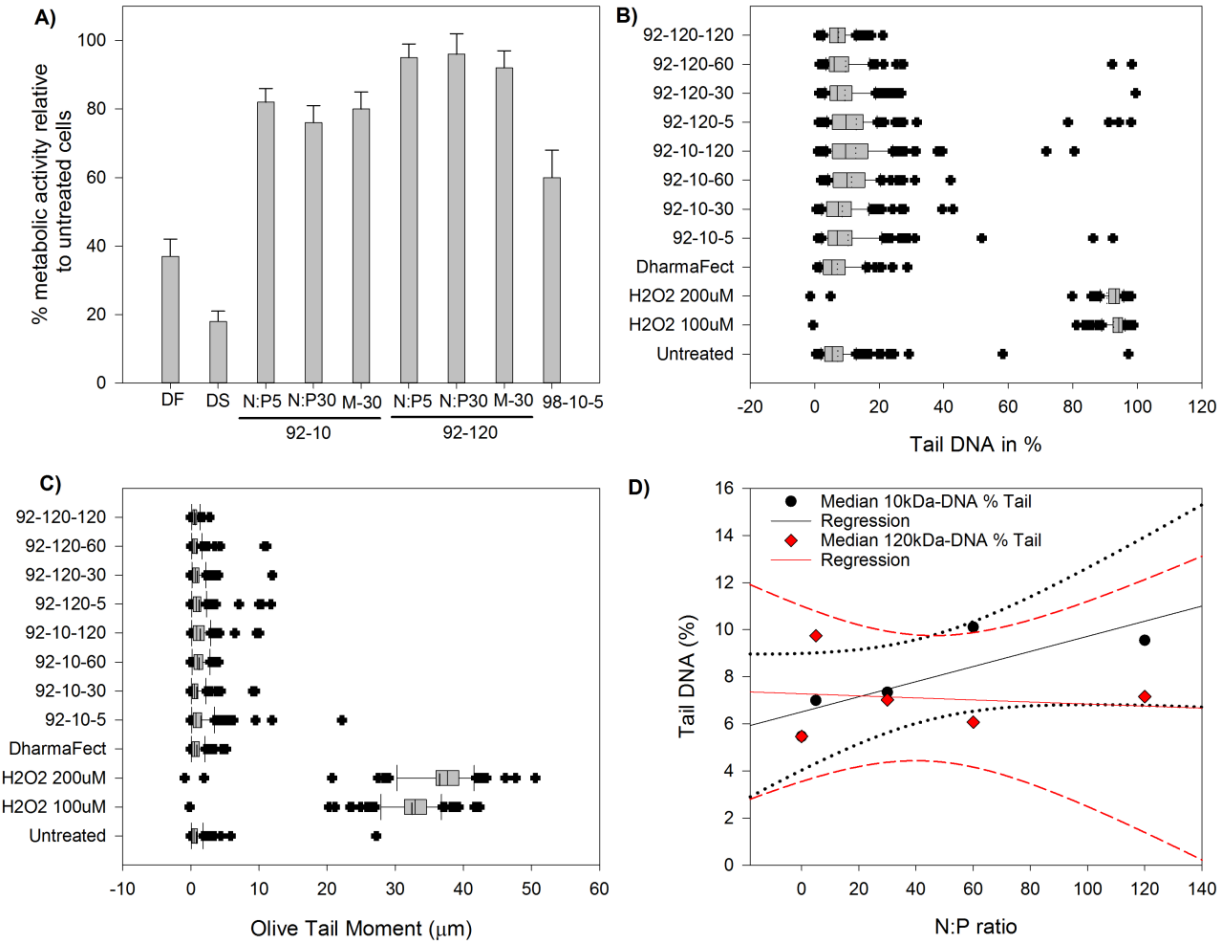

Figure 6-9 Effect of chitosan Mn and N:P ratio at 92% DDA on in vitro toxicity and genotoxicity. A) Metabolic activity relative to untreated EGFP^{+} H1299 cells measured by the alamarBlue® assay. Activity was measured 48 h posttransfection. Mock chitosan (M) was used at N:P 30 to assess the effect of siRNA encapsulation on metabolic activity. DharmaFect® 2 (DF), a commercial lipid-based system, was used as a comparator. Dimethyl sulfoxide (DS) was used as

positive control of toxicity. B) Effect of increasing Mn and N:P ratio on genotoxicity as measured using the comet assay parameter "% DNA in tail (PDT)". The PDT represents the percentage of DNA migrated in the tail of the comet or the proportion of damage to total DNA. C) Effect of increasing Mn and N:P ratio on genotoxicity as measured using the parameter "Olive tail moment (OTM)". OTM represents a parameter that is insensitive to the measurement of tail length. D) Correlation between median PDT and N:P ratio for 10 vs 120 kDa chitosan. For the alamarBlue® assay, data represent average metabolic activity ± standard deviation of 3 independent experiments with 2-3 technical replicates per experiment (N=3, n=6-9). For the comet assay, box plots were constructed from data of 2 independent experiments with more than 100 comet/experiment/treatment.

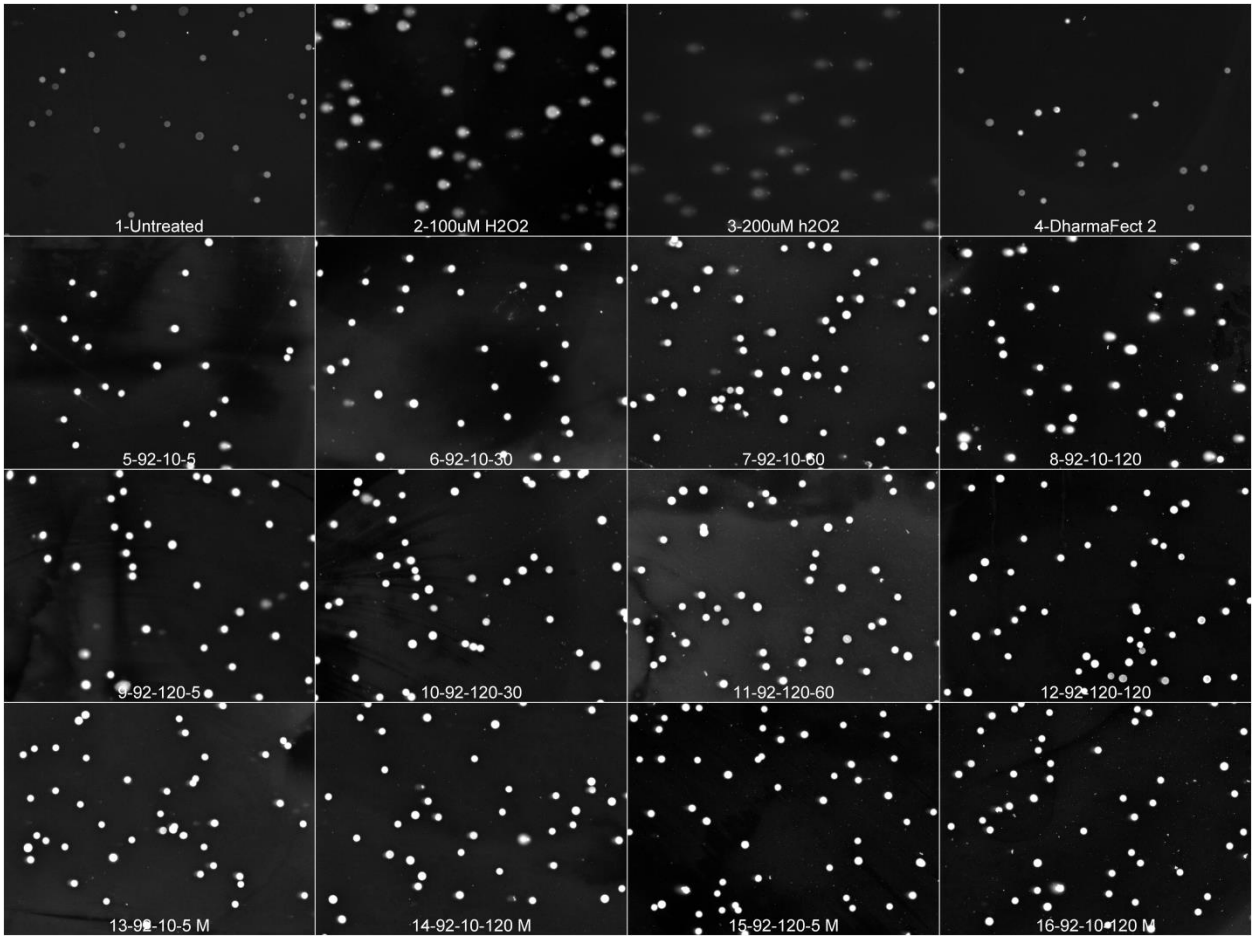

Figure S. 6-6 Representative images of comets 48 hours post transfection with nanoparticles. The montage was prepared with ImageJ. Hydrogen peroxide (H_2O_2) at 100 and 200 µM was used as

positive control for genotoxicity. DharmaFect® 2 siRNA nanoparticles were used as a comparator. Formulations at low and high Mn (92-10 and 92-120) were prepared at different N:P ratio (5, 30, 60 and 120) and transfected at final siRNA concentration of 100 nM (~0.00132 mg/mL). Equivalent concentration of chitosan at specific N:P ratio was 0.004, 0.018, 0.037 and 0.074 mg/mL for the N:P 5, 30, 60 and 120 respectively. Naked chitosan, or mock (M), was used as a control to account for the effect of the siRNA sequence. Typical comets are observed post treatment with the positive control. A dose-dependent increase in comet tail length can be seen when comparing 100 *vs* 200 µM H_2O_2.

Table S 6-2 Descriptive statistics of the data collected for genotoxicity parameters

Parameters tested		**% DNA tail**				**Olive Moment**				**Tail/Total Area**			
Treatment	**Size**	**Mean**	**Std Dev**	**Std. Error**	**C.I. of Mean**	**Mean**	**Std Dev**	**Std. Error**	**C.I. of Mean**	**Mean**	**Std Dev**	**Std. Error**	**C.I. of Mean**
Non-treated	203	7.2	8.7	0.6	1.2	0.8	2.0	0.1	0.3	17.4	10.0	0.7	1.4
100µM H_2O_2	207	92.6	9.7	0.9	1.9	32.4	4.9	0.5	0.9	92.7	9.6	0.9	1.9
200µM H_2O_2	285	90.6	14.0	1.5	3.0	36.5	7.0	0.7	1.5	90.3	13.2	1.4	2.8
DharmaFect 2	217	7.0	5.7	0.7	1.3	0.9	1.0	0.1	0.2	17.7	9.4	1.1	2.2
1992-10-05	251	10.4	13.0	1.2	2.4	1.5	2.6	0.2	0.5	21.7	14.3	1.3	2.6
1992-10-30	322	8.6	7.0	0.6	1.2	0.9	1.3	0.1	0.2	17.2	9.2	0.8	1.6
92-10-60	313	11.4	6.9	0.6	1.2	1.2	1.0	0.1	0.2	19.0	8.3	0.7	1.4
92-10-120	205	12.7	11.8	1.1	2.2	1.4	1.6	0.2	0.3	20.4	13.1	1.2	2.5
92-120-5	218	12.9	15.4	1.4	2.7	1.2	1.8	0.2	0.3	19.4	14.8	1.3	2.6
92-120-30	219	9.4	9.1	0.7	1.4	1.0	1.2	0.1	0.2	17.8	10.3	0.8	1.6
92-120-60	223	9.6	12.6	1.2	2.3	0.9	1.5	0.1	0.3	17.1	12.4	1.2	2.3
92-120-120	208	7.4	3.9	0.4	0.7	0.6	0.5	0.0	0.1	16.0	4.9	0.5	0.9

6.3.6 Chitosan induce Mn- and dose-dependent hemolysis and aggregation of red blood cells

Assessment of metabolic activity and genotoxicity demonstrated the safety of chitosan-based NPs *in vitro* (Figure 6-9). However, neither the alamarBlue® nor the comet assay are predictive of toxicity that might occur when nanoparticles interact with blood following intravenous administration (I.V.). As such, the effect of chain length (Mn) and dose on blood compatibility was

investigated according to the ASTM-E2524 standard [43]. As illustrated in Figure 6-10, a dose-dependent increase in hemolysis was observed for both low and high Mn chitosan. The 5 % ASTM hemolysis threshold was crossed at a blood concentration of 0.321 and 0.04 mg/mL for the 92-10-5 and 92-120-5 respectively. Assuming an N:P ratio of 5, the maximum siRNA dose that could potentially be intravenously (I.V.) administered at the observed threshold crossing point is 8 and 1 mg/kg respectively. Increasing the siRNA dose or chitosan concentration in blood from 0.040 to 0.321 mg/mL increased hemolysis by two-fold indicating a nonlinear relationship. Positive i.e. PLL and TX-100 and negative controls i.e. PEG and HA controls were within the ASTM standard (Figure 6-10, inset) whereas excipients (buffer) and siRNA were found to be non-hemolytic, i.e. below the threshold, confirming that dose dependent hemolysis is attributed to chitosan. In parallel to hemolysis, Mn and dose-dependent red blood cells (RBC) agglutination was investigated to further understand chitosan-blood interaction. Table 6-3 shows that both 92-10-5 and 92-120-5 induced dose-dependent RBC agglutination above a Circulating Blood Volume (tCBV) concentration of 0.04 mg/mL. The degree of hemagglutination, as qualitatively assessed by aggregate size, increased with both dose and Mn (Table 6-3).

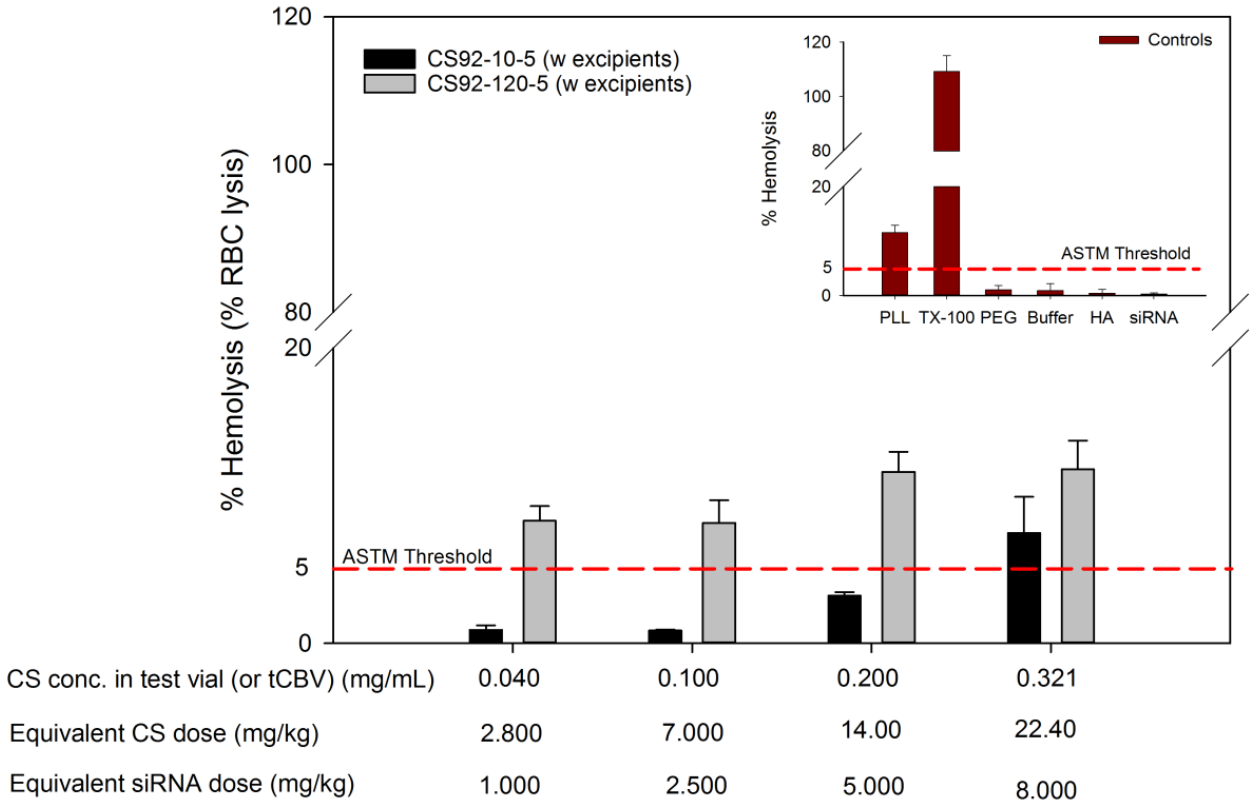

Figure 6-10 Effect of Mn and dose on hemocompatibility via red blood cell (RBC) lysis. Low (10 kDa) versus high (120 kDa) molecular weight chitosans were formulated with HPLC-grade siRNA at an N:P ratio of 5. Increasing doses of siRNA were mixed with human pooled blood and % hemolysis determined as per ASTM-E2524 [43]. The concentration of chitosan (mg/mL) in the test vial (equivalent to the concentration in total circulating blood volume or tCBV), the equivalent chitosan dose in mg/kg of body weight and the corresponding siRNA dose in mg/kg for N:P of 5 are shown. The inset shows data from positive and negative controls. Poly-L-Lysine (PLL), Triton-X-100 (TX-100), Polyethylene glycol (PEG), buffer (excipients at 1% trehalose, 5.8 mM histidine, pH 6.5), Hyaluronic acid 866 kDa (HA) and siRNA. Data represent the average ± standard deviation of 2 independent experiments with 3-6 technical replicate per experiment (N=2, n= 6-12).

Table 6-3 Effect of Mn and dose (concentration) on red blood cell agglutination. Agglutination was measured qualitatively and scored. (-) No aggregation, (+) Low agglutination, few aggregates (++) Medium agglutination, several large aggregates, (+++) Strong agglutination, clumps, (++++) Very strong agglutination, large clumps.

Formulation	**Chitosan dose (mg/kg)**	**Equivalent blood Conc. (mg/mL)**	**Aggregation**
92-10-05	2.8	0.04	-
	7	0.1	+
	14	0.2	++
	22.4	0.321	++
92-120-5	2.8	0.04	-
	7	0.1	+++
	14	0.2	++++
	22.4	0.321	++++
PEG	NA	Not calculated	-
Buffer	NA	Not calculated	-
HA	NA	1.26	-
siRNA	NA	0.321	-

6.3.7 Chitosan promotes extrahepatic siRNA delivery to proximal epithelial tubular cells of the kidney and induces target specific functional knockdown.

The effect of Mn on *in vivo* biodistribution using whole animal based *ex-vivo* imaging and CLSM was examined. As shown in Figure 6-11, chitosan based nanoparticles accumulated in the kidney and gallbladder of Balb/c nude mice following intravenous administration at a dose of 0.5 mg/kg (10 µg siRNA/animal). Naked siRNA followed its known tendency for elimination past the kidneys [35, 56-58]. However, siRNA accumulated in the kidneys many folds higher when complexed with chitosan suggesting a protective and targeting role of the delivery vector. Invivofectamine® 2.0 (InV) formulated siRNA, or InV LNP, showed a strong signal in liver/gallbladder, followed by spleen and kidneys. In order to examine the cellular accumulation of siRNA in the kidney, histological sections were generated and examined under confocal microscopy. As shown in Figure 6-12, the amount of siRNA in the kidney proximal tubules was greatly enhanced in comparison with naked siRNA and Invivofectamine® 2.0. Interestingly no glomerular accumulation was observed at this dose for either chitosan-based nanoparticle or controls (data not shown). Confocal microscopy showed punctate intracellular accumulation in proximal tubule cells (PTEC) indicating that siRNA was internalized across the brush border membrane lining PTECs (Figure 6-12). The efficacy of these uncoated systems to knockdown the glyceraldehyde-3 phosphate (GAPDH) gene was determined in the kidney cortex (Figure 6-13). In light of the *in vitro* performance described in this report, the effect of DDA and Mn was investigated *in vivo* through the comparison of compositions with different DDA (i.e. 98 *vs* 92%) and Mn (i.e. 10 *vs* 120 kDa). As shown Figure 6-13 A, nanoparticle physicochemical characteristics post-freeze drying, rehydration and injection (in excipients) demonstrated a similar Mn-dependent size increase as previously seen in NaCl (Figure 6-1). Low (10 kDa) and high (120 kDa) Mn chitosan were around 100 and 150 nm respectively (Figure 6-13). Cationic lipid nanoparticles (LNPs) and polymer based systems generally induce systemic toxicity, accompanied with a sharp reduction in body weight, upon intravenous administration through liver toxicity and immune stimulation. Our data show that multiple chitosan administration, below the hemolytic dose (Figure 6-13), did not induce a significant reduction in body weight except for the 98-10 formulation demonstrating tolerance. Mice injected with 98-10-5 quickly recovered upon the second administration (Figure 6-13, C). In

this study *in vivo* efficacy was demonstrated through functional GAPDH knockdown where both low Mn (10 kDa) chitosan demonstrated the highest efficacy (~ 40-50% knockdown) (Figure 6-13). In contrast to our *in vitro* data (Figure 6-8), high Mn (120 kDa) chitosans did not outperform their low Mn counterparts (Figure 6-13, D). As expected, chitosan improved knockdown efficiency in kidney cortex in comparison with naked siRNA with 30-35% more knockdown (Figure 6-13, D).

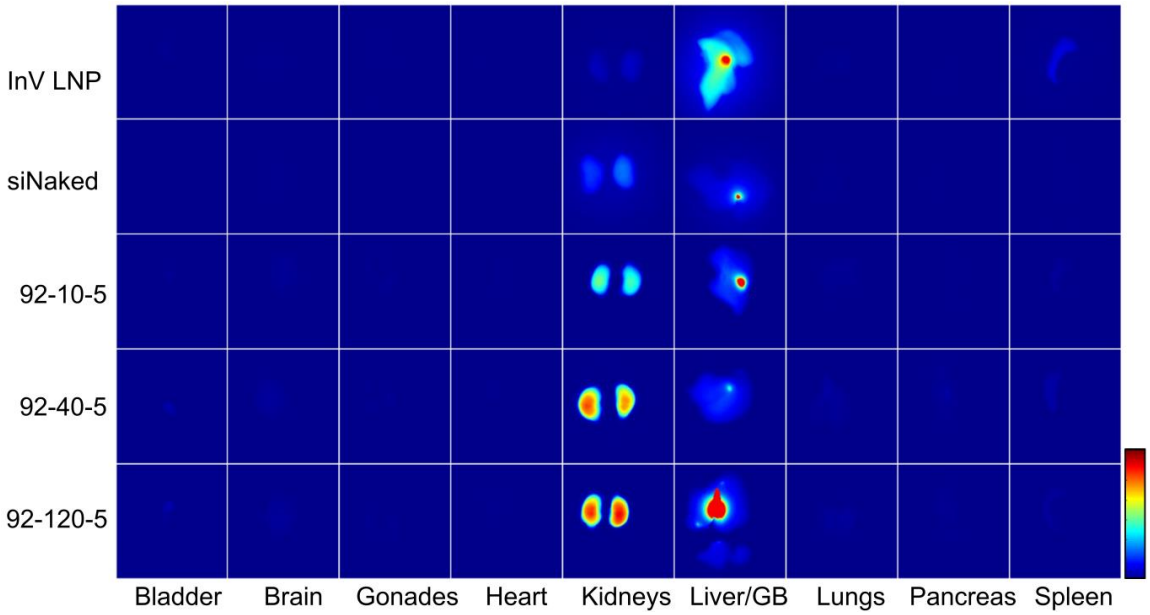

Figure 6-11Effect of Mn on the bio-distribution of chitosan-siRNA nanoparticles. Nanoparticles were injected in Balb/c nude mice at a dose of 0.5 mg/kg of DY^{647} labeled siRNA (equivalent dose of 1.4 mg/kg of chitosan) and organs imaged ex-vivo 4 hours post administration.

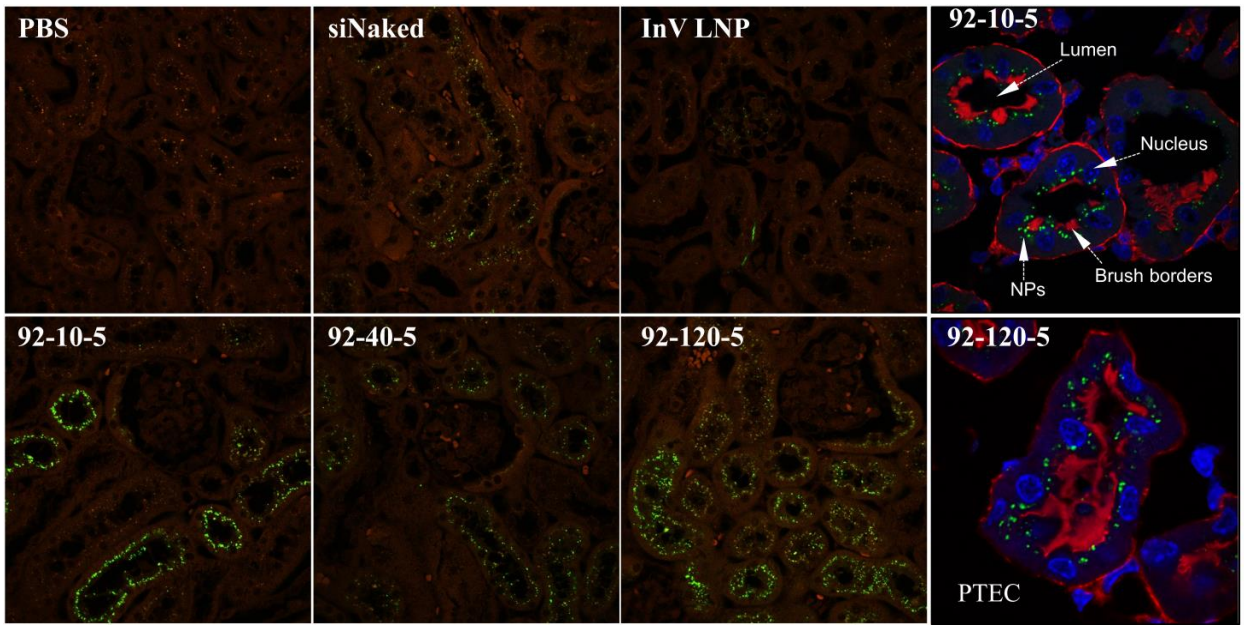

Figure 6-12 Histological and CLSM images of nanoparticles accumulated in PTEC. Nanoparticles were injected in Balb/c nude mice at a dose of 0.5 mg/kg of DY^{647} labeled siRNA (equivalent dose of 1.4 mg/kg of chitosan), organs perfused and collected 4 hours post administration, fixed and cryosectioned (5 µm). For CLSM, sections were stained with phalloidin red and Hoechst. (PBS) Phosphate Buffered Saline, (siNaked) naked DY^{647} labeled siRNA, (InV LNP) Invivofectamine® 2.0-DY^{647} siRNA-lipid nanoparticles, (PTEC) Proximal epithelial tubular cells, (NPs) Nanoparticles. DY^{647} siRNA = Green, Nucleus = Blue and Brush borders= Red (actin staining).

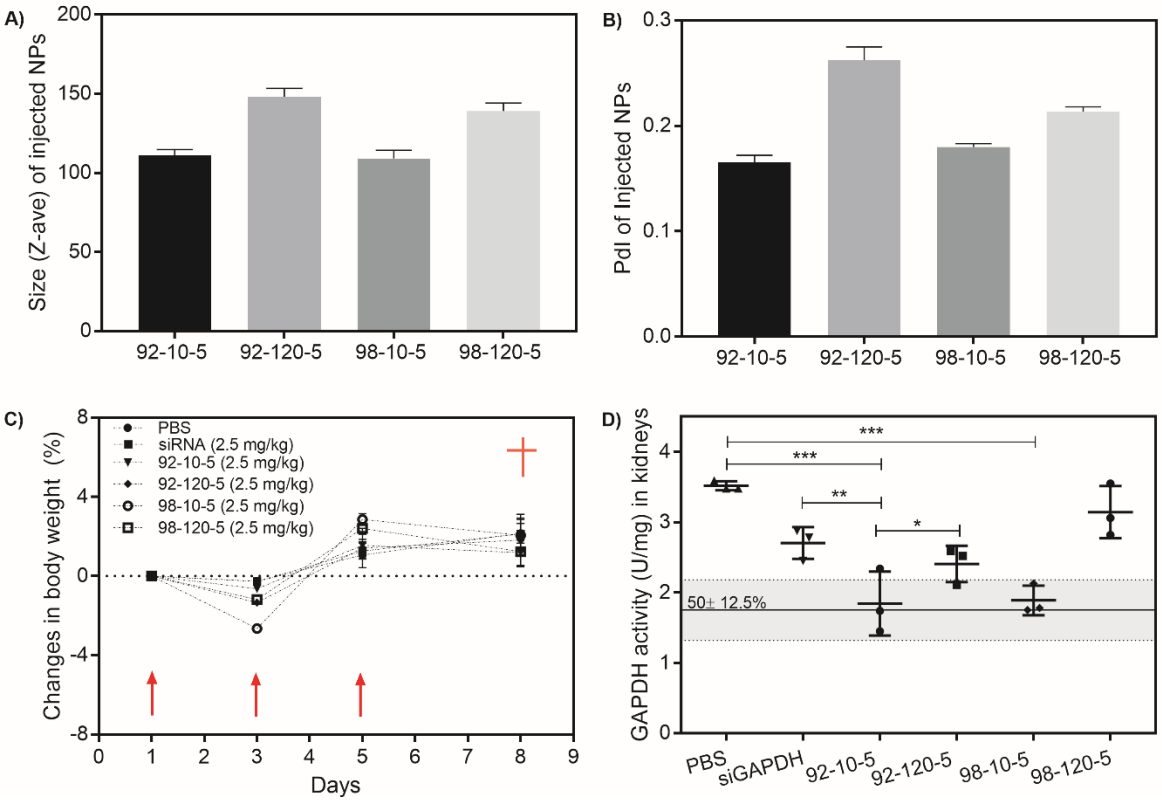

Figure 6-13 Effect of DDA and Mn on in vivo knockdown in the kidney. A) Size of the injected nanoparticles. Nanoparticles were rehydrated in excipients to reach a target dose of 2.5 mg/kg, injected and the remaining volume, diluted 1:8 in excipients and assessed for size using dynamic light scattering. B) Polydispersity index (PdI) of injected nanoparticles. The PdI was automatically computed during DLS in A. C) Changes in body weight following multiple injections. Mice body weight was monitored for a period of 8 days and measured before injection and at euthanasia as an indirect assessment of general toxicity. Arrows and cross represent injection and euthanasia respectively. D) Functional target knockdown in the kidney. Nanoparticles were manually prepared, freeze-dried, rehydrated with excipients and injected in Balb/c mice at a dose of 2.5 mg/kg siRNA. Seventy-two hours after the last administration, kidneys were collected, excised, lysed and the GAPDH enzymatic activity assessed using the KDalert® assay and normalized to total protein content. Cleveland dot plot represents 3 animals per treatment group, with average and standard deviation represented in the form of bars. Statistical significance was computed with One-Way ANOVA followed by Tukey test for multiple comparisons: *p< 0.01, **p <0.001, ***p < 0.00001

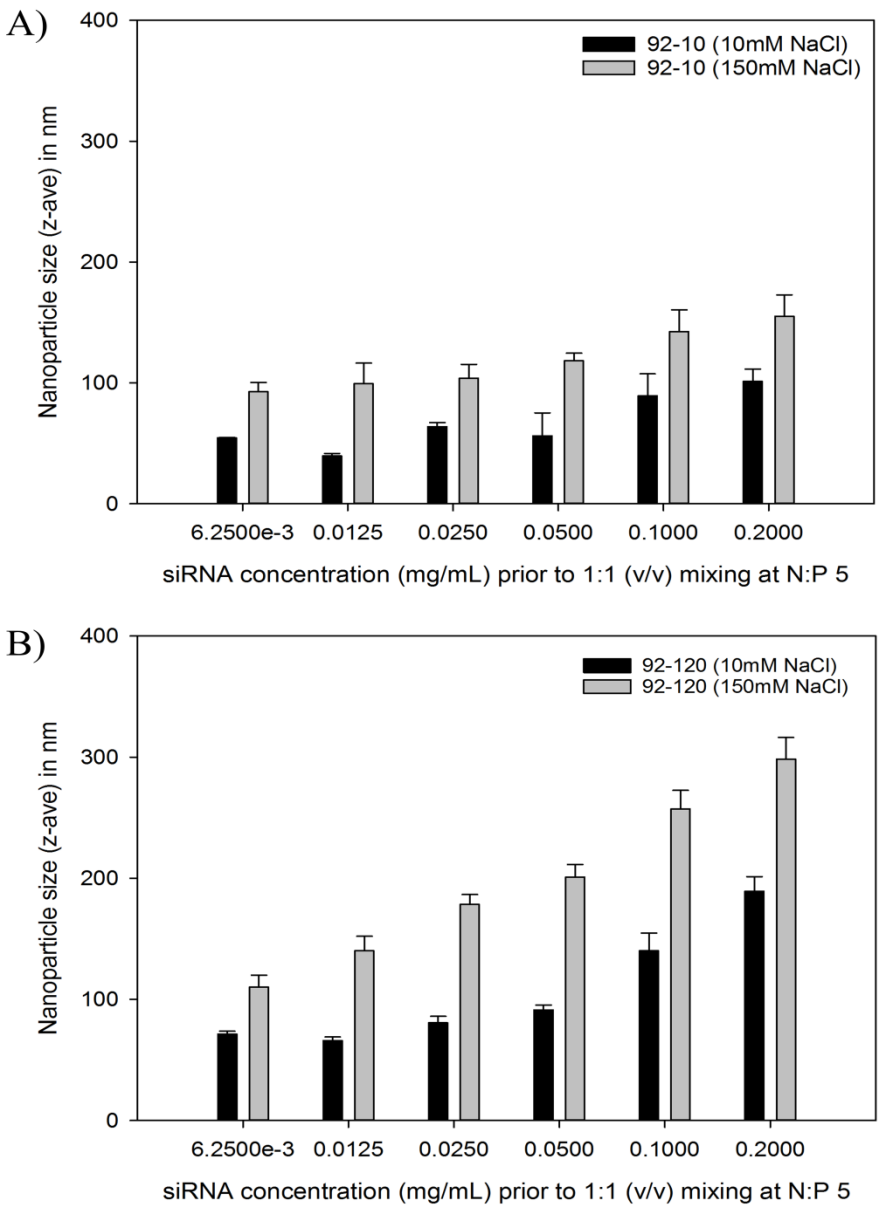

Figure S. 6-7 Effect of siRNA and salt concentration on nanoparticle size. In a previous experiment (Figure 6-1, A), the effect of DDA and N:P ratio on nanoparticle size was found to be negligible relative to Mn, when particles were mixed with siRNA (0.1mg/mL) and suspended in 10mM NaCl (pH 5.5). As a consequence, one chitosan and one N:P ratio i.e. DDA 92%; N:P 5 were selected to further study the effect of siRNA (mg/mL) and NaCl (mM) concentration on nanoparticle size. The latter was measured in 10mM NaCl using 10 versus 120kDa following manual mixing with specific siRNA concentration (mg/mL). For size measurements using dynamic light scattering, particles were formed as described in the materials and methods of this manuscript and diluted (1:8) either in 10 or 150mM NaCl and size measured after 2.5 min post-

incubation. A) 92-10-5 B) 92-120-5. Data represent the average ± standard deviation of two independent experiment with a technical triplicate in each experiment (N=2, n=6).

6.4 Discussion

This study demonstrates the importance of chitosan DDA (charge density), polymer length Mn, and N:P ratio on nanoparticle physicochemical properties and biological performance. The effect of chitosan DDA which controls charge density, or the number of protonatable amines (NH_2), played a predominant role in dictating successful *in vitro* knockdown (Figure 6-3). The positive effect of high charge density, achieved at high DDA, on knockdown efficiency can be attributed to several factors including increased binding affinity for siRNA, increased electrostatic interaction with cell membranes and increased endosomal buffering capacity. None of the previous studies [25-29, 31] investigating the influence of chitosan molecular parameters on siRNA delivery examined the biological relevance of DDA. Instead, these reports varied polymer length and the amine to phosphate molar ratio (N:P) to optimize *in vitro* knockdown efficiency (KD). In our study, the degree of polymerization, or chain length (Mn), and the N:P ratio had a positive but marginal effect on knockdown efficiency (Figure 6-3). This observation is in agreement with results reported previously [24, 26] where increased polymer length and N:P ratio had minimal effects on target knockdown efficiency. These findings are distinctly different from previous work on chitosan mediated plasmid delivery (pDNA), where a fine balance and coupling between Mn and DDA was found to be important for effective complexation and to promote intracellular decomplexation and transgene expression [16, 17, 20]. Those previous studies with plasmid as payload found that modulation of either chain length or charge density in order to reduce nanoparticle stability to a threshold where particles are able to protect pDNA and promote intracellular dissociation was required for efficient transgene expression. This dependence that coupled DDA to Mn achieve expression from plasmids is in contrast to siRNA, most likely since pDNA is a long and flexible molecule with an excess of phosphate binding sites on each molecule compared to amine sites on each chitosan chain, permitting a stronger and higher affinity binding of chitosan to pDNA *versus* chitosan to the shorter siRNA [16, 17, 20]. Compared to plasmid DNA, siRNA is a small and rigid molecule, that binds to chitosan with a lower affinity [24] compared to pDNA [19]. Our findings highlight differences in design principles for the development of chitosan-based nanoparticles for

the delivery of different types of nucleic acids. In the current study, we found a simultaneous increase in DDA, Mn and N:P ratio could optimise siRNA-based knockdown (Figure 6-2) *versus* the complex interaction of these parameters that need to be accounted for to optimize expression from plasmids.

In the current study, increased chain length (Mn) and N:P ratio increased biological performance and the former needed to be above a certain Mn threshold of 10 kDa (~60-70 monomers) (Figure 6-5). EGFP knockdown efficiency and nanoparticle internalization were both reduced when nanoparticles were formulated at 5 kDa and required an increase in Mn and/or N:P ratio to rescue efficiency. This observation is in agreement with previous findings [26, 29]. Low *in vitro* performance was not only attributed to nanoparticle integrity (Figure 6-2) at pH above chitosan pKa (6.5-6.9) but also due to the presence of serum (Figure 6-6). Low Mn formulations showed inferior performance in presence of serum and required an increase in Mn or N:P ratio for improved potency (Figure 6-6), suggesting nanoparticle destabilization occurring through competitive displacement with negatively charged serum components. The negative effect of serum on nanoparticle integrity has been previously demonstrated for cationic liposomes [59] and chitosan-PEI hybrid nanoparticles [25]. Although we could not elucidate the precise effect of serum, heparin and albumin were found to have antagonistic effects on siRNA release with heparin increasing and albumin decreasing release (Figure 6-8, C and D). Cooperation between competing serum components, ionic strength, pH and their effects on nanoparticles is believed to drive the need for higher Mn and N:P ratio for particle stability (Figure 6-1, 2 and 8). This observation was confirmed in the presence of relevant *in vivo* concentrations of serum, where nanoparticle performance decreased in a Mn and N:P dependent manner (Figure 6-8, A and B). The *in vivo* relevance of high N:P ratio and its effect on potency in the presence of physiological concentrations of serum may not be accurately estimated by the *in vitro* environment due to the ability of the free excess chitosan to partition to different compartments than the nanoparticles. However, these findings are important for the development of efficient *in vivo* delivery systems where a combination of high DDA and Mn needs to be used to maintain stability and induce efficient target knockdown. Nanoparticle size and surface charge are two important parameters that affect colloidal stability, pharmacokinetics, biocompatibility and nanoparticle-cell interactions [60]. In this study, size increased with increasing polymer length (Mn) and ionic strength (Figure 6-1). In contrast to size, nanoparticle ζ-potential, increased with increased DDA, Mn and N:P ratio and decreased with increasing ionic

strength. As expected, an increase in the DDA, or number of ionizable amine groups (NH_2) per chain (density), increases the charge density of the polymer and consequently has a direct and positive influence on ζ-potential. However, surface charge is not, at least theoretically, expected to increase with increasing Mn since 1) the pairing of chitosan positive charge and siRNA negative charge groups is not obviously Mn-dependent and 2) an increase in size, due to an increase in Mn, is translated to a lower electrophoretic mobility and thus a lower apparent ζ-potential. Nevertheless, this Mn-dependent increase in ζ-potential may be due to chains that are partly bound at the surface resulting in pendant chains that are longer for higher Mn that increase surface charge or possibly more chitosan chains are bound in particles through greater cooperativity of binding to siRNA. The reduction of ζ-potential at high ionic strength is due to surface charge screening. A decrease in surface potential decreases electrostatic repulsive forces between particles, therefore, causing colloidal instability and an apparent increase in size measured by dynamic light scattering (Figure 6-1). The effect of ionic strength on colloidal stability over time showed strong aggregation (Figure S. 6-1) and could, therefore, influence nanoparticle performance *in vivo* through unintended blood interactions. In this study, ζ-potential positively correlated with knockdown efficiency (Figure 6-4, C) confirming previous reports [16, 61]. As expected, the lack of correlation between size and EGFP knockdown could be explained by serum dependent size stabilization occurring through rapid protein corona formation [18].

siRNA and/or vector-based off-target effects continue to pose problems at the bench and the bedside [9, 62, 63]. A thorough evaluation of off-target effects was conducted in our study (Figure 6-5) with non-targeting siRNA (siNT) and mock transfections (M) performed in parallel to treatments. As shown in Figure 6-5 C and D, the delivery of siNT showed insignificant knockdown while mock transfections mediated a slight increase in EGFP expression for some chitosans. In both cases, target knockdown and/or expression reached a maximum of ±10% indicating a relatively safe profile. The pattern of EGFP knockdown and/or expression seem to follow a trend where long *vs* short chains appear to have opposite effects. This is reminiscent of the marginal toxicity observed when assessing metabolic activity in transfected cells (Figure 6-4 and 9A). Therefore, the decrease in EGFP expression for both siNT and mock transfections observed with short chains, and independent of the N:P ratio, is possibly associated with marginal metabolic toxicity observed at low Mn (Figure 6-4 and 6.9A). Consistent with this idea, Malmo et al [26] found that mock transfection with fully deacetylated chitosan consistently reduced EGFP

expression by about 10% and that a dose-dependent response was associated with around 0-25% decrease. Although no metabolic decrease was mentioned in [26], the number of seeded cells was above the linear response of the assay and therefore, toxicity was not accurately estimated for correlation with mock-induced EGFP knockdown. However, this toxicity issue, was indirectly highlighted during qPCR calibration relative to siNT treated instead of non-treated cells, which according to the authors was justified by differences in confluence between chitosan treated and untreated cells [26].

Since qPCR normalization to one reference gene is associated with a high error bias [41, 48, 49], a pilot study to identify the most stable reference genes under our experimental conditions was conducted. The relevance of our findings are not limited to the normalization strategy and reduction in quantification bias, but also since chitosan treatment influenced the stability of the reference gene panel assayed (Figure 6-7). This result suggested that chitosan, and depending on its DDA, Mn and N:P ratio, disturbs global gene expression indicative of a certain parallelism with linear polyethyleneimine (lPEI) [64] and cationic lipids [65]. The impact of chitosan on the global transcriptome might be due to random binding of chitosan with intracellular nucleic acids or molecular machines through electrostatic or hydrophobic interactions.

In order to mediate their intended effects, chitosan based nanoparticles are endocytosed, the payload released in the cytoplasm but could also accumulate in the nucleus [17]. In the cytoplasm, cationic polymers can interact with vesicular and mitochondrial membranes [66], disrupt normal protein synthesis via electrostatic interaction with polyanionic component in the cytoplasm, and/or induce the activation of molecular sensors. Endosomal release also exposes the cytoplasm to injuries from hydrolytic enzymes [60] while chitosan translocation into the nucleus could potentially induce genetic damage either through electrostatic interactions, hydrolysis from co-impurities or through physical obstruction during chromosomal separation at the anaphase. Formulations used in this study were relatively non-toxic with around 10±10% reduction in cell viability (Figure 6-9). Toxicity increased with lower molecular weight chitosan with high DDA (Figure 6-9D and 6.9A). The observed toxicity was demonstrated to be siRNA-independent as shown in mock transfections at high N:P ratio (Figure 6-9, A). These results are affirmed in other studies, where chitosan showed minimal toxicity when formulated at N:P ratio ranging from 5-60 [16, 21-24, 26, 28, 31]. In contrast, Liu et al. [29] have shown significantly reduced metabolic activity in H1299 cells. The apparent toxicity is probably due to the extremely high free chitosan

content (N:P 150), serum free conditions and assay specific differences. Chitosan-induced DNA damage was found to be statistically insignificant (Figure 6-9, D) indicating that neither the nanoparticle or the ascending concentrations of free chitosan or siRNA sequence were genotoxic.

The cationic nature of chitosan favors interaction with cellular blood components that could potentially have deleterious effects *in vivo*. However, this aspect of probable toxicity has been neglected [15-18, 20-29, 31, 33, 37, 67] with *in vivo* reports often using extremely high N:P ratios without reporting any signs of toxicities [28, 32-36]. However, high N:P ratio could pose serious adverse effects in light of reports suggesting blood-material interaction, reviewed in [68]. Our data show that chitosan-based nanoparticles could induce hemolysis and hemagglutination in a dose-dependent manner and, consequently highlight careful dosing to avoid hemotoxicity and/or embolism (Figure 6-10 and Table 6-3).

Intravenous administration of chitosan-siRNA nanoparticles showed accumulation in the kidneys. Finer examination of kidney structures revealed a punctate pattern of siRNA [17] in the cytoplasm of the proximal epithelial tubular cells (PTECs) suggesting translocation through the glomerular basement membrane (GBM) (Figure 6-12). Although naked siRNA filters through the kidneys ([69] and Figure 6-11) and a fraction accumulate in PTECs ([69] and Figure 6-12), our data clearly indicate a role for chitosan in increasing the efficiency of siRNA accumulation into PTECs (Figure 6-11 and 6-12) probably through glucosamine (Glc)-Megalin interaction and subsequent internalization [34, 70]. However, nanoparticle translocation through the GBM remains to be elucidated mechanistically since fenestration and the extracellular matrix limit nanoparticle translocation and diffusion. Translocation and PTEC accumulation could be achieved through either non-conventional mechanisms as observed with 200-300 nm carbon nanotubes [71] or through nanoparticle disassembly at the highly negative GBM and reassembly in the lumen as proposed for cyclodextrin-based nanoparticles [72]. Alternative delivery through the fenestrated peritubular capillaries could occur but also faces similar diffusion challenges through the negatively charged interstitium. Irrespective of the mechanism involved, chitosan based nanoparticles, not only accumulate in the cytoplasm of PTEC, but also induce functional knockdown (Figure 6-13) without causing deleterious effects on body weight. (Figure 6-13, D). In this study, *in vivo* efficacy was demonstrated through functional GAPDH knockdown where both low Mn (10 kDa) chitosans demonstrated the highest efficacy (~ 40-50% knockdown at the protein level) (Figure 6-13). In contrast to the *in vitro* data in Figure 6-8, high Mn (120kDa)

chitosans did not outperform their low Mn counterparts (Figure 6-13, D) highlighting fundamental differences between *in vitro* and *in vivo* validation. Gao et al [34] demonstrated that low Mn (40 kDa) fully deacetylated chitosan is able to achieve around 50% knockdown in PTEC when formulated at N:P ratio of 60 with higher Mn and/or lower N:P ratio unable distribute to the kidneys. In contrast, we have demonstrated that low and high Mn – except for the high Mn fully deacetylated chitosan – are able to achieve 40-50% target knockdown when formulated at low N:P ratio highlighting proper physicochemical characterization since nanoparticle physicochemical properties before injection, in [34], are highly questionable with non-homogenous and polydisperse NP (400-800 nm). The distribution of naked – LNA modified anti-GAPDH (siGAPDH) – siRNA in mice exhibited a predictable pattern based on the known propensity of oligonucleotides to accumulate in the kidneys [35, 73, 74] and resulted in poor (~ 15%) knockdown (Figure 6-13, D) confirming prior reports [69, 74]. Formulation with chitosan significantly increased knockdown efficiency by~30-35% compared to fresh naked siRNA suggesting a clear and positive role of the delivery system.

Compared to the potency of lipid systems (~70-90%) in advanced pre-clinical or clinical development [13, 75-77], functional target knockdown obtained with our system (~40-50%) appears to be lower. However, considerations such as half-life of the target gene (GAPDH *vs* FVII), potency of the payload, and tissue dependent technical challenges could explain these differences. Accurate estimation of target knockdown using conventional techniques, such as quantitative PCR, enzymatic activity or immunoblotting, depends on 1) the abundance of the target cell type (fraction of cells transfected relative to the organ), 2) the ability of the delivery system to transfect different cell types composing an organ and/or 3) the tissue – or cell – specificity of a target gene. Inasmuch as chitosan displays specific targeting to PTECs, a cell-type that represents a minor fraction of the cells in the kidney, assessment of target knockdown using conventional techniques is necessarily underestimated unless the target gene is PTEC specific and only expressed in this cell subtype. In contrast, LNPs accumulate in hepatocytes, the predominant cell type in the liver, permitting non-biased (accurate) estimation of target knockdown. Therefore, functional knockdown obtained in this report underestimates the true efficiency of our system to silence a target gene in PTECs, and suggest that precise evaluation of target knockdown requires the development of novel methods capable of estimating knockdown in a specific subset of cells composing an organ.

Hepatobiliary elimination in the gall bladder (Figure 6-11) indicates that a fraction of the injected nanoparticles is large enough to bypass liver fenestration and is probably in the size range of 0.3-1 µm in blood [78]. Taken together, our findings are of critical importance to siRNA delivery since extra-hepatic targeting could be naturally achieved without chemical modifications or ligand targeting and accumulation occurred in PTECs, with functional target knockdown around 50% in kidney cortex, further differentiating this system from cyclodextrin-based NPs that accumulate in glomeruli and podocytes [72]. As a consequence, unmodified chitosan-siRNA nanoparticles could potentially be used for the treatment of PTEC associated kidney fibrotic diseases.

6.5 Conclusion

This study highlights the importance of chitosan DDA (charge density), chain length and nanoparticle amine to phosphate molar ratio for efficient and nontoxic *in vitro* performance. Highly deacetylated chitosans are superior siRNA delivery systems compared to partially acetylated chitosans. Highly deacetylated chitosans provide the optimal balance between biological performance and toxicity. These specific formulations displayed potent knockdown, low toxicity, and present minimal non-specific effects and no genotoxicity. Most importantly, chitosan was demonstrated to exhibit extra-hepatic accumulation to kidney proximal epithelial tubular cells where functional knockdown of ~50% at the protein level was demonstrated. This study further suggests that increased colloidal stability may improve hemocompatibility and maintain their natural kidney targeting ability.

Acknowledgments

This work was supported by the Canadian Institutes of Health Research and ANRis pharmaceuticals. The funding source had no role in study design, data collection, analysis, interpretation of data, writing or decision to submit this manuscript. The authors would like to thank Mohammed Benhammadi and Rabeb Mouna Derbali for assistance with the siRNA encapsulation experiments, Daniel Del Balso for assisting in transfections and Julie Tremblay for quality control.

References

[1] K.E. Lundin, O. Gissberg, C.I. Smith, Oligonucleotide Therapies: The Past and the Present, Hum Gene Ther 26(8) (2015) 475-85.

[2] A. Wittrup, J. Lieberman, Knocking down disease: a progress report on siRNA therapeutics, Nat Rev Genet 16(9) (2015) 543-52.

[3] D.V. Morrissey, K. Blanchard, L. Shaw, K. Jensen, J.A. Lockridge, B. Dickinson, J.A. McSwiggen, C. Vargeese, K. Bowman, C.S. Shaffer, B.A. Polisky, S. Zinnen, Activity of stabilized short interfering RNA in a mouse model of hepatitis B virus replication, Hepatology 41(6) (2005) 1349-56.

[4] Y.L. Chiu, T.M. Rana, siRNA function in RNAi: a chemical modification analysis, RNA 9(9) (2003) 1034-48.

[5] D.V. Morrissey, J.A. Lockridge, L. Shaw, K. Blanchard, K. Jensen, W. Breen, K. Hartsough, L. Machemer, S. Radka, V. Jadhav, N. Vaish, S. Zinnen, C. Vargeese, K. Bowman, C.S. Shaffer, L.B. Jeffs, A. Judge, I. MacLachlan, B. Polisky, Potent and persistent in vivo anti-HBV activity of chemically modified siRNAs, Nat Biotechnol 23(8) (2005) 1002-7.

[6] A.D. Judge, G. Bola, A.C. Lee, I. MacLachlan, Design of noninflammatory synthetic siRNA mediating potent gene silencing in vivo, Mol Ther 13(3) (2006) 494-505.

[7] A.L. Jackson, J. Burchard, D. Leake, A. Reynolds, J. Schelter, J. Guo, J.M. Johnson, L. Lim, J. Karpilow, K. Nichols, W. Marshall, A. Khvorova, P.S. Linsley, Position-specific chemical modification of siRNAs reduces "off-target" transcript silencing, RNA 12(7) (2006) 1197-205.

[8] R. Kanasty, J.R. Dorkin, A. Vegas, D. Anderson, Delivery materials for siRNA therapeutics, Nat Mater 12(11) (2013) 967-77.

[9] K. Garber, Alnylam's RNAi therapy targets amyloid disease, Nat Biotechnol 33(6) (2015) 577.

[10] I. Arrowhead Pharmaceuticals, Arrowhead Pharmaceuticals Provides Update on Heparc-2004 Study, 2016.

[11] Ramanathan RK, Hamburg SI, e.a. Borad MJ, A Phase 1 dose escalation study of TKM-080301, a RNAi therapeutic directed against PLK1, in patients with advanced solid tumors, AACR 2013 Annual Meeting, Washington 2013.

[12] W. Tao, X. Mao, J.P. Davide, B. Ng, M. Cai, P.A. Burke, A.B. Sachs, L. Sepp-Lorenzino, Mechanistically probing lipid-siRNA nanoparticle-associated toxicities identifies Jak inhibitors effective in mitigating multifaceted toxic responses, Mol Ther 19(3) (2011) 567-75.

[13] M.T. Abrams, M.L. Koser, J. Seitzer, S.C. Williams, M.A. DiPietro, W. Wang, A.W. Shaw, X. Mao, V. Jadhav, J.P. Davide, P.A. Burke, A.B. Sachs, S.M. Stirdivant, L. Sepp-Lorenzino, Evaluation of efficacy, biodistribution, and inflammation for a potent siRNA nanoparticle: effect of dexamethasone co-treatment, Mol Ther 18(1) (2010) 171-80.

[14] C. Lorenzer, M. Dirin, A.M. Winkler, V. Baumann, J. Winkler, Going beyond the liver: progress and challenges of targeted delivery of siRNA therapeutics, J Control Release 203 (2015) 1-15.

[15] M.D. Buschmann, A. Merzouki, M. Lavertu, M. Jean, V. Darras, Chitosans for delivery of nucleic acids, Advanced Drug Delivery Reviews 65(9) (2013) 1234-1270.

[16] M. Lavertu, S. Methot, N. Tran-Khanh, M.D. Buschmann, High efficiency gene transfer using chitosan/DNA nanoparticles with specific combinations of molecular weight and degree of deacetylation, Biomaterials 27(27) (2006) 4815-24.

[17] M. Thibault, S. Nimesh, M. Lavertu, M.D. Buschmann, Intracellular trafficking and decondensation kinetics of chitosan-pDNA polyplexes, Mol Ther 18(10) (2010) 1787-95.

[18] S. Nimesh, M.M. Thibault, M. Lavertu, M.D. Buschmann, Enhanced gene delivery mediated by low molecular weight chitosan/DNA complexes: effect of pH and serum, Mol Biotechnol 46(2) (2010) 182-96.

[19] P.L. Ma, M. Lavertu, F.M. Winnik, M.D. Buschmann, New insights into chitosan-DNA interactions using isothermal titration microcalorimetry, Biomacromolecules 10(6) (2009) 1490-9.

[20] S.P. Strand, S. Lelu, N.K. Reitan, C. de Lange Davies, P. Artursson, K.M. Varum, Molecular design of chitosan gene delivery systems with an optimized balance between polyplex stability and polyplex unpacking, Biomaterials 31(5) (2010) 975-87.

[21] M. Alameh, M. Jean, D. Dejesus, M.D. Buschmann, A. Merzouki, Chitosanase-based method for RNA isolation from cells transfected with chitosan/siRNA nanocomplexes for real-time RT-PCR in gene silencing, Int J Nanomedicine 5 (2010) 473-81.

[22] M. Alameh, D. Dejesus, M. Jean, V. Darras, M. Thibault, M. Lavertu, M.D. Buschmann, A. Merzouki, Low molecular weight chitosan nanoparticulate system at low N:P ratio for nontoxic polynucleotide delivery, Int J Nanomedicine 7 (2012) 1399-414.

[23] M. Jean, M. Alameh, D. De Jesus, M. Thibault, M. Lavertu, V. Darras, M. Nelea, M.D. Buschmann, A. Merzouki, Chitosan-based therapeutic nanoparticles for combination gene therapy

and gene silencing of in vitro cell lines relevant to type 2 diabetes, Eur J Pharm Sci 45(1-2) (2012) 138-49.

[24] P. Holzerny, B. Ajdini, W. Heusermann, K. Bruno, M. Schuleit, L. Meinel, M. Keller, Biophysical properties of chitosan/siRNA polyplexes: profiling the polymer/siRNA interactions and bioactivity, J Control Release 157(2) (2012) 297-304.

[25] H. Ragelle, R. Riva, G. Vandermeulen, B. Naeye, V. Pourcelle, C.S. Le Duff, C. D'Haese, B. Nysten, K. Braeckmans, S.C. De Smedt, C. Jerome, V. Preat, Chitosan nanoparticles for siRNA delivery: optimizing formulation to increase stability and efficiency, J Control Release 176 (2014) 54-63.

[26] J. Malmo, H. Sorgard, K.M. Varum, S.P. Strand, siRNA delivery with chitosan nanoparticles: Molecular properties favoring efficient gene silencing, J Control Release 158(2) (2012) 261-8.

[27] H. Katas, H.O. Alpar, Development and characterisation of chitosan nanoparticles for siRNA delivery, J Control Release 115(2) (2006) 216-25.

[28] K.A. Howard, U.L. Rahbek, X. Liu, C.K. Damgaard, S.Z. Glud, M.O. Andersen, M.B. Hovgaard, A. Schmitz, J.R. Nyengaard, F. Besenbacher, J. Kjems, RNA interference in vitro and in vivo using a novel chitosan/siRNA nanoparticle system, Mol Ther 14(4) (2006) 476-84.

[29] X. Liu, K.A. Howard, M. Dong, M.O. Andersen, U.L. Rahbek, M.G. Johnsen, O.C. Hansen, F. Besenbacher, J. Kjems, The influence of polymeric properties on chitosan/siRNA nanoparticle formulation and gene silencing, Biomaterials 28(6) (2007) 1280-8.

[30] A.M. Ji, D. Su, O. Che, W.S. Li, L. Sun, Z.Y. Zhang, B. Yang, F. Xu, Functional gene silencing mediated by chitosan/siRNA nanocomplexes, Nanotechnology 20(40) (2009) 405103.

[31] J. Malmo, A. Sandvig, K.M. Varum, S.P. Strand, Nanoparticle mediated P-glycoprotein silencing for improved drug delivery across the blood-brain barrier: a siRNA-chitosan approach, PLoS One 8(1) (2013) e54182.

[32] C. Yang, S. Gao, J. Kjems, Folic acid conjugated chitosan for targeted delivery of siRNA to activated marcophages in vitro and in vivo, Journal of Materials Chemistry B 2 (2014) 8608-8615.

[33] E.J. Nielsen, J.M. Nielsen, D. Becker, A. Karlas, H. Prakash, S.Z. Glud, J. Merrison, F. Besenbacher, T.F. Meyer, J. Kjems, K.A. Howard, Pulmonary gene silencing in transgenic EGFP mice using aerosolised chitosan/siRNA nanoparticles, Pharm Res 27(12) (2010) 2520-7.

[34] S. Gao, S. Hein, F. Dagnaes-Hansen, K. Weyer, C. Yang, R. Nielsen, E.I. Christensen, R.A. Fenton, J. Kjems, Megalin-mediated specific uptake of chitosan/siRNA nanoparticles in mouse

kidney proximal tubule epithelial cells enables AQP1 gene silencing, Theranostics 4(10) (2014) 1039-51.

[35] S. Gao, F. Dagnaes-Hansen, E.J. Nielsen, J. Wengel, F. Besenbacher, K.A. Howard, J. Kjems, The effect of chemical modification and nanoparticle formulation on stability and biodistribution of siRNA in mice, Mol Ther 17(7) (2009) 1225-33.

[36] C. Yang, L. Nilsson, M.U. Cheema, Y. Wang, J. Frokiaer, S. Gao, J. Kjems, R. Norregaard, Chitosan/siRNA nanoparticles targeting cyclooxygenase type 2 attenuate unilateral ureteral obstruction-induced kidney injury in mice, Theranostics 5(2) (2015) 110-23.

[37] C. Corbet, H. Ragelle, V. Pourcelle, K. Vanvarenberg, J. Marchand-Brynaert, V. Preat, O. Feron, Delivery of siRNA targeting tumor metabolism using non-covalent PEGylated chitosan nanoparticles: Identification of an optimal combination of ligand structure, linker and grafting method, J Control Release 223 (2016) 53-63.

[38] S.A. Bustin, V. Benes, J.A. Garson, J. Hellemans, J. Huggett, M. Kubista, R. Mueller, T. Nolan, M.W. Pfaffl, G.L. Shipley, J. Vandesompele, C.T. Wittwer, The MIQE guidelines: minimum information for publication of quantitative real-time PCR experiments, Clin Chem 55(4) (2009) 611-22.

[39] M. Lavertu, Z. Xia, A.N. Serreqi, M. Berrada, A. Rodrigues, D. Wang, M.D. Buschmann, A. Gupta, A validated 1H NMR method for the determination of the degree of deacetylation of chitosan, J Pharm Biomed Anal 32(6) (2003) 1149-58.

[40] M. Zuker, Mfold web server for nucleic acid folding and hybridization prediction, Nucleic Acids Res 31(13) (2003) 3406-15.

[41] J. Vandesompele, K. De Preter, F. Pattyn, B. Poppe, N. Van Roy, A. De Paepe, F. Speleman, Accurate normalization of real-time quantitative RT-PCR data by geometric averaging of multiple internal control genes, Genome Biol 3(7) (2002) RESEARCH0034.

[42] B.M. Gyori, G. Venkatachalam, P.S. Thiagarajan, D. Hsu, M.V. Clement, OpenComet: an automated tool for comet assay image analysis, Redox Biol 2 (2014) 457-65.

[43] ASTM E2524-08: Standard Test Method for Analysis of Hemolytic Properties of Nanoparticles, 2013.

[44] S.J. Evani, A.K. Ramasubramanian, Chapter 13: Hemocompatibility of Nanoparticles, Nanobiomaterials Handbook, CRC Press2001, pp. 1-17.

[45] A. Tavakoli Naeini, O. Soliman, M. Alameh, M. Lavertu, M.D. Buschmann, Automated In-line Mixing System for Large Scale Production of Chitosan-based Polyplexes, Journal of Colloid and Interface Science (2017).

[46] M.H. Ullman-Cullere, C.J. Foltz, Body condition scoring: a rapid and accurate method for assessing health status in mice, Lab Anim Sci 49(3) (1999) 319-23.

[47] I. Richard, M. Thibault, G. De Crescenzo, M.D. Buschmann, M. Lavertu, Ionization behavior of chitosan and chitosan-DNA polyplexes indicate that chitosan has a similar capability to induce a proton-sponge effect as PEI, Biomacromolecules 14(6) (2013) 1732-40.

[48] K. Dheda, J.F. Huggett, S.A. Bustin, M.A. Johnson, G. Rook, A. Zumla, Validation of housekeeping genes for normalizing RNA expression in real-time PCR, Biotechniques 37(1) (2004) 112-4, 116, 118-9.

[49] K. Dheda, J.F. Huggett, J.S. Chang, L.U. Kim, S.A. Bustin, M.A. Johnson, G.A. Rook, A. Zumla, The implications of using an inappropriate reference gene for real-time reverse transcription PCR data normalization, Anal Biochem 344(1) (2005) 141-3.

[50] J. Huggett, K. Dheda, S. Bustin, A. Zumla, Real-time RT-PCR normalisation; strategies and considerations, Genes Immun 6(4) (2005) 279-84.

[51] J. Vermeulen, K. De Preter, S. Lefever, J. Nuytens, F. De Vloed, S. Derveaux, J. Hellemans, F. Speleman, J. Vandesompele, Measurable impact of RNA quality on gene expression results from quantitative PCR, Nucleic Acids Res 39(9) (2011) e63.

[52] S. Fleige, V. Walf, S. Huch, C. Prgomet, J. Sehm, M.W. Pfaffl, Comparison of relative mRNA quantification models and the impact of RNA integrity in quantitative real-time RT-PCR, Biotechnol Lett 28(19) (2006) 1601-13.

[53] S. Fleige, M.W. Pfaffl, RNA integrity and the effect on the real-time qRT-PCR performance, Mol Aspects Med 27(2-3) (2006) 126-39.

[54] H. Engelberg, Plasma heparin levels in normal man, Circulation 23 (1961) 578-81.

[55] P. Duez, G. Dehon, A. Kumps, J. Dubois, Statistics of the Comet assay: a key to discriminate between genotoxic effects, Mutagenesis 18(2) (2003) 159-66.

[56] Y. Huang, J. Hong, S. Zheng, Y. Ding, S. Guo, H. Zhang, X. Zhang, Q. Du, Z. Liang, Elimination pathways of systemically delivered siRNA, Mol Ther 19(2) (2011) 381-5.

[57] Y. Huang, Q. Cheng, J.L. Ji, S. Zheng, L. Du, L. Meng, Y. Wu, D. Zhao, X. Wang, L. Lai, H. Cao, K. Xiao, S. Gao, Z. Liang, Pharmacokinetic Behaviors of Intravenously Administered siRNA in Glandular Tissues, Theranostics 6(10) (2016) 1528-41.

[58] J. Soutschek, A. Akinc, B. Bramlage, K. Charisse, R. Constien, M. Donoghue, S. Elbashir, A. Geick, P. Hadwiger, J. Harborth, M. John, V. Kesavan, G. Lavine, R.K. Pandey, T. Racie, K.G. Rajeev, I. Rohl, I. Toudjarska, G. Wang, S. Wuschko, D. Bumcrot, V. Koteliansky, S. Limmer, M. Manoharan, H.P. Vornlocher, Therapeutic silencing of an endogenous gene by systemic administration of modified siRNAs, Nature 432(7014) (2004) 173-8.

[59] O. Zelphati, L.S. Uyechi, L.G. Barron, F.C. Szoka, Jr., Effect of serum components on the physico-chemical properties of cationic lipid/oligonucleotide complexes and on their interactions with cells, Biochim Biophys Acta 1390(2) (1998) 119-33.

[60] A.E. Nel, L. Madler, D. Velegol, T. Xia, E.M. Hoek, P. Somasundaran, F. Klaessig, V. Castranova, M. Thompson, Understanding biophysicochemical interactions at the nano-bio interface, Nat Mater 8(7) (2009) 543-57.

[61] M. Huang, C.W. Fong, E. Khor, L.Y. Lim, Transfection efficiency of chitosan vectors: effect of polymer molecular weight and degree of deacetylation, J Control Release 106(3) (2005) 391-406.

[62] S. Akhtar, I. Benter, Toxicogenomics of non-viral drug delivery systems for RNAi: potential impact on siRNA-mediated gene silencing activity and specificity, Adv Drug Deliv Rev 59(2-3) (2007) 164-82.

[63] C. Tschuch, A. Schulz, A. Pscherer, W. Werft, A. Benner, A. Hotz-Wagenblatt, L.S. Barrionuevo, P. Lichter, D. Mertens, Off-target effects of siRNA specific for GFP, BMC Mol Biol 9 (2008) 60.

[64] A. Beyerle, M. Irmler, J. Beckers, T. Kissel, T. Stoeger, Toxicity pathway focused gene expression profiling of PEI-based polymers for pulmonary applications, Mol Pharm 7(3) (2010) 727-37.

[65] S.A. Plautz, G. Boanca, J.M. Riethoven, A.K. Pannier, Microarray Analysis of Gene Expression Profiles in Cells Transfected With Nonviral Vectors, Mol Ther 19(12) (2011) 2144-2151.

[66] L. Parhamifar, H. Andersen, S.M. Moghimi, Lactate dehydrogenase assay for assessment of polycation cytotoxicity, Methods Mol Biol 948 (2013) 13-22.

[67] H. Ragelle, G. Vandermeulen, V. Preat, Chitosan-based siRNA delivery systems, J Control Release 172(1) (2013) 207-18.

[68] V. Balan, L. Verestiuc, Strategies to improve chitosan hemocompatibilities: A review, European Polymer Journal 53 (2014) 171-188.

[69] J.D. Thompson, D.J. Kornbrust, J.W. Foy, E.C. Solano, D.J. Schneider, E. Feinstein, B.A. Molitoris, S. Erlich, Toxicological and pharmacokinetic properties of chemically modified siRNAs targeting p53 RNA following intravenous administration, Nucleic Acid Ther 22(4) (2012) 255-64.

[70] Y. Lin, Y. Li, X. Wang, T. Gong, L. Zhang, X. Sun, Targeted drug delivery to renal proximal tubule epithelial cells mediated by 2-glucosamine, J Control Release 167(2) (2013) 148-56.

[71] A. Ruggiero, C.H. Villa, E. Bander, D.A. Rey, M. Bergkvist, C.A. Batt, K. Manova-Todorova, W.M. Deen, D.A. Scheinberg, M.R. McDevitt, Paradoxical glomerular filtration of carbon nanotubes, Proc Natl Acad Sci U S A 107(27) (2010) 12369-74.

[72] J.E. Zuckerman, A. Gale, P. Wu, R. Ma, M.E. Davis, siRNA delivery to the glomerular mesangium using polycationic cyclodextrin nanoparticles containing siRNA, Nucleic Acid Ther 25(2) (2015) 53-64.

[73] R.S. Geary, D. Norris, R. Yu, C.F. Bennett, Pharmacokinetics, biodistribution and cell uptake of antisense oligonucleotides, Adv Drug Deliv Rev 87 (2015) 46-51.

[74] B.A. Molitoris, P.C. Dagher, R.M. Sandoval, S.B. Campos, H. Ashush, E. Fridman, A. Brafman, A. Faerman, S.J. Atkinson, J.D. Thompson, H. Kalinski, R. Skaliter, S. Erlich, E. Feinstein, siRNA targeted to p53 attenuates ischemic and cisplatin-induced acute kidney injury, J Am Soc Nephrol 20(8) (2009) 1754-64.

[75] S.C. Semple, A. Akinc, J. Chen, A.P. Sandhu, B.L. Mui, C.K. Cho, D.W. Sah, D. Stebbing, E.J. Crosley, E. Yaworski, I.M. Hafez, J.R. Dorkin, J. Qin, K. Lam, K.G. Rajeev, K.F. Wong, L.B. Jeffs, L. Nechev, M.L. Eisenhardt, M. Jayaraman, M. Kazem, M.A. Maier, M. Srinivasulu, M.J. Weinstein, Q. Chen, R. Alvarez, S.A. Barros, S. De, S.K. Klimuk, T. Borland, V. Kosovrasti, W.L. Cantley, Y.K. Tam, M. Manoharan, M.A. Ciufolini, M.A. Tracy, A. de Fougerolles, I. MacLachlan, P.R. Cullis, T.D. Madden, M.J. Hope, Rational design of cationic lipids for siRNA delivery, Nat Biotechnol 28(2) (2010) 172-6.

[76] T.S. Zimmermann, A.C. Lee, A. Akinc, B. Bramlage, D. Bumcrot, M.N. Fedoruk, J. Harborth, J.A. Heyes, L.B. Jeffs, M. John, A.D. Judge, K. Lam, K. McClintock, L.V. Nechev, L.R. Palmer, T. Racie, I. Rohl, S. Seiffert, S. Shanmugam, V. Sood, J. Soutschek, I. Toudjarska, A.J. Wheat, E.

Yaworski, W. Zedalis, V. Koteliansky, M. Manoharan, H.P. Vornlocher, I. MacLachlan, RNAi-mediated gene silencing in non-human primates, Nature 441(7089) (2006) 111-4.

[77] A. Akinc, M. Goldberg, J. Qin, J.R. Dorkin, C. Gamba-Vitalo, M. Maier, K.N. Jayaprakash, M. Jayaraman, K.G. Rajeev, M. Manoharan, V. Koteliansky, I. Rohl, E.S. Leshchiner, R. Langer, D.G. Anderson, Development of lipidoid-siRNA formulations for systemic delivery to the liver, Mol Ther 17(5) (2009) 872-9.

[78] K.M. Tsoi, S.A. MacParland, X.Z. Ma, V.N. Spetzler, J. Echeverri, B. Ouyang, S.M. Fadel, E.A. Sykes, N. Goldaracena, J.M. Kaths, J.B. Conneely, B.A. Alman, M. Selzner, M.A. Ostrowski, O.A. Adeyi, A. Zilman, I.D. McGilvray, W.C. Chan, Mechanism of hard-nanomaterial clearance by the liver, Nat Mater 15(11) (2016) 1212-1221.

Chapter 7 ARTICLE 4: CHITOSAN SIRNA NANOPARTICLES PRODUCE SIGNIFICANT NON-TOXIC FUNCTIONAL GENE SILENCING IN KIDNEY CORTICES

Mohamad Alameh[2], Ashkan Tavakoli-Naeini[2], Yuan Chang[1], Garima Dwivedi[2], Nicolas Tran-Khan[1], Etienne Jeandupeux[2], Frederic Lesage[1], Marc Lavertu[1,2] and Michael D. Buschmann[1,2**]

[1] Polytechnique Montreal, Department of Chemical engineering, Montreal, QC, Canada. [2] Polytechnique Montreal, Institute of Biomedical engineering, Montreal, QC, Canada. [3] Polytechnique Montreal, Department of Electrical engineering, Montreal, QC, Canada

**Corresponding author

Submitted to the Journal of Controlled Release (2017)

Graphical Abstract:

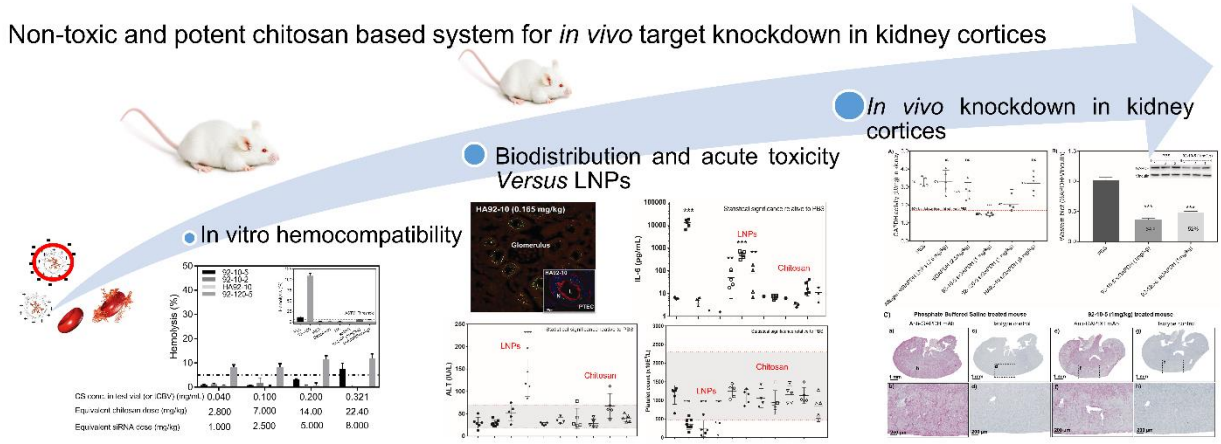

Abstract: Nanoparticle toxicity represents a major hurdle limiting clinical translation with both cationic lipids and polymers that can produce preclinical toxicity and serious adverse events in clinical trials. Advancements in cationic lipid head groups have improved the therapeutic window but clinical application still requires the administration of prophylactic anti-inflammatory steroids. Chitosans, a family of natural polycationic and bio-degradable polymers have shown *in vitro* and *in vivo* efficacy for nucleic acid delivery. However, the effect of chitosan molecular weight (Mn), dose and payload type – i.e. unmodified *versus* modified siRNA – on cytokine induction, hematological and serological responses, body weight and clinical signs have not been investigated nor reported following intravenous (I.V.) administration in mice. To understand the influence of Mn, dose, payload and hyaluronic acid (HA) coating, on *in vivo* toxicity, immune stimulation, biodistribution and efficacy, precisely characterized low (10 kDa) and high (120 kDa) Mn chitosans with a fixed degree of deacetylation of 92% were produced and formulated with unmodified (immune stimulating) *vs* chemically modified (non-immune stimulating) siRNA, and tested for hemocompatibility as per ASTM standards for dose selection and I.V. administration to mice. Cytokine induction (IL-1β, IL-6, TNF-α, IFN-γ and KC), hematological (Hb, Hematocrit, platelets, …) and serological (ALT, AST, BUN, Cr, ...) responses were assessed at 4 (Cytokine) and 24 hours (Serology) post-administration. HA was used to coat nanoparticle to improve hemocompatibility. Body weight and clinical signs were monitored following single *versus* multiple injections. *In vivo* biodistribution and the efficacy of uncoated and HA-coated formulations to induce functional target knockdown were also investigated, and compared with cationic lipid nanoparticles (Invivofectamine®). Hemolysis was found to be dose and Mn-dependent with HA coating

abrogating hemolysis. In comparison with cationic lipid nanoparticles (LNPs), uncoated and HA-coated chitosan NPs did not induce either immune stimulation or hematologic toxicity upon I.V. administration. Liver and kidney biomarkers remained unchanged with chitosan formulations while high doses of LNPs led, as previously reported, to increased transaminase levels and a decrease in body weight following repeated administration. *In vivo* biodistribution in mice show extra-hepatic accumulation of both uncoated and HA-coated NPs in the proximal epithelial tubules of the kidney with functional knockdown (measured by multiple techniques) reaching 60% suggesting potential applications in the treatment of kidney diseases.

7.1 Introduction

Small interfering RNA (siRNA) is a novel class of molecules with promising potential in treating previously un-druggable diseases via gene-specific knockdown. The clinical maturity of this potent and gene specific technology depends on the efficient delivery and cell uptake of these relatively large and negatively charged siRNA molecules without inducing any short or long term toxicities. Pharmacokinetic behavior, including absorption, distribution, metabolism, and excretion (ADME) depends on the chemical and structural architecture of these molecules [1]. Naked, and unmodified siRNA, are highly prone to nuclease degradation and are swiftly eliminated into the bladder resulting in poor target knockdown [2]. Modification of the sugar, and/or the backbone increases nuclease resistance, modifies pharmacokinetic/biodistribution profiles of these molecules via interaction with serum proteins and can reduce off-target effects. The modification pattern, type and position have been demonstrated to play an important role in abrogating off-target effects, improving guide strand loading into the RNA-Induced Silencing Complex (RISC) and dictating efficient target knockdown [1]. For instance, modifications such as 2’OMe were demonstrated to reduce immune activation [3, 4] and limit off-target effects via improved hybridization complementarity between the siRNA guide sequence and target mRNA [5]. Albeit very efficient, chemical modifications do not yet alleviate the problems of targeting siRNA delivery to the desired pharmacological site of action, limited endosomal release, or rapid renal elimination. Consequently, ligand-mediated targeting and encapsulation into delivery systems represent the two major delivery strategies used in clinical development. *N*-acetylgalactosamine (GalNAc)-conjugation directs siRNA to liver hepatocytes and demonstrates potent target gene knockdown in phase II/III clinical trials [6]. GalNAc conjugated siRNA has also been co-delivered to the liver

along a GalNAc targeted and polyethylene glycol masked endosomolytic peptide or polymer as part of the Dynamic Polyconjugate System (DPC) [7]. These two conjugation approaches require highly modified siRNA to achieve knockdown [8] and demonstrate potency in pre-clinical and clinical studies. However, these approaches face serious challenges with the recent discontinuation of the investigational Alnylam Revusiran and Arrowhead ARC- 520/521 programs [9, 10] in response to imbalanced mortality in the TTR amyloidosis with cardiomyopathy phase III trial compared to placebo [9] and the death of a non-human primate administered with high doses of DPCs [10]. However, association between observed mortality and components of the payload (i.e. siRNA, or the delivery system) or other factors [9] still need to be mechanistically understood.

Lipid-based nanoparticles (LNPs), physically protect the siRNA from serum nucleases and have a natural tendency to interact with negatively charged lipoproteins (i.e. ApoB A/E) and induce clinically meaningful target knockdown in liver hepatocytes [7, 9, 11]. In contrast to conjugates, LNPs require less chemical modification of the siRNA payload but are associated with serious side effects such as immune activation [12-15] and reduced potency following repeated administration [16, 17]. LNP clinical administration is preceded by and/or accompanied with prophylactic anti-inflammatory steroids [12, 14, 18]. Additionally, LNPs are limited in their ability to deliver nucleic acid cargos beyond the liver [19]. Therefore, delivery systems that meet criteria such as colloidal stability, high encapsulation efficiency, low toxicity, and deliver siRNA efficiently to extrahepatic organs are critically needed.

Chitosan is a family of cationic bio-copolymers composed of β (1-4) linked N-acetyl glucosamine (GlcNAc) and D-glucosamine (Glc) that has gained considerable attention for nucleic acid (NA) delivery due to its low toxicity, ease of production, and chemical modification. Chitosan can be fine-tuned to reach a specific degree of deacetylation (DDA), or fraction of protonatable amine (charge), and average molecular weights (Mw or Mn). The high degree of protonation of amino groups (NH_2) occurring at a pH below chitosan pKa (~6.5-6.9) favors spontaneous assembly of polyelectrolyte complexes, or nanoparticles, through electrostatic interactions and have been used to deliver siRNAs both *in vitro* [20-30] and *in vivo* [26, 30-35]. The system has been in part developed in our laboratory, where we previously demonstrated that siRNA could be delivered, both *in vitro* [20, 21, 36, 37] and *in vivo* [38, 39], at low nitrogen to phosphate molar (N:P) ratios to avoid limited dosing, blood incompatibility and non-specific effects due to large quantities of

free excess chitosan at higher N:P ratios. As a cationic polymer, chitosan can interact with blood components, activate platelets, induce erythrocyte lysis [40] and, depending on its DDA, cause cytokine induction through macrophage/monocyte stimulation [41, 42]. These aspects of toxicity, at least in the nanoparticle field, have been neglected [20-27, 29, 31, 35, 36, 43-46] with *in vivo* reports often using extremely high N:P ratios without reporting any signs of toxicity and/or parameters such as clinical signs, hematological and/or serological biomarkers [26, 30-34]. In addition, and in contrast to LNPs, *in vivo* induction of cytokines was never characterized. Therefore, a systemic study with accurately characterized chitosan that investigates hemocompatibility, *in vivo* acute toxicity and demonstrates knockdown following I.V. administration of nanoparticles is needed.

Here we report the complete hemocompatibility profile of uncoated and hyaluronic acid coated (HA) formulations and show that HA coating eliminates interaction with erythrocytes. Acute single ascending dose toxicity was assessed by measuring cytokine induction (4-hours post injection), hematological and serological biomarkers (24-hours post injection) and changes in body weight following single *vs* repeated administration. In addition, clinical signs and histopathological sections of main organs are reported to support the safety of our formulations. *In vivo* real-time imaging, and confocal microscopy was used to show the biodistribution profile and intracellular localization of both uncoated and HA coated nanoparticles. Functional target knockdown was measured by means of multiple techniques such as an enzymatic activity assay, western blotting and was qualitatively confirmed by immunohistochemistry. In this study, the biodistribution, toxicity, and efficacy of commercially available LNPs (Invivofectamine®) were compared with the uncoated and HA coated systems.

7.2 Material and Methods

7.2.1 Materials

Medical grade hyaluronic acid (HA, 866 kDa, HA1M-1) was purchased from Life Core Biomedical (Life Core Biomedical LLC, Chaska, MN, USA), Lipopolysaccharide (LPS) serotype O55:B5 (TLRgrade™) from Enzo Life Sciences (Enzo life sciences, Farmingdale, NY, USA), Isoflurane (Forane™) from Baxter (Baxter Canada, Mississauga, ON, Canada), BD Vacutainer SST Gold from WVR international (VWR International, Mont-Royal, QC, Canada), IDEXX green top

Lithium-Heparin and yellow top serum microtainers from IDEXX Laboratories (IDEXX Laboratories, Markham, ON, Canada), Altogen *in vivo* transfection kit from Altogen Biosystems (Altogen Biosystems, Las Vegas, NV, USA), Invivofectamine® 2.0 and 3.0, phosphate buffered saline (PBS), UltraPure™ DNase⁄RNase-Free water, 10% Neutral Buffer Formalin, AlexaFluor 546 phalloidin with ProLong® Diamond antifade containing DAPI and nuclease free water from Life Technologies (Burlington, ON, Canada). D-trehalose, L-histidine, diethyl pyrocarbonate (DEPC), 1N HCl, and RNaseZAP™ from Sigma-Aldrich (Sigma-Aldrich, Oakville, ON, Canada). Rabbit monoclonal anti-GAPDH (Ab181602) and, biotinylated goat anti-Rabbit IgG (Ab97049) were purchased from Abcam (Abcam, Cambridge, UK). Serum vials (223685, 223686 and 223687) were purchased from Wheaton (Wheaton, Millville, NJ, USA), and butyl Stoppers (73828A-21) from Kimble Chase (Kimble Chase, Rockwood, TN, USA). PVDF filters (.22 µm) and Amicon Ultra-15 centrifugal filter units were from EDM Millipore (EDM Millipore Ltd, Etobicoke, ON, Canada)

7.2.2 siRNA sequences and chitosan characterization

The native and 2’O methyl (2’OMe) modified anti-ApoB siRNA sequences were custom synthesized by Dharmacon Inc (GE Dharmacon, Lafayette, CO, USA). The anti-ApoB siRNA sense sequence was 5’- GUC AUC ACA CUG AAU ACC AAU -3’ and the antisense sequence was 5’-5' P.AUU GGU AUU CAG UGU GAU GAC AC -‘3, duplex Mw 14,053.5 g/mol with **P** denoting a phosphate group. The 2’OMe modified siRNA had the same antisense sequence and the following sense sequence 5’-GuC AuC ACA CuG AAu ACC AAu-‘3, with lower case letters denoting 2’O methylation and a duplex Mw of 14,122.8 g/mol. The anti-GAPDH siRNA was purchased from Life Technologies as a predesigned Ambion® *In Vivo* GAPDH Positive Control siRNA (Life Technologies, Burlington, ON, Canada). The anti-GAPDH sense sequence was 5’-GGU CAU CCA UGA CAA CUU UTT-3’, duplex Mw 13,400 g/mol. This siRNA sequence was LNA modified for increased stability. The position of the LNA modifications, as well as other Silencer™ modifications, was not disclosed by the manufacturer. All siRNA sequences were provided in a lyophilized format following HPLC purification and were subjected to quality control (i.e. endotoxin content, LC-MS, PAGE and UV/Vis spectrophotometric analysis).

Chitosans were obtained from Marinard, (Laval, QC, Canada) and depolymerized in our laboratory using nitrous acid to achieve specific number-average molecular weight targets (Mn) of 10 and 120 kDa (**Table 7-1**). Chitosan number and weight-average molecular weights (Mn and Mw) were determined by gel permeation chromatography (GPC) using a Shimadzu LC-20AD isocratic pump coupled with a Dawn HELEOS II multi-angle laser light scattering detector (Wyatt Technology Co, Santa Barbara, CA), an Optilab rEX interferometric refractometer (Wyatt Technology Co), and two Tosoh TSKgel (G6000PWxl-CP and G5000PWxl-CP; Tosoh Bioscience LLC, King of Prussia, PA) columns. Chitosans were eluted at pH 4.5 using an acetic acid (0.15 M)/sodium acetate (0.1 M)/sodium azide (4 mM) buffer. The injection volume was 100 µL, the flow rate 0.8 mL min^{-1} and temperature 25°C. The dn/dc value was determined at 0.208 using a laser's wavelength of 658 nm. The degree of deacetylation was determined by ^{1}H NMR as per *in house* published methods [47].

Table 7-1 Characterization of chitosans tested in this study. Different chitosans are denoted according to their chemical composition using the nomenclature [DDA-Mn] and are represented in the first column of the table. The degree of deacetylation (DDA) was determined by ^{1}H NMR. The number and weight average molecular weight (Mn and Mw) were determined by gel permeation chromatography (GPC). The polydispersity index (PdI) was calculated as M_w/M_n. The degree of polymerization (Dp) or chain length was computed using the following equation

$$\boldsymbol{Dp} = \frac{\boldsymbol{Mn\ chitosan}}{\boldsymbol{Average\ monomer\ molar\ mass\ at\ specific\ DDA}}$$

Chitosan	DDA (%)	Mn (kDa)	Mw (kDa)	PdI	Dp
92-10	92.0	9.0	13.7	1.52	55
92-120	91.9	138	181	1.31	836

7.2.3 Preparation of chitosan-based nanoparticles

7.2.3.1 Preparation of chitosan, hyaluronic acid, and siRNA working solutions

Low (10 kDa) and high (120 kDa) molecular weight chitosans were dissolved overnight in nuclease free water and 1N HCl, using a glucosamine to HCl ratio of 1:1, to a final concentration of 5 mg/mL. Hyaluronic acid (HA), was prepared by dissolving sodium hyaluronate in nuclease-free water at a final concentration of 1 mg/mL. The stock solutions were sterile filtered using a 0.22 µm PVDF filter and used to prepare solutions, containing 0.83% w/v trehalose and 5.83 mM histidine (toxicity) or 1% trehalose and 3.8 mM histidine (efficacy), at a specific amine: phosphate: HA carboxyl molar ratio (N:P:C = 2:1:1.5) by dilution in nuclease-free water, 4% w/v trehalose and 28 mM histidine (pH 6.5). Before complexation, anti-ApoB (native and 2'Ome modified) and anti-GAPDH siRNA stock solutions were diluted to 0.2 mg/mL in the same buffer as chitosan and/or HA (0.83% trehalose and 5.83 mM histidine or 1% trehalose and 3.8 mM histidine). Nanoparticles were prepared as described below.

7.2.3.2 Preparation, lyophilization and reconstitution of uncoated and HA-coated anti-ApoB nanoparticles (NPs) for the assessment of *in vivo* toxicity

Uncoated and HA-coated anti-ApoB nanoparticles were prepared at a final N:P:C ratio of 5:1:0 and 2:1:1.5 respectively using the advanced Automated Inline Mixing System (AIMS) as described in [37]. Chitosan at a specific N:P ratio (5:1 or 2:1) was mixed, using a closed and sterile system comprising an LS14 Pharmapure tubing (1/16") and two Masterflex L/S digital peristaltic pumps (Cole-Parmer, Montreal, QC, Canada), with siRNA (0.2 mg/mL) using a Y-connector and a mixing flow rate of 150 mL/min (Re=4000). Anti-ApoB nanoparticles prepared at N:P 2 were HA-coated to a final N:P:C of 2:1:1.5 using the primary version of the AIMS. The chitosan-siRNA nanoparticles (N:P:C of 2:1:0) were mixed with HA using a Y connector at a 1:2 vol:vol ratio and a mixing flow rate of 150 mL/min (nanoparticles) and 75 mL/min for HA. All nanoparticles were incubated for 30 min at room temperature upon preparation before analyses or freeze-drying. In order to inactivate possible nucleases, the whole closed system was treated with diethylpyrocarbonate (DEPC), autoclaved and flushed with nuclease free water.

Anti-ApoB nanoparticles were lyophilized, under sterile conditions, using a 3-day cycle as described in [48]. Nanoparticle volumes of 2 and 5 mL were pipetted into 5 and 10 mL serum vials

respectively, mounted with 20 mm butyl lyophilization stoppers, and freeze-dried using a Laboratory Series Freeze-Dryer PC/PLC (Millrock Technology, Kingston, NY, USA). Samples were backfilled with argon, stoppered, crimped, and stored at 4°C until reconstitution. All freeze-dried samples were reconstituted to 12 times their initial concentration using water for injection (208 or 417 µL to samples in 5 or 10 mL serum vials), respectively, incubated at room temperature for 5-10 minutes, and the concentration adjusted, by dilution with a nearly-isotonic aqueous solution of 10% w/v trehalose and 70 mM histidine (pH 6.5), so that the desired dosage (mg siRNA/kg animal body weight) would be reached upon injection of 10 µL of nanoparticle suspension per gram of body weight (BW).

7.2.3.3 Preparation of uncoated and HA-coated anti-GAPDH nanoparticles for assessment of *in vivo* target knockdown

Anti-GAPDH siRNA (0.2 mg/mL), Low Mn (10 kDa), high Mn (120 kDa) and hyaluronic acid (HA) working solutions were prepared as described above. Uncoated chitosan-siGAPDH nanoparticles were prepared at an N:P ratio of 5 by simple electrostatic mixing at a 1:1 vol:vol. HA coated nanoparticles, were prepared at an N:P ratio of 2.5:1 by manual mixing (1:1 vol:vol), incubated at room temperature for 15 minutes, and coated with HA by mixing 1 part of HA working solution (0.4 mg/mL) to 2 parts of chitosan-siGAPDH nanoparticles for a final N:P:C ratio of 2.5:1:2. The final volume never exceeded 1 mL and chitosan was pipetted into siRNA. Nanoparticles were kept at room temperature for 20-30 minutes before administration to animals.

7.2.4 Preparation of Invivofectamine®-siRNA-lipid nanoparticles (LNPs)

Invivofectamine® 2.0 and 3.0 were prepared as per manufacturer recommendation. For Invivofectamine® 2.0, a volume of 250 µL of anti-ApoB siRNA (3 mg/mL) was diluted (1:2) in complexation buffer, mixed with 500 µL of Invivofectamine® 2.0, vortexed for 30 seconds, incubated at 50 ºC for 30 minutes, diluted with 14 mL phosphate-buffered saline and concentrated at 4000 g using an Amicon Ultra-15 centrifugal filter unit (EDM Millipore Ltd, Etobicoke, ON, Canada) to a final volume of 872 µL (0.8 mg/mL siRNA).

For Invivofectamine®3.0, anti-GAPDH siRNA solution (2.4 mg/mL) was mixed with complexation buffer at 1:1 ratio and immediately added to Invivofectmine® 3.0 at a 1:1 vol/vol

ratio, vortexed for 30 seconds, incubated at 50ºC for 30 minutes and diluted to 0.25 mg/mL siRNA using PBS (pH 7.4). All LNPs were subjected to quality control (i.e. DLS, Doppler velocimetry, UV measurements and sterility assessment), stored at 4ºC for 10-16 hours before administration into mice. **Note:** Invivofectamine® 3.0 was used as a replacement for Invivofectamine® 2.0 which was discontinued at the time of the efficacy study.

7.2.5 Determination of size and surface charge

Size and surface charge (ζ-potential) of nanoparticles were determined by Dynamic Light Scattering (DLS) and Laser Doppler velocimetry using a ZetaSizer Nano ZS device (Malvern Instruments Ltd, Malvern, UK). The scattering angle of the detector was fixed at 173º and measurements were performed at 25ºC using the viscosity of water as sample diluent. Nanoparticles were diluted to 1X their initial concentration using nuclease-free water, followed by a dilution 1:4 and 1:8 using sterile filtered 1% trehalose solution before determination of size and ζ-potential respectively. The Smoluchowski equation was used to calculate ζ-potential from the measured electrophoretic mobility. All measurements were done in triplicate and replicated at least once (N=2-3, n=6-9).

7.2.6 Hemocompatibility

Hemolytic and hemagglutination properties of uncoated and HA-coated nanoparticles were tested according to ASTM E2524 [49] and Evani et al [50] respectively. Human blood was collected on consenting and healthy donors following protocol approval by the University Ethics Committee. Anti-ApoB nanoparticles were prepared as described above, freeze-dried (FD) in the presence of 0.83% w/v trehalose, and 5.8 mM histidine (pH 6.5), and rehydrated to 12X the pre-FD concentration using nuclease free water to reach the highest tested concentration (or dose) at iso-osmolality and then serially diluted using 10% w/v trehalose buffer (300 mOsm) to a final siRNA concentration of 0.1, 0.25, 0.5, and 0.8 mg/mL. The plasma-free hemoglobin (PFH) in the blood was measured at 0.49 mg/mL prior to initiating the assay. Total blood hemoglobin (TBH) was adjusted with PBS to a concentration of 10 ± 1 mg/mL (dTBH). Nanoparticles were mixed with PBS and diluted in dTBH at a 1:7:1 volumetric ratio, with 100 µL of nanoparticles at the target concentration pipetted into an Eppendorf tube containing 700 µL PBS and 100 µL of blood (dTBH 10 ± 1 mg/mL). For colorimetric determination of hemolysis, samples (700 µL) were incubated for

3 h in a water bath at 37°C and visually inspected every 30 minutes for nanoparticle flocculation, dispersion, sinking or floating. The supernatant was collected following centrifugation at 800 g for 15 min and absorbance measured at 540 nm on a TECAN Infinite® M200 PRO microplate system (Tecan Systems, Mannedorf, Switzerland). A four-parameter regression algorithm (4PL) was used to obtain the calibration curve required to calculate the hemoglobin concentration in the supernatant of each sample (PFH sample). The percentage of hemolysis was computed as $Hemolysis\ (\%) = 100 \times (PFH_{sample}/TBHd)$. For hemagglutination, the remaining 200 µL of each sample prepared above were pipetted in 96 well assay plates, incubated for 3h, visualized using an Axiovert light microscope and the area covered by red blood cells (RBCs) estimated and scored.

7.2.7 *In vivo* studies

All *in vivo* experiments described in this manuscript were randomized double blinded and approved by the University of Montreal Ethics Committee (CDEA) and the Montreal Heart Institute Research Center Ethics Committee. Mice were purchased from Charles Rivers (Charles River, Quebec, Canada), housed and acclimatized in a specific pathogen-free facility with unrestricted access to water and food. Mice had body condition scores (BCS) of 3 [51] and their body weights (BW) were in the range of 20-25 g at the time of injection. All injection volumes were calculated as 10 µL/g of BW and injections performed within 10-15 seconds. Mice were euthanized under anesthesia (mixture of 3% Forane™ and 20-80% oxygen-air vol/vol) by cardiac puncture followed by cervical dislocation.

7.2.7.1 Determination of chitosan-siRNA biodistribution using *ex-vivo* organ imaging

Balb/c nude female (♀) mice aged 6 weeks and weighing 20-22 g were injected for the biodistribution experiments. All test articles i.e. naked siRNA, Invivofectamine® 2.0 and chitosan based nanoparticles formulated at an N:P:C of 5:1:0 or 2:1:1.5 (Mn 10 and 120 kDa) were administered at a dose of 0.25 mg/kg DY^{647} labeled siRNA, except for the HA-coated NPs which were administered at 0.165 mg/kg. The DY^{647} fluorophore was administered at a dose of 0.5 mg/kg. Mice were euthanized 4 hours post administration and immediately perfused using PBS (1 X 20 mL) and 10% Neutral Buffer Formalin (NBF, 1 X 40 mL). *Ex-vivo* imaging on collected organs was performed using a whole animal imaging system mounted with an EMCCD EM N2 camera

(NUVU Cameras, Montreal, QC, Canada). Controls included PBS, naked DY^{647} labeled siRNA, DY^{647} alone, and commercially available lipid control Invivofectamine® 2.0.

7.2.7.2 Determination of chitosan-siRNA nanoparticle in *vivo* toxicity

CD-1® (ICR) female (♀) and male (♂) mice aged 4-5 weeks and weighing 22-24g were used for the toxicity study. Mice (7 / group; 4 ♀ and 3 ♂) were administered the test and control articles. Mandibular blood collection was performed prior and 4 hours post administration of test articles, and serum separated at 10,000 g following 10-minute incubation at room temperature and stored at -80°C. Two out of the 7 mice (2/7) were euthanized at 4 hours (1 ♀ and 1 ♂), and the remaining five mice per group (4 ♀ and 1 ♂) euthanized 24 hours post administration of test articles. At each time point (4 *versus* 24 h), the total circulating blood volume (tCBV) was collected by intracardiac puncture, and organs harvested, washed in PBS, split in half and one-half immediately stored in Liquid nitrogen (LiqN) while the second half fixed in 10% NFB.

7.2.7.3 Hematological and serological parameters

The total circulating blood volume was split into lithium heparin (LH) and serum separation tubes (SST), serum separated and samples stored on ice and sent to IDEXX Laboratories for the comprehensive complete blood count (CCBC) and the CC4 clinical chemistry panels. Analysis was performed in less than 24 hours using a Sysmex XTV 2000 (Sysmex, Mississauga, ON, Canada) and Beckman AU680 analyzers (Beckman Coulter Ltd, Mississauga, ON, Canada).

7.2.7.4 Determination of cytokine levels

Serum samples collected at baseline (0 h) and 4 hours post-administration of test articles were assayed for the induction of pro-inflammatory cytokine (TNF-α, IL-1β, IL-6, KC and IFN-γ) using the Luminex® technology. Plates were designed using the Bio-Plex® assay builder (Bio-Rad Laboratories, Mississauga, ON, Canada) and subjected to the manufacturer quality control. For each plate, a standard curve was prepared by diluting the Bio-Plex® Pro Mouse Cytokine Standard 23-Plex in the Bio-Plex® in standard diluent followed by 4-fold serial dilutions from 1:4 to 1:65536 in the same diluent. Samples were thawed on ice, cleared by centrifugation (10,000 g, 10 minutes, 4°C), diluted 1:4 using the Bio-Plex® Sample diluent (Bio-Rad Laboratories, Mississauga, ON, Canada), and a volume of 20 µL transferred to assay plates pre filled pooled capture antibodies. The plates were incubated for 30 minutes under orbital shaking (800 rpm, room temperature),

washed as per manufacturer recommendation using a Bio-Plex® Pro II Wash Station (Bio-Rad Laboratories, Mississauga, ON, Canada), incubated with biotinylated detection antibodies (30 minutes, 800 rpm, RT), washed and revealed post-incubation for 10 minutes with streptavidin-phycoerythrin (800 rpm, RT). Data was acquired on a Bio-Plex® 200 system using RP1 PMT setting (Bio-Rad Laboratories, Mississauga, ON, Canada) with a minimum of 50 beads per region analyzed. For each cytokine, a 5-parameter regression algorithm (5-PL) was used to fit the data and interpolate cytokine values in serum samples. In order to account for inter-plate variability, two samples (i.e. one LPS and one Invivofectamine® 2.0 (8 mg/kg) sample) were used as interplate calibrators (IPC).

7.2.8 Determination of chitosan-siRNA nanoparticle in *vivo* efficacy

Balb/c male (♂) mice aged 6-7 weeks and weighing 22-25g were used for the efficacy study. Uncoated anti-GAPDH NPs (viz. 92-10-5 and 92-120-5) and HA coated nanoparticles (viz. HA92-10) were administered at 1 mg/kg (uncoated) and 8 mg/kg siRNA (HA coated) every other day for a total of three injections. Mice were sacrificed 72 hours following the last injection. Naked anti-GAPDH siRNA (siGAPDH) and Altogen lipid nanoparticles (Altogen LNP) were I.V. administered at 2.5 mg/kg every other day for a total of three injections and sacrificed 72 hours following the last administration. The liver targeting Invivofectamine® 3.0 lipid nanoparticles (Inv LNP), were I.V. injected at 2.5mg/kg as a single injection and mice were sacrificed 72 hours post administration. Mice were euthanized as previously described and tCBV and organs collected. tCBV was serum separated and immediately stored at -80 ^{o}C, and organs split into halves and stored in LiqN and fixed in 10% NBF before protein extraction, determination of GAPDH enzymatic activity, western blotting, histology, and immunohistochemistry.

7.2.8.1 Assessment of GAPDH enzymatic activity using the KDalert® assay

Following collection, organs were snap frozen in liquid nitrogen and stored at -80°C until use. Frozen tissues were cut on dry ice, weighed (~20 mg), and disrupted using the TissueLyzer® II system (Qiagen Inc, Toronto, ON, Canada). Tissues were disrupted using the 5 mm steel beads (Qiagen Inc, Toronto, ON, Canada) under the following conditions: 2 x 30 Hz, 20 seconds per cycle. Homogenized tissues were resuspended in 750 µL of KDalert™ lysis buffer (Life Technologies, Burlington, ON, Canada), and incubated on ice for 30 minutes with inversions every

10 minutes. Lysates were clarified by centrifugation (2270 g, 30 minutes, 4°C), transferred to new tubes, and diluted (1:20), in KDalert™ lysis buffer. The standard curve was prepared by diluting GAPDH stock solution (26 U/mL) with lysis buffer at a 1:100 ratio (GAPDH: Lysis), followed by 2-fold serial dilutions from 1:5 to 1:320. Twenty microliters of diluted samples, and standards were transferred into 96 well plates (Corning, NY, USA), and 180 µL of the KDalert™ Master Mix (Life Technologies, Burlington, ON, Canada) was pipetted into each well. Plates were incubated for 15 minutes at room temperature and absorbance measured at 610 (±10) nm using a TECAN Infinite® F-500 microplate system (Tecan Systems, Mannedorf, Switzerland). GAPDH activity was computed from the standard curve and normalized to total protein content of the lysate sample as determined using the BioRad DC Protein assay kit (Bio-Rad Laboratories, Mississauga, ON, Canada).

7.2.8.2 Western blotting

Affinity-purified monoclonal antibodies used were against GAPDH and vinculin. Kidney cortex were excised, homogenized using the TissueLyzer® II system (Qiagen Inc, Toronto, ON, Canada) as described above and suspended in KD Alert lysis solution (Life Technologies, Mississauga, ON, Canada) in the presence of a protease cocktail inhibitor, and centrifuged at 2,270 g for 30 minutes at 4°C. The supernatant was quantified using the the BioRad DC Protein assay kit (Bio-Rad Laboratories, Mississauga, ON, Canada) and diluted in SDS buffer containing a final concentration of 62 mM Tris (hydroxymethyl)-aminomethane, 0.1 M SDS, 8.7% glycerol, 0.09 mM bromophenol blue, and 0.04 M dithiothreitol (DTT). Samples were heated for 5 min at 90°C, loaded into Protean mini TGX SDS-PAGE (4–12%) gradient polyacrylamide gels (Bio-Rad Laboratories, Mississauga, ON, Canada), and overnight wet transferred to Amersham™ HyBond® P PVDF membranes (GE Lifesciences, Mississauga, ON, Canada). Membranes were dried and blocked for 1 h at room temperature in 5% nonfat milk, probed overnight at 4°C with anti-GAPDH primary antibody (1:1000), washed (3X, 15 min, 1% Triton in the presence of blocking buffer), and incubated with HRP conjugated anti-rabbit IgG1 secondary antibody (1:500) for 1h, washed, revealed using the Clarity Max™ ECL substrate (Bio-Rad Laboratories, Mississauga, ON, Canada) and visualized using the ChemiDoc MP™ system (Bio-Rad Laboratories, Mississauga, ON, Canada). Protein band quantification was performed using ChemiDoc MP™ software.

7.2.8.3 Clinical signs and body weight

Mice clinical signs were determined for a period of 4-hours post-administration of test articles and at euthanasia. The clinical signs were recorded by trained personnel and qualified animal care technicians. Clinical signs were scored for body condition, general aspect, natural behavior, and provoked behavior. The Mouse Grimace Scale (MGS) was also used for scoring of clinical signs in case of distress. Body weight was recorded prior to each injection and at euthanasia using an Avery Berkel scale (Avery Berkel, Fairmont, MN, USA). Body weight was expressed as percent change relative to the previous injection.

7.2.8.4 Histology and immunohistochemistry

Samples were fixed in 10% neutral buffered formalin (NBF) prefilled HistoTainer™ II (Simport, Beloeil, QC, Canada), dehydrated in graded ethanol series, cleared with xylene and embedded in paraffin. Sections (5 µm) were collected on Superfrost™ Plus stain slides (Fisher Scientific, Ottawa, ON, Canada), and stained with Hematoxylin and Eosin. Prior to immunohistochemistry, antigen retrieval was performed with 10 mM Tris/1 mM EDTA pH 9 at 60ºC. Sections were blocked with 20% (v/v) goat serum/0.1 % (v/v) Triton X-100/PBS for 1 hour at room temperature and then incubated for 16 hours at 4ºC with Rabbit monoclonal anti-GAPDH (Ab181602) diluted 1:250 in 10% (v/v) goat serum/0.1 % (v/v) Triton X-100/PBS. Sections were then incubated for 1 hour at room temperature with Biotinylated goat anti-Rabbit IgG (Ab97049) diluted 1:500 in 10% (v/v) goat serum/0.1 % (v/v) Triton X-100/PBS. Revelation was performed with the Vectastain Avidin-Biotin Complex (ABC)-Alkaline Phosphatase (AP) and AP Red substrate kits (Vector Laboratories, Burlingame, CA, USA). Sections were counterstained with Weigert Iron Hematoxylin prior to dehydration, clearing, and mounting. Slides were scanned using a NanoZoomer digital slide scanner (Hamamatsu, Boston, MA, USA) and visualized using the NDP® view 2.0 software (Hamamatsu, Boston, MA, USA).

7.2.8.5 Confocal laser scanning microscopy

For *in vivo* biodistribution and subcellular localization of DY^{647} labeled siRNA, organs were cryosectioned (5 µm), actin stained using AlexaFluor 546 phalloidin and mounted with ProLong® Diamond antifade containing DAPI. Sections were imaged in a multitrack mode using a Zeiss LSM 510 META confocal Axioplan 200 microscope (Carl Zeiss AG, Feldbach, Switzerland).

7.2.9 Statistical analysis

Data were collected and expressed as the average ± standard deviation (stdev). Statistical analysis was conducted using GraphPad Prism® 7.0 (GraphPad Software Inc, La Jolla, CA, USA) software package. Unless otherwise stated, One-Factor ANOVA followed by Dunnet test for multiple comparisons was performed on collected data.

7.3 Results

7.3.1 Uncoated chitosan NPs induced hemolysis and hemagglutination at high doses which were abrogated by hyaluronic acid (HA) coating

Cationic polymers and lipids are often associated with an ability to interact with blood proteins and erythrocytes leading to decreased transfection, rapid clearance, embolism and hemolysis with abrogation of these negative effects achieved through PEGylation and/or the use of helper lipids (i.e. balancing between hydrophobic and cationic components). In order to select for dose, and investigate the effect of polymer length (Mn), free chitosan and hyaluronic acid coating (HA) on blood compatibility, erythrocyte hemolysis, and agglutination were investigated according to the ASTM-E2524 standard [49] and Evani et al [50] respectively. As shown in Figure 7-1, a dose-dependent increase in hemolysis was observed for both low (10 kDa) and high (120 kDa) Mn chitosan. Erythrocyte lysis was abolished with a reduction in free chitosan from N:P 5 to 2 followed by HA coating. As a consequence, the maximum siRNA dose that could potentially be intravenously administered with chitosan depends on Mn, N:P ratio (or the fraction of free chitosan) and HA coating. According to the ASTM standard, a hemolytic index below 5% is regarded as safe [49]. In as much as doses of 5 and 1 mg/kg siRNA could be administered with low (10 kDa) and high (120 kDa) Mn chitosan, respectively, when formulated at N:P 5 and doses of at least 8 mg/kg siRNA for N:P 2 and HA-coated nanoparticles (Figure 7-1). Hemolysis increased two-fold with an increase in siRNA dose or chitosan concentration in blood from 0.040 to 0.321 mg/mL indicating a nonlinear relationship for high Mn chitosan. Positive i.e. PLL and TX-100 and negative controls i.e. PEG and HA controls were within the ASTM standard [49] (Figure 7-1, Inset) whereas excipients (buffer) and siRNA were found to be non-hemolytic, i.e. below the threshold, confirming that dose dependent hemolysis be attributed to chitosan.

Lipid nanoparticles (InvLNP) assayed at 1 and 8 mg/kg siRNA showed around 5% hemolysis with no dose effect (Figure 7-1, Inset) indicating minimal interaction with blood erythrocytes at pH 7.4, consistent with previous data for ionizable/cationic (pKa ~ 6.5) and PEGylated LNPs [52-54]. The influence of dose, Mn, N:P ratio and HA coating on hemagglutination, or erythrocyte aggregation was investigated to better understand chitosan-blood interaction and limit potential *in vivo* toxicity. **Supplemental** Figure S. 7-1 shows that both low and high Mn chitosan induced dose-dependent

hemagglutination above a threshold of 1 mg/kg siRNA, but could be eliminated with the reduction of free chitosan and HA coating.

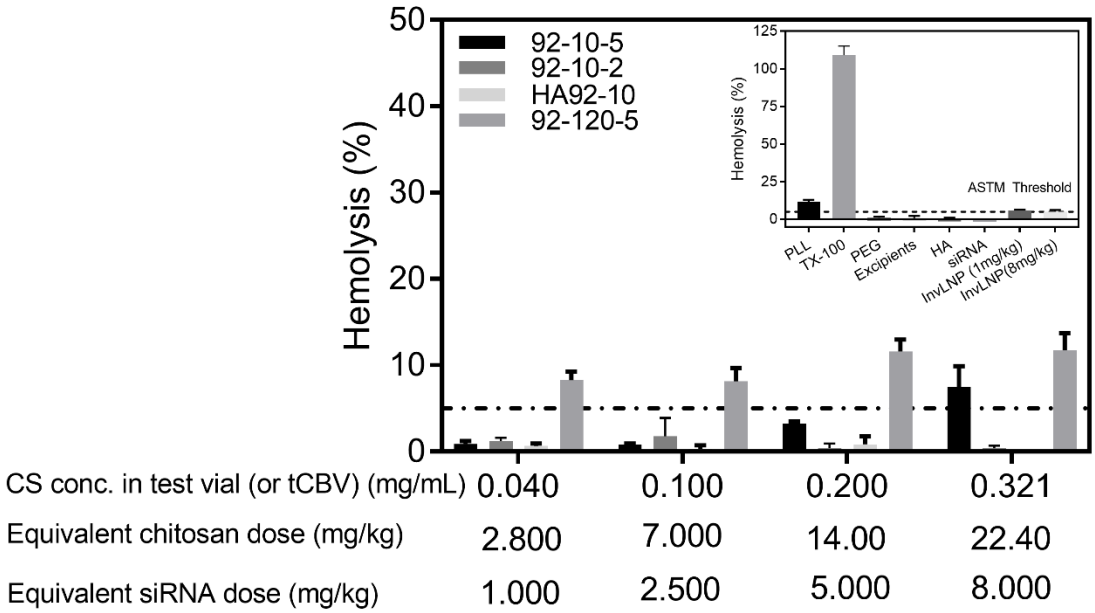

Figure 7-1 Hemocompatibility profiling of uncoated and HA coated chitosan-siRNA nanoparticles via red blood cell (RBC) lysis. Low (10 kDa) versus high (120 kDa) molecular weight chitosans were formulated with HPLC-grade siRNA at an N:P ratio of 5. HA coated formulations were formulated at an N:P:C of 2:1:1.5. Increasing doses of siRNA were mixed with human pooled blood and % hemolysis determined as per ASTM-E2524 [49]. The concentration of chitosan (mg/mL) in the test vial (equivalent to the concentration in total circulating blood volume or tCBV), the equivalent chitosan dose in mg/kg of body weight and the corresponding siRNA dose in mg/kg for N:P of 5 are shown. Inset shows data from positive and negative controls. Poly-L-Lysine (PLL), Triton-X-100 (TX-100), Polyethylene glycol (PEG), Excipients (1% trehalose, 5.8 mM histidine, pH 6.5), Hyaluronic acid 866 kDa (HA), siRNA (8 mg/kg) and Invivofectamine® 2.0 (1 versus 8 mg/kg of siRNA). Data represent the average ± standard deviation of 2 independent experiments with 3-6 technical replicates per experiment (N=2, n= 6-12).

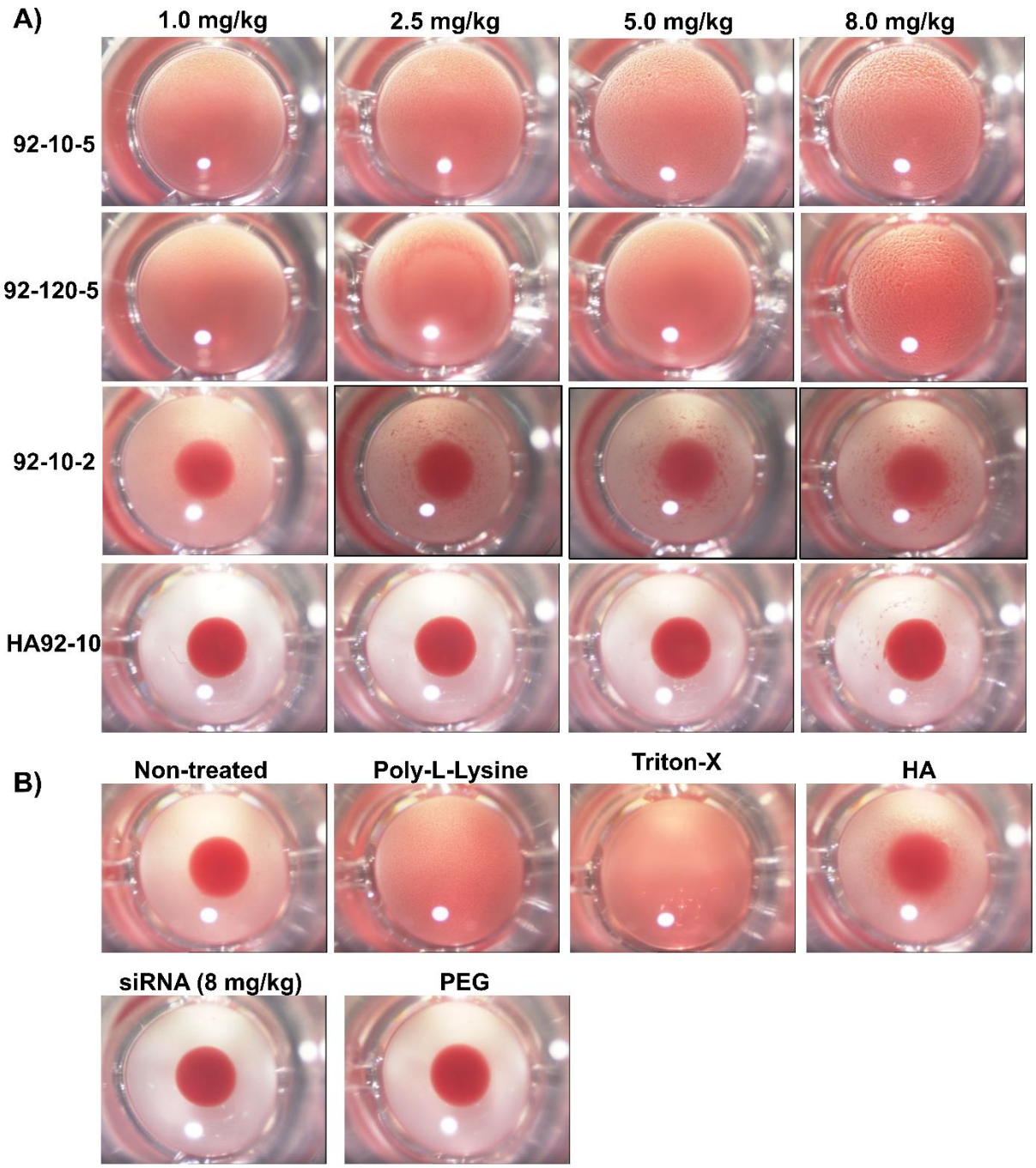

Figure S. 7-1Hemocompatibility profiling of uncoated and HA coated chitosan-siRNA nanoparticles via erythrocyte aggregation. Low (10 kDa) versus high (120 kDa) molecular weight chitosans were formulated with HPLC-grade siRNA at an N:P ratio of 5. HA coated formulations were formulated at an N:P:C of 2:1:1.5. Increasing doses of siRNA were mixed with human pooled blood, incubated and imaged for qualitative assessment of hemagglutination. In the absence of hemagglutination, erythrocytes (RBC) deposit in the bottom of the U-shaped well and

form a ring (see Non-treated, PEG, siRNA in **B**). In contrast, when hemagglutination occurs, aggregates become visible, stay suspended in solution and depending on the extent of agglutination may prevent the formation of the ring. **A)** Treatment samples at different doses of siRNA. **B)** Controls.

7.3.2 Uncoated and HA coated chitosan NPs promoted extrahepatic delivery of siRNA to kidney proximal tubular epithelial cells (PTEC)

Next, we examined the effect of polymer length (Mn) and HA coating on *in-vivo* biodistribution using whole animal based *ex-vivo* imaging and confocal laser scanning microscopy (CLSM). As illustrated in Figure 7-2, chitosan based NPs accumulated in the kidney and gallbladder following intravenous administration of 0.25 mg/kg (5 µg siRNA/animal). Hyaluronic acid coating of the NPs seemed to increase siRNA accumulation in the kidney and gallbladder without altering the biodistribution profile observed with uncoated NPs. In contrast to polyethyleneimine (PEI)-siRNA based nanoparticles, chitosan, whether coated or uncoated, did not accumulate in the lungs or spleen indicating striking differences with the PEI delivery platform [55]. Controls, such as Invivofectamine® 2.0 LNPs (Inv LNP), naked siRNA and DY^{647} alone, accumulated in the liver and spleen (Inv LNP), kidney (naked siRNA) and bladder (DY^{647}) respectively (data not shown). The fluorescent signal intensity of siRNA in the kidney was several folds lower compared to chitosan and HA chitosan NPs indicating a clear role of the delivery system in enhancing siRNA accumulation in the kidney. In order to examine cellular accumulation of siRNA in the kidney, histological sections were examined under confocal laser scanning microscopy (CLSM). As shown in Figure 7-2 B, siRNA formulated in NPs accumulated predominantly in the proximal tubule epithelial cells (PTECs) independent of chitosan Mn and HA coating. Nevertheless, siRNA accumulation in PTECs was greatly enhanced with HA coating as exemplified with an increase in fluorescence at a lower dose of 0.165 *vs* 0.25 mg/kg for uncoated NPs. Actin staining using phalloidin red revealed a typical punctuate siRNA pattern across the brush border membrane lining the PTEC, indicating intracellular localization (Figure 7-2, **Insets**). In contrast to lipid NPs, chitosan-based NPs accumulation in the kidney represents a new approach to treat PTEC dependent pathologies.

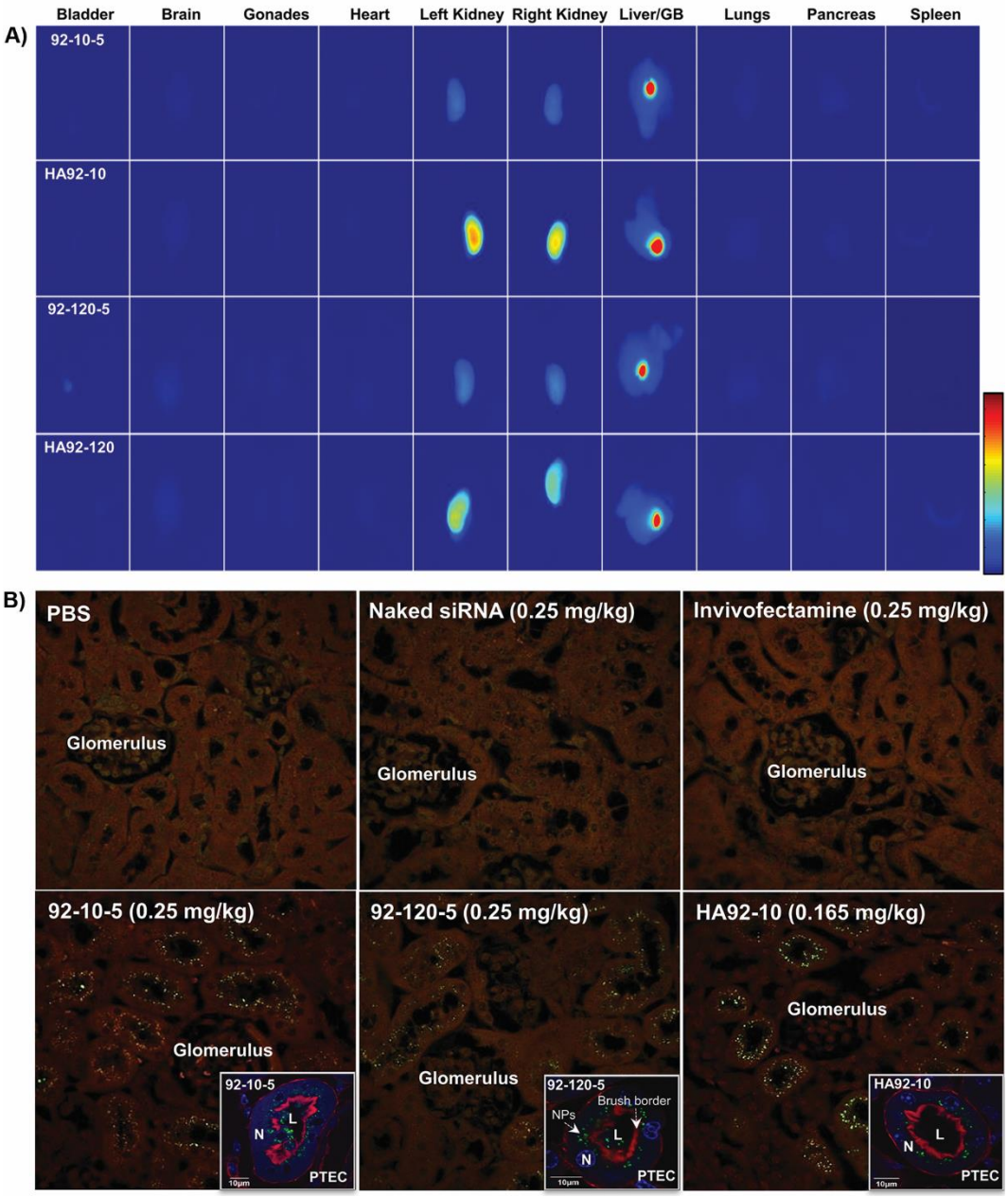

Figure 7-2 *In vivo* Biodistribution of uncoated and HA coated chitosan-siRNA nanoparticles. A) Effect of Mn and HA coating on the biodistribution of chitosan-siRNA nanoparticles. Uncoated nanoparticles were injected in Balb/c nude mice at a dose of 0.25 mg/kg of DY^{647} labelled siRNA (equivalent dose of 0.7 mg/kg of chitosan), HA coated nanoparticles were injected at a dose of 0.165 mg/kg of DY^{647} labelled siRNA (equivalent dose of 0.2 mg/kg of chitosan) and organs imaged ex-vivo 4 hours post administration. B) Histological and CLSM images of nanoparticles accumulated in PTEC. Nanoparticles were injected as described above, organs perfused and collected 4 hours post-administration, fixed and cryosectioned (5 µm). For CLSM insets, sections

were stained with phalloidin red and DAPI. (PBS) Phosphate Buffered Saline, (siNaked) naked DY^{647} labeled siRNA, (Invivofectamine) lipid nanoparticles, (PTEC) Proximal epithelial tubular cells, (NPs) Nanoparticles. Lumen (L), DY^{647} siRNA = Green, Nucleus (N) = Blue and Brush borders= Red (actin staining).

7.3.3 Characterization of the injected nanoparticles

As shown in Figure 7-3 A, lipid and chitosan based NPs were in the range of 60-100 nm with hyaluronic acid coating (HA) increasing chitosan NP size by two-fold. The polydispersity index (PdI), a dimensionless measure of dispersion around the mean, was below 0.2 indicating homogeneous particles. As expected, chitosan based NPs were positively charged with a ζ-potential between 25-30 mV. Hyaluronic acid (HA) coating at an N:P:C ratio of 2:1:1.5 inverted the surface charge to around -30 mV representative of HA coating. Lipid nanoparticles (Inv LNP) were quasi-neutral (~ 8-10 mV). Although the exact composition of Inv LNPs is not disclosed by the manufacturer, a quasi-neutral surface charge is probably associated with PEGylation or the use of an increased molar ratio of neutral to cationic lipids in the formulation.

Compared with inline mixed NPs (Figure 7-3, A and C), manually mixed chitosan-based nanoparticles had a similar size and surface charge (Figure 7-3 D and F) but a higher PdI indicating a homogenous but more disperse population of particles. As expected, and although theoretically less likely, surface charge increased with an increase in polymer length (Mn). The effect of siRNA composition and chemical modification had no impact on NP physicochemical characteristics (Figure 7-3). A slight concomitant increase in size and decrease in surface charge was observed for Inv LNP (Figure 7-3 A and C, *vs* D and E) and is considered to be composition dependent since Invivofectamine® 3.0 (Figure 7-3, D, E and F) is a novel formulation with higher potency than its previous counterpart Invivofectamine® 2.0 (Figure 7-3 A, B and C). The Altogen LNP, a liposome-based formulation claiming kidney targeting ability, showed a size around 325 nm and ζ-potential around 5-10 mV.

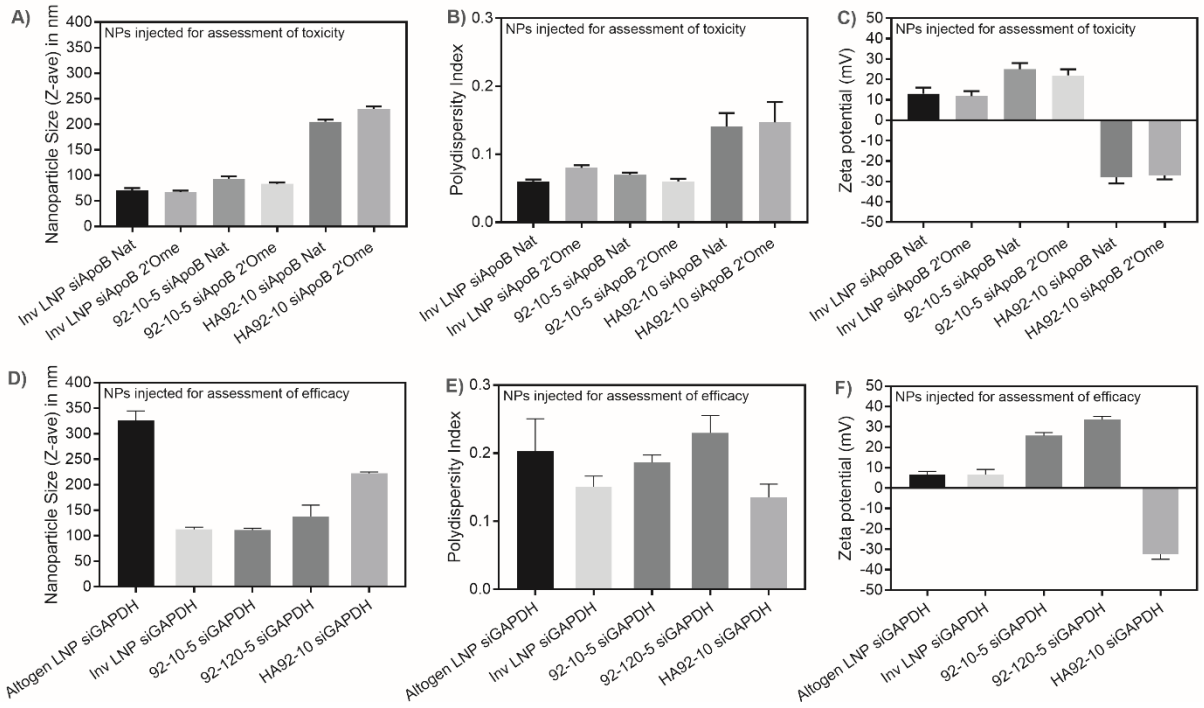

Figure 7-3 Size, polydispersity index and surface charge (ζ-potential) of chitosan-based siRNA nanoparticles and lipid-based nanoparticles (LNPs). Invivofectamine® 2.0 (Inv LNP) were formulated with unmodified (siApoB Nat) or 2'O-methyl modified anti-ApoB siRNA (2'Ome siApoB) sequences (panels A, B and C). Invivofectamine® 3.0 and Altogen LNPs were formulated with LNA-modified anti-GAPDH siRNA (panels D, E and F). Low molecular weight chitosan, with a degree of deacetylation of 92% and molecular weight (Mn) of 10 kDa (92-10) was formulated with siApoB Nat or 2'Ome siApoB at an amine to phosphate ratio (N:P ratio) of 5 (panels A, B and C). Low Mn (10 kDa) and high Mn (120 kDa) chitosans were formulated with LNA-modified anti-GAPDH siRNA at an N:P ratio of 5 (panels D, E and F). Hyaluronic acid (HA, 866 kDa) coated chitosan nanoparticles (HA92-10) were prepared at an N:P ratio of 2 and coated with HA at a phosphate to carboxyl ratio (P:C) of 1.5 (panels A, B, C, D, E and F). Size, PdI and ζ-potential of lipid nanoparticles (LNPs) were measured in phosphate buffered saline (PBS, pH 7.4). Size, PdI and ζ-potential of uncoated and HA coated chitosan-siRNA nanoparticles were measured in excipients (1% trehalose (w/w), 5.8 or 3.5 mM histidine, pH 6.5). A) Size (Z-ave diameter in nm), B) Polydispersity index (pdI), and C) Surface charge (ζ-potential) of nanoparticles injected for the assessment of toxicity. D) Size (Z-ave diameter in nm), E) Polydispersity index (pdI), and F) Surface charge (ζ-potential) of nanoparticles injected

for the assessment of in vivo knockdown efficacy. Data represent the average ± standard deviation of 3 independent experiments with 2 technical replicates per experiment (N=3, n=6).

7.3.4 Unlike Lipid nanoparticles, uncoated and HA coated chitosan NPs did not induce immune stimulation and hematologic toxicity upon intravenous administration

Systemic acute *in vivo* immune stimulation was investigated following I.V. administration of single ascending dose and compared with commercially available LNPs (Invivofectamine®). In order to exclude the role of siRNA in immune stimulation, all NPs were formulated with either unmodified or 2'O-methyl (2'Ome) modified anti-ApoB siRNA sequence (siApoB). This specific anti-ApoB sequence was previously demonstrated to activate the immune system and induce systemic toxicity when formulated with Chol: DSPC: PEG-cDMA: DLinDMA (molar ratio 48:20:2:30) based liposomes (SNALPs) or polyethyleneimine (PEI) [4] with the aforementioned deleterious side effects abrogated through selective and position dependent chemical modifications of the ribose backbone. As illustrated in Figure 7-4, pro-inflammatory type I cytokines (IL-1β, TNF-α, IFN-γ, IL-6 and KC) measured in serum 4 hours post-injection were markedly induced by bacterial lipopolysaccharide (LPS), a potent TLR-4 activator [56, 57], and lipid nanoparticles (Inv LNP) with no significant induction observed for uncoated and HA coated nanoparticles. Inv LNPs showed a dose-dependent and statistically significant induction of IFN-γ, IL-6 and KC and a minor TNF-α increase in serum. As expected, chemical modification (2'Ome) of the uridine (U) and guanine (G) nucleotides of the anti-ApoB siRNA (siApoB 2'Ome) abolished cytokine induction except for the murine IL-8 functional homolog KC (CXCL1). In contrast, uncoated and HA coated chitosan, and irrespective of the injected dose or payload did not significantly induce any of the assayed pro-inflammatory cytokines (i.e. IL-1β, TNF-α, IFN-γ, IL-6 and KC) demonstrating low *in vivo* immune stimulating potential following intravenous injection of chitosan-based systems. Interestingly, a small but statistically significant reduction in IL-1β was observed with all formulations containing chitosan regardless of the payload (Figure 7-4). Although, the decrease in IL-1β was only observed with chitosan injected mice, pre *versus* post-injection levels of IL-1β and TNF-α showed no significant changes and were generally lower than the PBS and excipient groups

(Figure 7-4 *vs* Supplemental Fig.S2), consequently excluding a treatment effect. However, the baseline difference between negative controls (i.e. PBS and Excipients) and chitosan treated groups could be attributed to different batches of mice (two orders of mice from the same supplier). In addition, pre *versus* post-injection (4h) indicate that KC levels increased by two-fold upon chitosan administration, yet remained statistically insignificant.

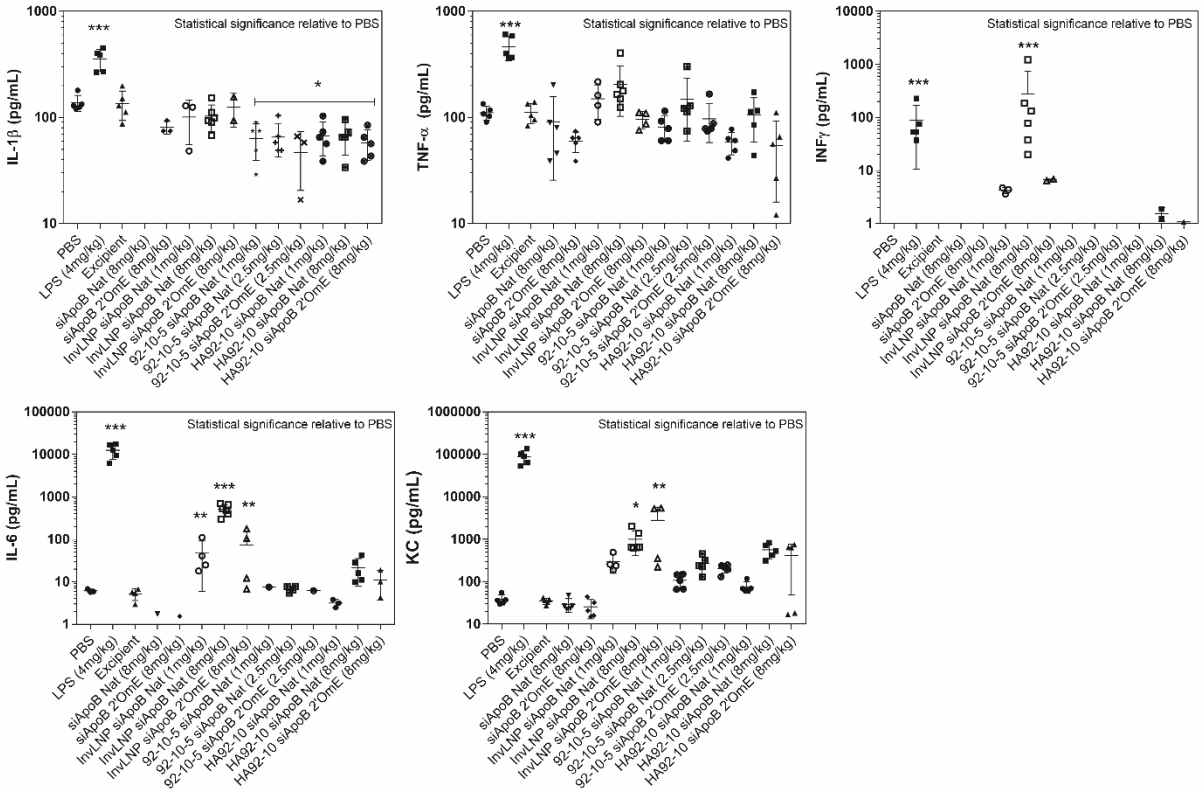

Figure 7-4 Cytokine induction 4 hours post injection of a single ascending dose of Invivofectamine® 2.0, uncoated and HA coated chitosan-siRNA nanoparticles in CD-1® (ICR) mice. PBS (Phosphate buffered saline), LPS (Lipopolysaccharide), Inv LNP (Invivofectamine® 2.0-siRNA Lipid Nanoparticles), siApoB Nat (unmodified anti-ApoB siRNA sequence), siApoB 2'Ome (2'O methyl-modified anti-ApoB siRNA sequence), and HA (Hyaluronic acid, 866 kDa). Mice were I.V. injected with test articles, serum collected and analyzed 4 hours post injection using the BioPlex™ 200 system. Each symbol represents an animal and data represent average values ± standard deviation of 5-7 animals. Statistical significance versus PBS-treated animals was computed with One-Way ANOVA followed by Dunnett test for multiple comparisons: *p< 0.01, **p <0.001, ***p < 0.00001. Note: In order to not bias the average, cytokine levels

(animals) below the range of detection (< OOR) were excluded and not considered as 0 or LLOQ (pg/mL).

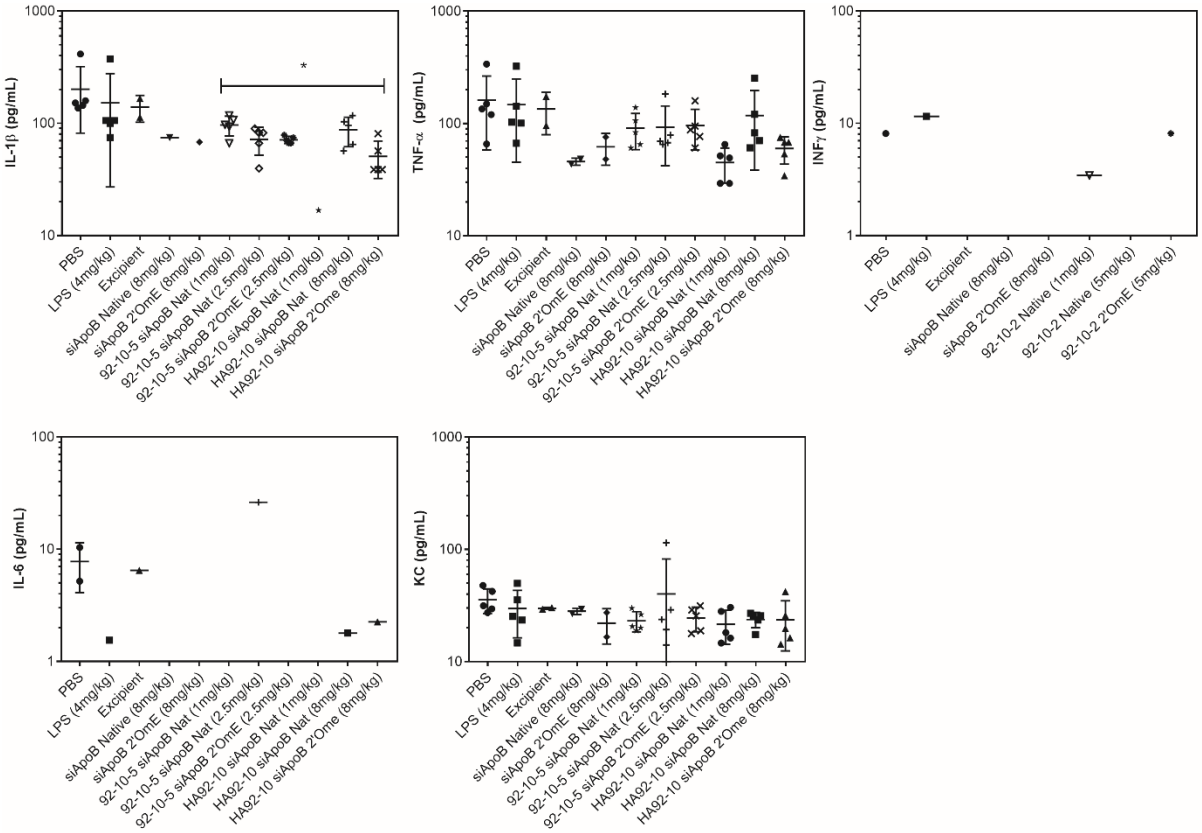

Figure S. 7-2 Cytokine levels pre-injection of Invivofectamine® 2.0, uncoated and HA coated chitosan-siRNA nanoparticles into CD1 mice. PBS (Phosphate buffered saline), LPS (Lipopolysaccharide), Inv LNP (Invivofectamine® 2.0-siRNA Lipid Nanoparticles), siApoB Nat (unmodified anti-ApoB siRNA sequence), siApoB 2'Ome (2'O methyl-modified anti-ApoB siRNA sequence), and HA (Hyaluronic acid, 866kDa). Mice were intravenously injected with test articles, serum collected and analyzed 4 hours post injection using the BioPlex 200 system. Each symbol represents an animal. Note: In order to not artificially manipulate the average, cytokine levels (animals) that were below the range of detection (< OOR) were excluded and not considered as 0 or LLOQ (pg/mL).

We next examined the acute effect of NPs on hematological parameters and immune cells 24 hours post administration. As illustrated in Figure 7-5, hemoglobin and hematocrit levels decreased,

relative to PBS treated mice, with high doses of LNPs (8 mg/kg) and increased with uncoated chitosan NPs at high dose (2.5 mg/kg) with no correlation observed when these values were compared to the absolute reticulocyte count. Platelet counts decreased significantly with both LPS and InV LNPs encapsulating the native ApoB sequence (siApoB Nat) indicating acute thrombocytopenia (decreased platelet counts). The use of chemically modified siRNA (siApoB 2'Ome) abrogated the sharp decline in platelets (Figure 7-5) confirming previous results where thrombocytopenia was linked to both the dianophore (i.e. chemical modifications) and pharmacophore (i.e. sequence motifs) of the encapsulated nucleic acid [58]. In contrast to the LNPs used in this study, no sequence or vector dependent thrombocytopenic effect was observed with both uncoated and HA coated chitosan NPs (Figure 7-5). LPS, Inv LNPs, and high doses of uncoated (2.5 mg/kg) and HA coated (8 mg/kg) chitosan-based NPs, decreased the circulating lymphocyte count (Figure 7-5) with an ostensible sequence dependent lymphopenic effect. However, the effect of chitosan-based NPs in decreasing the lymphocyte count was weaker than lipid NPs with values at the lower limit of the CD-1® (ICR) normal reference values. Basophils, eosinophils, neutrophils and monocytes were all unaffected by any of the treatments administered to both male and female CD-1® (ICR) mice (Figure 7-5).

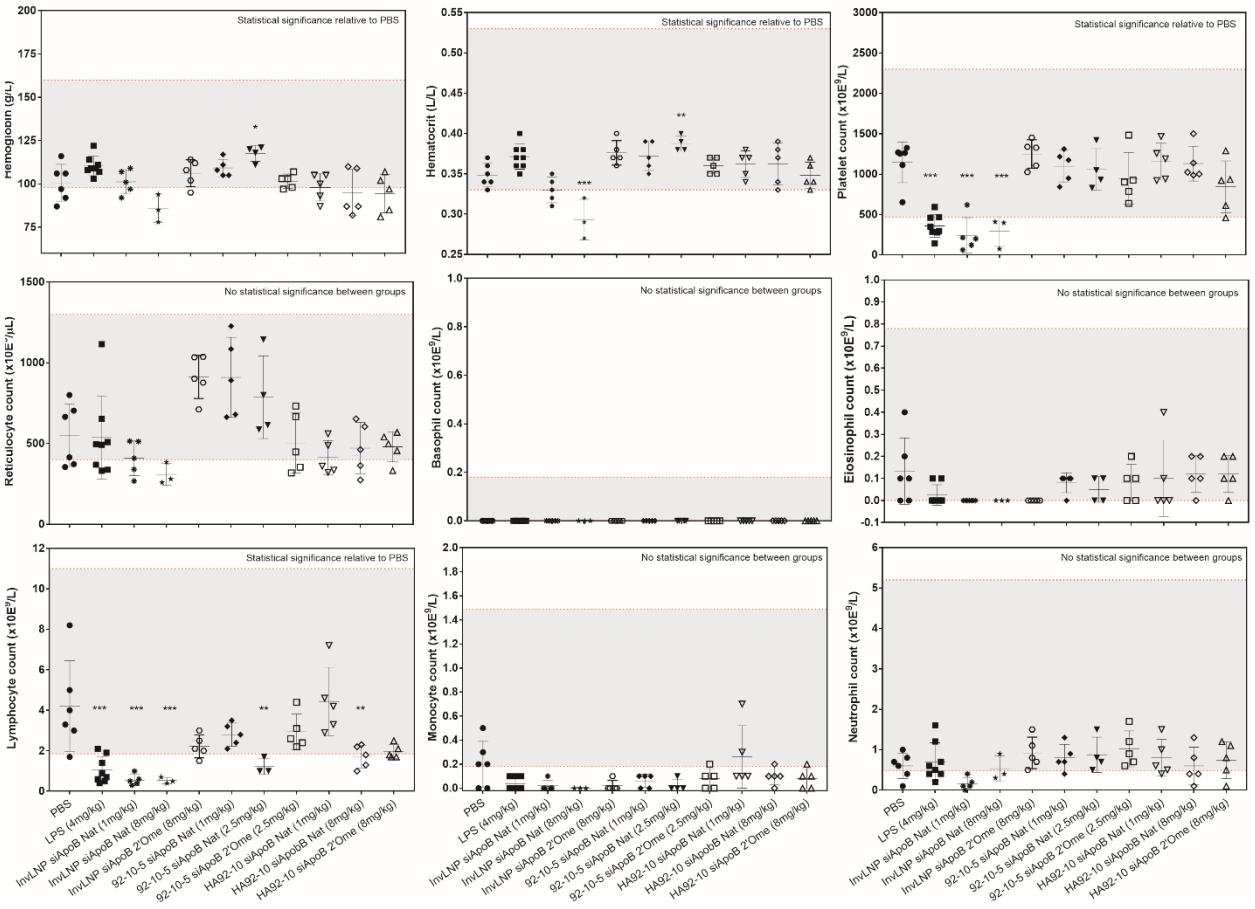

Figure 7-5 Hematological profiling of Invivofectamine® 2.0, uncoated and HA coated chitosan-siRNA nanoparticles following single ascending dose administration in CD-1® (ICR) mice. PBS (Phosphate buffered saline), LPS (Lipopolysaccharide), Inv LNP (Invivofectamine® 2.0-siRNA Lipid Nanoparticles), siApoB Nat (unmodified anti-ApoB siRNA sequence), siApoB 2'Ome (2'O methyl-modified anti-ApoB siRNA sequence), and HA (Hyaluronic acid, 866 kDa). Mice were intravenously injected with test articles, blood collected and analyzed 24 hours post injection at IDEXX Laboratories. Each symbol represents an animal and lines represent average values ± standard deviation of 5-7 animals except for InvLNP siApoB Nat (8 mg/kg) where 3 animals were assayed for hematology. The gray shaded area represents the normal values (95% confidence interval, N= 266 divided as 133 ♀ and 133 ♂) of 8-12 week old CD-1® (ICR) mice from Charles Rivers Laboratories (North American colonies) [59]. Statistical significance versus PBS-treated animals was computed with One-Way ANOVA followed by Dunnett test for multiple comparisons: *p< 0.01, **p <0.001, ***p < 0.00001. Note: Normal range limits in this figure are not firm boundaries and should be used as guidelines since a large range of values was

reported in the literature and could be accounted for by variation in age, sex, sampling technique and testing methodology (i.e. instrument, technique …).

7.3.5 Liver and kidney biomarkers remain unchanged with uncoated and HA coated chitosan NPs while high doses of lipid NPs led to increased transaminase levels

Since cationic lipid-based systems and liposomes, in addition to their immune stimulating properties, are known inducers of liver biomarkers such as alanine transaminase (ALT) and aspartate transaminase (AST), we investigated the effect of our formulations on serum biomarkers and compared them with LNPs (Figure 7-6) As shown in Figure 7-6, blood urea nitrogen (BUN) and creatinine (Cr), both byproducts of protein and creatine catabolism in the liver and muscles respectively and considered clinically relevant indicators (biomarkers) of kidney function, were within the normal reference ranges and statistically comparable to the PBS control group following injection with uncoated and HA coated chitosan-based NPs. Our results indicated that chitosan-based NPs (uncoated and HA coated) targeting kidney PTEC (Figure 7-2) were well tolerated for at least 24 hours post-injection with no changes in kidney biomarkers (i.e. function). An increase in BUN with a concomitant decrease in Cr was observed for the LPS treated group consistent with increased protein catabolism, reduced clearance and induction of cytokines (Figure 7-4) associated with fever like symptoms or infections. Surprisingly a decrease in Cr with a normal BUN value was observed with Invivofectamine® 2.0-siRNA LNP (Inv LNP siApoB Nat) only at low dose. In contrast to lipid nanoparticles (LNPs) or liposomes, information on liver (or systemic) toxicity following administration of uncoated (positively charged) and HA coated (negatively charged) chitosan NPs is lacking. As illustrated in Figure 7-6, ALT, AST and ALP levels were within the normal range and comparable to the PBS control 24 hours post-administration of chitosan-based NPs indicating the absence of liver (or systemic) toxicity. As expected, cationic LNPs (Inv LNPs) demonstrated a dose-dependent increase in liver biomarkers with 2 to 3-fold increase in the ALT/AST ratio consistent with previous data [60, 61]. γ-glutamyl transferase (γGT), a relevant biomarker for liver and bile duct injury, total bilirubin (TBil) and creatine kinase (CK), a biomarker for muscle toxicity, were within the normal range for all formulations tested (i.e. Inv LNPs,

uncoated and HA coated chitosan). Despite the statistically significant increase in γGT observed for the high dose Inv LNP formulation, the clinical relevance of this increase is anecdotal due to high variability in γGT normal range (i.e. 0-12 IU/L). The lack of γGT expression 24 hours following administration of uncoated and HA coated nanoparticle indicate that hepatobiliary excretion (Figure 7-2, A) of these formulations is safe. Lipopolysaccharide (LPS) induced a decrease in alkaline phosphatase (ALP) and albumin/globulin ratio with no effect on ALT, AST, γGT, TBil and CK.

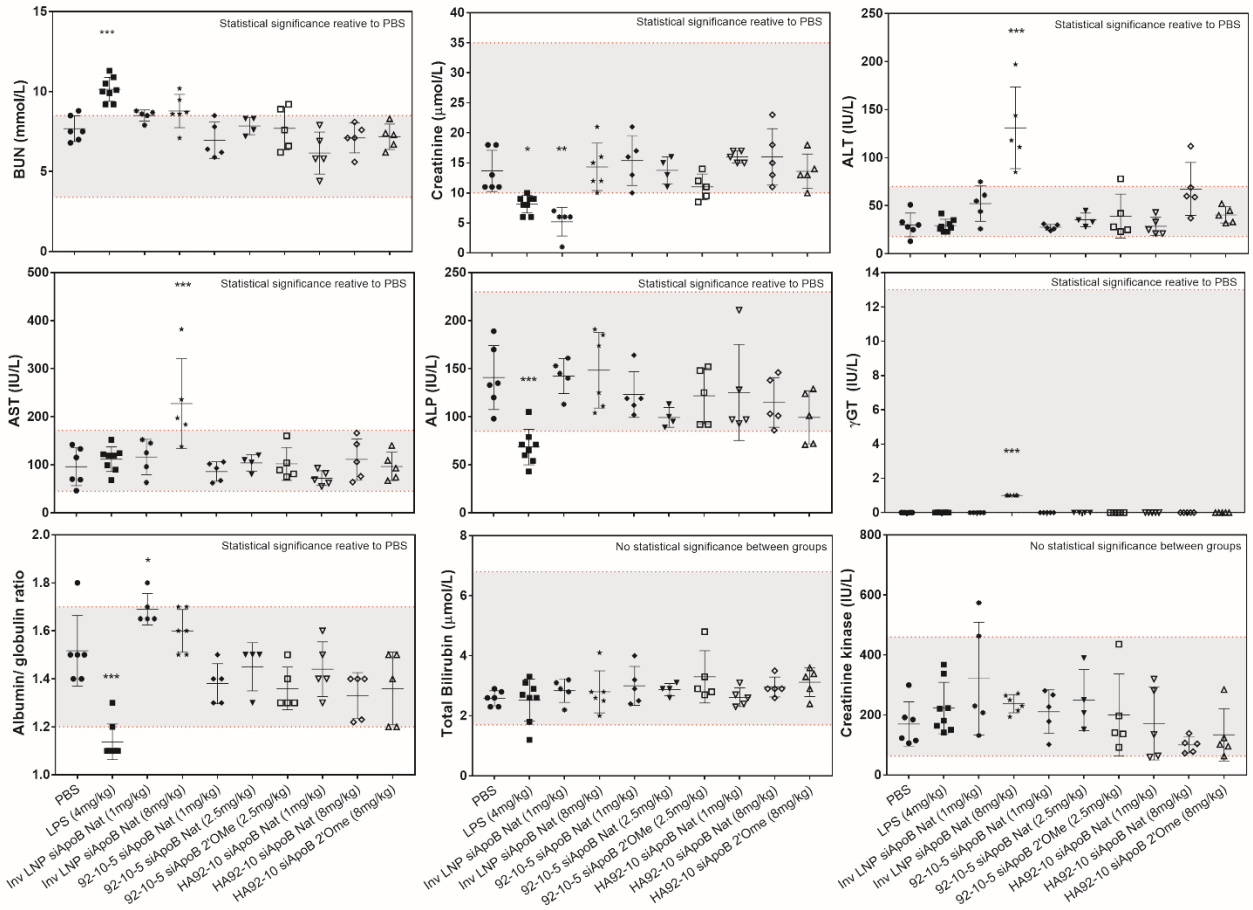

Figure 7-6 Serological profiling of Invivofectamine® 2.0, uncoated and HA coated chitosan-siRNA nanoparticles following single ascending dose administration in CD-1® (ICR) mice. PBS (Phosphate buffered saline), LPS (Lipopolysaccharide), Inv LNP (Invivofectamine® 2.0-siRNA Lipid Nanoparticles), siApoB Nat (unmodified anti-ApoB siRNA sequence), siApoB 2'Ome (2'O methyl-modified anti-ApoB siRNA sequence), and HA (Hyaluronic acid, 866 kDa), BUN (Blood Urea Nitrogen), ALT (alanine transaminase), AST (aspartate transaminase), ALP (Alkaline phosphatase), γGTT (gamma glutamyl transferase). Mice were intravenously injected

with test articles, blood collected and analyzed 24 hours post injection at IDEXX Laboratories. Each symbol represents an animal and data represent average values ± standard deviation of 5-7 animals except for InvLNP siApoB Nat (8 mg/kg) where 3 animals were assayed for hematology. The gray shaded area represents the normal values (95% confidence interval, N= 266 divided as 133 ♀ and 133 ♂) of 8-12 week old CD-1® (ICR) mice from Charles Rivers Laboratories (North American colonies) [59]. Statistical significance versus PBS-treated animals was computed with One-Way ANOVA followed by Dunnett test for multiple comparisons: *p< 0.01, **p <0.001, ***p < 0.00001. Note: Normal range limits in this figure are not firm boundaries and should be used as guidelines since a large range of values was reported in the literature and could be accounted for by variation in age, sex, sampling technique and testing methodology (i.e. instrument, technique …).

7.3.6 Despite normal clinical signs post-administration of NPs, a decrease in body weight was observed with cationic lipid nanoparticles, specifically following multiple injections

Next, we examined global changes in body weight (BW) following single (Figure 7-7**,** A) and multiple (Figure 7-7, B) intravenous administrations of uncoated, HA-coated and lipid nanoparticles formulated with either native or chemically modified siRNA. Cationic lipid nanoparticles at doses between 1 to 8 mg/kg have been shown to induce a reduction in BW which was associated with vector and/or sequence dependent immune stimulation, and/or elevated ALT/AST [58, 62, 63]. As shown in Figure 7-7, a small decrease in BW (~ 0-2 %) was observed for quasi-neutral Inv LNPs (ζ-potential ~ 11 ± 3 mV), HA coated NPs (ζ-potential ~ -25 ± 5 mV) and low doses (1 mg/kg) of uncoated NPs (ζ-potential ~ 25 ± 5 mV) following a single I.V. injection. However, and due to variability, the observed difference was not statistically significant compared with PBS, excipient and naked siRNA groups that showed a steady, or a small (< 1 %) increase in, body weight. The LPS treated group showed a sharp decline in BW (4 ± 0.5 %) that could possibly be linked with elevated cytokine levels (i.e. IL-1β, IL-6, TNF-α, IFN-γ and KC) compared with other groups that had lower (i.e. Inv LNP) or did not induce cytokine release (i.e. uncoated and HA coated NPs) (Figure 7-4). The sharp decrease in BW correlated with clinical

signs (Table 7-2) where LPS injected mice showed signs of lethargy, delayed responsiveness to stimuli and changes in their general appearance around 4 hours post-injection and with decreased ALP levels (Figure 7-6). Given the demonstrated safety of uncoated and HA coated NPs (Figure 7-4, 5, 6 and 7) administered as a single injection, we assumed no changes in cytokine induction, hematological and serological parameter upon multiple injections. However, we monitored clinical signs, body weights, and gross organ pathology as a general toxic assessment following multiple injections (Figure 7-7and **Table S.1**). As expected, uncoated and HA coated chitosan NPs did not induce a decrease in BW. Interestingly, an initial decrease in BW between 0.5 and 2 % was observed for uncoated chitosan upon the first injection, followed by a steady increase in BW after the second injection (day 3). Moreover, there was no difference between low (10 kDa) and high Mn (120 kDa) formulations on BW. Invivofectamine® 3.0, a cationic lipid formulation with improved potency relative to its previous 2.0 generation, induced a sharp decrease (4 ± 1 %) in body weight typical of lipid based and liposomal formulations [15, 58, 62, 63].

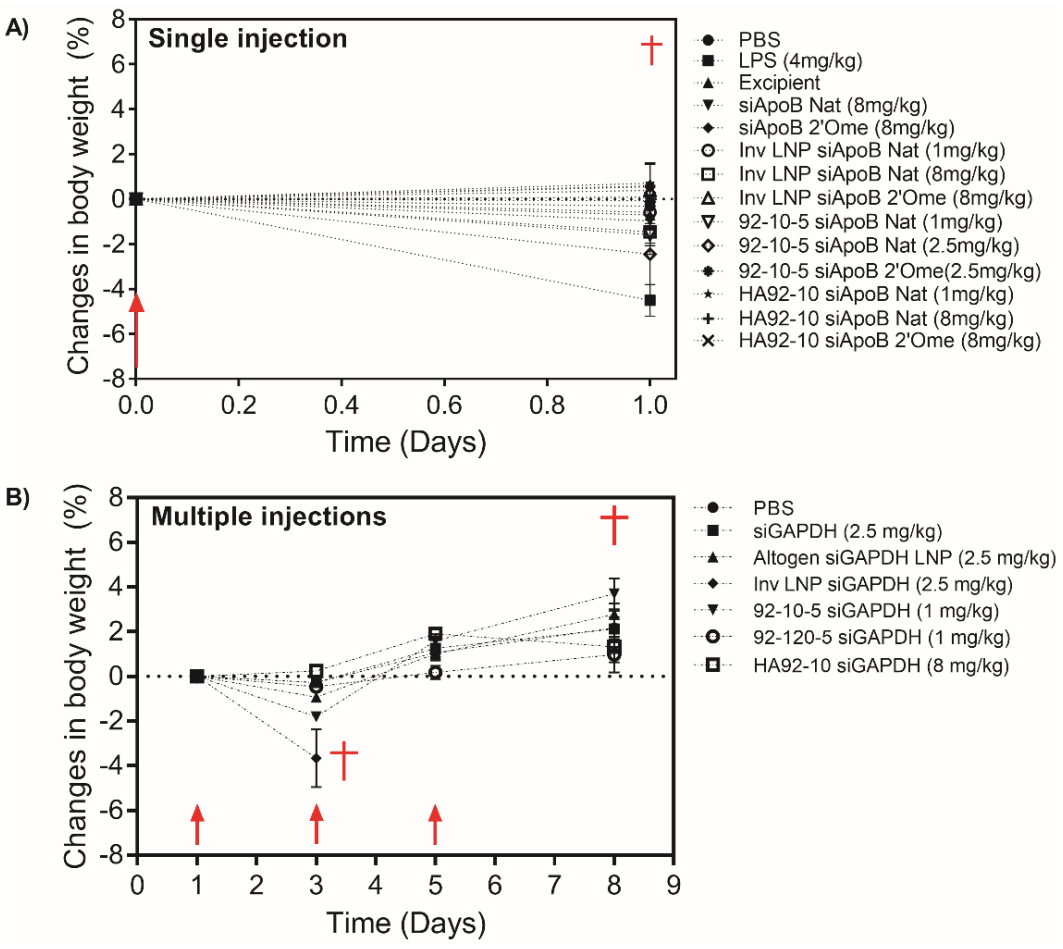

Figure 7-7 Changes in body weight following intravenous nanoparticle administration. A) Percent change in body weight following a single intravenous injection in CD-1® (ICR) mice. Invivofectamine® 2.0 lipid nanoparticles (Inv LNP) were formulated with unmodified (siApoB Nat) and 2'O-methyl modified ApoB siRNA (siApoB 2'Ome) and injected at 1 and 8 mg/kg. Uncoated chitosan was formulated with siApoB Nat and siApoB 2'Ome at an N:P ratio of 5 and injected at 1 and 2.5 mg/kg. Hyaluronic acid (HA, 866 kDa) coated nanoparticles were prepared at an N:P:C of 2:1:1.5 and injected at 1 and 8 mg/kg. The injected doses were chosen from the hemocompatibility data (Figure 7-1) where the maximum dose results in hemolysis below the ASTM threshold. B) Percent change in body weight following three I.V. injections in Balb/c mice. Invivofectamine® 3.0 (Inv LNP) and Altogen (Altogen LNP) lipid nanoparticles were formulated with LNA-modified GAPDH siRNA (siGAPDH) and injected at 2.5 mg/kg. Low Mn (10 kDa) and high Mn (120 kDa) chitosan nanoparticles were formulated with siGAPDH at an N:P ratio of 5 and I.V. injected at 1 mg/kg. Hyaluronic acid (HA, 866 kDa) coated nanoparticles

were prepared at an N:P:C of 2:1:1.5 and injected at 8 mg/kg. The injected doses were chosen from the hemocompatibility data (Figure 7-1) where the maximum dose results in hemolysis below the ASTM threshold and following personal communication with the manufacturers of Invivofectamine® 3.0 and Altogen. For panel A and B, body weight (g) was collected before each injection and at euthanasia. Red arrows and crosses illustrate injection and euthanasia respectively. Data represent the average ± standard deviation of 5-7 mice/group. Phosphate buffered saline (PBS) and lipopolysaccharide (LPS) were used as controls.

Table 7-2 Clinical signs collected following a single ascending dose of LNPs, uncoated and HA coated chitosan-siRNA nanoparticles. General aspect score (GAS), or the general physical aspect of the animal (i.e. hunchback position, piloerection, vocalization …), the natural behaviour score (NBS), or the behavioral aspect of the animal relative to its habitat and littermates (i.e. litter aspect, activity, nesting …) and the provoked behaviour score (PKBS), or the animal response to stimuli (i.e. pen tap on the cage …) were collected by three independent scorers and reported in this table along with the frequency.

TA (dose)	Clinical signs parameters	Time (h) post injection	
		4h (frequency)	24h (frequency)
PBS	GAS	0 (7/7)	0 (7/7)
	NBS	0 (7/7)	0 (7/7)
	PKBS	0 (7/7)	0 (7/7)
LPS (4mg/kg)	GAS	3 (7/7)	0 (7/7)
	NBS	0 (7/7)	0 (7/7)
	PKBS	3 (7/7)	0 (7/7)
siApoB Nat (8 mg/kg)	GAS	0 (7/7)	0 (7/7)
	NBS	0 (7/7)	0 (7/7)
	PKBS	0 (7/7)	0 (7/7)
siApoB 2’Ome (8mg/kg)	GAS	0 (7/7)	0 (7/7)
	NBS	0 (7/7)	0 (7/7)
	PKBS	0 (7/7)	0 (7/7)
InvLNP siApoB Nat (1 mg/kg)	GAS	0 (7/7)	0 (7/7)
	NBS	0 (7/7)	0 (7/7)

	PKBS	0 (7/7)	0 (7/7)
InvLNP siApoB Nat (8 mg/kg)	GAS	1 (7/7)	0 (7/7)
	NBS	0 (7/7)	0 (7/7)
	PKBS	1 (7/7)	0 (7/7)
InvLNP siApoB 2'Ome (8 mg/kg)	GAS	1 (7/7)	0 (7/7)
	NBS	0 (7/7)	0 (7/7)
	PKBS	1 (7/7)	0 (7/7)
92-10-5 siApoB Nat (1mg/kg)	GAS	0 (7/7)	0 (7/7)
	NBS	0 (7/7)	0 (7/7)
	PKBS	0 (7/7)	0 (7/7)
92-10-5 siApoB Nat (2.5 mg/kg)	GAS	1 (7/7)	0 (7/7)
	NBS	0 (7/7)	0 (7/7)
	PKBS	1 (7/7)	0 (7/7)
92-10-5 siApoB 2'Ome (2.5 mg/kg)	GAS	1 (4/7)	0 (7/7)
	NBS	0 (7/7)	0 (7/7)
	PKBS	1 (3/7)	0 (7/7)
HA92-10 siApoB Nat (1 mg/kg)	GAS	0 (7/7)	0 (7/7)
	NBS	0 (7/7)	0 (7/7)
	PKBS	0 (7/7)	0 (7/7)
HA92-10 siApoB Nat (8 mg/kg)	GAS	0 (7/7)	0 (7/7)
	NBS	0 (7/7)	0 (7/7)
	PKBS	0 (7/7)	0 (7/7)
HA92-10 siApoB 2'Ome (8 mg/kg)	GAS	0 (7/7)	0 (7/7)
	NBS	0 (7/7)	0 (7/7)
	PKBS	0 (7/7)	0 (7/7)

7.3.7 Uncoated and HA coated chitosan NPs did not induce histopathological changes in main organs following I.V injection at low and high doses

Histopathological changes are often associated with nanoparticle toxicity and accumulation in target organs. We, therefore, monitored gross and microscopic morphological changes in main organs 24 hours post-injection. As shown in Figure 7-8, tissue sections from liver and kidney display no difference relative to PBS-treated group indicating that NPs accumulating in PTECs (Figure 7-2) are relatively safe. A thorough examination of these organs showed no changes in cell morphology, absence of apoptotic cells and/or immune infiltration. Similar results were obtained at lower doses of uncoated and HA coated NPs and for other organs such as the heart, lungs, and spleen (Figure S. 7-1 and S-4) highlighting the safety of these formulations. Histopathological examination of tissues upon multiple injections underlined the safety of these NPs (data not shown) with similar results obtained in comparison with a single injection. In contrast to chitosan-based NPs, immune cell infiltration close to liver sinusoids was observed for the high dose of Inv LNP (8 mg/kg) (Data not shown).

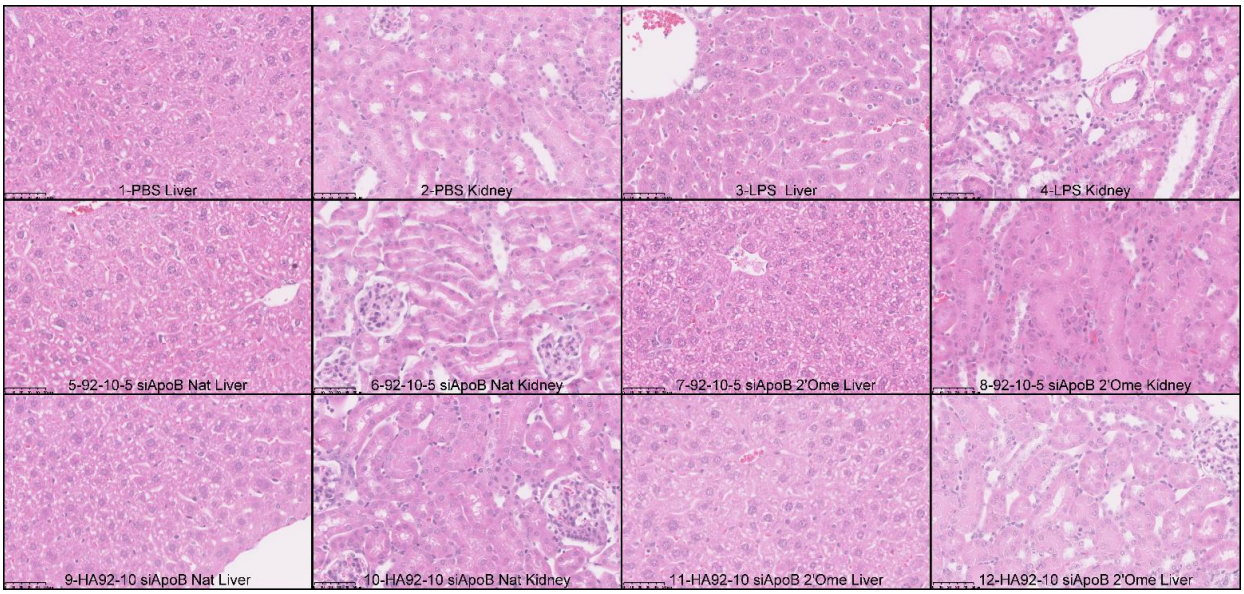

Figure 7-8 Histopathological comparison of liver and kidney tissue sections following intravenous administration of high doses of uncoated and HA coated nanoparticles. Uncoated and HA coated nanoparticles were formulated with both unmodified (siApoB Nat) and 2'O-methyl modified ApoB siRNA sequences (2'Ome siApoB) at an N:P:C of 5:1:0 for uncoated and 2:1:1.5 for HA-coated formulations, freeze-dried, rehydrated using excipients and I.V. injected at a dose

of 2.5 (uncoated) and 8 (HA coated) mg/kg siRNA. Animals were euthanatized 24 hours post-administration, organ collected, fixed and processed for histopathological analysis. Phosphate buffered saline (PBS) and lipopolysaccharide (LPS) were used as controls. Organs from at least two animals per treatment group were processed and analyzed. Heart, Lungs and Spleen tissues from low (1 mg/kg) and high doses (2.5 and 8 mg/kg) are depicted in Supplemental Figure S. 7-4. Tissues show the absence of morphological changes, alterations, clots, apoptotic/necrotic cells or infiltration of immune cells.

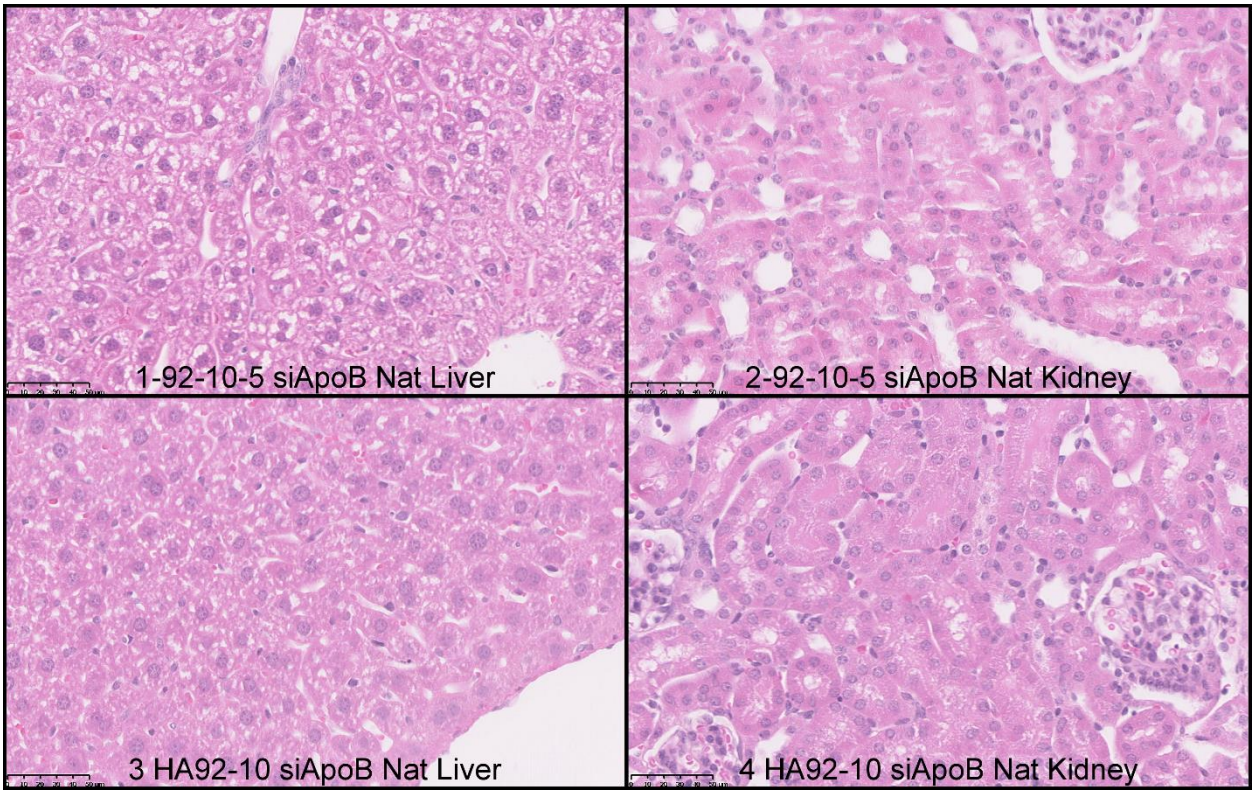

Figure S. 7-3 Histopathological comparison of liver and kidney tissue sections following intravenous administration of low doses of uncoated and HA coated nanoparticles. Uncoated and HA coated nanoparticles were formulated with unmodified (siApoB Nat) at an N:P:C ratio of 5:1:0 for uncoated and 2:1:1.5 for HA-coated formulations, freeze-dried, rehydrated using excipients and intravenously injected at a dose of 1 mg/kg siRNA. Animals were euthanatized 24 hours post-administration, organ collected, fixed and processed for histopathological analysis. Tissues show the absence of morphological changes, alterations, clots, apoptotic/necrotic cells or infiltration of immune cells.

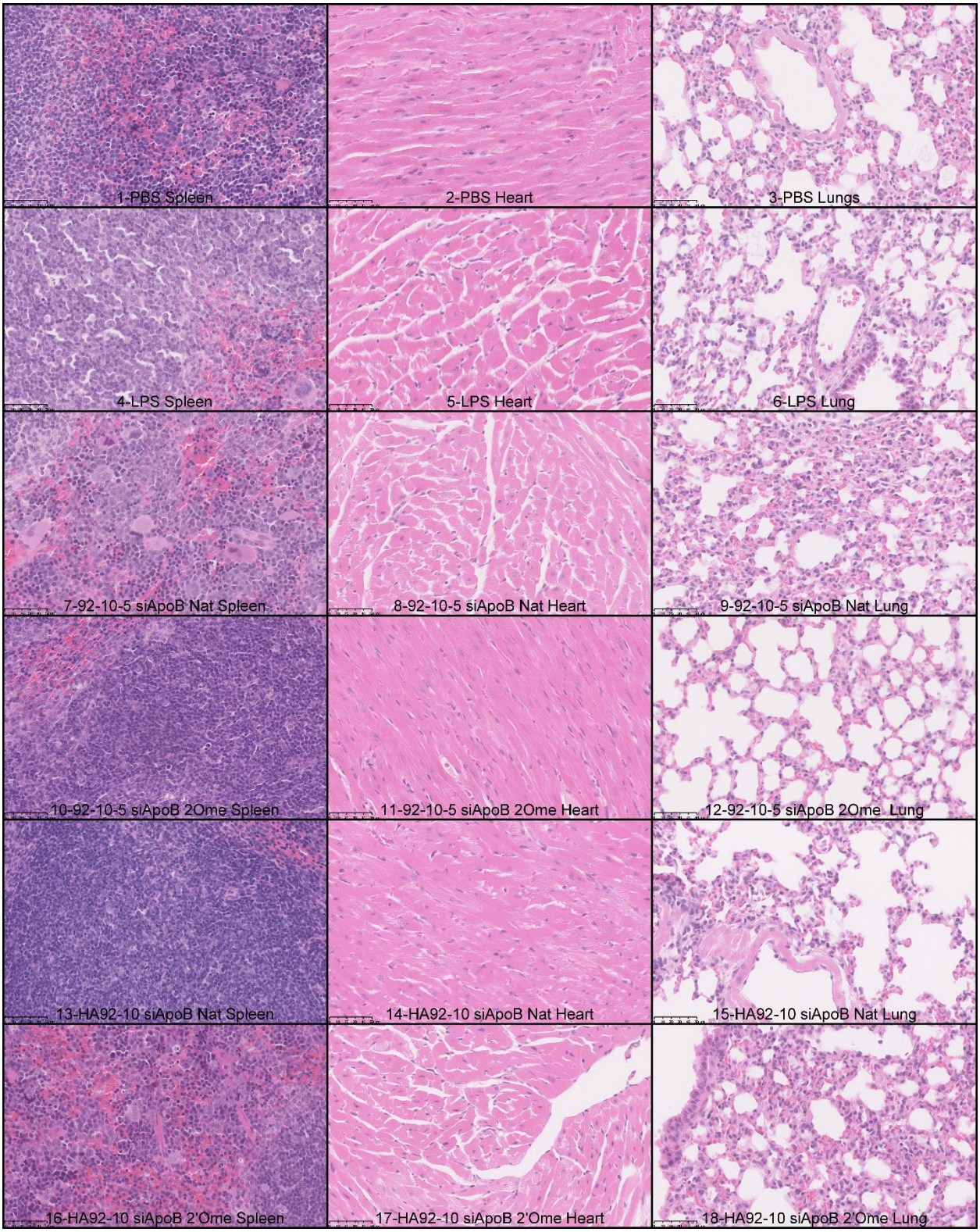

Figure S. 7-4 Histopathological comparison of spleen, heart and lung tissue sections following intravenous administration of high doses of uncoated and HA coated nanoparticles. Uncoated and

HA coated nanoparticles were formulated with either unmodified (siApoB Nat) or 2'O-methyl modified ApoB siRNA (2'Ome ApoB) at an N:P:C ratio of 5:1:0 for uncoated and 2:1:1.5 for HA-coated formulations, freeze-dried, rehydrated using excipients and intravenously injected at a dose of 2.5 (uncoated) and 8 (HA coated) mg/kg siRNA. Animals were euthanatized 24 hours post-administration, organ collected, fixed and processed for histopathological analysis. Phosphate buffered saline (PBS) and lipopolysaccharide (LPS) were used as controls. Organs from at least two animals per treatment group were processed and analyzed. Tissues show absence of morphological changes, alterations, clots, apoptotic/necrotic cells or infiltration of immune cells.

7.3.8 Uncoated chitosan NPs demonstrated functional gene-specific knockdown in kidney cortex independent of polymer length (Mn)

We next examined the efficacy of uncoated and HA-coated NPs through the assessment of functional GAPDH knockdown in inbred Balb/c mice. Nanoparticles were manually prepared, and injected via the tail vein, except for the HA formulation which was freeze-dried (FD), following manual mixing, to reach the specific dose and rehydrated before injection. As illustrated in Figure 7-9, statistically significant functional knockdown of 55%, as assessed by GAPDH enzymatic activity (Figure 7-9, A), was achieved in the kidney cortex following administration of 1 mg/kg of uncoated chitosan NPs. Low (10 kDa) and high (120 kDa) Mn chitosan achieved similar knockdown efficiency with a small, but improved performance observed with low Mn chitosan (Figure 7-9, A and B). Assessment of GAPDH knockdown by western blot showed a similar trend in knockdown between low *versu*s high Mn chitosan with minor differences that could be attributed to the different techniques used for target knockdown assessment (Enzymatic *versus* immune detection). Interestingly, the HA coated formulation, injected at the higher dose of 8 mg/kg, produced no knockdown of the target gene. Naked siRNA has a natural tendency to accumulate in the kidney [33, 64-67] and is used as a strategy in phase III clinical trial to target p53 in ischemia-reperfusion kidney injury (NCT02610296). In our study, chemically modified siRNA, containing Locked Nucleic Acid (LNA) combined with other AMBION Silencer® Select modifications (undisclosed), resulted in only 16% target knockdown when injected at a dose of 2.5 mg/kg

indicating a clear, and positive effect, of the chitosan delivery system to improve siRNA knockdown efficiency nearly 4 fold to 55%. Surprisingly, a commercially available kidney-targeted liposome, Altogen LNP, did not achieve knockdown possibly due to its large size (~ 300 nm) pre-injection which could increase to around 400-500 nm upon injection in blood. Qualitative confirmation of target knockdown was performed using immunohistochemistry on kidney sections from chitosan and PBS-treated mice. As shown in Figure 7-9 C, specific target knockdown was achieved in the cortex of chitosan NP treated kidneys. Taken together, our data showed that uncoated chitosans (both high and low Mn) with a degree of deacetylation (DDA) of 92%, are safe (Figure 7-5 and 6), non-immune stimulating delivery systems (Figure 7-4**)** that targets kidney PTECs (Figure 7-2), and are well tolerated upon single and multiple injection to achieve significant functional knockdown in kidney cortices (Figure 7-9**,** A, B and C).

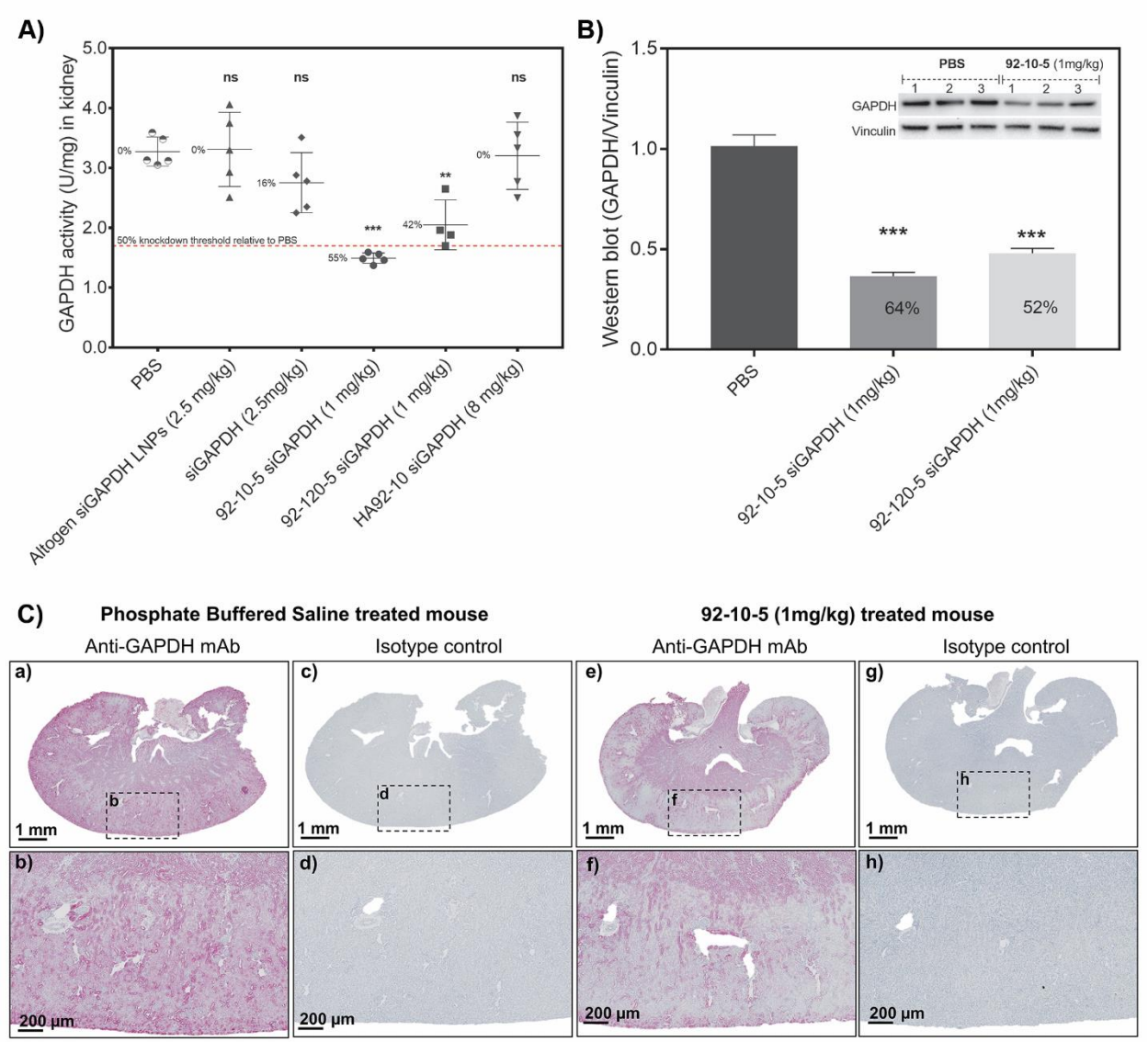

Figure 7-9 Efficacy of in vivo target knockdown. A) GAPDH activity (U) normalized per tissue mass (mg). Kidneys were collected, snap frozen in liquid nitrogen, and cortex excised, homogenized, protein extracted and assayed using the GAPDH KDalert™ enzymatic kit. (ns) non-significant and numbers express % knockdown relative to PBS. B) Western blot detection of GAPDH in kidney lysate. GAPDH signal was normalized to the vinculin loading control. The inset shows an actual example of a western blot membrane used for quantification. The membrane shows three different animals injected with PBS (control) and with 92-10-5 (1 mg/kg siGAPDH). Numbers in the histogram columns represent % knockdown relative to PBS. C) Qualitative assessment of GAPDH knockdown in the kidney by immunohistochemistry. Panels a, b, c, and d show a kidney section collected from a PBS-treated animal, stained with anti-GAPDH

antibody (a and b) and isotype control (c and d). Panels e, f, g, and h show a kidney section collected from a chitosan (92-10-5) treated animal, stained with anti-GAPDH antibody (e and f) and isotype control (g and h). Data represent average values ± standard deviation of 5 animals except for 92-120-5 siGAPDH (1 mg/kg) where 4 animals were assayed. Statistical significance versus PBS-treated animals was computed with One-Way ANOVA followed by Dunnett test for multiple comparisons: *p< 0.01, **p <0.001, ***p < 0.00001.

7.4 Discussion

Here, we investigated the effect of chitosan polymer length, dose, and surface modification with hyaluronic acid (HA) on the hemolytic potential, acute and organ toxicity, cytokine induction, *in vivo* biodistribution and target knockdown efficacy in addition to comparing chitosan NPs with commercially available cationic lipid nanoparticles (Invivofectamine®). Hemolytic and hemagglutination properties have been well characterized for cationic polymers such as PEI [68, 69] and chitosan [40] with chitooligosaccharide (Mn < 5 kDa) found to be non-hemolytic but cause dose-dependent erythrocyte aggregation [70]. In our study, we have shown that uncoated chitosan NPs display dose and molecular weight dependent hemolytic and hemagglutination properties that could be abrogated with the use of nanoparticles prepared at low nitrogen to phosphate ratio (N:P ratio) or following HA coating (Figure 7-1) consequently highlighting careful dosing to avoid hemotoxicity and/or embolism. The hemolytic/hemagglutination potential of chitosan could occur through interaction with negatively charged erythrocyte (RBC) membranes via a pore forming mechanism, followed by a subsequence osmotic shock, and/or through regulation of surface protein and increase in surface roughness as demonstrated for methacrylate based polymers [71] and chitooligosaccharides [70] respectively. In addition, the interaction between chitosan amino groups and acidic groups on erythrocytes could promote polyelectrolyte complex formation leading to RBC aggregation as seen for other biomaterials [72]. NP coating with HA, a biocompatible and negatively charged molecule, eliminated both hemolysis and RBC aggregation possibly due to limited interaction with erythrocyte membranes through electrostatic repulsion and reduced interaction with serum components (Figure 7-1. In contrast to uncoated chitosan, lipid nanoparticles (LNPs) did not show dose-dependent hemolysis (Figure 7-1**, Inset)** probably due to

surface PEGylation implied by the quasi-neutral ζ-potential ~ 8-10mV (Figure 7-3). Shielding with polyethylene glycol (PEG) has been the method of choice to limit LNP hemolysis with high PEG density required for improved biocompatibility and reduced cytokine induction [52] and is incorporated in most if not all LNPs that are commercially available or in clinical development. In contrast to PEGylation, electrostatic coating with HA has demonstrated a similar protective effect permitting dose increase to at least 8 mg/kg (Figure 7-1).

Immune stimulating properties of nanoparticles, or their payloads, can be studied by monitoring the expression of cytokines in plasma, serum or target tissues [4, 58, 62, 63] and represent one of the major hurdles for clinical translation [14]. In the current study, uncoated and HA-coated chitosan NPs did not induce type I pro-inflammatory cytokines (IL-1β, TNF-α, IFN-γ and IL-6) except for a small but statistically insignificant increase in KC, a human IL-8 homolog (Figure 7-4) indicating a non-immunogenic effect 4 hours post-administration. KC is a chemoattractant cytokine with distinct, or quasi-unique target specificity for neutrophils and is produced by a variety of epithelial and endothelial cells (EC) [73, 74]. The absence of neutrophil invasion, 24 hours post-administration, in main organs (**Supplemental Fig. S3 and S4**) and in kidney tissues (Figure 7-8) where chitosan has been found to accumulate (Figure 7-2) suggests an epithelial cell-independent mechanism of KC expression. However, platelet activation, aggregation and cytokine release (i.e. TGF-β1, PDGF-AB) have been observed following *in vitro* assessment of chitosan in hemostatic aggregation experiments [75] suggesting that KC levels post-administration of chitosan (Figure 7-4) could be attributed to platelet activation and their release from Weibel-Palade bodies. The adjuvant and immune stimulating effect of chitosan have been well described both *in vitro* and *in vivo*, and involve the activation of dendritic cells, and the secretion of Type-I pro-inflammatory cytokines (i.e. IFN-α/β/γ, IL-1β, TNF-α …), through NLRP3 inflammasome activation and the recently discovered cGAS/STING pathway for lower DDA (80%) chitosans [41, 42, 76-78]. The apparent contradiction between the lack of cytokine activation (Figure 7-4) and the literature could be explained by differences in routes of administration, dose, degrees of deacetylation and priming of immune cells. For instance, most studies demonstrating the anti-allergic properties of chitin and chitosan (Th_2 inhibition) via the expression of Type-I cytokines have been tested *in vitro* and/or using the intranasal, intraperitoneal, intraocular and intravaginal routes of administration [42, 76]. However, in all these studies, priming strategies were used and could explain cytokine induction consistent with the finding that chitosan stimulated significant cytokine release only from primed

BMMΦ [77]. In this study, we did not measure cytokine levels at subsequent time points which could also explain the absence of cytokine induction, that only appeared around 9 h and peaked 24 hours post stimulation [42]. Other considerations such as Mn, contaminants, particle size may also contribute to the observed difference.

Lipid nanoparticles (LNPs), and liposomes are known, and potent, immune activators *in vitro* and *in vivo* with immune stimulation governed by the lipid and cationic head groups, and/or the combination with the nucleic acid payload [4, 15, 52, 58, 63]. In this study, Invivofectamine® LNPs demonstrated a dose-dependent induction of IFN-γ, IL-6 and KC and a minor TNF-α increase in serum (Figure 7-4). Immune stimulation was abrogated with the 2'Ome modified siRNA confirming previous results with LNPs [4, 58] highlighting major differences with our chitosan system where cytokine induction was not observed with any payload. In this study, we chose TNF-α because it is a potent cytokine that is invariably activated, and immediately released, by all Toll-Like receptors (TLRs) [79, 80]. Therefore, the TNF-α stimulation observed with lipid nanoparticle used in this study, while not induced with chitosan, suggests a TLR based mechanism of immune induction reminiscent of Chol:DSPC:DOTAP (3:1:1) cationic liposomes [63].

In the absence of cytokine induction (Figure 7-4), we next examined the acute toxic effects of chitosan, dose, siRNA sequence, HA-coating on hematological and serological parameters. Hematocrit (HCT) and total hemoglobin (Hb) levels were unchanged relative to PBS and within the normal reference ranges of CD-1® (ICR) mice indicating a relatively safe and non-hemolytic profile for all formulation tested. Lower Hb, but not HCT, levels compared with the reference range could be observed intragroup and might be due to differences in gender, age and quantification techniques used to establish the reference ranges [59, 81]. However, Hb levels were comparable to the PBS group and considered normal in this study. In contrast to chitosan NP, and their HA coated form, LNPs used in this study sharply decreased platelet counts consistent with previous observations [15, 58]. In this study, platelet decreases, or thrombocytopenia, post-LNP injection was sequence dependent consistent with [58]. Thrombocytopenia was also observed for antisense oligonucleotide (ASO) administered at doses above 200 mg/kg, which resulted in a halt in both the IONIS CARDIO-TTR and the NEURO-TTR phase III trials, and could be traced to the phosphorothioate (PS) backbone modification [82]. In the present study, as seen in a previous study [58], the anti-ApoB siRNA was not PS modified, supporting further mechanistic investigation.

Interestingly, lymphocyte counts decreased with both lipid and chitosan based formulations when formulated with the native immune stimulatory [4] anti-ApoB sequence Figure 7-5). All other parameters tested such as circulating basophils, eosinophils, monocytes, and neutrophils were normal and within the normal standard ranges for CD-1® (ICR) mice [59, 81].

Chitosan accumulation in the kidney (Figure 7-2) did not impair kidney function since levels of blood urea nitrogen and creatine remained normal (Figure 7-6). However, one major drawback of this study consists of the lack of BUN and creatinine measurements in urine which is more predictive than their serum counterparts as they permit the computation of the glomerular filtration rate (GFR), a clinical indicator of renal function. BUN and creatinine, are also indirect indicators of liver health, and therefore support the absence of liver toxicity as indicated by normal transaminase levels such as ALT, AST and ALP (Figure 7-6). In contrast to uncoated and HA coated NPs, lipid nanoparticles showed a typical dose-dependent increase in transaminases (Figure 7-6) indicating transient liver toxicity [15, 62, 63]. This was further accompanied by a reduction in body weight (Figure 7-7) further highlighting systemic (liver) toxicity with LNPs. In general, a decrease in body weight has been observed with lipid nanoparticles [15, 58, 62, 63] and could be attributed to either the lipids [15, 62, 63] or to properties of the encapsulated nucleic acid payload [58]. In the present study, the decrease in body weight is believed to be due to the general toxicity induced by the lipid system, since injections were performed with a Locked Nucleic Acid (LNA) modified sequence containing 2’Ome and phosphorothioate (PS). However, further examination of the immune stimulation properties of this sequence, in the lipid encapsulated form is required. Lipopolysaccharide (LPS) treatment increased BUN, and decreased Cr levels in serum typical of catabolic processes induced following induction of cytokines (Figure 7-4) in fever like symptoms or infections [83]. Alkaline phosphatase (AP), an enzyme endowed with LPS detoxifying properties decreased following I.V. injection of LPS (Figure 7-6). The reduction is mainly attributed to malnutrition and weight loss (Figure 7-7A), and correlates with overt clinical signs including lethargy, decreased reactivity to stimuli and changed in the general appearance of mice (Table 7-2). However, and under the current experimental conditions, we cannot rule out another, less possible but valid, hypothesis to explain AP reduction in serum, likely due to AP depletion following LPS detoxification.

Organ and tissue toxicity is generally recognized by morphological changes, immune infiltration, apoptosis and/or necrosis. In the current study, no morphological changes, including an absence of infiltrating neutrophils, apoptotic and/or necrotic cells were observed in main organs upon single (Figure 7-8 and Supplemental Figure S. 7-3 and S4) and multiple injections (data not shown) further confirming the safety of uncoated and HA coated NPs. However, immune infiltration in liver was observed with high doses (8 mg/kg) of Invivofectamine® 2.0 (data not shown) supporting immune stimulation data (Figure 7-4). Considering the data discussed above, sub-acute and chronic toxicity studies should be performed as per the international conference on harmonization (ICH) and the Food and Drug Administration (FDA) guidelines, with cytokine induction assessed at multiple time points, in order to draw a complete toxicity profile.

Intravenous administration was shown to cause accumulation of chitosan-siRNA NPs in kidneys (Figure 7-2) and promote siRNA translocation through the glomerular basement membrane (GBM) as evidenced by the intracytoplasmic localization and punctuate pattern of siRNA Figure 7-2, B and Inset). PTEC internalization of chitosan has been previously demonstrated to be dependent on glucosamine (Glc)-Megalin interaction and subsequent endocytosis [32, 84]. Hyaluronic acid coating modified the physicochemical properties of nanoparticles, with a shift in size and ζ-potential indicating effective coating (Figure 7-3), without modifying the kidney-targeted biodistribution pattern possibly via CD44 internalization. Indeed, PTECs express at least five CD44 splice variants that play an important role in HA internalization and could be blocked using anti-CD44 antibodies [85]. In addition, HA has been shown to increase colloidal stability of NPs in serum [23] but HA could shed in circulation, therefore, exposing the chitosan-siRNA core (N:P 2) that subsequently accumulate in PTEC via Megalin-mediated endocytosis. This two hypothesis, could be validated through a PK/PD study in CD44 and Megalin double negative transgenic mice or CD44 negative with drug-induced Megalin shedding. Independent of the observed PTEC accumulation, the mechanism of NP translocation through GBM still remains unclear since fenestration and ECM restrict translocation and diffusion of NPs. Non-conventional mechanisms such as those observed with 200-300 nm carbon nanotubes [86], or through nanoparticle disassembly at the highly negative GBM and reassembly in the lumen as proposed for cyclodextrin-based nanoparticles [87] might provide an explanation for GBM translocation and PTEC accumulation. Alternative delivery through the fenestrated peritubular capillaries could occur but also faces similar diffusion challenges through the negatively charged interstitium. In addition to

kidney, uncoated and HA-coated NPs accumulate in the gallbladder (Gb) (Figure 7-2) suggesting hepatobiliary elimination of nanoparticles, or a fraction thereof, with a size above liver fenestrations suggesting that a fraction of the injected NPs was in the range of 0.3-1 µm [88].

Considering the biodistribution and the toxicity assessment of uncoated and HA-coated NPs, we next examined the efficacy of these NPs to induce target specific knockdown. The glyceraldehyde 3-phosphate (GAPDH) gene was selected as a target due to its ubiquitous expression in tissues and the availability of *in vivo* validated, and chemically modified, siRNA sequences. In this study, functional GAPDH knockdown in the kidney cortex was achieved upon three injections of uncoated NPs (Figure 7-9, A). GAPDH enzymatic activity was reduced in kidney lysate by around 55% and 45% using low (10 kDa) and high (120 kDa) Mn chitosan respectively. Western blot analysis and qualitative immunohistochemistry confirmed the enzymatic activity data and showed cortex specific knockdown (Figure 7-9, B and C). In contrast to uncoated chitosan, HA-coated NPs accumulated in the kidney (Figure 7-3) but did not induce target knockdown (Figure 7-9, A). This result could be explained by the need of excess chitosan (N:P = 5:1 in uncoated *vs* 2.5:1 in HA-coated) to promote endosomal release [89], possibly through the proton sponge effect. As a consequence, it is likely that HA-coated NPs formulated at an N:P:C 2.5:1:2 are able to translocate to the cytoplasm of PTEC (Figure 7-2) but remain sequestrated in endolysosomal compartments due to poor endosomal buffering capacity and reduced proton sponge effect. In addition, the negatively charged HA molecule, if co-localizing with chitosan, could contribute to lower endosomal release by masking positive charge in the endosome, therefore, reducing the capacity of endocytosed chitosan to mediate endosomal rupture. Independent of the two hypotheses, further validation through *in vivo* rescue experiments – i.e. injection of HA-coated NPs, followed by, or co-injected with, free chitosan – and intracellular trafficking studies are needed. In contrast to HA-coated NPs (N:P:C of 2.5:1:2), uncoated chitosan formulations prepared at an N:P ratio of 5 contain around 70% free chitosan [90] that could colocalize in PTEC endosomes and promote endosomal rupture, explaining the observed efficacy (Figure 7-9). Endosomal colocalization strategies involving cholesterol-conjugated siRNA and GalNAc-conjugated endosomodisruptive polymers have been previously described and applied in the clinic as a Dynamic Polyconjugate (DPC) system.

In contrast to chitosan, Invivofectamine® LNPs accumulated in liver (data not shown) and induced target knockdown (**Supplemental Fig.S5**) confirming previous findings with the same delivery system [91]. Knockdown levels obtained in this study with LNPs are lower than previously reported data [64, 91] and could be explained by differences in target gene half-lives ($t_{1/2}$). Full depletion of the target protein after complete mRNA knockdown (> 95%), given steady and long-term knockdown, requires around 5 half-lives indicating the importance of time point selection for knockdown assessment. As such, knockdown is underestimated for long (i.e. GAPDH >35 h [92]) *versus* short half-life targets (i.e. factor VII, tearoyl-CoA Desaturase or tbid …).

Compared to the potency of LNPs in biopharmaceutical pipelines (~70-90%) [18, 93], functional target knockdown obtained with our system (~50-60%) appears lower. However, considerations such as half-life of the target gene, potency of the siRNA, and tissue dependent technical challenges could explain these differences. Given that chitosan accumulates in PTECs (minor cell subtype of the kidney) *versus* LNPs in hepatocytes (predominant cell type in liver), assessment of target knockdown using conventional techniques (i.e. qPCR, enzymatic activity, western blotting…) that average expression levels across all cell types in the tissue sample is inevitably underestimated. Therefore, functional knockdown obtained in this report underestimates the true efficiency of our system to silence a target gene in PTECs, and highlight that precise evaluation of knockdown requires the development of methods capable of estimating knockdown in a specific subset of cells composing an organ.

Taken together, our findings are critically important in revealing that uncoated and HA-coated NPs display no toxicity along with extra-hepatic delivery of siRNA leading to a functional knockdown in kidney cortices. The efficacy of our uncoated system in inducing functional target knockdown in PTECs specifically differentiates it from cyclodextrin-based NPs accumulating in the glomerulus and podocytes [87]. This study also highlights the potential of hyaluronic acid coated chitosan hybrid system as a potential system that accumulates in the kidney and could be delivered at high doses without hemolytic and/or adverse events. Further investigation is needed to elucidate the mechanism of PTEC accumulation and lack of knockdown efficacy observed with the HA-coated system in this report despite similar distribution properties.

7.5 Conclusion

Uncoated chitosan NPs were shown to have hemolytic potential in a dose and Mn-dependent manner with hyaluronic acid coating abrogating this negative effect. In contrast to lipid-based nanoparticles, and liposomes, uncoated and HA coated chitosan NPs did not induce proinflammatory Type-I cytokines except for a small but statistically insignificant increase observed with the human IL-8 homolog, KC. Toxicological profiling showed that both uncoated and HA coated chitosan NPs injected at low and high doses were safe as demonstrated by normal hematological parameters and serological biomarkers. In this study, lipid nanoparticles (Invivofectamine®), induced a dose-dependent cytokine release and caused acute toxicity exemplified by increased serum transaminases and a sharp reduction in body weight. *In vivo* biodistribution showed cytoplasmic accumulation of siRNA in the proximal tubular epithelial cells of the kidney, with a clear role for chitosan, whether uncoated or HA-coated, in improved bioaccumulation. Nanoparticle efficacy showed 50-65% functional knockdown with a clear confinement to the kidney cortex after I.V. administration. In contrast, we have found that HA coating sharply reduced knockdown despite accumulation in the kidney cortex suggesting the incorporation of endosomolytic moieties in such NPs may improve endosomal release. Taken together, our data indicate that chitosan NPs are safe delivery systems with the potential to treat kidney diseases, specifically in PTEC related pathologies.

Acknowledgments

This work was supported by the Canadian Institutes of Health Research and ANRis pharmaceuticals. The funding sources had no role in study design, data collection, analysis, interpretation of data, writing or decision to submit this manuscript. The authors would like to thank Genevieve Picard and Colleen Mathieu (MSc) for assistance with histology, Dr Vaijayanthimala Vairakkannu (PhD), Dr Wafaa Yahyaoui (PhD), Almas-Fatima Siddiqui (MSc), Isabelle Caron, Eric Bouchard and Dr Melania Gombos (MedVet) for assisting during animal experiments, Ibtissam Kheiri (BSc) for designing, implementing and maintaining the animal studies database, Professor Caroline Hoemann (PhD) for providing the BioPlex® system, and Julie Tremblay (BSc) for quality control.

References

[1] A. Khvorova, J.K. Watts, The chemical evolution of oligonucleotide therapies of clinical utility, Nat Biotechnol, 35 (2017) 238-248.

[2] J.M. Layzer, A.P. McCaffrey, A.K. Tanner, Z. Huang, M.A. Kay, B.A. Sullenger, In vivo activity of nuclease-resistant siRNAs, RNA, 10 (2004) 766-771.

[3] D.V. Morrissey, J.A. Lockridge, L. Shaw, K. Blanchard, K. Jensen, W. Breen, K. Hartsough, L. Machemer, S. Radka, V. Jadhav, N. Vaish, S. Zinnen, C. Vargeese, K. Bowman, C.S. Shaffer, L.B. Jeffs, A. Judge, I. MacLachlan, B. Polisky, Potent and persistent in vivo anti-HBV activity of chemically modified siRNAs, Nat Biotechnol, 23 (2005) 1002-1007.

[4] A.D. Judge, G. Bola, A.C. Lee, I. MacLachlan, Design of noninflammatory synthetic siRNA mediating potent gene silencing in vivo, Mol Ther, 13 (2006) 494-505.

[5] A.L. Jackson, J. Burchard, D. Leake, A. Reynolds, J. Schelter, J. Guo, J.M. Johnson, L. Lim, J. Karpilow, K. Nichols, W. Marshall, A. Khvorova, P.S. Linsley, Position-specific chemical modification of siRNAs reduces "off-target" transcript silencing, RNA, 12 (2006) 1197-1205.

[6] A. Wittrup, J. Lieberman, Knocking down disease: a progress report on siRNA therapeutics, Nat Rev Genet, 16 (2015) 543-552.

[7] R. Kanasty, J.R. Dorkin, A. Vegas, D. Anderson, Delivery materials for siRNA therapeutics, Nat Mater, 12 (2013) 967-977.

[8] T.P. Prakash, G.A. Kinberger, H.M. Murray, A. Chappell, S. Riney, M.J. Graham, W.F. Lima, E.E. Swayze, P.P. Seth, Synergistic effect of phosphorothioate, 5'-vinylphosphonate and GalNAc modifications for enhancing activity of synthetic siRNA, Bioorg Med Chem Lett, 26 (2016) 2817-2820.

[9] K. Garber, Alnylam's RNAi therapy targets amyloid disease, Nat Biotechnol, 33 (2015) 577.

[10] I. Arrowhead Pharmaceuticals, Arrowhead Pharmaceuticals Provides Update on Heparc-2004 Study, in, 2016.

[11] Ramanathan RK, Hamburg SI, e.a. Borad MJ, A Phase 1 dose escalation study of TKM-080301, a RNAi therapeutic directed against PLK1, in patients with advanced solid tumors, in: AACR 2013 Annual Meeting, Washington 2013.

[12] J. Tabernero, G.I. Shapiro, P.M. LoRusso, A. Cervantes, G.K. Schwartz, G.J. Weiss, L. Paz-Ares, D.C. Cho, J.R. Infante, M. Alsina, M.M. Gounder, R. Falzone, J. Harrop, A.C. White, I. Toudjarska, D. Bumcrot, R.E. Meyers, G. Hinkle, N. Svrzikapa, R.M. Hutabarat, V.A. Clausen, J.

Cehelsky, S.V. Nochur, C. Gamba-Vitalo, A.K. Vaishnaw, D.W. Sah, J.A. Gollob, H.A. Burris, 3rd, First-in-humans trial of an RNA interference therapeutic targeting VEGF and KSP in cancer patients with liver involvement, Cancer Discov, 3 (2013) 406-417.

[13] T. Coelho, D. Adams, A. Silva, P. Lozeron, P.N. Hawkins, T. Mant, J. Perez, J. Chiesa, S. Warrington, E. Tranter, M. Munisamy, R. Falzone, J. Harrop, J. Cehelsky, B.R. Bettencourt, M. Geissler, J.S. Butler, A. Sehgal, R.E. Meyers, Q. Chen, T. Borland, R.M. Hutabarat, V.A. Clausen, R. Alvarez, K. Fitzgerald, C. Gamba-Vitalo, S.V. Nochur, A.K. Vaishnaw, D.W. Sah, J.A. Gollob, O.B. Suhr, Safety and efficacy of RNAi therapy for transthyretin amyloidosis, N Engl J Med, 369 (2013) 819-829.

[14] W. Tao, X. Mao, J.P. Davide, B. Ng, M. Cai, P.A. Burke, A.B. Sachs, L. Sepp-Lorenzino, Mechanistically probing lipid-siRNA nanoparticle-associated toxicities identifies Jak inhibitors effective in mitigating multifaceted toxic responses, Mol Ther, 19 (2011) 567-575.

[15] J.D. Tousignant, A.L. Gates, L.A. Ingram, C.L. Johnson, J.B. Nietupski, S.H. Cheng, S.J. Eastman, R.K. Scheule, Comprehensive analysis of the acute toxicities induced by systemic administration of cationic lipid:plasmid DNA complexes in mice, Hum Gene Ther, 11 (2000) 2493-2513.

[16] S.C. Semple, T.O. Harasym, K.A. Clow, S.M. Ansell, S.K. Klimuk, M.J. Hope, Immunogenicity and rapid blood clearance of liposomes containing polyethylene glycol-lipid conjugates and nucleic Acid, J Pharmacol Exp Ther, 312 (2005) 1020-1026.

[17] A. Judge, K. McClintock, J.R. Phelps, I. Maclachlan, Hypersensitivity and loss of disease site targeting caused by antibody responses to PEGylated liposomes, Mol Ther, 13 (2006) 328-337.

[18] M.T. Abrams, M.L. Koser, J. Seitzer, S.C. Williams, M.A. DiPietro, W. Wang, A.W. Shaw, X. Mao, V. Jadhav, J.P. Davide, P.A. Burke, A.B. Sachs, S.M. Stirdivant, L. Sepp-Lorenzino, Evaluation of efficacy, biodistribution, and inflammation for a potent siRNA nanoparticle: effect of dexamethasone co-treatment, Mol Ther, 18 (2010) 171-180.

[19] C. Lorenzer, M. Dirin, A.M. Winkler, V. Baumann, J. Winkler, Going beyond the liver: progress and challenges of targeted delivery of siRNA therapeutics, J Control Release, 203 (2015) 1-15.

[20] M. Alameh, M. Jean, D. Dejesus, M.D. Buschmann, A. Merzouki, Chitosanase-based method for RNA isolation from cells transfected with chitosan/siRNA nanocomplexes for real-time RT-PCR in gene silencing, Int J Nanomedicine, 5 (2010) 473-481.

[21] M. Alameh, D. Dejesus, M. Jean, V. Darras, M. Thibault, M. Lavertu, M.D. Buschmann, A. Merzouki, Low molecular weight chitosan nanoparticulate system at low N:P ratio for nontoxic polynucleotide delivery, Int J Nanomedicine, 7 (2012) 1399-1414.

[22] P. Holzerny, B. Ajdini, W. Heusermann, K. Bruno, M. Schuleit, L. Meinel, M. Keller, Biophysical properties of chitosan/siRNA polyplexes: profiling the polymer/siRNA interactions and bioactivity, J Control Release, 157 (2012) 297-304.

[23] H. Ragelle, R. Riva, G. Vandermeulen, B. Naeye, V. Pourcelle, C.S. Le Duff, C. D'Haese, B. Nysten, K. Braeckmans, S.C. De Smedt, C. Jerome, V. Preat, Chitosan nanoparticles for siRNA delivery: optimizing formulation to increase stability and efficiency, J Control Release, 176 (2014) 54-63.

[24] J. Malmo, H. Sorgard, K.M. Varum, S.P. Strand, siRNA delivery with chitosan nanoparticles: Molecular properties favoring efficient gene silencing, J Control Release, 158 (2012) 261-268.

[25] H. Katas, H.O. Alpar, Development and characterisation of chitosan nanoparticles for siRNA delivery, J Control Release, 115 (2006) 216-225.

[26] K.A. Howard, U.L. Rahbek, X. Liu, C.K. Damgaard, S.Z. Glud, M.O. Andersen, M.B. Hovgaard, A. Schmitz, J.R. Nyengaard, F. Besenbacher, J. Kjems, RNA interference in vitro and in vivo using a novel chitosan/siRNA nanoparticle system, Mol Ther, 14 (2006) 476-484.

[27] X. Liu, K.A. Howard, M. Dong, M.O. Andersen, U.L. Rahbek, M.G. Johnsen, O.C. Hansen, F. Besenbacher, J. Kjems, The influence of polymeric properties on chitosan/siRNA nanoparticle formulation and gene silencing, Biomaterials, 28 (2007) 1280-1288.

[28] A.M. Ji, D. Su, O. Che, W.S. Li, L. Sun, Z.Y. Zhang, B. Yang, F. Xu, Functional gene silencing mediated by chitosan/siRNA nanocomplexes, Nanotechnology, 20 (2009) 405103.

[29] J. Malmo, A. Sandvig, K.M. Varum, S.P. Strand, Nanoparticle mediated P-glycoprotein silencing for improved drug delivery across the blood-brain barrier: a siRNA-chitosan approach, PLoS One, 8 (2013) e54182.

[30] C. Yang, S. Gao, J. Kjems, Folic acid conjugated chitosan for targeted delivery of siRNA to activated marcophages in vitro and in vivo, Journal of Materials Chemistry B, 2 (2014) 8608-8615.

[31] E.J. Nielsen, J.M. Nielsen, D. Becker, A. Karlas, H. Prakash, S.Z. Glud, J. Merrison, F. Besenbacher, T.F. Meyer, J. Kjems, K.A. Howard, Pulmonary gene silencing in transgenic EGFP mice using aerosolised chitosan/siRNA nanoparticles, Pharm Res, 27 (2010) 2520-2527.

[32] S. Gao, S. Hein, F. Dagnaes-Hansen, K. Weyer, C. Yang, R. Nielsen, E.I. Christensen, R.A. Fenton, J. Kjems, Megalin-mediated specific uptake of chitosan/siRNA nanoparticles in mouse kidney proximal tubule epithelial cells enables AQP1 gene silencing, Theranostics, 4 (2014) 1039-1051.

[33] S. Gao, F. Dagnaes-Hansen, E.J. Nielsen, J. Wengel, F. Besenbacher, K.A. Howard, J. Kjems, The effect of chemical modification and nanoparticle formulation on stability and biodistribution of siRNA in mice, Mol Ther, 17 (2009) 1225-1233.

[34] C. Yang, L. Nilsson, M.U. Cheema, Y. Wang, J. Frokiaer, S. Gao, J. Kjems, R. Norregaard, Chitosan/siRNA nanoparticles targeting cyclooxygenase type 2 attenuate unilateral ureteral obstruction-induced kidney injury in mice, Theranostics, 5 (2015) 110-123.

[35] C. Corbet, H. Ragelle, V. Pourcelle, K. Vanvarenberg, J. Marchand-Brynaert, V. Preat, O. Feron, Delivery of siRNA targeting tumor metabolism using non-covalent PEGylated chitosan nanoparticles: Identification of an optimal combination of ligand structure, linker and grafting method, J Control Release, 223 (2016) 53-63.

[36] M. Jean, M. Alameh, D. De Jesus, M. Thibault, M. Lavertu, V. Darras, M. Nelea, M.D. Buschmann, A. Merzouki, Chitosan-based therapeutic nanoparticles for combination gene therapy and gene silencing of in vitro cell lines relevant to type 2 diabetes, Eur J Pharm Sci, 45 (2012) 138-149.

[37] A. Tavakoli Naeini, O. Soliman, M. Alameh, M. Lavertu, M.D. Buschmann, Automated In-line Mixing System for Large Scale Production of Chitosan-based Polyplexes, Journal of Colloid and Interface Science, (2017).

[38] M. Jean, M. Alameh, M.D. Buschmann, A. Merzouki, Effective and safe gene-based delivery of GLP-1 using chitosan/plasmid-DNA therapeutic nanocomplexes in an animal model of type 2 diabetes, Gene Ther, 18 (2011) 807-816.

[39] M. Jean, F. Smaoui, M. Lavertu, S. Methot, L. Bouhdoud, M.D. Buschmann, A. Merzouki, Chitosan-plasmid nanoparticle formulations for IM and SC delivery of recombinant FGF-2 and PDGF-BB or generation of antibodies, Gene Ther, 16 (2009) 1097-1110.

[40] V. Balan, L. Verestiuc, Strategies to improve chitosan hemocompatibilities: A review, European Polymer Journal, 53 (2014) 171-188.

[41] D. Fong, P. Gregoire-Gelinas, A.P. Cheng, T. Mezheritsky, M. Lavertu, S. Sato, C.D. Hoemann, Lysosomal rupture induced by structurally distinct chitosans either promotes a type 1 IFN response or activates the inflammasome in macrophages, Biomaterials, 129 (2017) 127-138.

[42] E.C. Carroll, L. Jin, A. Mori, N. Munoz-Wolf, E. Oleszycka, H.B. Moran, S. Mansouri, C.P. McEntee, E. Lambe, E.M. Agger, P. Andersen, C. Cunningham, P. Hertzog, K.A. Fitzgerald, A.G. Bowie, E.C. Lavelle, The Vaccine Adjuvant Chitosan Promotes Cellular Immunity via DNA Sensor cGAS-STING-Dependent Induction of Type I Interferons, Immunity, 44 (2016) 597-608.

[43] M. Lavertu, S. Methot, N. Tran-Khanh, M.D. Buschmann, High efficiency gene transfer using chitosan/DNA nanoparticles with specific combinations of molecular weight and degree of deacetylation, Biomaterials, 27 (2006) 4815-4824.

[44] S. Nimesh, M.M. Thibault, M. Lavertu, M.D. Buschmann, Enhanced gene delivery mediated by low molecular weight chitosan/DNA complexes: effect of pH and serum, Mol Biotechnol, 46 (2010) 182-196.

[45] M. Thibault, S. Nimesh, M. Lavertu, M.D. Buschmann, Intracellular trafficking and decondensation kinetics of chitosan-pDNA polyplexes, Mol Ther, 18 (2010) 1787-1795.

[46] S.P. Strand, S. Lelu, N.K. Reitan, C. de Lange Davies, P. Artursson, K.M. Varum, Molecular design of chitosan gene delivery systems with an optimized balance between polyplex stability and polyplex unpacking, Biomaterials, 31 (2010) 975-987.

[47] M. Lavertu, Z. Xia, A.N. Serreqi, M. Berrada, A. Rodrigues, D. Wang, M.D. Buschmann, A. Gupta, A validated 1H NMR method for the determination of the degree of deacetylation of chitosan, J Pharm Biomed Anal, 32 (2003) 1149-1158.

[48] D. Veilleux, M. Nelea, K. Biniecki, M. Lavertu, M.D. Buschmann, Preparation of Concentrated Chitosan/DNA Nanoparticle Formulations by Lyophilization for Gene Delivery at Clinically Relevant Dosages, J Pharm Sci, 105 (2016) 88-96.

[49] ASTM E2524-08: Standard Test Method for Analysis of Hemolytic Properties of Nanoparticles, in, 2013.

[50] S.J. Evani, A.K. Ramasubramanian, Chapter 13: Hemocompatibility of Nanoparticles, in: Nanobiomaterials Handbook, CRC Press, 2001, pp. 1-17.

[51] M.H. Ullman-Cullere, C.J. Foltz, Body condition scoring: a rapid and accurate method for assessing health status in mice, Lab Anim Sci, 49 (1999) 319-323.

[52] V. Kumar, J. Qin, Y. Jiang, R.G. Duncan, B. Brigham, S. Fishman, J.K. Nair, A. Akinc, S.A. Barros, P.V. Kasperkovitz, Shielding of Lipid Nanoparticles for siRNA Delivery: Impact on Physicochemical Properties, Cytokine Induction, and Efficacy, Mol Ther Nucleic Acids, 3 (2014) e210.

[53] Y. Sato, H. Hatakeyama, M. Hyodo, H. Akita, H. Harashima, [Development of an efficient short interference RNA (siRNA) delivery system with a new pH-sensitive cationic lipid], Yakugaku Zasshi, 132 (2012) 1355-1363.

[54] Y. Sato, H. Hatakeyama, Y. Sakurai, M. Hyodo, H. Akita, H. Harashima, A pH-sensitive cationic lipid facilitates the delivery of liposomal siRNA and gene silencing activity in vitro and in vivo, J Control Release, 163 (2012) 267-276.

[55] O.M. Merkel, I. Rubinstein, T. Kissel, siRNA delivery to the lung: what's new?, Adv Drug Deliv Rev, 75 (2014) 112-128.

[56] C.M. McKee, M.B. Penno, M. Cowman, M.D. Burdick, R.M. Strieter, C. Bao, P.W. Noble, Hyaluronan (HA) fragments induce chemokine gene expression in alveolar macrophages. The role of HA size and CD44, J Clin Invest, 98 (1996) 2403-2413.

[57] D. Jiang, J. Liang, J. Fan, S. Yu, S. Chen, Y. Luo, G.D. Prestwich, M.M. Mascarenhas, H.G. Garg, D.A. Quinn, R.J. Homer, D.R. Goldstein, R. Bucala, P.J. Lee, R. Medzhitov, P.W. Noble, Regulation of lung injury and repair by Toll-like receptors and hyaluronan, Nat Med, 11 (2005) 1173-1179.

[58] A.D. Judge, V. Sood, J.R. Shaw, D. Fang, K. McClintock, I. MacLachlan, Sequence-dependent stimulation of the mammalian innate immune response by synthetic siRNA, Nat Biotechnol, 23 (2005) 457-462.

[59] C. River, CD-1 IGS Mouse Model Infromation Sheet, in, Charles River, http://www.criver.com/products-services/basic-research/find-a-model/cd-1-mouse, 2011.

[60] Invivofectamine® 3.0 Reagent, in, Life technologies, world wide web.

[61] S. Wada, S. Obika, M.A. Shibata, T. Yamamoto, M. Nakatani, T. Yamaoka, H. Torigoe, M. Harada-Shiba, Development of a 2',4'-BNA/LNA-based siRNA for Dyslipidemia and Assessment of the Effects of Its Chemical Modifications In Vivo, Mol Ther Nucleic Acids, 1 (2012) e45.

[62] D. Landesman-Milo, D. Peer, Toxicity profiling of several common RNAi-based nanomedicines: a comparative study, Drug Deliv Transl Res, 4 (2014) 96-103.

[63] R. Kedmi, N. Ben-Arie, D. Peer, The systemic toxicity of positively charged lipid nanoparticles and the role of Toll-like receptor 4 in immune activation, Biomaterials, 31 (2010) 6867-6875.

[64] Y. Huang, Q. Cheng, J.L. Ji, S. Zheng, L. Du, L. Meng, Y. Wu, D. Zhao, X. Wang, L. Lai, H. Cao, K. Xiao, S. Gao, Z. Liang, Pharmacokinetic Behaviors of Intravenously Administered siRNA in Glandular Tissues, Theranostics, 6 (2016) 1528-1541.

[65] Y. Huang, J. Hong, S. Zheng, Y. Ding, S. Guo, H. Zhang, X. Zhang, Q. Du, Z. Liang, Elimination pathways of systemically delivered siRNA, Mol Ther, 19 (2011) 381-385.

[66] J. Soutschek, A. Akinc, B. Bramlage, K. Charisse, R. Constien, M. Donoghue, S. Elbashir, A. Geick, P. Hadwiger, J. Harborth, M. John, V. Kesavan, G. Lavine, R.K. Pandey, T. Racie, K.G. Rajeev, I. Rohl, I. Toudjarska, G. Wang, S. Wuschko, D. Bumcrot, V. Koteliansky, S. Limmer, M. Manoharan, H.P. Vornlocher, Therapeutic silencing of an endogenous gene by systemic administration of modified siRNAs, Nature, 432 (2004) 173-178.

[67] J.D. Thompson, D.J. Kornbrust, J.W. Foy, E.C. Solano, D.J. Schneider, E. Feinstein, B.A. Molitoris, S. Erlich, Toxicological and pharmacokinetic properties of chemically modified siRNAs targeting p53 RNA following intravenous administration, Nucleic Acid Ther, 22 (2012) 255-264.

[68] S. Boeckle, K. von Gersdorff, S. van der Piepen, C. Culmsee, E. Wagner, M. Ogris, Purification of polyethylenimine polyplexes highlights the role of free polycations in gene transfer, J Gene Med, 6 (2004) 1102-1111.

[69] U. Lungwitz, M. Breunig, T. Blunk, A. Gopferich, Polyethylenimine-based non-viral gene delivery systems, Eur J Pharm Biopharm, 60 (2005) 247-266.

[70] J.C. Fernandes, P. Eaton, H. Nascimento, L. Belo, S. Rocha, R. Vitorino, F. Amado, J. Gomes, A. Santos-Silva, M.E. Pintado, F.X. Malcata, Effects of chitooligosaccharides on human red blood cell morphology and membrane protein structure, Biomacromolecules, 9 (2008) 3346-3352.

[71] I. Sovadinova, E.F. Palermo, R. Huang, L.M. Thoma, K. Kuroda, Mechanism of polymer-induced hemolysis: nanosized pore formation and osmotic lysis, Biomacromolecules, 12 (2011) 260-268.

[72] B.D. Ratner, S.J. Bryant, Biomaterials: where we have been and where we are going, Annu Rev Biomed Eng, 6 (2004) 41-75.

[73] E. Kolaczkowska, P. Kubes, Neutrophil recruitment and function in health and inflammation, Nat Rev Immunol, 13 (2013) 159-175.

[74] J. Hol, L. Wilhelmsen, G. Haraldsen, The murine IL-8 homologues KC, MIP-2, and LIX are found in endothelial cytoplasmic granules but not in Weibel-Palade bodies, J Leukoc Biol, 87 (2010) 501-508.

[75] Y. Okamoto, R. Yano, K. Miyatake, I. Tomohiro, Y. Shigemasa, S. Minami, Effects of chitin and chitosan on blood coagulation, Carbohydrate Polymers, 53 (2003) 337-342.

[76] R.A. Muzzarelli, Chitins and chitosans as immunoadjuvants and non-allergenic drug carriers, Mar Drugs, 8 (2010) 292-312.

[77] C.L. Bueter, C.K. Lee, J.P. Wang, G.R. Ostroff, C.A. Specht, S.M. Levitz, Spectrum and mechanisms of inflammasome activation by chitosan, J Immunol, 192 (2014) 5943-5951.

[78] C.L. Bueter, C.K. Lee, V.A. Rathinam, G.J. Healy, C.H. Taron, C.A. Specht, S.M. Levitz, Chitosan but not chitin activates the inflammasome by a mechanism dependent upon phagocytosis, J Biol Chem, 286 (2011) 35447-35455.

[79] A. Elouahabi, J.M. Ruysschaert, Formation and intracellular trafficking of lipoplexes and polyplexes, Mol Ther, 11 (2005) 336-347.

[80] P. Miossec, Diseases that may benefit from manipulating the Th17 pathway, Eur J Immunol, 39 (2009) 667-669.

[81] L.M. Serfilippi, D.R. Pallman, B. Russell, Serum clinical chemistry and hematology reference values in outbred stocks of albino mice from three commonly used vendors and two inbred strains of albino mice, Contemp Top Lab Anim Sci, 42 (2003) 46-52.

[82] U. Flierl, T.L. Nero, B. Lim, J.F. Arthur, Y. Yao, S.M. Jung, E. Gitz, A.Y. Pollitt, M.T. Zaldivia, M. Jandrot-Perrus, A. Schafer, B. Nieswandt, R.K. Andrews, M.W. Parker, E.E. Gardiner, K. Peter, Phosphorothioate backbone modifications of nucleotide-based drugs are potent platelet activators, J Exp Med, 212 (2015) 129-137.

[83] A.O. Hosten, BUN and Creatinine, in: H.K. Walker, W.D. Hall, J.W. Hurst (Eds.) Clinical Methods: The History, Physical, and Laboratory Examinations, Boston, 1990.

[84] Y. Lin, Y. Li, X. Wang, T. Gong, L. Zhang, X. Sun, Targeted drug delivery to renal proximal tubule epithelial cells mediated by 2-glucosamine, J Control Release, 167 (2013) 148-156.

[85] S.G. Jones, T. Ito, A.O. Phillips, Regulation of proximal tubular epithelial cell CD44-mediated binding and internalisation of hyaluronan, Int J Biochem Cell Biol, 35 (2003) 1361-1377.

[86] A. Ruggiero, C.H. Villa, E. Bander, D.A. Rey, M. Bergkvist, C.A. Batt, K. Manova-Todorova, W.M. Deen, D.A. Scheinberg, M.R. McDevitt, Paradoxical glomerular filtration of carbon nanotubes, Proc Natl Acad Sci U S A, 107 (2010) 12369-12374.

[87] J.E. Zuckerman, A. Gale, P. Wu, R. Ma, M.E. Davis, siRNA delivery to the glomerular mesangium using polycationic cyclodextrin nanoparticles containing siRNA, Nucleic Acid Ther, 25 (2015) 53-64.

[88] K.M. Tsoi, S.A. MacParland, X.Z. Ma, V.N. Spetzler, J. Echeverri, B. Ouyang, S.M. Fadel, E.A. Sykes, N. Goldaracena, J.M. Kaths, J.B. Conneely, B.A. Alman, M. Selzner, M.A. Ostrowski, O.A. Adeyi, A. Zilman, I.D. McGilvray, W.C. Chan, Mechanism of hard-nanomaterial clearance by the liver, Nat Mater, 15 (2016) 1212-1221.

[89] M. Thibault, M. Astolfi, N. Tran-Khanh, M. Lavertu, V. Darras, A. Merzouki, M.D. Buschmann, Excess polycation mediates efficient chitosan-based gene transfer by promoting lysosomal release of the polyplexes, Biomaterials, 32 (2011) 4639-4646.

[90] P.L. Ma, M. Lavertu, F.M. Winnik, M.D. Buschmann, New insights into chitosan-DNA interactions using isothermal titration microcalorimetry, Biomacromolecules, 10 (2009) 1490-1499.

[91] A. Eguchi, X. De Mollerat Du Jeu, C.D. Johnson, A. Nektaria, A.E. Feldstein, Liver Bid suppression for treatment of fibrosis associated with non-alcoholic steatohepatitis, J Hepatol, 64 (2016) 699-707.

[92] H.A. Franch, S. Sooparb, J. Du, N.S. Brown, A mechanism regulating proteolysis of specific proteins during renal tubular cell growth, J Biol Chem, 276 (2001) 19126-19131.

[93] S.C. Semple, A. Akinc, J. Chen, A.P. Sandhu, B.L. Mui, C.K. Cho, D.W. Sah, D. Stebbing, E.J. Crosley, E. Yaworski, I.M. Hafez, J.R. Dorkin, J. Qin, K. Lam, K.G. Rajeev, K.F. Wong, L.B. Jeffs, L. Nechev, M.L. Eisenhardt, M. Jayaraman, M. Kazem, M.A. Maier, M. Srinivasulu, M.J. Weinstein, Q. Chen, R. Alvarez, S.A. Barros, S. De, S.K. Klimuk, T. Borland, V. Kosovrasti, W.L. Cantley, Y.K. Tam, M. Manoharan, M.A. Ciufolini, M.A. Tracy, A. de Fougerolles, I. MacLachlan, P.R. Cullis, T.D. Madden, M.J. Hope, Rational design of cationic lipids for siRNA delivery, Nat Biotechnol, 28 (2010) 172-176.

Chapter 8 GENERAL DISCUSSION

This study was carried out with the purpose of identifying molecular properties favoring efficient, and non-toxic, *in vitro and in vivo* delivery of siRNA (Objective 1 & 2). Furthermore, the efficacy of selected formulations to induce potent functional gene knockdown was tested in mice after thorough profiling of hemocompatibility, single ascending dose acute toxicity and biodistribution (Objective 3). This study demonstrates the importance of chitosan degree of deacetylation (charge density), polymer length, and N:P ratio on nanoparticle physicochemical properties and biological performance. Results showed that nanoparticle uptake and target gene knockdown positively correlated with an increase in all three parameters, with polymer length and N:P ratio playing positive but marginal roles. Systemic administration of sub-hemolytic doses revealed extrahepatic distribution to the cytoplasm of renal proximal epithelial tubular cells. Nanoparticles were non-toxic compared to their lipid counterparts and had no impact on clinical signs, hematological and serological biomarkers, cytokine induction and changes in body weight. Functional target knockdown reached 50-60% in renal cortices.

Our data show that chitosan degree of deacetylation (DDA), or the number of protonatable amines (NH_2), played a predominant role in dictating successful *in vitro* knockdown. The positive effect of high charge density, achieved at high DDA, on knockdown efficiency can be attributed to several factors including increased binding affinity for siRNA, increased electrostatic interaction with cell membranes and increased endosomal buffering capacity. None of the previous studies [20-23, 25, 27] investigating the influence of chitosan molecular parameters on siRNA delivery examined the biological relevance of DDA. Instead, polymer length and the amine to phosphate molar ratio (N:P) was varied to optimize *in vitro* knockdown efficiency. In our study, the molecular weight, or chain length (Mn), and the N:P ratio had a positive but marginal effect on knockdown efficiency. This observation is in agreement with results reported previously [20, 29] where increased polymer length and N:P ratio had minimal effects on target knockdown efficiency. However, and as hypothesised in Objective 1, our findings are distinctly different from previous work on chitosan mediated plasmid delivery (pDNA), where a fine balance or the modulation of either the molecular weight (chain length) or the degree of deacetylation (charge density) was required in order to reduce nanoparticle stability to a threshold where particles are able to protect pDNA and promote intracellular dissociation for efficient transgene expression [37, 39, 40]. These differences could

be due to different affinities between chitosan and the nucleic acids. pDNA is a large and flexible molecule able to form multiple interchain bridges with high affinity [210] (avidity) with the polymer compared to the short and rigid siRNA molecule [29].

In the current study, the importance of chain length (Mn) and N:P ratio was demonstrated below a certain Mn threshold where nanoparticle internalization and target knockdown were both reduced when nanoparticles were formulated below 10 kDa. Low *in vitro* performance was not only attributed to nanoparticle integrity at pH above chitosan pKa (6.5-6.9) but also due to the presence of serum. Low Mn formulations showed inferior performance in presence of serum and required an increase in Mn or N:P ratio for improved potency, suggesting nanoparticle destabilization occurring through competitive displacement with negatively charged serum components. The negative effect of serum on nanoparticle integrity has been previously demonstrated for cationic liposomes [126] and chitosan-PEI hybrid nanoparticles [21] with the inclusion of helper lipids i.e DOPE and cholesterol or surface modification (e.g. PEGylation or HA coating) abrogating these negative effects. Although we could not elucidate the precise effect of serum, heparin and albumin were found to have antagonistic effects on siRNA release with heparin increasing and albumin decreasing release partially confirming our hypothesis (Hypothesis 1). These opposed effects confirm previous findings with albumin antagonizing the negative effects of heparin and oleic acid on cationic liposomes formulated without helper lipids [126]. In our study, cooperation between competing serum components, ionic strength, pH and their effects on nanoparticles is believed to drive the need for higher Mn and N:P ratio for particle stability. This observation was confirmed in the presence of relevant *in vivo* concentrations of serum, where nanoparticle performance decreased in a Mn and N:P dependent manner.

Nanoparticle size and surface charge are two important parameters that affect colloidal stability, pharmacokinetics, biocompatibility and nanoparticle-cell interactions [237]. In this study, size increased with increasing polymer length (Mn) and ionic strength. In contrast to size, nanoparticle ζ-potential, increased with increased DDA, Mn and N:P ratio and decreased with increasing ionic strength. As expected, an increase in the number of ionizable amine groups (NH_2) per chain (DDA), increases the charge density of the polymer and consequently has a direct and positive influence on ζ-potential. However, surface charge is not, at least theoretically, expected to increase with increasing Mn since **1)** the pairing of chitosan positive charge and siRNA negative charge groups is not obviously Mn-dependent and **2)** an increase in size, due to an increase in Mn, is translated to

a lower electrophoretic mobility and thus a lower apparent ζ-potential. Nevertheless, this Mn-dependent increase in ζ-potential may be due to chains that are partly bound at the surface resulting in pendant chains that are longer for higher Mn that increase surface charge, or possibly more chitosan chains are bound in particles through greater cooperativity of binding to siRNA. The effect of ionic strength on colloidal stability over time showed strong aggregation and could, therefore, influence nanoparticle performance *in vivo* through unintended blood interactions. In this study, ζ-potential positively correlated with knockdown efficiency confirming previous reports [37, 238]. However, a lack of correlation between size and EGFP knockdown was observed and could be explained by serum dependent size stabilization occurring through rapid protein corona formation [38]. Nimesh *et al* found that the size of chitosan-based nanoparticles rapidly increases in the presence of serum then stabilizes around 300-500 nm without loss in performance [38].

siRNA and/or vector-based off-target effects continue to pose problems at the bench and the bedside [239-241]. A thorough evaluation of off-target effects was conducted in our study with non-targeting siRNA (siNT) and mock transfections (M) performed in parallel to treatments. The delivery of siNT showed insignificant knockdown while mock transfections mediated a slight increase in EGFP expression for some chitosans. In both cases, target knockdown and/or expression reached a maximum of ±10% indicating a relatively safe profile. The pattern of EGFP knockdown and/or expression seem to follow a trend where long *vs* short chains appear to have opposite effects. This is reminiscent of the marginal toxicity observed when assessing metabolic activity in transfected cells. Therefore, the decrease in EGFP expression for both siNT and mock transfections observed with short chains, and independent of the N:P ratio, is possibly associated with marginal metabolic toxicity observed at low Mn. Consistent with this idea, Malmo et al [20] found that mock transfection with fully deacetylated chitosan consistently reduced EGFP expression by about 10% and that a dose-dependent response was associated with around 0-25% decrease. Although no metabolic decrease was mentioned in [20], the number of seeded cells was above the linear response of the assay and therefore, toxicity was not accurately estimated for correlation with mock-induced EGFP knockdown. However, this toxicity issue was indirectly highlighted during qPCR calibration relative to siNT treated instead of non-treated cells, which according to the authors was justified by differences in confluence between chitosan treated and untreated cells [20].

Our results suggested that chitosan, and depending on its DDA, Mn and N:P ratio, disturbs global gene expression indicative of a certain parallelism with linear polyethyleneimine (lPEI) [242] and cationic lipids [243]. PEI has been shown to induce the expression of apoptotic genes, inflammation and oxidative stress responses while cationic lipids were generally associated with increased expression of stress-related genes. The impact of chitosan on the global transcriptome might be due to random binding of chitosan with intracellular nucleic acids or molecular machines through electrostatic or hydrophobic interactions.

Nanoparticle toxicity is a major hurdle for clinical translation and could be due to 1) physical interactions with vesicular and mitochondrial membranes [244], 2) disruption of normal protein synthesis via electrostatic interaction with polyanionic component in the cytoplasm, and/or 3) injuries from hydrolytic enzymes released during endosomal escape [237]. Formulations used in this study were relatively non-toxic with around 10±10% reduction in cell viability confirming our hypothesis (Objective 2). Toxicity increased with lower molecular weight chitosan with high DDA. Mock transfections demonstrated that toxicity is payload independent. These results are affirmed in other studies, where chitosan showed minimal toxicity when formulated at N:P ratio ranging from 5-60 [20, 22, 27, 29, 33, 34, 36, 37]. In contrast, Liu et al. [23] have shown significantly reduced metabolic activity in H1299 cells. The apparent toxicity is probably due to the extremely high free chitosan content (N:P 150), serum free conditions and assay specific differences. Chitosan translocation into the nucleus could potentially induce genetic damage either through electrostatic interactions, hydrolysis from co-impurities or through physical obstruction during chromosomal separation at the anaphase. We found DNA damage to be statistically insignificant indicating that neither the nanoparticle nor the ascending concentrations of free chitosan or siRNA sequence were genotoxic and therefore confirming our hypothesis (Objective 2).

The cationic nature of chitosan favors interaction with cellular blood components that could potentially have deleterious effects *in vivo*. However, this aspect of probable toxicity has been neglected [20-25, 27-29, 33-40, 245] with *in vivo* reports often using extremely high N:P ratios without reporting any signs of toxicities [22, 24, 41-44]. However, high N:P ratio could pose serious adverse effects in light of reports suggesting blood-material interaction [30]. In our study, we showed that uncoated chitosan NPs display dose and molecular weight dependent hemolytic and hemagglutination properties that could be abrogated with the use of nanoparticles prepared at low nitrogen to phosphate ratio (N:P ratio) or following HA coating confirming our hypothesis

(Objective 2) and consequently highlighting careful dosing to avoid hemotoxicity and/or embolism. The hemolytic/hemagglutination potential of chitosan could occur through interaction with negatively charged erythrocyte (RBC) membranes via a pore forming mechanism, followed by a subsequence osmotic shock, and/or through regulation of surface protein and increase in surface roughness as demonstrated for methacrylate based polymers [246] and chitooligosaccharides [247], respectively. In addition, the interaction between chitosan amino groups and acidic groups on erythrocytes could promote polyelectrolyte complex formation leading to RBC aggregation as seen for other biomaterials [248]. NP coating with HA, a biocompatible and negatively charged molecule, eliminated both hemolysis and RBC aggregation possibly due to limited interaction with erythrocyte membranes through electrostatic repulsion and reduced interaction with serum components permitting dose increase to at least 8 mg/kg. In contrast to uncoated chitosan, lipid nanoparticles (LNPs) did not show dose-dependent hemolysis probably due to surface PEGylation implied by the quasi-neutral surface charge. Shielding with polyethylene glycol (PEG) has been the method of choice to limit LNP hemolysis with high PEG density required for improved biocompatibility and reduced cytokine induction [249] and is incorporated in most if not all LNPs that are commercially available or in clinical development.

Immune stimulating properties of nanoparticles or their payloads represent one of the major hurdles for clinical translation [250]. In the current study, uncoated and HA-coated chitosan NPs did not induce type I pro-inflammatory cytokines (IL-1β, TNF-α, IFN-γ and IL-6) except for a small but statistically insignificant increase in KC, a human IL-8 homolog indicating a non-immunogenic effect 4 hours post-administration. KC is a chemoattractant cytokine with distinct, or quasi-unique target specificity for neutrophils and is produced by a variety of epithelial and endothelial cells (EC) [251, 252]. The absence of neutrophil invasion, 24 hours post-administration, in main organs and in kidney tissues where chitosan has been found to accumulate suggests an epithelial cell-independent mechanism of KC expression. However, platelet activation, aggregation and cytokine release (i.e. TGF-β1, PDGF-AB) have been observed following *in vitro* assessment of chitosan in hemostatic aggregation experiments [253] suggesting that KC levels post-administration of chitosan could be attributed to platelet activation and their release from Weibel-Palade bodies. The adjuvant and immune stimulating effect of chitosan have been well described both *in vitro* and *in vivo*, and involve the activation of dendritic cells, and the secretion of Type-I pro-inflammatory cytokines (i.e. IFN-α/β/γ, IL-1β, TNF-α …), through NLRP3 inflammasome activation and the

recently discovered cGAS/STING pathway for lower DDA (80%) chitosans [31, 32, 208, 254, 255]. The apparent contradiction between the lack of cytokine activation and the literature could be explained by differences in routes of administration, dose, degrees of deacetylation and priming of immune cells. For instance, most studies demonstrating the anti-allergic properties of chitin and chitosan (Th_2 inhibition) via the expression of Type-I cytokines have been tested *in vitro* and/or using the intranasal, intraperitoneal, intraocular and intravaginal routes of administration [32, 208]. However, in all these studies, priming strategies were used and could explain cytokine induction consistent with the finding that chitosan stimulated significant cytokine release only from primed BMMΦ [254]. In this study, we did not measure cytokine levels at subsequent time points which could also explain the absence of cytokine induction, that only appeared around 9 h and peaked 24 hours post stimulation [32]. Other considerations such as Mn, contaminants, particle size may also contribute to the observed difference.

Lipid nanoparticles (LNPs) and liposomes are known immune activators with several groups demonstrating that immune stimulation is governed by the lipid and cationic head groups, and/or the combination with the nucleic acid payload [14, 76, 81, 249, 256]. In this study, Invivofectamine® LNPs demonstrated a dose-dependent induction of IFNγ, IL-6 and KC and a minor TNF-α increase in serum. Immune stimulation was abrogated with the 2'OMe modified siRNA confirming previous results with LNPs [76, 81] highlighting major differences with our chitosan system where cytokine induction was not observed with any payload. In this study, we chose TNF-α because it is a potent cytokine that is invariably activated, and immediately released, by all Toll-Like receptors (TLRs) [257, 258]. Therefore, the TNF-α stimulation observed with lipid nanoparticle used in this study, while not induced with chitosan, suggests a TLR based mechanism of immune induction reminiscent of Chol:DSPC:DOTAP (3:1:1) cationic liposomes [14].

In the absence of cytokine induction, hematocrit (HCT) and total hemoglobin (Hb) levels were unchanged relative to PBS and within the normal reference ranges of CD-1® (ICR) mice indicating a relatively safe and non-hemolytic profile for all formulation tested. Lower Hb, but not HCT, levels compared with the reference range could be observed intragroup and might be due to differences in gender, age and quantification techniques used to establish the reference ranges [259, 260]. However, Hb levels were comparable to the PBS group and considered normal in this study. In contrast to chitosan NP, and their HA coated form, LNPs used in this study sharply decreased platelet counts consistent with previous observations [76, 256]. Thrombocytopenia was only

observed with LNPs confirming previous data [76]. Interestingly, lymphocyte counts decreased with both lipid and chitosan based formulations when formulated with the native immune stimulatory sequence [81]. All other parameters tested such as circulating basophils, eosinophils, monocytes, and neutrophils were normal and within the normal standard ranges for CD-1® (ICR) mice [259, 260].

Chitosan accumulation in the kidney did not impair kidney function since levels of blood urea nitrogen and creatine remained normal. However, one major drawback of this study consists of the lack of BUN and creatinine measurements in urine which are more predictive than their serum counterparts as they permit the computation of the glomerular filtration rate (GFR), a clinical indicator of renal function. BUN and creatinine, are also indirect indicators of liver health, and therefore support the absence of liver toxicity as indicated by normal transaminase levels. In contrast to uncoated and HA coated NPs, lipid nanoparticles showed a typical dose-dependent increase in transaminases accompanied by a reduction in body weight indicating transient liver toxicity and highlighting systemic toxicity [14, 256, 261]. In general, a decrease in body weight has been observed with lipid nanoparticles [14, 76, 256, 261] and could be attributed to either the lipids [14, 256, 261] or to properties of the encapsulated nucleic acid payload [76]. In the present study, the decrease in body weight is believed to be due to the general toxicity induced by the lipid system, since injections were performed with a non-immune stimulatory LNA modified sequence containing methylated sugars and PS modification in the backbone. Lipopolysaccharide (LPS) treatment increased BUN, and decreased Cr levels in serum typical of catabolic processes induced following induction of cytokines in fever like symptoms or infections [262], and further confirming that negative data obtained with chitosan are not due to assay dependent technical issues. Alkaline phosphatase (AP), an enzyme endowed with LPS detoxifying properties decreased following I.V. injection of LPS, can probably be attributed to malnutrition and weight loss, which correlated with overt clinical signs including lethargy, decreased reactivity to stimuli and changed in the general appearance of mice. However, and under the current experimental conditions, we cannot rule out another, less possible but valid hypothesis to explain AP reduction in serum, likely due to AP depletion following LPS detoxification. The absence of toxicity was confirmed by histopathology with no morphological changes, including an absence of infiltrating neutrophils, apoptotic and/or necrotic cells observed in main organs.

In contrast to polyethyleneimine (PEI), intravenous administration of chitosan-siRNA nanoparticles showed exclusive accumulation in the kidneys. Finer examination of kidney structures revealed a punctate pattern of siRNA [39] in the cytoplasm of the proximal epithelial tubular cells (PTECs) suggesting translocation through the glomerular basement membrane (GBM). PEI a cationic polymer that spontaneously form nanoparticles with similar physicochemical properties and colloidal stability compared to chitosan has been found to accumulate in lungs, liver, spleen and kidneys following intravenous administration [41]. Although naked siRNA filters through the kidneys [263] and a fraction accumulate in PTECs [263], our data clearly indicate a role for chitosan in increasing the efficiency of siRNA accumulation into PTECs probably through glucosamine (Glc)-Megalin interaction and subsequent internalization [42, 264]. In contrast to our hypothesis (Objective 3), hyaluronic acid coating modified physicochemical properties of nanoparticles without alteration of the kidney-targeted biodistribution pattern.

PTECs express at least five CD44 splice variants that play an important role in HA internalization and could be blocked using anti-CD44 antibodies [265]. In addition, HA has been shown to increase colloidal stability of NPs in serum [21] but could shed in circulation, therefore, exposing the chitosan-siRNA core (N:P 2) that subsequently accumulate in PTEC via Megalin-mediated endocytosis. In either case, nanoparticle translocation through the GBM remains to be elucidated mechanistically since fenestration and the extracellular matrix limit nanoparticle translocation and diffusion. Translocation and PTEC accumulation could be achieved through either non-conventional mechanisms as observed with 200-300 nm carbon nanotubes [266] or through nanoparticle disassembly at the highly negative GBM and reassembly in the lumen as proposed for cyclodextrin-based nanoparticles [174]. Alternative delivery through the fenestrated peritubular capillaries could occur but also faces similar diffusion challenges through the negatively charged interstitium.

Irrespective of the mechanism involved, chitosan based nanoparticles, not only accumulate in the cytoplasm of PTEC, but also induce functional knockdown without causing deleterious effects on body weight. In this study, *in vivo* efficacy was demonstrated through functional GAPDH knockdown where both low Mn (10 kDa) chitosans demonstrated the highest efficacy (~ 40-50% knockdown at the protein level). Western blot analysis and qualitative immunohistochemistry confirmed the enzymatic activity data and showed cortex specific knockdown. In contrast to the *in vitro* data, high Mn (120 kDa) chitosans did not outperform their low Mn counterparts emphasizing

fundamental differences between *in vitro* and *in vivo* validation. Gao *et al* [42] demonstrated that low Mn (40 kDa) fully deacetylated chitosan is able to achieve around 50 % knockdown in PTECs when formulated at N:P ratio of 60 with higher Mn and/or lower N:P ratio unable to distribute to the kidneys. In contrast, we have demonstrated that low and high Mn – except for the high Mn fully decetylated chitosan – are able to achieve 40-50% target knockdown when formulated at low N:P ratio. The discrepancy between our data and those presented in [42] \ is most probably due to aggregation since physicochemical properties of the injected nanoparticles [42] are questionable with non-homogenous and polydisperse NPs (400-800 nm). The distribution of naked siRNA in mice exhibited a predictable pattern based on the known propensity of oligonucleotides to accumulate in the kidneys [41, 267, 268] and resulted in poor (~ 15%) knockdown confirming prior reports [263, 268]. Formulation with chitosan significantly increased knockdown efficiency by~30-35% compared to fresh naked siRNA suggesting a clear and positive role of the delivery system (3-fold improvement).

HA-coated NPs accumulated in the kidney but did not induce target knockdown even at higher doses compared to uncoated nanoparticles consequently refuting our hypothesis (Objective 3). This result could be explained by the need for excess chitosan (N:P = 5:1 in uncoated *vs* 2.5:1 in HA coated) to promote endosomal release [216], possibly through the proton sponge effect. As a consequence, it is likely that HA coated NPs formulated at an N:P:C 2.5:1:2 are able to translocate to the cytoplasm of PTEC but remain sequestrated in endolysosomal compartments due to poor endosomal buffering capacity and reduced proton sponge effect. In addition, the negatively charged HA molecule, assumed to colocalize with chitosan, could contribute to lower endosomal release by masking positive charge in the endosome, therefore, reducing the capacity of endocytosed chitosan to mediate endosomal rupture. In contrast to HA-coated NPs (N:P:C of 2.5:1:2), uncoated chitosan formulations prepared at an N:P ratio of 5 contain around 70% free chitosan [210] that could colocalize in PTEC endosomes and promote endosomal rupture, explaining the observed efficacy.

Compared to the potency of lipid systems (~70-90%) in advanced pre-clinical or clinical development [121, 139, 140, 142], functional target knockdown obtained with our system (~40-50%) appears to be lower. However, considerations such as half-life of the target gene (GAPDH

versus factor VII), potency of the payload, and tissue dependent technical challenges could explain these differences. Accurate estimation of target knockdown using conventional techniques, such as quantitative PCR, enzymatic activity or immunoblotting, depends on **1)** the abundance of the target cell type (fraction of cells transfected relative to the organ), **2)** the ability of the delivery system to transfect different cell types composing an organ and/or **3)** the tissue – or cell – specificity of a target gene. Inasmuch as chitosan displays specific targeting to PTECs, a cell-type that represents a minor fraction of the cells in the kidney, assessment of target knockdown using conventional techniques is necessarily underestimated unless the target gene is PTEC specific and only expressed in this cell subtype. In contrast, LNPs accumulate in hepatocytes, the predominant cell type in the liver, permitting non-biased (accurate) estimation of target knockdown. Therefore, functional knockdown obtained in this report underestimates the true efficiency of our system to silence a target gene in PTECs, and suggest that precise evaluation of target knockdown requires the development of novel methods capable of estimating knockdown in a specific subset of cells composing an organ.

Taken together, our findings are of critical importance to siRNA delivery since extra-hepatic targeting could be naturally achieved without chemical modifications or ligand targeting and accumulation occurred in PTECs, with functional target knockdown around 50% in kidney cortex, further differentiating this system from cyclodextrin-based NPs that accumulate in glomeruli and podocytes [174]. As a consequence, unmodified chitosan-siRNA nanoparticles could potentially be used for the treatment of PTEC associated kidney fibrotic diseases.

Chapter 9 CONCLUSION AND RECOMMENDATIONS

The work presented in this thesis demonstrates the application of chitosan in nucleic acid delivery *in vitro* and *in vivo* and highlight the role of chitosan molecular parameters on nanoparticle physicochemical characteristics and bioactivity. In a first study, we showed that a simple method based on the enzymatic digestion of chitosan permits the extraction and recovery of total RNA for subsequent quantification of gene expression and downstream molecular analysis (**Chapter 4**). In addition, the method was found suitable for the removal of membrane-bound chitosan during flow cytometry-based assessment of nanoparticle uptake and demonstrated that assessment of nanoparticle internalization is biased by ~10-15% (**Chapter 4**). In a subsequent study, we found that nanoparticles can be formulated at a low N:P ratio (N:P 5), and induce potent and nontoxic *in vitro* knockdown in multiple cell lines. In contrast to previously published data, we showed that low molecular weight chitosan, prepared at low N:P ratio, effectively complex nucleic acids into stable particles and protect the payload from nuclease digestion in slightly acidic conditions. The modification of the electrophoresis buffer from basic to slightly acidic showed that nanoparticles with low N:P ratio could be selected based on their stability (**Chapter 5**).

In a subsequent study (**Chapter 6**), we found the following: **1)** both *in vitro* nanoparticle internalization and target gene knockdown were maximized with a concomitant increase in the degree of deacetylation, molecular weight and N:P ratio, **2)** minimal molecular weight (10 kDa) is required for efficient transfection and target knockdown, **3)** serum had a negative impact on the transfection efficiency of low molecular weight formulations, which could be abrogated by increasing both Mn and the N:P ratio, **4)** increasing serum concentrations decreased knockdown efficiency in a dose-dependent manner, with formulations at high Mn/N:P ratio being the most performant due to increased stability, **5)** *in vitro* treatment with chitosan influenced the expression of a panel of reference genes and **6)** irrespective of the Mn and N:P ratio, absence of genotoxic effect at 4 and 48 hours were demonstrated in this study. These findings revealed the exact molecular requirement for potent and nontoxic *in vitro* target knockdown and the selection of optimal formulation for further development and testing in animals.

In vivo, chitosan was found to accumulate in the proximal tubules epithelial cells of the kidney (**Chapters 6 & 7**), with undetectable toxic effects *as per* evaluation of serological and hematological biomarkers (**Chapter 7**). In addition, chitosan did not induce pro-inflammatory cytokines at the maximum tested dose for both uncoated and hyaluronic acid-coated formulations further confirming the safety of this system in comparison with Invivofectamine® (Lipid nanoparticle) (**Chapter 7**). Perhaps the most important finding in this thesis, along with the absence of toxic effects (**Chapter 7**), is the demonstrated potent functional gene knockdown in kidney cortices (**Chapter 6 & 7**). Interestingly, nanoparticle surface decoration (electrostatic) with hyaluronic acid did not impair biodistribution but mitigated potency (**Chapter 7**).

The comprehensive analysis of diverse factors studied in this research project revealed underlying important factor for the development of chitosan-based nanoparticles for the delivery of small interfering RNA. In addition, these studies demonstrated the safety of specific formulations for *in vivo* application and in a proof of concept study showed potent functional gene knockdown in kidney cortices. In sum, formulations with extrahepatic capabilities were identified and are believed to have promising potential for the treatment of kidney related diseases and cancer. All through this thesis, we realized significant progress in advancing the field of chitosan for the delivery of short oligonucleotides; however, with each finding, technical challenge, and conclusion, more questions were open for contemplation, which when answered can make further contributions toward the development of advanced chitosan-based systems intended to deliver small interfering RNA *in vivo*.

Although beyond the scope of this research, the following recommendations are worth considering in the future:

1. *Demonstration of higher knockdown in PTEC isolates* – In this study, nanoparticles were shown to accumulate in kidney cortices, specifically in the *proximal epithelial tubular cells* (PTECs). Since PTECs represent only a fraction of the renal cortex, assessment of target gene knockdown is undoubtedly underestimated using conventional techniques that averages expression levels across all cell types of a tissue sample. Therefore, isolation of primary PTECs, following intravenous administration of nanoparticles, would allow for

further development in the efficacy of the delivery system through increased PTEC specific knockdown.

2. *Evaluation of therapeutic efficiency in a model of kidney fibrosis* – Proximal epithelial tubular cells have been demonstrated to cause fibrotic diseases through activation of the TGF-β pathway. The unilateral ureteral obstruction (UUO) or streptozotocin-induced type-1 diabetes models are relatively simple models of renal fibrosis mimicking features in humans. These models could be used to demonstrate the therapeutic effect of nanoparticles targeting a TGF-β downstream target, known as SMAD-3.
3. *Validation of hypothesis for limited HA-coated nanoparticle efficacy* – HA-coated nanoparticles demonstrated excellent biocompatibility and safety profiles but failed to induce target gene knockdown. We, therefore, hypothesized that the lack of free chitosan reduces endosomal escape, and supported our claims, with published observations by members of our group. Here we propose to validate our hypothesis by injecting HA coated nanoparticles, followed by an injection of free chitosan. This fraction of chitosan colocalize in the endosome promoting the release of HA coated samples and subsequent gene knockdown. We also propose to test other hyaluronic acid polymers with different degrees of sulfation and molecular weight to exclude a specific problem with the HA polymer used in this thesis (HA, 866 kDa).
4. *Characterization of endosomal escape and comparison with lipid nanoparticles* – As mentioned throughout this thesis, endosomal escape is the most rate-limiting step in gene delivery. Improvement of target knockdown and therapeutic window can be achieved by improving endosomal escape. In comparison with lipid nanoparticle, awareness in the endosomal escape mechanisms for chitosan nanoparticle is embryonic with most studies hypothesizing on the mechanism of release without its quantitative assessment. Prior studies in our laboratory determined the kinetics of escape for plasmid DNA. Here we suggest to study endocytosis, and endosomal escape in primary PTEC cultures using live cell imaging and spinning disk confocal microscopy.
5. *Improvement of colloidal stability and inclusion of endosomolytic moieties* – Colloidal stability in the presence of high ionic strength and serum protein need to be addressed for uncoated nanoparticles through PEGylation or surface coating (i.e. polyacrylic acid). However, limited *in vivo* efficiency, probably due to reduced endosomal release in the

absence of free chitosan might limits strategies to improve colloidal stability. As a consequence, we suggest the inclusion of endosomolytic moieties in nanoparticle during the colloidal stabilization process to circumvent poor endosomal release.

6. *Evaluation of repeated dose toxicity* – Proper development of delivery systems, or drug molecules, requires the assessment of both acute and chronic toxicity. Since chitosan biodegradable properties depend on the degree of deacetylation, and to a lesser extent on molecular weight, formulation with high degree of deacetylation i.e. 92 and 98%, can accumulate in kidney PTEC eliciting long-term toxicity. Studies targeted at evaluation of repeated dose toxicity on a period of 3-6 month to understand elimination kinetics, design novel formulations with biodegradable linkers, and limit renal toxicity can be undertaken in future.

BIBLIOGRAPHY

[1] R.C. Wilson, J.A. Doudna, Molecular mechanisms of RNA interference, Annu Rev Biophys 42 (2013) 217-39.

[2] S.F. Dowdy, Overcoming cellular barriers for RNA therapeutics, Nat Biotechnol 35(3) (2017) 222-229.

[3] R.L. Kanasty, K.A. Whitehead, A.J. Vegas, D.G. Anderson, Action and reaction: the biological response to siRNA and its delivery vehicles, Mol Ther 20(3) (2012) 513-24.

[4] A. Khvorova, J.K. Watts, The chemical evolution of oligonucleotide therapies of clinical utility, Nat Biotechnol 35(3) (2017) 238-248.

[5] A.L. Jackson, P.S. Linsley, Recognizing and avoiding siRNA off-target effects for target identification and therapeutic application, Nat Rev Drug Discov 9(1) (2010) 57-67.

[6] A. Judge, I. MacLachlan, Overcoming the innate immune response to small interfering RNA, Hum Gene Ther 19(2) (2008) 111-24.

[7] A.K. Vaishnaw, J. Gollob, C. Gamba-Vitalo, R. Hutabarat, D. Sah, R. Meyers, T. de Fougerolles, J. Maraganore, A status report on RNAi therapeutics, Silence 1(1) (2010) 14.

[8] A. de Fougerolles, H.P. Vornlocher, J. Maraganore, J. Lieberman, Interfering with disease: a progress report on siRNA-based therapeutics, Nat Rev Drug Discov 6(6) (2007) 443-53.

[9] M. Dominska, D.M. Dykxhoorn, Breaking down the barriers: siRNA delivery and endosome escape, J Cell Sci 123(Pt 8) (2010) 1183-9.

[10] A. Schroeder, C.G. Levins, C. Cortez, R. Langer, D.G. Anderson, Lipid-based nanotherapeutics for siRNA delivery, J Intern Med 267(1) (2010) 9-21.

[11] R. Kanasty, J.R. Dorkin, A. Vegas, D. Anderson, Delivery materials for siRNA therapeutics, Nat Mater 12(11) (2013) 967-77.
[12] A. Wittrup, J. Lieberman, Knocking down disease: a progress report on siRNA therapeutics, Nat Rev Genet 16(9) (2015) 543-52.
[13] K. Fitzgerald, S. White, A. Borodovsky, B.R. Bettencourt, A. Strahs, V. Clausen, P. Wijngaard, J.D. Horton, J. Taubel, A. Brooks, C. Fernando, R.S. Kauffman, D. Kallend, A. Vaishnaw, A. Simon, A Highly Durable RNAi Therapeutic Inhibitor of PCSK9, N Engl J Med 376(1) (2017) 41-51.
[14] R. Kedmi, N. Ben-Arie, D. Peer, The systemic toxicity of positively charged lipid nanoparticles and the role of Toll-like receptor 4 in immune activation, Biomaterials 31(26) (2010) 6867-75.
[15] D. Landesman-Milo, D. Peer, Toxicity profiling of several common RNAi-based nanomedicines: a comparative study, Drug Deliv. and Transl. Res. (2013).
[16] H. Lv, S. Zhang, B. Wang, S. Cui, J. Yan, Toxicity of cationic lipids and cationic polymers in gene delivery, J Control Release 114(1) (2006) 100-9.
[17] H.Y. Xue, S. Liu, H.L. Wong, Nanotoxicity: a key obstacle to clinical translation of siRNA-based nanomedicine, Nanomedicine (Lond) 9(2) (2014) 295-312.
[18] C. Lorenzer, M. Dirin, A.M. Winkler, V. Baumann, J. Winkler, Going beyond the liver: progress and challenges of targeted delivery of siRNA therapeutics, J Control Release 203 (2015) 1-15.
[19] M.D. Buschmann, A. Merzouki, M. Lavertu, M. Thibault, M. Jean, V. Darras, Chitosans for delivery of nucleic acids, Adv Drug Deliv Rev 65(9) (2013) 1234-70.
[20] J. Malmo, H. Sorgard, K.M. Varum, S.P. Strand, siRNA delivery with chitosan nanoparticles: Molecular properties favoring efficient gene silencing, J Control Release 158(2) (2012) 261-8.

[21] H. Ragelle, R. Riva, G. Vandermeulen, B. Naeye, V. Pourcelle, C.S. Le Duff, C. D'Haese, B. Nysten, K. Braeckmans, S.C. De Smedt, C. Jerome, V. Preat, Chitosan nanoparticles for siRNA delivery: optimizing formulation to increase stability and efficiency, J Control Release 176 (2014) 54-63.

[22] K.A. Howard, U.L. Rahbek, X. Liu, C.K. Damgaard, S.Z. Glud, M.O. Andersen, M.B. Hovgaard, A. Schmitz, J.R. Nyengaard, F. Besenbacher, J. Kjems, RNA interference in vitro and in vivo using a novel chitosan/siRNA nanoparticle system, Mol Ther 14(4) (2006) 476-84.

[23] X. Liu, K.A. Howard, M. Dong, M.O. Andersen, U.L. Rahbek, M.G. Johnsen, O.C. Hansen, F. Besenbacher, J. Kjems, The influence of polymeric properties on chitosan/siRNA nanoparticle formulation and gene silencing, Biomaterials 28(6) (2007) 1280-8.

[24] E.J. Nielsen, J.M. Nielsen, D. Becker, A. Karlas, H. Prakash, S.Z. Glud, J. Merrison, F. Besenbacher, T.F. Meyer, J. Kjems, K.A. Howard, Pulmonary gene silencing in transgenic EGFP mice using aerosolised chitosan/siRNA nanoparticles, Pharm Res 27(12) (2010) 2520-7.

[25] H. Katas, H.O. Alpar, Development and characterisation of chitosan nanoparticles for siRNA delivery, J Control Release 115(2) (2006) 216-25.

[26] A.M. Ji, D. Su, O. Che, W.S. Li, L. Sun, Z.Y. Zhang, B. Yang, F. Xu, Functional gene silencing mediated by chitosan/siRNA nanocomplexes, Nanotechnology 20(40) (2009) 405103.

[27] J. Malmo, A. Sandvig, K.M. Varum, S.P. Strand, Nanoparticle mediated P-glycoprotein silencing for improved drug delivery across the blood-brain barrier: a siRNA-chitosan approach, PLoS One 8(1) (2013) e54182.

[28] M.D. Buschmann, A. Merzouki, M. Lavertu, M. Jean, V. Darras, Chitosans for delivery of nucleic acids, Advanced Drug Delivery Reviews 65(9) (2013) 1234-1270.

[29] P. Holzerny, B. Ajdini, W. Heusermann, K. Bruno, M. Schuleit, L. Meinel, M. Keller, Biophysical properties of chitosan/siRNA polyplexes: profiling the polymer/siRNA interactions and bioactivity, J Control Release 157(2) (2012) 297-304.

[30] V. Balan, L. Verestiuc, Strategies to improve chitosan hemocompatibilities: A review, European Polymer Journal 53 (2014) 171-188.

[31] D. Fong, P. Gregoire-Gelinas, A.P. Cheng, T. Mezheritsky, M. Lavertu, S. Sato, C.D. Hoemann, Lysosomal rupture induced by structurally distinct chitosans either promotes a type 1 IFN response or activates the inflammasome in macrophages, Biomaterials 129 (2017) 127-138.

[32] E.C. Carroll, L. Jin, A. Mori, N. Munoz-Wolf, E. Oleszycka, H.B. Moran, S. Mansouri, C.P. McEntee, E. Lambe, E.M. Agger, P. Andersen, C. Cunningham, P. Hertzog, K.A. Fitzgerald, A.G. Bowie, E.C. Lavelle, The Vaccine Adjuvant Chitosan Promotes Cellular Immunity via DNA Sensor cGAS-STING-Dependent Induction of Type I Interferons, Immunity 44(3) (2016) 597-608.

[33] M. Alameh, D. Dejesus, M. Jean, V. Darras, M. Thibault, M. Lavertu, M.D. Buschmann, A. Merzouki, Low molecular weight chitosan nanoparticulate system at low N:P ratio for nontoxic polynucleotide delivery, Int J Nanomedicine 7 (2012) 1399-414.

[34] M. Alameh, M. Jean, D. Dejesus, M.D. Buschmann, A. Merzouki, Chitosanase-based method for RNA isolation from cells transfected with chitosan/siRNA nanocomplexes for real-time RT-PCR in gene silencing, Int J Nanomedicine 5 (2010) 473-81.

[35] C. Corbet, H. Ragelle, V. Pourcelle, K. Vanvarenberg, J. Marchand-Brynaert, V. Preat, O. Feron, Delivery of siRNA targeting tumor metabolism using non-covalent PEGylated chitosan nanoparticles: Identification of an optimal

combination of ligand structure, linker and grafting method, J Control Release 223 (2016) 53-63.
[36] M. Jean, M. Alameh, D. De Jesus, M. Thibault, M. Lavertu, V. Darras, M. Nelea, M.D. Buschmann, A. Merzouki, Chitosan-based therapeutic nanoparticles for combination gene therapy and gene silencing of in vitro cell lines relevant to type 2 diabetes, Eur J Pharm Sci 45(1-2) (2012) 138-49.
[37] M. Lavertu, S. Methot, N. Tran-Khanh, M.D. Buschmann, High efficiency gene transfer using chitosan/DNA nanoparticles with specific combinations of molecular weight and degree of deacetylation, Biomaterials 27(27) (2006) 4815-24.
[38] S. Nimesh, M.M. Thibault, M. Lavertu, M.D. Buschmann, Enhanced gene delivery mediated by low molecular weight chitosan/DNA complexes: effect of pH and serum, Mol Biotechnol 46(2) (2010) 182-96.
[39] M. Thibault, S. Nimesh, M. Lavertu, M.D. Buschmann, Intracellular trafficking and decondensation kinetics of chitosan-pDNA polyplexes, Mol Ther 18(10) (2010) 1787-95.
[40] S.P. Strand, S. Lelu, N.K. Reitan, C. de Lange Davies, P. Artursson, K.M. Varum, Molecular design of chitosan gene delivery systems with an optimized balance between polyplex stability and polyplex unpacking, Biomaterials 31(5) (2010) 975-87.
[41] S. Gao, F. Dagnaes-Hansen, E.J. Nielsen, J. Wengel, F. Besenbacher, K.A. Howard, J. Kjems, The effect of chemical modification and nanoparticle formulation on stability and biodistribution of siRNA in mice, Mol Ther 17(7) (2009) 1225-33.
[42] S. Gao, S. Hein, F. Dagnaes-Hansen, K. Weyer, C. Yang, R. Nielsen, E.I. Christensen, R.A. Fenton, J. Kjems, Megalin-mediated specific uptake of chitosan/siRNA nanoparticles in mouse kidney proximal tubule epithelial cells enables AQP1 gene silencing, Theranostics 4(10) (2014) 1039-51.

[43] C. Yang, S. Gao, J. Kjems, Folic acid conjugated chitosan for targeted delivery of siRNA to activated marcophages in vitro and in vivo, Journal of Materials Chemistry B 2 (2014) 8608-8615.
[44] C. Yang, L. Nilsson, M.U. Cheema, Y. Wang, J. Frokiaer, S. Gao, J. Kjems, R. Norregaard, Chitosan/siRNA nanoparticles targeting cyclooxygenase type 2 attenuate unilateral ureteral obstruction-induced kidney injury in mice, Theranostics 5(2) (2015) 110-23.
[45] M.E. Davis, J.E. Zuckerman, C.H. Choi, D. Seligson, A. Tolcher, C.A. Alabi, Y. Yen, J.D. Heidel, A. Ribas, Evidence of RNAi in humans from systemically administered siRNA via targeted nanoparticles, Nature 464(7291) (2010) 1067-70.
[46] K. Fitzgerald, M. Frank-Kamenetsky, S. Shulga-Morskaya, A. Liebow, B.R. Bettencourt, J.E. Sutherland, R.M. Hutabarat, V.A. Clausen, V. Karsten, J. Cehelsky, S.V. Nochur, V. Kotelianski, J. Horton, T. Mant, J. Chiesa, J. Ritter, M. Munisamy, A.K. Vaishnaw, J.A. Gollob, A. Simon, Effect of an RNA interference drug on the synthesis of proprotein convertase subtilisin/kexin type 9 (PCSK9) and the concentration of serum LDL cholesterol in healthy volunteers: a randomised, single-blind, placebo-controlled, phase 1 trial, Lancet 383(9911) (2014) 60-8.
[47] Y. Lee, K. Jeon, J.T. Lee, S. Kim, V.N. Kim, MicroRNA maturation: stepwise processing and subcellular localization, EMBO J 21(17) (2002) 4663-70.
[48] Y. Lee, C. Ahn, J. Han, H. Choi, J. Kim, J. Yim, J. Lee, P. Provost, O. Radmark, S. Kim, V.N. Kim, The nuclear RNase III Drosha initiates microRNA processing, Nature 425(6956) (2003) 415-9.
[49] H. Wu, H. Xu, L.J. Miraglia, S.T. Crooke, Human RNase III is a 160-kDa protein involved in preribosomal RNA processing, J Biol Chem 275(47) (2000) 36957-65.

[50] J. Han, Y. Lee, K.H. Yeom, J.W. Nam, I. Heo, J.K. Rhee, S.Y. Sohn, Y. Cho, B.T. Zhang, V.N. Kim, Molecular basis for the recognition of primary microRNAs by the Drosha-DGCR8 complex, Cell 125(5) (2006) 887-901.

[51] E. Lund, S. Guttinger, A. Calado, J.E. Dahlberg, U. Kutay, Nuclear export of microRNA precursors, Science 303(5654) (2004) 95-8.

[52] R. Yi, Y. Qin, I.G. Macara, B.R. Cullen, Exportin-5 mediates the nuclear export of pre-microRNAs and short hairpin RNAs, Genes Dev 17(24) (2003) 3011-6.

[53] N.H. Tolia, L. Joshua-Tor, Slicer and the argonautes, Nat Chem Biol 3(1) (2007) 36-43.

[54] A. Khvorova, A. Reynolds, S.D. Jayasena, Functional siRNAs and miRNAs exhibit strand bias, Cell 115(2) (2003) 209-16.

[55] D.S. Schwarz, G. Hutvagner, T. Du, Z. Xu, N. Aronin, P.D. Zamore, Asymmetry in the assembly of the RNAi enzyme complex, Cell 115(2) (2003) 199-208.

[56] Y. Huang, J. Hong, S. Zheng, Y. Ding, S. Guo, H. Zhang, X. Zhang, Q. Du, Z. Liang, Elimination pathways of systemically delivered siRNA, Mol Ther 19(2) (2011) 381-5.

[57] R. Rodewald, M.J. Karnovsky, Porous substructure of the glomerular slit diaphragm in the rat and mouse, J Cell Biol 60(2) (1974) 423-33.

[58] J. Soutschek, A. Akinc, B. Bramlage, K. Charisse, R. Constien, M. Donoghue, S. Elbashir, A. Geick, P. Hadwiger, J. Harborth, M. John, V. Kesavan, G. Lavine, R.K. Pandey, T. Racie, K.G. Rajeev, I. Rohl, I. Toudjarska, G. Wang, S. Wuschko, D. Bumcrot, V. Koteliansky, S. Limmer, M. Manoharan, H.P. Vornlocher, Therapeutic silencing of an endogenous gene by systemic administration of modified siRNAs, Nature 432(7014) (2004) 173-8.

[59] H. Yin, R.L. Kanasty, A.A. Eltoukhy, A.J. Vegas, J.R. Dorkin, D.G. Anderson, Non-viral vectors for gene-based therapy, Nat Rev Genet 15(8) (2014) 541-55.
[60] J. Gilleron, W. Querbes, A. Zeigerer, A. Borodovsky, G. Marsico, U. Schubert, K. Manygoats, S. Seifert, C. Andree, M. Stoter, H. Epstein-Barash, L. Zhang, V. Koteliansky, K. Fitzgerald, E. Fava, M. Bickle, Y. Kalaidzidis, A. Akinc, M. Maier, M. Zerial, Image-based analysis of lipid nanoparticle-mediated siRNA delivery, intracellular trafficking and endosomal escape, Nat Biotechnol 31(7) (2013) 638-46.
[61] A. Wittrup, A. Ai, X. Liu, P. Hamar, R. Trifonova, K. Charisse, M. Manoharan, T. Kirchhausen, J. Lieberman, Visualizing lipid-formulated siRNA release from endosomes and target gene knockdown, Nat Biotechnol 33(8) (2015) 870-6.
[62] J.B. Bramsen, M.M. Pakula, T.B. Hansen, C. Bus, N. Langkjaer, D. Odadzic, R. Smicius, S.L. Wengel, J. Chattopadhyaya, J.W. Engels, P. Herdewijn, J. Wengel, J. Kjems, A screen of chemical modifications identifies position-specific modification by UNA to most potently reduce siRNA off-target effects, Nucleic Acids Res 38(17) (2010) 5761-73.
[63] P.Y. Chen, L. Weinmann, D. Gaidatzis, Y. Pei, M. Zavolan, T. Tuschl, G. Meister, Strand-specific 5'-O-methylation of siRNA duplexes controls guide strand selection and targeting specificity, RNA 14(2) (2008) 263-74.
[64] S.L. Ameres, J. Martinez, R. Schroeder, Molecular basis for target RNA recognition and cleavage by human RISC, Cell 130(1) (2007) 101-12.
[65] Z.J. Lu, D.H. Mathews, OligoWalk: an online siRNA design tool utilizing hybridization thermodynamics, Nucleic Acids Res 36(Web Server issue) (2008) W104-8.

[66] A. Reynolds, D. Leake, Q. Boese, S. Scaringe, W.S. Marshall, A. Khvorova, Rational siRNA design for RNA interference, Nat Biotechnol 22(3) (2004) 326-30.
[67] A.L. Jackson, S.R. Bartz, J. Schelter, S.V. Kobayashi, J. Burchard, M. Mao, B. Li, G. Cavet, P.S. Linsley, Expression profiling reveals off-target gene regulation by RNAi, Nature Biotechnology 21(6) (2003) 635-637.
[68] A.L. Jackson, J. Burchard, D. Leake, A. Reynolds, J. Schelter, J. Guo, J.M. Johnson, L. Lim, J. Karpilow, K. Nichols, W. Marshall, A. Khvorova, P.S. Linsley, Position-specific chemical modification of siRNAs reduces "off-target" transcript silencing, RNA 12(7) (2006) 1197-205.
[69] Q. Boese, D. Leake, A. Reynolds, S. Read, S.A. Scaringe, W.S. Marshall, A. Khvorova, Mechanistic insights aid computational short interfering RNA design, Method Enzymol 392 (2005) 73-+.
[70] Y. Naito, K. Ui-Tei, siRNA Design Software for a Target Gene-Specific RNA Interference, Front Genet 3 (2012) 102.
[71] Y. Naito, J. Yoshimura, S. Morishita, K. Ui-Tei, siDirect 2.0: updated software for designing functional siRNA with reduced seed-dependent off-target effect, BMC Bioinformatics 10 (2009) 392.
[72] S. Petri, A. Dueck, G. Lehmann, N. Putz, S. Rudel, E. Kremmer, G. Meister, Increased siRNA duplex stability correlates with reduced off-target and elevated on-target effects, RNA 17(4) (2011) 737-49.
[73] N. Vaish, F. Chen, S. Seth, K. Fosnaugh, Y. Liu, R. Adami, T. Brown, Y. Chen, P. Harvie, R. Johns, G. Severson, B. Granger, P. Charmley, M. Houston, M.V. Templin, B. Polisky, Improved specificity of gene silencing by siRNAs containing unlocked nucleobase analogs, Nucleic Acids Res 39(5) (2011) 1823-32.
[74] C.A. Sledz, M. Holko, M.J. de Veer, R.H. Silverman, B.R. Williams, Activation of the interferon system by short-interfering RNAs, Nat Cell Biol 5(9) (2003) 834-9.

[75] K. Kariko, P. Bhuyan, J. Capodici, H. Ni, J. Lubinski, H. Friedman, D. Weissman, Exogenous siRNA mediates sequence-independent gene suppression by signaling through toll-like receptor 3, Cells Tissues Organs 177(3) (2004) 132-8.
[76] A.D. Judge, V. Sood, J.R. Shaw, D. Fang, K. McClintock, I. MacLachlan, Sequence-dependent stimulation of the mammalian innate immune response by synthetic siRNA, Nat Biotechnol 23(4) (2005) 457-62.
[77] M. Sioud, Induction of inflammatory cytokines and interferon responses by double-stranded and single-stranded siRNAs is sequence-dependent and requires endosomal localization, J Mol Biol 348(5) (2005) 1079-90.
[78] V. Hornung, M. Guenthner-Biller, C. Bourquin, A. Ablasser, M. Schlee, S. Uematsu, A. Noronha, M. Manoharan, S. Akira, A. de Fougerolles, S. Endres, G. Hartmann, Sequence-specific potent induction of IFN-alpha by short interfering RNA in plasmacytoid dendritic cells through TLR7, Nat Med 11(3) (2005) 263-70.
[79] J.T. Marques, T. Devosse, D. Wang, M. Zamanian-Daryoush, P. Serbinowski, R. Hartmann, T. Fujita, M.A. Behlke, B.R. Williams, A structural basis for discriminating between self and nonself double-stranded RNAs in mammalian cells, Nat Biotechnol 24(5) (2006) 559-65.
[80] G.F. Deleavey, J.K. Watts, M.J. Damha, Chemical modification of siRNA, Curr Protoc Nucleic Acid Chem Chapter 16 (2009) Unit 16 3.
[81] A.D. Judge, G. Bola, A.C. Lee, I. MacLachlan, Design of noninflammatory synthetic siRNA mediating potent gene silencing in vivo, Mol Ther 13(3) (2006) 494-505.
[82] E. Koller, S. Propp, H. Murray, W. Lima, B. Bhat, T.P. Prakash, C.R. Allerson, E.E. Swayze, E.G. Marcusson, N.M. Dean, Competition for RISC binding predicts in vitro potency of siRNA, Nucleic Acids Res 34(16) (2006) 4467-76.

[83] D. Castanotto, K. Sakurai, R. Lingeman, H. Li, L. Shively, L. Aagaard, H. Soifer, A. Gatignol, A. Riggs, J.J. Rossi, Combinatorial delivery of small interfering RNAs reduces RNAi efficacy by selective incorporation into RISC, Nucleic Acids Res 35(15) (2007) 5154-64.

[84] D. Grimm, L. Wang, J.S. Lee, N. Schurmann, S. Gu, K. Borner, T.A. Storm, M.A. Kay, Argonaute proteins are key determinants of RNAi efficacy, toxicity, and persistence in the adult mouse liver, J Clin Invest 120(9) (2010) 3106-19.

[85] J.L. McBride, R.L. Boudreau, S.Q. Harper, P.D. Staber, A.M. Monteys, I. Martins, B.L. Gilmore, H. Burstein, R.W. Peluso, B. Polisky, B.J. Carter, B.L. Davidson, Artificial miRNAs mitigate shRNA-mediated toxicity in the brain: implications for the therapeutic development of RNAi, Proc Natl Acad Sci U S A 105(15) (2008) 5868-73.

[86] R.L. Boudreau, I. Martins, B.L. Davidson, Artificial microRNAs as siRNA shuttles: improved safety as compared to shRNAs in vitro and in vivo, Mol Ther 17(1) (2009) 169-75.

[87] A.A. Khan, D. Betel, M.L. Miller, C. Sander, C.S. Leslie, D.S. Marks, Transfection of small RNAs globally perturbs gene regulation by endogenous microRNAs, Nat Biotechnol 27(6) (2009) 549-55.

[88] K. Garber, Alnylam terminates revusiran program, stock plunges, Nat Biotechnol 34(12) (2016) 1213-1214.

[89] Y.L. Chiu, T.M. Rana, siRNA function in RNAi: a chemical modification analysis, RNA 9(9) (2003) 1034-48.

[90] S.M. Elbashir, J. Harborth, W. Lendeckel, A. Yalcin, K. Weber, T. Tuschl, Duplexes of 21-nucleotide RNAs mediate RNA interference in cultured mammalian cells, Nature 411(6836) (2001) 494-8.

[91] S.M. Elbashir, J. Martinez, A. Patkaniowska, W. Lendeckel, T. Tuschl, Functional anatomy of siRNAs for mediating efficient RNAi in Drosophila melanogaster embryo lysate, EMBO J 20(23) (2001) 6877-88.
[92] F. Czauderna, M. Fechtner, S. Dames, H. Aygun, A. Klippel, G.J. Pronk, K. Giese, J. Kaufmann, Structural variations and stabilising modifications of synthetic siRNAs in mammalian cells, Nucleic Acids Research 31(11) (2003) 2705-2716.
[93] S. Choung, Y.J. Kim, S. Kim, H.O. Park, Y.C. Choi, Chemical modification of siRNAs to improve serum stability without loss of efficacy, Biochem Bioph Res Co 342(3) (2006) 919-927.
[94] G. Dorn, S. Patel, G. Wotherspoon, M. Hemmings-Mieszczak, J. Barclay, F.J. Natt, P. Martin, S. Bevan, A. Fox, P. Ganju, W. Wishart, J. Hall, siRNA relieves chronic neuropathic pain, Nucleic Acids Res 32(5) (2004) e49.
[95] J.M. Layzer, A.P. McCaffrey, A.K. Tanner, Z. Huang, M.A. Kay, B.A. Sullenger, In vivo activity of nuclease-resistant siRNAs, RNA 10(5) (2004) 766-71.
[96] D.A. Braasch, S. Jensen, Y. Liu, K. Kaur, K. Arar, M.A. White, D.R. Corey, RNA interference in mammalian cells by chemically-modified RNA, Biochemistry 42(26) (2003) 7967-75.
[97] J. Harborth, S.M. Elbashir, K. Vandenburgh, H. Manninga, S.A. Scaringe, K. Weber, T. Tuschl, Sequence, chemical, and structural variation of small interfering RNAs and short hairpin RNAs and the effect on mammalian gene silencing, Antisense Nucleic Acid Drug Dev 13(2) (2003) 83-105.
[98] R.A. Blidner, R.P. Hammer, M.J. Lopez, S.O. Robinson, W.T. Monroe, Fully 2'-deoxy-2'-fluoro substituted nucleic acids induce RNA interference in mammalian cell culture, Chem Biol Drug Des 70(2) (2007) 113-22.
[99] T. Dowler, D. Bergeron, A.L. Tedeschi, L. Paquet, N. Ferrari, M.J. Damha, Improvements in siRNA properties mediated by 2'-deoxy-2'-fluoro-beta-D-arabinonucleic acid (FANA), Nucleic Acids Res 34(6) (2006) 1669-75.

[100] J.K. Watts, K. Sadalapure, N. Choubdar, B.M. Pinto, M.J. Damha, Synthesis and conformational analysis of 2'-fluoro-5-methyl-4'-thioarabinouridine (4'S-FMAU), J Org Chem 71(3) (2006) 921-5.
[101] M.J. Damha, A. Noronha, Recognition of nucleic acid double helices by homopyrimidine 2', 5'-linked RNA, Nucleic Acids Res 26(22) (1998) 5152-6.
[102] C.J. Wilds, M.J. Damha, 2'-Deoxy-2'-fluoro-beta-D-arabinonucleosides and oligonucleotides (2'F-ANA): synthesis and physicochemical studies, Nucleic Acids Res 28(18) (2000) 3625-35.
[103] S. Parrish, J. Fleenor, S. Xu, C. Mello, A. Fire, Functional anatomy of a dsRNA trigger: differential requirement for the two trigger strands in RNA interference, Mol Cell 6(5) (2000) 1077-87.
[104] K. Ui-Tei, Y. Naito, K. Nishi, A. Juni, K. Saigo, Thermodynamic stability and Watson-Crick base pairing in the seed duplex are major determinants of the efficiency of the siRNA-based off-target effect, Nucleic Acids Res 36(22) (2008) 7100-9.
[105] K. Ui-Tei, Y. Naito, S. Zenno, K. Nishi, K. Yamato, F. Takahashi, A. Juni, K. Saigo, Functional dissection of siRNA sequence by systematic DNA substitution: modified siRNA with a DNA seed arm is a powerful tool for mammalian gene silencing with significantly reduced off-target effect, Nucleic Acids Res 36(7) (2008) 2136-51.
[106] J.B. Bramsen, J. Kjems, Development of Therapeutic-Grade Small Interfering RNAs by Chemical Engineering, Front Genet 3 (2012) 154.
[107] M. Amarzguioui, T. Holen, E. Babaie, H. Prydz, Tolerance for mutations and chemical modifications in a siRNA, Nucleic Acids Res 31(2) (2003) 589-95.
[108] D.S. Schwarz, Y. Tomari, P.D. Zamore, The RNA-induced silencing complex is a Mg2+-dependent endonuclease, Curr Biol 14(9) (2004) 787-791.

[109] A.H. Hall, J. Wan, E.E. Shaughnessy, B. Ramsay Shaw, K.A. Alexander, RNA interference using boranophosphate siRNAs: structure-activity relationships, Nucleic Acids Res 32(20) (2004) 5991-6000.

[110] T.P. Prakash, C.R. Allerson, P. Dande, T.A. Vickers, N. Sioufi, R. Jarres, B.F. Baker, E.E. Swayze, R.H. Griffey, B. Bhat, Positional effect of chemical modifications on short interference RNA activity in mammalian cells, J Med Chem 48(13) (2005) 4247-53.

[111] P. Dande, T.P. Prakash, N. Sioufi, H. Gaus, R. Jarres, A. Berdeja, E.E. Swayze, R.H. Griffey, B. Bhat, Improving RNA interference in mammalian cells by 4'-thio-modified small interfering RNA (siRNA): effect on siRNA activity and nuclease stability when used in combination with 2'-O-alkyl modifications, J Med Chem 49(5) (2006) 1624-34.

[112] V. Hornung, J. Ellegast, S. Kim, K. Brzozka, A. Jung, H. Kato, H. Poeck, S. Akira, K.K. Conzelmann, M. Schlee, S. Endres, G. Hartmann, 5'-Triphosphate RNA is the ligand for RIG-I, Science 314(5801) (2006) 994-7.

[113] K. Sipa, E. Sochacka, J. Kazmierczak-Baranska, M. Maszewska, M. Janicka, G. Nowak, B. Nawrot, Effect of base modifications on structure, thermodynamic stability, and gene silencing activity of short interfering RNA, RNA 13(8) (2007) 1301-16.

[114] C. Lorenz, P. Hadwiger, M. John, H.P. Vornlocher, C. Unverzagt, Steroid and lipid conjugates of siRNAs to enhance cellular uptake and gene silencing in liver cells, Bioorg Med Chem Lett 14(19) (2004) 4975-7.

[115] J.K. Watts, G.F. Deleavey, M.J. Damha, Chemically modified siRNA: tools and applications, Drug Discov Today 13(19-20) (2008) 842-55.

[116] J.B. Bramsen, M.B. Laursen, C.K. Damgaard, S.W. Lena, B.R. Babu, J. Wengel, J. Kjems, Improved silencing properties using small internally segmented interfering RNAs, Nucleic Acids Res 35(17) (2007) 5886-97.

[117] J. Martinez, A. Patkaniowska, H. Urlaub, R. Luhrmann, T. Tuschl, Single-stranded antisense siRNAs guide target RNA cleavage in RNAi, Cell 110(5) (2002) 563-74.
[118] D.H. Kim, M.A. Behlke, S.D. Rose, M.S. Chang, S. Choi, J.J. Rossi, Synthetic dsRNA Dicer substrates enhance RNAi potency and efficacy, Nat Biotechnol 23(2) (2005) 222-6.
[119] M.A. Minks, D.K. West, S. Benvin, C. Baglioni, Structural requirements of double-stranded RNA for the activation of 2',5'-oligo(A) polymerase and protein kinase of interferon-treated HeLa cells, J Biol Chem 254(20) (1979) 10180-3.
[120] A. Akinc, W. Querbes, S. De, J. Qin, M. Frank-Kamenetsky, K.N. Jayaprakash, M. Jayaraman, K.G. Rajeev, W.L. Cantley, J.R. Dorkin, J.S. Butler, L. Qin, T. Racie, A. Sprague, E. Fava, A. Zeigerer, M.J. Hope, M. Zerial, D.W. Sah, K. Fitzgerald, M.A. Tracy, M. Manoharan, V. Koteliansky, A. Fougerolles, M.A. Maier, Targeted delivery of RNAi therapeutics with endogenous and exogenous ligand-based mechanisms, Mol Ther 18(7) (2010) 1357-64.
[121] T.S. Zimmermann, A.C. Lee, A. Akinc, B. Bramlage, D. Bumcrot, M.N. Fedoruk, J. Harborth, J.A. Heyes, L.B. Jeffs, M. John, A.D. Judge, K. Lam, K. McClintock, L.V. Nechev, L.R. Palmer, T. Racie, I. Rohl, S. Seiffert, S. Shanmugam, V. Sood, J. Soutschek, I. Toudjarska, A.J. Wheat, E. Yaworski, W. Zedalis, V. Koteliansky, M. Manoharan, H.P. Vornlocher, I. MacLachlan, RNAi-mediated gene silencing in non-human primates, Nature 441(7089) (2006) 111-4.
[122] M. Jayaraman, S.M. Ansell, B.L. Mui, Y.K. Tam, J. Chen, X. Du, D. Butler, L. Eltepu, S. Matsuda, J.K. Narayanannair, K.G. Rajeev, I.M. Hafez, A. Akinc, M.A. Maier, M.A. Tracy, P.R. Cullis, T.D. Madden, M. Manoharan, M.J. Hope, Maximizing the potency of siRNA lipid nanoparticles for hepatic gene silencing in vivo, Angew Chem Int Ed Engl 51(34) (2012) 8529-33.

[123] M.A. Maier, M. Jayaraman, S. Matsuda, J. Liu, S. Barros, W. Querbes, Y.K. Tam, S.M. Ansell, V. Kumar, J. Qin, X. Zhang, Q. Wang, S. Panesar, R. Hutabarat, M. Carioto, J. Hettinger, P. Kandasamy, D. Butler, K.G. Rajeev, B. Pang, K. Charisse, K. Fitzgerald, B.L. Mui, X. Du, P. Cullis, T.D. Madden, M.J. Hope, M. Manoharan, A. Akinc, Biodegradable lipids enabling rapidly eliminated lipid nanoparticles for systemic delivery of RNAi therapeutics, Mol Ther 21(8) (2013) 1570-8.

[124] R.W. Malone, P.L. Felgner, I.M. Verma, Cationic liposome-mediated RNA transfection, Proc Natl Acad Sci U S A 86(16) (1989) 6077-81.

[125] I.M. Hafez, P.R. Cullis, Roles of lipid polymorphism in intracellular delivery, Adv Drug Deliv Rev 47(2-3) (2001) 139-48.

[126] O. Zelphati, L.S. Uyechi, L.G. Barron, F.C. Szoka, Jr., Effect of serum components on the physico-chemical properties of cationic lipid/oligonucleotide complexes and on their interactions with cells, Biochim Biophys Acta 1390(2) (1998) 119-33.

[127] K. Buyens, B. Lucas, K. Raemdonck, K. Braeckmans, J. Vercammen, J. Hendrix, Y. Engelborghs, S.C. De Smedt, N.N. Sanders, A fast and sensitive method for measuring the integrity of siRNA-carrier complexes in full human serum, J Control Release 126(1) (2008) 67-76.

[128] K. Buyens, M. Meyer, E. Wagner, J. Demeester, S.C. De Smedt, N.N. Sanders, Monitoring the disassembly of siRNA polyplexes in serum is crucial for predicting their biological efficacy, J Control Release 141(1) (2010) 38-41.

[129] D. Litzinger, Limitations of Cationic Liposomes for Antisense Oligonucleotide Delivery in Vivo, Journal of Liposome Research (7) (1997) 51-61.

[130] P.R. Cullis, A. Chonn, S.C. Semple, Interactions of liposomes and lipid-based carrier systems with blood proteins: Relation to clearance behaviour in vivo, Adv Drug Deliv Rev 32(1-2) (1998) 3-17.

[131] S.M. Moghimi, A.C. Hunter, T.L. Andresen, Factors controlling nanoparticle pharmacokinetics: an integrated analysis and perspective, Annu Rev Pharmacol Toxicol 52 (2012) 481-503.
[132] B. Romberg, W.E. Hennink, G. Storm, Sheddable coatings for long-circulating nanoparticles, Pharm Res 25(1) (2008) 55-71.
[133] B.L. Mui, Y.K. Tam, M. Jayaraman, S.M. Ansell, X. Du, Y.Y. Tam, P.J. Lin, S. Chen, J.K. Narayanannair, K.G. Rajeev, M. Manoharan, A. Akinc, M.A. Maier, P. Cullis, T.D. Madden, M.J. Hope, Influence of Polyethylene Glycol Lipid Desorption Rates on Pharmacokinetics and Pharmacodynamics of siRNA Lipid Nanoparticles, Mol Ther Nucleic Acids 2 (2013) e139.
[134] S.C. Semple, T.O. Harasym, K.A. Clow, S.M. Ansell, S.K. Klimuk, M.J. Hope, Immunogenicity and rapid blood clearance of liposomes containing polyethylene glycol-lipid conjugates and nucleic Acid, J Pharmacol Exp Ther 312(3) (2005) 1020-6.
[135] A. Judge, K. McClintock, J.R. Phelps, I. Maclachlan, Hypersensitivity and loss of disease site targeting caused by antibody responses to PEGylated liposomes, Mol Ther 13(2) (2006) 328-37.
[136] Y. Wang, L. Miao, A. Satterlee, L. Huang, Delivery of oligonucleotides with lipid nanoparticles, Adv Drug Deliv Rev 87 (2015) 68-80.
[137] S.C. Semple, S.K. Klimuk, T.O. Harasym, N. Dos Santos, S.M. Ansell, K.F. Wong, N. Maurer, H. Stark, P.R. Cullis, M.J. Hope, P. Scherrer, Efficient encapsulation of antisense oligonucleotides in lipid vesicles using ionizable aminolipids: formation of novel small multilamellar vesicle structures, Biochim Biophys Acta 1510(1-2) (2001) 152-66.
[138] J. Heyes, L. Palmer, K. Bremner, I. MacLachlan, Cationic lipid saturation influences intracellular delivery of encapsulated nucleic acids, J Control Release 107(2) (2005) 276-87.

[139] M.T. Abrams, M.L. Koser, J. Seitzer, S.C. Williams, M.A. DiPietro, W. Wang, A.W. Shaw, X. Mao, V. Jadhav, J.P. Davide, P.A. Burke, A.B. Sachs, S.M. Stirdivant, L. Sepp-Lorenzino, Evaluation of efficacy, biodistribution, and inflammation for a potent siRNA nanoparticle: effect of dexamethasone co-treatment, Mol Ther 18(1) (2010) 171-80.
[140] S.C. Semple, A. Akinc, J. Chen, A.P. Sandhu, B.L. Mui, C.K. Cho, D.W. Sah, D. Stebbing, E.J. Crosley, E. Yaworski, I.M. Hafez, J.R. Dorkin, J. Qin, K. Lam, K.G. Rajeev, K.F. Wong, L.B. Jeffs, L. Nechev, M.L. Eisenhardt, M. Jayaraman, M. Kazem, M.A. Maier, M. Srinivasulu, M.J. Weinstein, Q. Chen, R. Alvarez, S.A. Barros, S. De, S.K. Klimuk, T. Borland, V. Kosovrasti, W.L. Cantley, Y.K. Tam, M. Manoharan, M.A. Ciufolini, M.A. Tracy, A. de Fougerolles, I. MacLachlan, P.R. Cullis, T.D. Madden, M.J. Hope, Rational design of cationic lipids for siRNA delivery, Nat Biotechnol 28(2) (2010) 172-6.
[141] T. Coelho, D. Adams, A. Silva, P. Lozeron, P.N. Hawkins, T. Mant, J. Perez, J. Chiesa, S. Warrington, E. Tranter, M. Munisamy, R. Falzone, J. Harrop, J. Cehelsky, B.R. Bettencourt, M. Geissler, J.S. Butler, A. Sehgal, R.E. Meyers, Q. Chen, T. Borland, R.M. Hutabarat, V.A. Clausen, R. Alvarez, K. Fitzgerald, C. Gamba-Vitalo, S.V. Nochur, A.K. Vaishnaw, D.W. Sah, J.A. Gollob, O.B. Suhr, Safety and efficacy of RNAi therapy for transthyretin amyloidosis, N Engl J Med 369(9) (2013) 819-29.
[142] A. Akinc, M. Goldberg, J. Qin, J.R. Dorkin, C. Gamba-Vitalo, M. Maier, K.N. Jayaprakash, M. Jayaraman, K.G. Rajeev, M. Manoharan, V. Koteliansky, I. Rohl, E.S. Leshchiner, R. Langer, D.G. Anderson, Development of lipidoid-siRNA formulations for systemic delivery to the liver, Mol Ther 17(5) (2009) 872-9.
[143] A. Akinc, A. Zumbuehl, M. Goldberg, E.S. Leshchiner, V. Busini, N. Hossain, S.A. Bacallado, D.N. Nguyen, J. Fuller, R. Alvarez, A. Borodovsky, T. Borland, R. Constien, A. de Fougerolles, J.R. Dorkin, K. Narayanannair

Jayaprakash, M. Jayaraman, M. John, V. Koteliansky, M. Manoharan, L. Nechev, J. Qin, T. Racie, D. Raitcheva, K.G. Rajeev, D.W. Sah, J. Soutschek, I. Toudjarska, H.P. Vornlocher, T.S. Zimmermann, R. Langer, D.G. Anderson, A combinatorial library of lipid-like materials for delivery of RNAi therapeutics, Nat Biotechnol 26(5) (2008) 561-9.

[144] K.T. Love, K.P. Mahon, C.G. Levins, K.A. Whitehead, W. Querbes, J.R. Dorkin, J. Qin, W. Cantley, L.L. Qin, T. Racie, M. Frank-Kamenetsky, K.N. Yip, R. Alvarez, D.W. Sah, A. de Fougerolles, K. Fitzgerald, V. Koteliansky, A. Akinc, R. Langer, D.G. Anderson, Lipid-like materials for low-dose, in vivo gene silencing, Proc Natl Acad Sci U S A 107(5) (2010) 1864-9.

[145] M.S. Shim, Y.J. Kwon, Acid-responsive linear polyethylenimine for efficient, specific, and biocompatible siRNA delivery, Bioconjug Chem 20(3) (2009) 488-99.

[146] D.E. Owens, 3rd, N.A. Peppas, Opsonization, biodistribution, and pharmacokinetics of polymeric nanoparticles, Int J Pharm 307(1) (2006) 93-102.

[147] M.E. Bonnet, P. Erbacher, A.L. Bolcato-Bellemin, Systemic delivery of DNA or siRNA mediated by linear polyethylenimine (L-PEI) does not induce an inflammatory response, Pharm Res 25(12) (2008) 2972-82.

[148] O.M. Merkel, R. Urbanics, P. Bedocs, Z. Rozsnyay, L. Rosivall, M. Toth, T. Kissel, J. Szebeni, In vitro and in vivo complement activation and related anaphylactic effects associated with polyethylenimine and polyethylenimine-graft-poly(ethylene glycol) block copolymers, Biomaterials 32(21) (2011) 4936-42.

[149] S. Boeckle, K. von Gersdorff, S. van der Piepen, C. Culmsee, E. Wagner, M. Ogris, Purification of polyethylenimine polyplexes highlights the role of free polycations in gene transfer, J Gene Med 6(10) (2004) 1102-11.

[150] J.M. Williford, J. Wu, Y. Ren, M.M. Archang, K.W. Leong, H.Q. Mao, Recent advances in nanoparticle-mediated siRNA delivery, Annu Rev Biomed Eng 16 (2014) 347-70.
[151] A.C. Hunter, S.M. Moghimi, Cationic carriers of genetic material and cell death: a mitochondrial tale, Biochim Biophys Acta 1797(6-7) (2010) 1203-9.
[152] S. Mao, M. Neu, O. Germershaus, O. Merkel, J. Sitterberg, U. Bakowsky, T. Kissel, Influence of polyethylene glycol chain length on the physicochemical and biological properties of poly(ethylene imine)-graft-poly(ethylene glycol) block copolymer/SiRNA polyplexes, Bioconjug Chem 17(5) (2006) 1209-18.
[153] T. Nomoto, Y. Matsumoto, K. Miyata, M. Oba, S. Fukushima, N. Nishiyama, T. Yamasoba, K. Kataoka, In situ quantitative monitoring of polyplexes and polyplex micelles in the blood circulation using intravital real-time confocal laser scanning microscopy, J Control Release 151(2) (2011) 104-9.
[154] O.M. Merkel, D. Librizzi, A. Pfestroff, T. Schurrat, K. Buyens, N.N. Sanders, S.C. De Smedt, M. Behe, T. Kissel, Stability of siRNA polyplexes from poly(ethylenimine) and poly(ethylenimine)-g-poly(ethylene glycol) under in vivo conditions: effects on pharmacokinetics and biodistribution measured by Fluorescence Fluctuation Spectroscopy and Single Photon Emission Computed Tomography (SPECT) imaging, J Control Release 138(2) (2009) 148-59.
[155] S. Patnaik, K.C. Gupta, Novel polyethylenimine-derived nanoparticles for in vivo gene delivery, Expert Opin Drug Deliv 10(2) (2013) 215-28.
[156] L. Buscail, B. Bournet, F. Vernejoul, G. Cambois, H. Lulka, N. Hanoun, M. Dufresne, A. Meulle, A. Vignolle-Vidoni, L. Ligat, N. Saint-Laurent, F. Pont, S. Dejean, M. Gayral, F. Martins, J. Torrisani, O. Barbey, F. Gross, R. Guimbaud, P. Otal, F. Lopez, G. Tiraby, P. Cordelier, First-in-man phase 1 clinical trial of gene therapy for advanced pancreatic cancer: safety, biodistribution, and preliminary clinical findings, Mol Ther 23(4) (2015) 779-89.

[157] L. D, L. R, Degradable Poly(β-amino esters): Synthesis, Characterization, and Self-Assembly with Plasmid DNA, J. Am. Chem. Soc 122(44) (2000) 10761–10768.

[158] J.J. Green, R. Langer, D.G. Anderson, A combinatorial polymer library approach yields insight into nonviral gene delivery, Acc Chem Res 41(6) (2008) 749-59.

[159] Y. Rui, G. Quinones, J.J. Green, Biodegradable and Bioreducible Poly(Beta-Amino Ester) Nanoparticles for Intracellular Delivery to Treat Brain Cancer, AIChE 63(5) (2017) 1470-1482.

[160] T.J. Harris, J.J. Green, P.W. Fung, R. Langer, D.G. Anderson, S.N. Bhatia, Tissue-specific gene delivery via nanoparticle coating, Biomaterials 31(5) (2010) 998-1006.

[161] D.M. Lynn, D.G. Anderson, D. Putnam, R. Langer, Accelerated discovery of synthetic transfection vectors: parallel synthesis and screening of a degradable polymer library, J Am Chem Soc 123(33) (2001) 8155-6.

[162] A. Akinc, R. Langer, Measuring the pH environment of DNA delivered using nonviral vectors: implications for lysosomal trafficking, Biotechnol Bioeng 78(5) (2002) 503-8.

[163] J.C. Sunshine, D.Y. Peng, J.J. Green, Uptake and transfection with polymeric nanoparticles are dependent on polymer end-group structure, but largely independent of nanoparticle physical and chemical properties, Mol Pharm 9(11) (2012) 3375-83.

[164] C.J. Bishop, B. Abubaker-Sharif, T. Guiriba, S.Y. Tzeng, J.J. Green, Gene delivery polymer structure-function relationships elucidated via principal component analysis, Chem Commun (Camb) 51(60) (2015) 12134-7.

[165] R.B. Shmueli, J.C. Sunshine, Z. Xu, E.J. Duh, J.J. Green, Gene delivery nanoparticles specific for human microvasculature and macrovasculature, Nanomedicine 8(7) (2012) 1200-7.

[166] H. Guerrero-Cazares, S.Y. Tzeng, N.P. Young, A.O. Abutaleb, A. Quinones-Hinojosa, J.J. Green, Biodegradable polymeric nanoparticles show high efficacy and specificity at DNA delivery to human glioblastoma in vitro and in vivo, ACS Nano 8(5) (2014) 5141-53.

[167] S.Y. Tzeng, H. Guerrero-Cazares, E.E. Martinez, J.C. Sunshine, A. Quinones-Hinojosa, J.J. Green, Non-viral gene delivery nanoparticles based on poly(beta-amino esters) for treatment of glioblastoma, Biomaterials 32(23) (2011) 5402-10.

[168] A. Mangraviti, S.Y. Tzeng, K.L. Kozielski, Y. Wang, Y. Jin, D. Gullotti, M. Pedone, N. Buaron, A. Liu, D.R. Wilson, S.K. Hansen, F.J. Rodriguez, G.D. Gao, F. DiMeco, H. Brem, A. Olivi, B. Tyler, J.J. Green, Polymeric nanoparticles for nonviral gene therapy extend brain tumor survival in vivo, ACS Nano 9(2) (2015) 1236-49.

[169] J.C. Kaczmarek, A.K. Patel, K.J. Kauffman, O.S. Fenton, M.J. Webber, M.W. Heartlein, F. DeRosa, D.G. Anderson, Polymer-Lipid Nanoparticles for Systemic Delivery of mRNA to the Lungs, Angew Chem Int Ed Engl 55(44) (2016) 13808-13812.

[170] S. Hu-Lieskovan, J.D. Heidel, D.W. Bartlett, M.E. Davis, T.J. Triche, Sequence-specific knockdown of EWS-FLI1 by targeted, nonviral delivery of small interfering RNA inhibits tumor growth in a murine model of metastatic Ewing's sarcoma, Cancer Res 65(19) (2005) 8984-92.

[171] J.D. Heidel, J.Y. Liu, Y. Yen, B. Zhou, B.S. Heale, J.J. Rossi, D.W. Bartlett, M.E. Davis, Potent siRNA inhibitors of ribonucleotide reductase subunit RRM2

reduce cell proliferation in vitro and in vivo, Clin Cancer Res 13(7) (2007) 2207-15.
[172] J.D. Heidel, Z. Yu, J.Y. Liu, S.M. Rele, Y. Liang, R.K. Zeidan, D.J. Kornbrust, M.E. Davis, Administration in non-human primates of escalating intravenous doses of targeted nanoparticles containing ribonucleotide reductase subunit M2 siRNA, Proc Natl Acad Sci U S A 104(14) (2007) 5715-21.
[173] J.E. Zuckerman, I. Gritli, A. Tolcher, J.D. Heidel, D. Lim, R. Morgan, B. Chmielowski, A. Ribas, M.E. Davis, Y. Yen, Correlating animal and human phase Ia/Ib clinical data with CALAA-01, a targeted, polymer-based nanoparticle containing siRNA, Proc Natl Acad Sci U S A 111(31) (2014) 11449-54.
[174] J.E. Zuckerman, A. Gale, P. Wu, R. Ma, M.E. Davis, siRNA delivery to the glomerular mesangium using polycationic cyclodextrin nanoparticles containing siRNA, Nucleic Acid Ther 25(2) (2015) 53-64.
[175] C. Wolfrum, S. Shi, K.N. Jayaprakash, M. Jayaraman, G. Wang, R.K. Pandey, K.G. Rajeev, T. Nakayama, K. Charrise, E.M. Ndungo, T. Zimmermann, V. Koteliansky, M. Manoharan, M. Stoffel, Mechanisms and optimization of in vivo delivery of lipophilic siRNAs, Nat Biotechnol 25(10) (2007) 1149-57.
[176] M.S. Brown, J.L. Goldstein, The receptor model for transport of cholesterol in plasma, Ann N Y Acad Sci 454 (1985) 178-82.
[177] E. Ikonen, Cellular cholesterol trafficking and compartmentalization, Nat Rev Mol Cell Biol 9(2) (2008) 125-38.
[178] W.M. Winston, C. Molodowitch, C.P. Hunter, Systemic RNAi in C. elegans requires the putative transmembrane protein SID-1, Science 295(5564) (2002) 2456-9.
[179] K. Nishina, T. Unno, Y. Uno, T. Kubodera, T. Kanouchi, H. Mizusawa, T. Yokota, Efficient In Vivo Delivery of siRNA to the Liver by Conjugation of alpha-Tocopherol, Mol Ther 16(4) (2008) 734-740.

[180] N.S. Petrova, I.V. Chernikov, M.I. Meschaninova, I.S. Dovydenko, A.G. Venyaminova, M.A. Zenkova, V.V. Vlassov, E.L. Chernolovskaya, Carrier-free cellular uptake and the gene-silencing activity of the lipophilic siRNAs is strongly affected by the length of the linker between siRNA and lipophilic group, Nucleic Acids Res 40(5) (2012) 2330-44.

[181] S.C. Wong, J.J. Klein, H.L. Hamilton, Q. Chu, C.L. Frey, V.S. Trubetskoy, J. Hegge, D. Wakefield, D.B. Rozema, D.L. Lewis, Co-injection of a targeted, reversibly masked endosomolytic polymer dramatically improves the efficacy of cholesterol-conjugated small interfering RNAs in vivo, Nucleic Acid Ther 22(6) (2012) 380-90.

[182] T.P. Prakash, G.A. Kinberger, H.M. Murray, A. Chappell, S. Riney, M.J. Graham, W.F. Lima, E.E. Swayze, P.P. Seth, Synergistic effect of phosphorothioate, 5'-vinylphosphonate and GalNAc modifications for enhancing activity of synthetic siRNA, Bioorg Med Chem Lett 26(12) (2016) 2817-20.

[183] M. Byrne, R. Tzekov, Y. Wang, A. Rodgers, J. Cardia, G. Ford, K. Holton, L. Pandarinathan, J. Lapierre, W. Stanney, K. Bulock, S. Shaw, L. Libertine, K. Fettes, A. Khvorova, S. Kaushal, P. Pavco, Novel hydrophobically modified asymmetric RNAi compounds (sd-rxRNA) demonstrate robust efficacy in the eye, J Ocul Pharmacol Ther 29(10) (2013) 855-64.

[184] J.F. Alterman, L.M. Hall, A.H. Coles, M.R. Hassler, M.C. Didiot, K. Chase, J. Abraham, E. Sottosanti, E. Johnson, E. Sapp, M.F. Osborn, M. Difiglia, N. Aronin, A. Khvorova, Hydrophobically Modified siRNAs Silence Huntingtin mRNA in Primary Neurons and Mouse Brain, Mol Ther Nucleic Acids 4 (2015) e266.

[185] M.F. Osborn, J.F. Alterman, M. Nikan, H. Cao, M.C. Didiot, M.R. Hassler, A.H. Coles, A. Khvorova, Guanabenz (Wytensin) selectively enhances uptake and

efficacy of hydrophobically modified siRNAs, Nucleic Acids Res 43(18) (2015) 8664-72.
[186] D.H. Wakefield, J.J. Klein, J.A. Wolff, D.B. Rozema, Membrane activity and transfection ability of amphipathic polycations as a function of alkyl group size, Bioconjug Chem 16(5) (2005) 1204-8.
[187] D.B. Rozema, D.L. Lewis, D.H. Wakefield, S.C. Wong, J.J. Klein, P.L. Roesch, S.L. Bertin, T.W. Reppen, Q. Chu, A.V. Blokhin, J.E. Hagstrom, J.A. Wolff, Dynamic PolyConjugates for targeted in vivo delivery of siRNA to hepatocytes, Proc Natl Acad Sci U S A 104(32) (2007) 12982-7.
[188] D. Lewis, Dynamic Polyconjugates (DPC) Technology: An Elegant Solution to the siRNA Delivery Problem (White Paper), (2011).
[189] S.R. Mudd, V.S. Trubetskoy, A.V. Blokhin, J.P. Weichert, J.A. Wolff, Hybrid PET/CT for noninvasive pharmacokinetic evaluation of dynamic PolyConjugates, a synthetic siRNA delivery system, Bioconjug Chem 21(7) (2010) 1183-9.
[190] C.I. Wooddell, D.B. Rozema, M. Hossbach, M. John, H.L. Hamilton, Q. Chu, J.O. Hegge, J.J. Klein, D.H. Wakefield, C.E. Oropeza, J. Deckert, I. Roehl, K. Jahn-Hofmann, P. Hadwiger, H.P. Vornlocher, A. McLachlan, D.L. Lewis, Hepatocyte-targeted RNAi therapeutics for the treatment of chronic hepatitis B virus infection, Mol Ther 21(5) (2013) 973-85.
[191] Yuen Man-Fung, K. Liu, H. Chan, B. Given, T. Schluep, J. Hamilton, C. Lai, S. Locarnini, J. Lau, C. Ferrari, R. Gish, Prolonged RNA interference therapy with ARC-520 Injection in treatment naïve, HBeAg positive and negative patients with chronic HBV results in significant reductions of HBs antigen, The International Liver Congress™ 2017 (EASL). Amsterdam, 2017.
[192] A. Turner, J. Stolk, R. Bals, J. Lickliter, J. Hamilton, R. Christianson, B. Given, J. Burdon, R. Loomba, J. Stoller, J. Teckman, Hepatic targeted RNA

interference provides deep and prolonged knockdown of alpha-1 antitrypsin levels in ZZ patients, he International Liver Congress™ 2017 (AESL), Amsterdam, 2017.
[193] E. Gane, C. Schwabe, B. Given, T. Schluep, J. Hamilton, C. Lai, S. Locarnini, J. Lau, C. Ferrari, R. Gish, A phase 1 study to evaluate safety and tolerability of escalating single doses of the HBV RNA interference drug ARC-521 in a healthy volunteer and HBV patient population, The International Liver Congress™ 2017 (EASL), 2017.
[194] I. Arrowhead Pharmaceuticals, Arrowhead Pharmaceuticals Focuses Resources on Subcutaneous and Extra-Hepatic RNAi Therapeutics, 2016.
[195] J.K. Nair, J.L. Willoughby, A. Chan, K. Charisse, M.R. Alam, Q. Wang, M. Hoekstra, P. Kandasamy, A.V. Kel'in, S. Milstein, N. Taneja, J. O'Shea, S. Shaikh, L. Zhang, R.J. van der Sluis, M.E. Jung, A. Akinc, R. Hutabarat, S. Kuchimanchi, K. Fitzgerald, T. Zimmermann, T.J. van Berkel, M.A. Maier, K.G. Rajeev, M. Manoharan, Multivalent N-acetylgalactosamine-conjugated siRNA localizes in hepatocytes and elicits robust RNAi-mediated gene silencing, J Am Chem Soc 136(49) (2014) 16958-61.
[196] K.G. Rajeev, J.K. Nair, M. Jayaraman, K. Charisse, N. Taneja, J. O'Shea, J.L. Willoughby, K. Yucius, T. Nguyen, S. Shulga-Morskaya, S. Milstein, A. Liebow, W. Querbes, A. Borodovsky, K. Fitzgerald, M.A. Maier, M. Manoharan, Hepatocyte-specific delivery of siRNAs conjugated to novel non-nucleosidic trivalent N-acetylgalactosamine elicits robust gene silencing in vivo, Chembiochem 16(6) (2015) 903-8.
[197] A. Sehgal, S. Barros, L. Ivanciu, B. Cooley, J. Qin, T. Racie, J. Hettinger, M. Carioto, Y. Jiang, J. Brodsky, H. Prabhala, X. Zhang, H. Attarwala, R. Hutabarat, D. Foster, S. Milstein, K. Charisse, S. Kuchimanchi, M.A. Maier, L. Nechev, P. Kandasamy, A.V. Kel'in, J.K. Nair, K.G. Rajeev, M. Manoharan, R. Meyers, B. Sorensen, A.R. Simon, Y. Dargaud, C. Negrier, R.M. Camire, A. Akinc, An RNAi

therapeutic targeting antithrombin to rebalance the coagulation system and promote hemostasis in hemophilia, Nat Med 21(5) (2015) 492-7.
[198] A.A. D'Souza, P.V. Devarajan, Asialoglycoprotein receptor mediated hepatocyte targeting - strategies and applications, J Control Release 203 (2015) 126-39.
[199] M. Manoharan, GalNAc-siRNA with Enhanced Stabilization Chemistry: ESC-GalNAc-siRNA, TIDES: Oligonucleotide and Peptide Research, Providence, 2014.
[200] X. Huang, J.C. Leroux, B. Castagner, Well-Defined Multivalent Ligands for Hepatocytes Targeting via Asialoglycoprotein Receptor, Bioconjug Chem 28(2) (2017) 283-295.
[201] M. Spiess, The asialoglycoprotein receptor: a model for endocytic transport receptors, Biochemistry 29(43) (1990) 10009-18.
[202] T. Onizuka, H. Shimizu, Y. Moriwaki, T. Nakano, S. Kanai, I. Shimada, H. Takahashi, NMR study of ligand release from asialoglycoprotein receptor under solution conditions in early endosomes, FEBS J 279(15) (2012) 2645-56.
[203] K.G. Rajeev, Conjugation Strategies for In Vivo siRNA Delivery, 8th Annual Meeting of the Oligonucleotide Therapeutics Society, Boston, MA, USA, 2012.
[204] M. Rinaudo, Chitin and chitosan: Properties and applications, Progress in Polymer Scence (7) (2006) 603-632.
[205] M. Lavertu, Z. Xia, A.N. Serreqi, M. Berrada, A. Rodrigues, D. Wang, M.D. Buschmann, A. Gupta, A validated 1H NMR method for the determination of the degree of deacetylation of chitosan, J Pharm Biomed Anal 32(6) (2003) 1149-58.
[206] S. Mao, W. Sun, T. Kissel, Chitosan-based formulations for delivery of DNA and siRNA, Adv Drug Deliv Rev 62(1) (2010) 12-27.
[207] H. Onishi, Y. Machida, Biodegradation and distribution of water-soluble chitosan in mice, Biomaterials 20(2) (1999) 175-82.

[208] R.A. Muzzarelli, Chitins and chitosans as immunoadjuvants and non-allergenic drug carriers, Mar Drugs 8(2) (2010) 292-312.
[209] I. Richard, M. Thibault, G. De Crescenzo, M.D. Buschmann, M. Lavertu, Ionization behavior of chitosan and chitosan-DNA polyplexes indicate that chitosan has a similar capability to induce a proton-sponge effect as PEI, Biomacromolecules 14(6) (2013) 1732-40.
[210] P.L. Ma, M. Lavertu, F.M. Winnik, M.D. Buschmann, New insights into chitosan-DNA interactions using isothermal titration microcalorimetry, Biomacromolecules 10(6) (2009) 1490-9.
[211] T. Kiang, J. Wen, H.W. Lim, K.W. Leong, The effect of the degree of chitosan deacetylation on the efficiency of gene transfection, Biomaterials 25(22) (2004) 5293-301.
[212] T. Sato, T. Ishii, Y. Okahata, In vitro gene delivery mediated by chitosan. effect of pH, serum, and molecular mass of chitosan on the transfection efficiency, Biomaterials 22(15) (2001) 2075-80.
[213] S.P. Strand, M.M. Issa, B.E. Christensen, K.M. Varum, P. Artursson, Tailoring of chitosans for gene delivery: novel self-branched glycosylated chitosan oligomers with improved functional properties, Biomacromolecules 9(11) (2008) 3268-76.
[214] M. Koping-Hoggard, I. Tubulekas, H. Guan, K. Edwards, M. Nilsson, K.M. Varum, P. Artursson, Chitosan as a nonviral gene delivery system. Structure-property relationships and characteristics compared with polyethylenimine in vitro and after lung administration in vivo, Gene Ther 8(14) (2001) 1108-21.
[215] P.L. Ma, M.D. Buschmann, F.M. Winnik, One-step analysis of DNA/chitosan complexes by field-flow fractionation reveals particle size and free chitosan content, Biomacromolecules 11(3) (2010) 549-54.

[216] M. Thibault, M. Astolfi, N. Tran-Khanh, M. Lavertu, V. Darras, A. Merzouki, M.D. Buschmann, Excess polycation mediates efficient chitosan-based gene transfer by promoting lysosomal release of the polyplexes, Biomaterials 32(20) (2011) 4639-46.

[217] K. Khatri, A.K. Goyal, P.N. Gupta, N. Mishra, S.P. Vyas, Plasmid DNA loaded chitosan nanoparticles for nasal mucosal immunization against hepatitis B, Int J Pharm 354(1-2) (2008) 235-41.

[218] E.A. Klausner, Z. Zhang, R.L. Chapman, R.F. Multack, M.V. Volin, Ultrapure chitosan oligomers as carriers for corneal gene transfer, Biomaterials 31(7) (2010) 1814-20.

[219] M. Jean, M. Alameh, M.D. Buschmann, A. Merzouki, Effective and safe gene-based delivery of GLP-1 using chitosan/plasmid-DNA therapeutic nanocomplexes in an animal model of type 2 diabetes, Gene Ther 18(8) (2011) 807-16.

[220] M. Jean, F. Smaoui, M. Lavertu, S. Methot, L. Bouhdoud, M.D. Buschmann, A. Merzouki, Chitosan-plasmid nanoparticle formulations for IM and SC delivery of recombinant FGF-2 and PDGF-BB or generation of antibodies, Gene Ther 16(9) (2009) 1097-110.

[221] S.A. Bustin, V. Benes, J.A. Garson, J. Hellemans, J. Huggett, M. Kubista, R. Mueller, T. Nolan, M.W. Pfaffl, G.L. Shipley, J. Vandesompele, C.T. Wittwer, The MIQE guidelines: minimum information for publication of quantitative real-time PCR experiments, Clin Chem 55(4) (2009) 611-22.

[222] I. Nawroth, J. Alsner, B.W. Deleuran, F. Dagnaes-Hansen, C. Yang, M.R. Horsman, J. Overgaard, K.A. Howard, J. Kjems, S. Gao, Peritoneal macrophages mediated delivery of chitosan/siRNA nanoparticle to the lesion site in a murine radiation-induced fibrosis model, Acta Oncol 52(8) (2013) 1730-8.

[223] E.S. Swenson, J.G. Price, T. Brazelton, D.S. Krause, Limitations of green fluorescent protein as a cell lineage marker, Stem Cells 25(10) (2007) 2593-600.
[224] K.A. Howard, S.R. Paludan, M.A. Behlke, F. Besenbacher, B. Deleuran, J. Kjems, Chitosan/siRNA nanoparticle-mediated TNF-alpha knockdown in peritoneal macrophages for anti-inflammatory treatment in a murine arthritis model, Mol Ther 17(1) (2009) 162-8.
[225] B. Ghosn, A. Singh, M. Li, A.V. Vlassov, C. Burnett, N. Puri, K. Roy, Efficient gene silencing in lungs and liver using imidazole-modified chitosan as a nanocarrier for small interfering RNA, Oligonucleotides 20(3) (2010) 163-72.
[226] G. Sahay, D.Y. Alakhova, A.V. Kabanov, Endocytosis of nanomedicines, J Control Release 145(3) (2010) 182-95.
[227] N. Oh, J.H. Park, Endocytosis and exocytosis of nanoparticles in mammalian cells, Int J Nanomedicine 9 Suppl 1 (2014) 51-63.
[228] I. Canton, G. Battaglia, Endocytosis at the nanoscale, Chem Soc Rev 41(7) (2012) 2718-39.
[229] G.J. Doherty, H.T. McMahon, Mechanisms of endocytosis, Annu Rev Biochem 78 (2009) 857-902.
[230] X. Gao, L. Huang, Cationic liposome-mediated gene transfer, Gene Ther 2(10) (1995) 710-22.
[231] C. Foged, siRNA delivery with lipid-based systems: promises and pitfalls, Curr Top Med Chem 12(2) (2012) 97-107.
[232] I.M. Hafez, N. Maurer, P.R. Cullis, On the mechanism whereby cationic lipids promote intracellular delivery of polynucleic acids, Gene Ther 8(15) (2001) 1188-96.
[233] H. Takahashi, K. Sinoda, I. Hatta, Effects of cholesterol on the lamellar and the inverted hexagonal phases of dielaidoylphosphatidylethanolamine, Biochim Biophys Acta 1289(2) (1996) 209-16.

[234] D.W. Pack, A.S. Hoffman, S. Pun, P.S. Stayton, Design and development of polymers for gene delivery, Nat Rev Drug Discov 4(7) (2005) 581-93.
[235] F. Labat-Moleur, A.M. Steffan, C. Brisson, H. Perron, O. Feugeas, P. Furstenberger, F. Oberling, E. Brambilla, J.P. Behr, An electron microscopy study into the mechanism of gene transfer with lipopolyamines, Gene Ther 3(11) (1996) 1010-7.
[236] G. van den Bogaart, J.V. Guzman, J.T. Mika, B. Poolman, On the mechanism of pore formation by melittin, J Biol Chem 283(49) (2008) 33854-7.
[237] A.E. Nel, L. Madler, D. Velegol, T. Xia, E.M. Hoek, P. Somasundaran, F. Klaessig, V. Castranova, M. Thompson, Understanding biophysicochemical interactions at the nano-bio interface, Nat Mater 8(7) (2009) 543-57.
[238] M. Huang, C.W. Fong, E. Khor, L.Y. Lim, Transfection efficiency of chitosan vectors: effect of polymer molecular weight and degree of deacetylation, J Control Release 106(3) (2005) 391-406.
[239] K. Garber, Alnylam's RNAi therapy targets amyloid disease, Nat Biotechnol 33(6) (2015) 577.
[240] S. Akhtar, I. Benter, Toxicogenomics of non-viral drug delivery systems for RNAi: potential impact on siRNA-mediated gene silencing activity and specificity, Adv Drug Deliv Rev 59(2-3) (2007) 164-82.
[241] C. Tschuch, A. Schulz, A. Pscherer, W. Werft, A. Benner, A. Hotz-Wagenblatt, L.S. Barrionuevo, P. Lichter, D. Mertens, Off-target effects of siRNA specific for GFP, BMC Mol Biol 9 (2008) 60.
[242] A. Beyerle, M. Irmler, J. Beckers, T. Kissel, T. Stoeger, Toxicity pathway focused gene expression profiling of PEI-based polymers for pulmonary applications, Mol Pharm 7(3) (2010) 727-37.

[243] S.A. Plautz, G. Boanca, J.M. Riethoven, A.K. Pannier, Microarray Analysis of Gene Expression Profiles in Cells Transfected With Nonviral Vectors, Mol Ther 19(12) (2011) 2144-2151.
[244] L. Parhamifar, H. Andersen, S.M. Moghimi, Lactate dehydrogenase assay for assessment of polycation cytotoxicity, Methods Mol Biol 948 (2013) 13-22.
[245] H. Ragelle, G. Vandermeulen, V. Preat, Chitosan-based siRNA delivery systems, J Control Release 172(1) (2013) 207-18.
[246] I. Sovadinova, E.F. Palermo, R. Huang, L.M. Thoma, K. Kuroda, Mechanism of polymer-induced hemolysis: nanosized pore formation and osmotic lysis, Biomacromolecules 12(1) (2011) 260-8.
[247] J.C. Fernandes, P. Eaton, H. Nascimento, L. Belo, S. Rocha, R. Vitorino, F. Amado, J. Gomes, A. Santos-Silva, M.E. Pintado, F.X. Malcata, Effects of chitooligosaccharides on human red blood cell morphology and membrane protein structure, Biomacromolecules 9(12) (2008) 3346-52.
[248] B.D. Ratner, S.J. Bryant, Biomaterials: where we have been and where we are going, Annu Rev Biomed Eng 6 (2004) 41-75.
[249] V. Kumar, J. Qin, Y. Jiang, R.G. Duncan, B. Brigham, S. Fishman, J.K. Nair, A. Akinc, S.A. Barros, P.V. Kasperkovitz, Shielding of Lipid Nanoparticles for siRNA Delivery: Impact on Physicochemical Properties, Cytokine Induction, and Efficacy, Mol Ther Nucleic Acids 3 (2014) e210.
[250] W. Tao, X. Mao, J.P. Davide, B. Ng, M. Cai, P.A. Burke, A.B. Sachs, L. Sepp-Lorenzino, Mechanistically probing lipid-siRNA nanoparticle-associated toxicities identifies Jak inhibitors effective in mitigating multifaceted toxic responses, Mol Ther 19(3) (2011) 567-75.
[251] E. Kolaczkowska, P. Kubes, Neutrophil recruitment and function in health and inflammation, Nat Rev Immunol 13(3) (2013) 159-75.

[252] J. Hol, L. Wilhelmsen, G. Haraldsen, The murine IL-8 homologues KC, MIP-2, and LIX are found in endothelial cytoplasmic granules but not in Weibel-Palade bodies, J Leukoc Biol 87(3) (2010) 501-8.

[253] Y. Okamoto, R. Yano, K. Miyatake, I. Tomohiro, Y. Shigemasa, S. Minami, Effects of chitin and chitosan on blood coagulation, Carbohydrate Polymers 53 (2003) 337-342.

[254] C.L. Bueter, C.K. Lee, J.P. Wang, G.R. Ostroff, C.A. Specht, S.M. Levitz, Spectrum and mechanisms of inflammasome activation by chitosan, J Immunol 192(12) (2014) 5943-51.

[255] C.L. Bueter, C.K. Lee, V.A. Rathinam, G.J. Healy, C.H. Taron, C.A. Specht, S.M. Levitz, Chitosan but not chitin activates the inflammasome by a mechanism dependent upon phagocytosis, J Biol Chem 286(41) (2011) 35447-55.

[256] J.D. Tousignant, A.L. Gates, L.A. Ingram, C.L. Johnson, J.B. Nietupski, S.H. Cheng, S.J. Eastman, R.K. Scheule, Comprehensive analysis of the acute toxicities induced by systemic administration of cationic lipid:plasmid DNA complexes in mice, Hum Gene Ther 11(18) (2000) 2493-513.

[257] A. Elouahabi, J.M. Ruysschaert, Formation and intracellular trafficking of lipoplexes and polyplexes, Mol Ther 11(3) (2005) 336-47.

[258] P. Miossec, Diseases that may benefit from manipulating the Th17 pathway, Eur J Immunol 39(3) (2009) 667-9.

[259] L.M. Serfilippi, D.R. Pallman, B. Russell, Serum clinical chemistry and hematology reference values in outbred stocks of albino mice from three commonly used vendors and two inbred strains of albino mice, Contemp Top Lab Anim Sci 42(3) (2003) 46-52.

[260] C. River, CD-1 IGS Mouse Model Infromation Sheet, Charles River, http://www.criver.com/products-services/basic-research/find-a-model/cd-1-mouse, 2011.

[261] D. Landesman-Milo, D. Peer, Toxicity profiling of several common RNAi-based nanomedicines: a comparative study, Drug Deliv Transl Res 4(1) (2014) 96-103.
[262] A.O. Hosten, BUN and Creatinine, in: H.K. Walker, W.D. Hall, J.W. Hurst (Eds.), Clinical Methods: The History, Physical, and Laboratory Examinations, Boston, 1990.
[263] J.D. Thompson, D.J. Kornbrust, J.W. Foy, E.C. Solano, D.J. Schneider, E. Feinstein, B.A. Molitoris, S. Erlich, Toxicological and pharmacokinetic properties of chemically modified siRNAs targeting p53 RNA following intravenous administration, Nucleic Acid Ther 22(4) (2012) 255-64.
[264] Y. Lin, Y. Li, X. Wang, T. Gong, L. Zhang, X. Sun, Targeted drug delivery to renal proximal tubule epithelial cells mediated by 2-glucosamine, J Control Release 167(2) (2013) 148-56.
[265] S.G. Jones, T. Ito, A.O. Phillips, Regulation of proximal tubular epithelial cell CD44-mediated binding and internalisation of hyaluronan, Int J Biochem Cell Biol 35(9) (2003) 1361-77.
[266] A. Ruggiero, C.H. Villa, E. Bander, D.A. Rey, M. Bergkvist, C.A. Batt, K. Manova-Todorova, W.M. Deen, D.A. Scheinberg, M.R. McDevitt, Paradoxical glomerular filtration of carbon nanotubes, Proc Natl Acad Sci U S A 107(27) (2010) 12369-74.
[267] R.S. Geary, D. Norris, R. Yu, C.F. Bennett, Pharmacokinetics, biodistribution and cell uptake of antisense oligonucleotides, Adv Drug Deliv Rev 87 (2015) 46-51.
[268] B.A. Molitoris, P.C. Dagher, R.M. Sandoval, S.B. Campos, H. Ashush, E. Fridman, A. Brafman, A. Faerman, S.J. Atkinson, J.D. Thompson, H. Kalinski, R. Skaliter, S. Erlich, E. Feinstein, siRNA targeted to p53 attenuates ischemic and cisplatin-induced acute kidney injury, J Am Soc Nephrol 20(8) (2009) 1754-64.